PICOSECOND DYNAMICS OF INTRAMOLECULAR VIBRATIONAL-ENERGY REDISTRIBUTION (IVR) IN JET-COOLED MOLECULES

Thesis by

Peter Mark Felker

In Partial Fulfillment of the Requirements

for the Degree of

Doctor of Philosophy

California Institute of Technology

Pasadena, California

1985

(submitted December 4, 1984)

ACKNOWLEDGEMENTS

Being a believer in a creative, loving God, I also believe that all that is of worth in this thesis has come into being through His power. For this and for the joys of scientific research, I am thankful.

I am greatly indebted to many people who have contributed directly and indirectly to the work reported on in these pages. It has been a pleasure to be under the supervision of Professor Ahmed Zewail. I thank him for his sound direction, his contagious enthusiasm, his drive to attack difficult scientific problems, and his willingness to treat his students as colleagues. If I had to do it over again, I would gladly choose to work under him.

I have been substantially aided by interactions with many members of the Zewail research group. In particular, I thank Bill Lambert, whose experimental guidance has been invaluable to me. I also thank Tina Wood for typing numerous manuscripts.

I have benefitted in many ways from friends and institutions at Caltech. I thank my cronies at the Lambert memorial table: Dean Neikirk, James Garvey, Wyman Williams, and Don Caldwell for uncountable fun-filled hours. I thank my old roomate Rich Durand for being such a self-sacrificing friend. And, I acknowledge the importance of the Caltech Men's Glee Club in providing a valuable escape from the everyday pressures of research.

My family has never failed to be supportive of my career as a perpetual student. For this and for more things than can be written down or expressed, I thank my wife, my parents, my grandparents, and all the members of my family. Finally, I thank again my wife Patti for her love and for her patience, even in the times when I slip from doing science, to being obsessed with science.

Financial support for this research was made available through National Science Foundation grant nos. DMR-8105034 and CHE-8211356 awarded to Professor Ahmed H. Zewail. I am grateful to IBM for their support in the form of a fellowship.

To my parents,

David and Mary Anne Felker

ABSTRACT

Theoretical and experimental results concerning the dynamical manifestations of intramolecular vibrational-energy redistribution (IVR) in the temporally resolved fluorescence of jet-cooled molecules are presented. A first concern is with the derivation of the characteristics of the beat-modulated fluorescence decays which arise from *multilevel* vibrational coupling within a molecule. Relations connecting quantum beat frequencies, phases, and modulation depths to coupling parameters are presented. Likely sources of deviations of experimental results from theoretical predictions are considered. And, the direct link between IVR and time-resolved fluorescence experiments is discussed with emphasis placed on the physical interpretation of vibrational quantum beats and the nature of IVR as a function of vibrational energy in a molecule. Secondly, the results of picosecond time-resolved measurements of IVR on jet-cooled anthracene at different excess energies are reported and analyzed. The nature of IVR as a function of vibrational energy, the relevant timescales for the process, and the details of pertinent vibrational couplings are determined. Thirdly, experimental and theoretical results pertaining to the role of molecular rotations in IVR are presented. Finally, experimental results on jet-cooled *t*-stilbene are reported and analyzed with the aim of assessing the generality of our theoretical treatment and the anthracene results.

TABLE OF CONTENTS

CHAPTER 1

INTRODUCTION

Among the most fundamental of current problems in chemical physics is the characterization of dynamical processes in individual molecules effectively isolated from external perturbations. Such intramolecular processes, which arise following the excitation of a gaseous molecule, may be expected to be markedly dependent on the nature of the initially excited state. In large part, it is this expected dependence of dynamics on initial state that provides the justification for detailed studies of these processes, for it implies that one may be able to intimately control the physics and/or chemistry of a molecule simply by varying excitation parameters. Thus, for the past twenty years experimentalists and theorists have been interested in developing propensity rules by which one can predict intramolecular dynamics given knowledge of molecular parameters and the initially prepared state.

Without question, and perhaps not surprisingly, the greatest success in this effort has been at the coarsest level of molecular level structure—that is, at the level of the electronic state. The reasons for this success are many, but for the most part are related to: 1) the relatively small number of relevant electronic states, 2) the success which theories of electronic structure have had both in characterizing these states and their couplings to other electronic states, and 3) the fact that the rates of the relevant processes can be directly measured by experiment.

For the next coarsest regime of molecular level structure, the vibrational regime, the characterization of intramolecular processes is not nearly as complete. This relative lack of knowledge of vibrational effects compared to the knowledge of electronic effects on intramolecular dynamics is due primarily to the larger number of relevant states, less precise knowledge of relevant couplings, and experimental difficulties in measuring vibrational state-specific rates. But it is precisely at the vibrational level where one might expect initial state-dependent processes to yield the greatest measure and variety of control over subsequent dynamics. For chemical processes this expectation derives from the nature of molecular motions as distortions of chemical bonds, which implies that different vibrational motions lend different reactivities to the molecule. For photophysical processes, Franck-Condon factors and

promoting vibrational modes are expected to be intimately involved in determining rates. Numerous processes such as multiphoton dissociation, laser-selective chemistry, radiationless transitions, and unimolecular reactions may therefore be strongly dependent on the vibrational state initially excited.[1]

At the heart of the question of vibrational state specificity in intramolecular dynamics is the matter of intramolecular vibrational energy redistribution (IVR).[2] This is the process by which energy that is initially localized in a particular vibrational motion redistributes in time such that different vibrational motions gain energy at the expense of the initial motion. One can readily see that the extent to which this redistribution occurs and the timescale on which it happens has direct bearing on vibrational state-specific processes. For if IVR spreads energy over a large number of vibrations in a time short compared to other intramolecular decay processes, then memory of the initial state will be lost and with it the possibility of state-specific dynamics. Thus, insofar as vibrational character influences molecular dynamics, the characterization of IVR is essential to the understanding of the dynamics. It is with the aim of contributing to this characterization that the work comprising this thesis is presented.

Experimental approaches to the study of IVR typically have tended to fall into one of two classes of experiments;[2a] the measurement of unimolecular reaction rates or the steady-state measurement of molecular emission upon excitation. In the former approach information concerning the IVR process is obtained by comparison of the observed rates of gas phase reactions with rates calculated assuming instantaneous and complete vibrational energy randomization subsequent to excitation of the molecule. In many cases the predictions of such "statistical" theories (*e.g.*, RRKM theory[3]) closely match observed behavior, which agreement implies rapid and extensive IVR. The latter approach relies on the fact that the spectral characteristics of emission from a molecule will depend intimately on the vibrational character of the molecular excited state. If one prepares a gaseous molecule in a well-defined vibrational state and subsequently observes emission bands which

would not be expected to arise from this initially prepared state, then some IVR process can be inferred. Moreover, a "rate" can be calculated for this process by comparing the intensities of expected emission bands (so-called vibrationally unrelaxed emission) and unexpected emission bands (vibrationally relaxed emission).

Until the development of seeded supersonic jets for molecular spectroscopy both of the above-mentioned general methods of studying IVR processes were seriously handicapped by the requirement that the gaseous samples be at temperatures on the order of, or greater than, room temperature just to achieve vapor densities large enough to render experiments possible. For reasonably large molecules (*e.g.*, napthalene and anthracene) at such temperatures, the thermal distribution of rovibrational levels is composed of a large number of states with significant population. The situation makes it all but impossible to excite well-defined initial states, even with narrow band light sources. Thus, experiments done in the gas bulb generally suffer severe ambiguities in interpretation due to this thermal congestion effect.

The use of ultra-cold gaseous samples generated by free-jet expansion[4] can eliminate much of the ambiguity associated with thermal effects while still providing a sample in which the molecules of interest are effectively isolated. In the past decade or so, these features of jet-cooled samples have been extensively exploited in the study of IVR by both unimolecular reaction rate measurements[5] and emission spectroscopy[2] (or combinations of both). The results of these studies have been very fruitful in contributing to the characterization of IVR processes. Nevertheless, it has been apparent that deficiencies are present in these jet experiments as well. These deficiencies arise from the fact that the measurements made do not directly monitor the IVR process in time, but instead are time-integrated quantities that can only be related to IVR indirectly.

In an effort to directly study the IVR processes of large molecules in the time domain, we have been led to use picosecond spectroscopic techniques to make measurements on molecules cooled by free-jet expansion (the so-called "picosecond-jet" technique[5]). In this manner we have hoped to eliminate both the ambiguity asso-

ciated with thermal congestion (although it must be noted that even in the jet at very low temperatures, significant rotational thermal congestion persists for large molecules) and the deficiencies of time-integrated experiments. The key features, therefore, of this experimental technique are the relative absence of thermal congestion in the molecular samples (and the concomitant ability to prepare well-defined initial states) and the capability of observing dynamical processes on a picosecond timescale.

The specific work which is reported on in this thesis involves the use of the picosecond-jet technique to measure the time- and frequency-resolved fluorescence of two molecules as function of initially prepared vibrational level in their first excited singlet electronic states (S_1) and in this manner to directly probe IVR within the S_1 manifolds. As a prototypical example of IVR in large aromatics, results for the anthracene molecule are first presented. The intent is to examine the detailed nature of vibrational energy flow in this rigid, "unreactive" molecule and to discover the ways in which the amount of vibrational energy and the rotational level structure affect this flow. Particular emphasis is placed on the phenomenon of phase-shifted quantum beats,[6] which occurs for excitation energies within a small energy range of the anthracene S_1 manifold and which represents the manifestation of IVR amongst a small number of vibrational levels (restricted IVR). Emphasis is also placed on how the character of the energy flow changes at higher vibrational energies to encompass a larger number of levels and to become dissipative in nature.[7] The second molecule studied is *trans*-stilbene. It differs in significant ways from the anthracene molecule in that it is reactive in the S_1 state[8] (it undergoes a *trans-cis* photoisomerization), is much less rigid, has many low frequency vibrational modes, and has reduced symmetry. It therefore represents an interesting test of the general applicability of IVR trends deduced from the anthracene results. Moreover, its study sheds some light on the interplay between IVR and reactive dynamical processes.

The structure of the main body of the thesis takes the following form. In

Chapter 2 a brief discussion of the principles underlying the picosecond-jet technique is presented. Chapter 3[9] deals with the theory of how the dynamics of IVR is manifested as coherence effects in fluorescence decays. Chapter 4[10] is a presentation of results pertaining to IVR in the S_1 manifold of anthracene. The ways in which the rotational level structure of molecules can influence the manifestations of IVR in fluorescence decay measurements is the subject of Chapter 5.[11] Finally, Chapters 6[12] and 7[13] deal with results pertinent to IVR in S_1 *t*-stilbene. All of the Chapters 3–7 were written as manuscripts to be submitted as papers to journals. This might have the effect of rendering the thesis somewhat disjointed to the reader. For this I apologize and ask the reader's indulgence. The thesis also has four appendices, three of which are published reports[6,7] of our initial work on restricted and dissipative IVR. The fourth appendix consists of the FORTRAN computer program used in the Fourier analysis of fluorescence decays.

REFERENCES

1. See, for example, N. Bloembergen and E. Yablonovitch, Phys. Today, **31**, 23 (1978); A. H. Zewail, Phys. Today **33**, 27 (1980).

2. For reviews see: (a) R. H. P. Rettschnick, in *Radiationless Transitions*, edited by S. H. Lin (Academic, New York, 1980); (b) R. E. Smalley, J. Phys. Chem. **86**, 3504 (1982); (c) C. S. Parmenter, Faraday Discuss. Chem. Soc. **75**, 7 (1983).

3. R. A. Marcus, J. Chem. Phys. **20**, 359 (1952).

4. R. E. Smalley, L. Wharton, and D. H. Levy, Accts. Chem. Res. **10**, 139 (1977).

5. For example, see: P. M. Felker and A. H. Zewail, in *Applications of Picosecond Spectroscopy to Chemistry*, edited by K. B. Eisenthal (Reidel, Dortrecht, 1984); and references therein.

6. (a) P. M. Felker and A. H. Zewail, Chem. Phys. Lett. **102**, 113 (1983); (b) P. M. Felker and A. H. Zewail, Phys. Rev. Lett. **53**, 501 (1984).

7. P. M. Felker and A. H. Zewail, Chem. Phys. Lett. **108**, 303 (1984).

8. J. A. Syage, W. R. Lambert, P. M. Felker, A. H. Zewail, and R. M. Hochstrasser, Chem. Phys. Lett. **88**, 266 (1982); and references therein.

9. P. M. Felker and A. H. Zewail, J. Chem. Phys. - submitted.

10. P. M. Felker and A. H. Zewail, J. Chem. Phys. - submitted.

11. P. M. Felker and A. H. Zewail, J. Chem. Phys. - submitted.

12. P. M. Felker, W. R. Lambert, and A. H. Zewail, J. Chem. Phys. - submitted.

13. P. M. Felker and A. H. Zewail, J. Phys. Chem. - submitted.

CHAPTER 2

EXPERIMENTAL

In this chapter the intent is to present a discussion of the principles underlying the picosecond-jet technique.[1] As has been stated in Chapter 1, the utility of this experimental approach to the study of IVR derives from the combination of two features—the use of a free-jet expansion to cool the gaseous molecular sample and the use of picosecond spectroscopic techniques to probe dynamical processes in the time domain. Thus, we shall be concerned with elucidating the mechanism by which a freely expanding gas is cooled, and explaining the fundamentals of the spectroscopic technique by which we measure fluorescence decays on a picosecond timescale. At the end of the chapter an overview of the experimental apparatus and a discussion of the sensitivity of the method are given. Detailed information concerning the design of the apparatus may be found elsewhere.[2] Specific experimental conditions relevant to the results dealt with in subsequent chapters will be presented in those chapters.

I. COOLING BY FREE-JET EXPANSION

A. Useful relations

The expansion of a high pressure gas through an orifice of diameter D into a region of low pressure, with D being large in comparison to the mean free path of the gas molecules, is termed a free-jet expansion.[3] The effect of such an expansion is to convert, *via* collisions, the random thermal velocity of the gas before the orifice into directed flow and, in so doing, to reduce the translational temperature of the gas. To the extent that the translational degrees of freedom communicate with any internal degrees of freedom that exist in the gas (*i.e.*, the rotational and vibrational motions of any polyatomic constituents) these are cooled as well.

Probably the most convenient method of calculating the thermodynamic properties of a free-jet expansion is that which involves the treatment of the gaseous flow in the hydrodynamic limit and the expansion taken to be isentropic.[4] In this manner one can obtain a number of useful equations relating gas expansion parameters to jet translational temperature and density. For instance, for a monatomic gas in the hydrodynamic regime, the translational temperature T as a function of

D; x, the distance from the orifice; and nozzle temperature T_0, is given by:[4]

$$T = \frac{T_0}{1 + 1.09(\frac{x}{D})^{4/3}}. \tag{1.1}$$

The gas density $\rho(x, \theta, D)$ for an ideal monatomic gas at distance x, off-expansion axis angle θ, and orifice diameter D, is found to be:[5]

$$\rho(x, \theta, D) \simeq 0.16\rho_0 \cos^2\theta(\frac{D}{x})^2, \tag{1.2}$$

where ρ_0 is the density of the gas before the orifice.

Going beyond the continuum approximation, as is necessary for large x, is somewhat more complicated since it involves treating the expansion on a microscopic level. Nevertheless, analyses have been made and have produced results[6] of interest to the spectroscopist. In particular, unlike that which is suggested by (1.1), T does not continue decreasing as $x \to \infty$. Instead, a terminal translational temperature T_t is reached at large x, and is a function of the product of P_0D, where P_0 is the nozzle gas pressure. For argon,[4]

$$T_t = \frac{1}{1 + 5900(P_0D)^{.8}}, \tag{1.3}$$

with P_0 in atmospheres and D in centimeters. This equation, besides indicating the influence of nozzle pressure in the cooling process, also suggests the importance of collisions in translational cooling, being that the total number of two body collisons in the expansion is proportional to P_0D.[5]

Besides translational temperature and gas density, a third quantity is of interest to the spectroscopist; the two body collision rate in the jet. One would expect this rate to decrease with density and therefore to be a function of x/D. Lubman, *et al.*,[7] have calculated hard sphere collision rates for a variety of expansion parameters and x/D values. Their findings indicate that for typical conditions and reasonably large x/D values (≥ 25), collision rates in a jet are about two orders of magnitude less than typical large molecule fluorescence decay rates ($\sim 10^7 - 10^8$ sec^{-1}). This, of course, is important to those who undertake to study intramolecular decay rates

in a supersonic jet. The steep dependence of collision rate on x/D is also of use in a practical sense. It suggests an empirical assessment of collisional influences on experimental observables *via* the measurement of such observables as a function of x.

B. A microscopic picture of cooling

The results surveyed above concerning the parameters which affect cooling, density, and collision rate in a free-jet expansion are of obvious importance to the free-jet spectroscopist. They were presented to aid the unfamiliar reader in assessing the experimental results presented later in the thesis. Unfortunately, they reveal little of the mechanism by which gases are cooled in the process of expansion. To try to provide a qualitative picture of this process is the aim of this section.

We start with the assumption that translational cooling is the result of collisional interactions.[5] But obviously, all collisions between gas molecules are not cooling collisions. Thus, the task is to derive the requirements that must be fulfilled if a collision between two hard sphere gas molecules is to be a "cooling" collision, and then to argue that there is a bias towards such collisions in a freely expanding gas. Once an intuitive feel for translational cooling is established, it is then a relatively easy matter to give a qualitative explanation of the rotational and vibrational cooling experienced by a polyatomic molecule seeded in a monatomic carrier gas.

Consider the identical hard spheres 1 and 2 of radius a heading on a collision course with velocities in the laboratory frame $\vec{v}_{1i}$ and $\vec{v}_{2i}$. Choose the x direction in space as the direction of the relative velocity $\vec{v}_r \equiv \vec{v}_{1i} - \vec{v}_{2i}$, and the y direction such that the centers of the two spheres initially lie in the xy plane. With this axes choice, the centers of the two spheres at any instant of time are at the same z value. Thus one can analyze the collisional interaction in two dimensions. Keeping the x and y spatial directions for the x' and y' directions, respectively, in the center of mass (cm) frame (see Fig. 1), the velocities of the spheres are $\vec{v}_{1i}^{cm} = (|\frac{\vec{v}_r}{2}|, 0, 0)$ and $\vec{v}_{2i}^{cm} = (-|\frac{\vec{v}_r}{2}|, 0, 0)$, and they approach each other moving parallel to the x'-axis. An impact parameter b is defined by the quantity $y_2' - y_1'$, where y_2' is the constant y' value that sphere 2 travels along and y_1' is the analogous value for sphere 1. The value of b can range from $-2a$ to $+2a$.

After colliding, the velocities of the spheres in the cm frame become

$$\vec{v}_{1f}^{cm} = \frac{|v_r|}{2}\hat{e} = -\vec{v}_{2f}^{cm}, \tag{1.4}$$

where $\hat{e}$ is the unit vector $(\cos 2\theta, -\sin 2\theta, 0)$ and $\theta = \cos^{-1}(\frac{b}{2a})$. In the laboratory frame the final velocities are given by

$$\vec{v}_{1f} = \vec{V} + \frac{\vec{v}_{1f}^{cm}}{2} \tag{1.5a}$$

and

$$\vec{v}_{2f} = \vec{V} - \frac{\vec{v}_{1f}^{cm}}{2}, \tag{1.5b}$$

where $\vec{V}$ is the cm velocity $\frac{1}{2}(\vec{v}_{1f} + \vec{v}_{2f}) = \frac{1}{2}(\vec{v}_{1i} + \vec{v}_{2i})$. We are interested in determining those collisions which change the magnitudes of the velocities of the two spheres such that they are closer together after collision than they were before. For such "cooling" collisions to occur

$$||\vec{v}_{1f}| - |\vec{v}_{2f}|| < ||\vec{v}_{1i}| - |\vec{v}_{2i}||. \tag{1.6}$$

Squaring both sides and noting that

$$|\vec{v}_{1f}|^2 + |\vec{v}_{2f}|^2 = |\vec{v}_{1i}|^2 + |\vec{v}_{2i}|^2, \tag{1.7}$$

(1.6) reduces to

$$|\vec{v}_{1f}||\vec{v}_{2f}| > |\vec{v}_{1i}||\vec{v}_{2i}|. \tag{1.8}$$

Now,

$$|\vec{v}_{1f}||\vec{v}_{2f}| = (|\vec{V}|^4 + \frac{|\vec{V}|^2|\vec{v}_r|^2}{2} + \frac{|\vec{v}_r|^4}{16} - |\vec{v}_r|^2|\vec{V}\cdot\hat{e}|^2)^{\frac{1}{2}} \tag{1.9a}$$

and

$$|\vec{v}_{1i}||\vec{v}_{2i}| = (|\vec{V}|^4 + \frac{|\vec{V}|^2|\vec{v}_r|^2}{2} + \frac{|\vec{v}_r|^4}{16} - |\vec{V}\cdot\vec{v}_r|^2)^{\frac{1}{2}}. \tag{1.9b}$$

Thus (1.8) amounts to

$$|\vec{v}_r|^2|\vec{V}\cdot\hat{e}|^2 < |\vec{V}\cdot\vec{v}_r|^2. \tag{1.10}$$

Since $\vec{v}_r = (|\vec{v}_r|, 0, 0,)$ this becomes

$$|\vec{v}_r|^2(V_x \cos 2\theta - V_y \sin 2\theta)^2 < |\vec{v}_r|^2 V_x^2, \tag{1.11a}$$

which can be reduced to

$$V_y^2 - V_x^2 < 2V_x V_y \frac{\cos 2\theta}{\sin 2\theta}, \tag{1.11b}$$

where V_x and V_y are the x and y components, respectively, of $\vec{V}$. Now if we average the right side of (1.11b) over all possible values of the impact parameter by integration over b:

$$\int_{-2a}^{2a} \frac{\cos 2\theta}{\sin 2\theta} db = \int_{\pi}^{0} -2a \frac{\sin\theta \cos 2\theta}{\sin 2\theta} d\theta = 0, \tag{1.12}$$

we finally obtain the b-averaged condition for a cooling collision:

$$V_y^2 < V_x^2. \tag{1.13}$$

This condition can be expressed in terms of the angle ($\equiv \phi$) between the projections of $\vec{V}$ and $\vec{v}_r$ in the xy scattering plane by using

$$\cos\phi = \frac{V_x|\vec{v}_r|}{|\vec{v}_r|(V_x^2 + V_y^2)^{\frac{1}{2}}} \tag{1.14}$$

and (1.13) to obtain $|\cos\phi| > \frac{1}{\sqrt{2}}$ or

$$-\frac{\pi}{4} < \phi < \frac{\pi}{4} \quad \text{and} \quad \frac{3\pi}{4} < \phi < \frac{5\pi}{4}, \tag{1.15}$$

the condition for cooling collisions. ***Qualitively this means that collisions between two spheres travelling in similar directions at different speeds will tend to be cooling collisions, while collisions between spheres travelling in very different directions at similar speeds will tend not to be cooling collisions.***

In a confined gas there is no geometrical preference for any given values of ϕ. One can see this by noting that the Boltzmann factor for the probability that the vectors $\vec{V}$ and $\vec{v}_r$ characterize the sphere 1-sphere 2 two body problem depends on

$$\vec{v}_{1i} \cdot \vec{v}_{1i} + \vec{v}_{2i} \cdot \vec{v}_{2i} = 2|\vec{V}|^2 + \frac{|\vec{v}_r|^2}{2} \tag{1.16}$$

and is independent of ϕ. Thus, one does not expect a predominance of either cooling or noncooling collisions in a gas at equilibrium. A freely expanding gas is different, however. As gas atoms travel from the expansion orifice into the evacuated chamber, those atoms with velocities pointing in similar directions will tend to travel along the same streamline emanating from the expansion orifice. This geometrical sorting effect spatially localizes atoms travelling in the same direction. In turn, it provides an environment in which cooling collisions are more likely to occur than noncooling ones, for a given atom's most likely collision partners are those atoms which are travelling in the same direction as it is.

This qualitative picture of the translational cooling process is treated more rigorously and quantitatively by Toennies and Winkelmann.[8] By assuming a spherically symmetric expansion and by invoking Maxwellian velocity distributions for atoms travelling along a given streamline, they solve, as a function of radial distance, the Boltzmann equation for the translational temperatures parallel ($T_{||}$) and perpendicular ($T_{\perp}$) to the streamline. The treatment allows them to deduce that the effect of collisions in an expansion is to reduce $T_{||}$ at the expense of increasing random motion in the perpendicular direction, where geometrical sorting then serves to reduces $T_{\perp}$. Thus, geometrical sorting is the means by which an environment is created in which cooling collisions predominate.

C. Rotational and vibrational cooling

Translational cooling is not the only cooling which occurs in a free-jet expansion when the expanding gas is composed in part of polyatomics. In such cases the rotational and vibrational degrees of freedom of the polyatomic gas molecules are also cooled.[4,5] This happens as a result of the translational cooling. To see this, imagine what will happen if a small amount of some polyatomic is mixed in with gaseous atoms (*i.e.*, the carrier gas) undergoing expansion. Collisions will occur during expansion which will tend to equalize the velocities of the various species in the jet. In addition, collisions between atoms and molecules will induce energy flow to and from the internal degrees of freedom of the molecules. However, as the

translational velocity distribution sharpens, the average collision energies decrease. As a result, less collisions between the atomic gas and the polyatomic will be able to excite internal degrees of freedom. No comparable conservation of energy constraints exist on de-excitation collisions, however. Collision induced energy flow involving the internal degrees of freedom of the polyatomic will therefore become one-sided toward de-excitation and vibrational-rotational cooling will result.

In general, the rotational and vibrational temperatures achieved in an expansion are not as low as that for translation. For the most part rotational temperatures have been found to follow translational temperatures ($\sim 0-5$ K) fairly closely[4] and to be on the order of 10 K or less, while vibrational temperatures tend to have somewhat higher values[4] (< 50 K) owing to the generally smaller cross sections for vibrational-translational energy exchange compared to rotational-translational energy exchange. The degree of rotational and vibrational cooling depends on the particular polyatomic involved and the particular carrier gas, as well as on the expansion parameters.

II. MEASUREMENT OF FLUORESCENCE DECAYS BY TIME-CORRELATED SINGLE PHOTON COUNTING (TSPC).

A. General Scheme

The TSPC method[9] of observing fluorescence decays has proven very useful in application to samples with lifetimes of $\sim$ 10 psec to hundreds of nanoseconds. Detection does not require strongly fluorescing samples or a very intense excitation source. Moreover, excellent signal-to-noise ratios are obtained with data collection often lasting less than ten minutes. In short, TSPC detection can be applied with excellent results to a large variety of samples.

The method of TSPC depends on the assumption that by individually timing many single photon emission events from an ensemble of molecules and by consequently producing a histogram of events *vs.* time, one can faithfully reproduce the fluorescence decay of an "average" molecule in that ensemble. This is accomplished as follows (see Fig. 2): Light from a pulsed source is split into two directions. One part serves to produce an electrical pulse *via* a fast photodiode (PD). This electrical pulse, after appropriate shaping by timing electronics (PSE), starts a timing clock (TAC). The other part of the light pulse, meanwhile, is directed toward the fluorescent sample (S). Optics collect and focus a portion of the resulting fluorescence on the photocathode of a fast photomultiplier (PMT). If a fluorescence photon is detected, the resulting PMT electrical pulse serves to stop the clock started *via* the photodiode. (The TSPC scheme can be used in a reverse configuration also, in which the PMT pulse starts the clock and the PD pulse is delayed and then stops the clock.) If both start and stop events occur, the time on the clock is read by an analyzer and the event is stored in a memory slot designated for its particular clock time. If no stop pulse arrives at the clock for a given time after its start, the clock is automatically set to zero to await restarting. Also, a stop pulse has no effect if no start pulse has triggered the clock. The storage locations of the analyzer add up all the start-stop events characterized by like clock times. In doing so, a histogram of events *vs.* time is produced. The result is a reconstruction of the fluorescence

decay of the sample.

Consideration of the above reveals that there is a limitation of the TSPC scheme. That is, it is possible to detect only one photon from any given excitation pulse. If the excitation intensity is such that two or more photons reach the photocathode an appreciable fraction of the times that only one photon does, the observed decay will reflect this as anomalous intensity at early times. In other words, due to biased data collection, the decay will appear faster than it is. This effect can be made negligible simply by reducing the fluorescence intensity such that the number of multiple photon detection events is only a small fraction of single photon events. In practice, this is accomplished in this laboratory by keeping the photon counting rate at less than about one percent of the excitation source repetition rate.

B. Excitation Source

The nature of the TSPC scheme dictates the ideal characteristics for the excitation source to be used in its application. Firstly, of course, it should be pulsed and should produce pulses with widths that do not limit the temporal resolution of detection. Secondly, it should be able to produce pulses at repetition rates high enough that, despite the necessary limitations imposed on the photon counting rate, decays can be collected in a reasonable amount of time. Thirdly, the pulse repetition rate should be variable to allow operation at the highest repetition rate consistent with the requirement that the sample be allowed to relax fully between pulses. Finally (and independent of the mode of detection), the source should be tunable.

All of these requirements are met well by laser systems known as synchronously pumped, mode-locked, cavity dumped dye lasers.[10] These systems, which typically consist of a mode-locked argon ion laser pumping a cavity length-matched dye laser, produce tunable $\sim$ 15 psec pulses at repetition rates variable from about 80 MHz down into the few KHz range. Although the peak pulse powers of such lasers are typically smaller by a factor of one thousand or more compared to other, low

repetition rate sources, this is compensated for by the high laser repetition rate and the inherent sensitivity of TSPC detection.

C. Temporal resolution

The temporal resolution available with TSPC using a picosecond laser is typically not limited by the excitation source. In most systems, the limit arises from timing jitter in the photomultiplier. This jitter is primarily the result of the thermal distribution of photoelectrons in the photocathode of the detector and of the distribution of distances over which photoelectrons must travel before reaching the gain portion of the device. These two factors introduce a spread in the interval between the collision of a photon with the photocathode and the ultimate production of an electrical pulse by the photomultiplier. Photomultiplier products designed to reduce this transit time jitter allow one to limit it to approximately 80 psec. Given the typical jitter of $\sim$ 20 psec in the other timing electronics and a 15 psec laser pulsewidth, this still represents a limiting value for the overall temporal resolution of a TSPC system.

Finite temporal resolution has the effect of distorting measured fluorescence decays away from "true" molecular fluorescence decays. The effect can be succinctly expressed mathematically by means of an integral that relates the observed decay $F(t)$ to the convolution of the true decay $I(t)$ with the "system response function" $R(t)$:[11]

$$F(t) = \int_0^t R(t')I(t-t')dt'. \tag{2.1}$$

The system response function represents that decay which would be observed if the true molecular fluorescence decay were a δ-function in time. It thus takes into account the overall temporal response of the measurement apparatus. Response functions can be accurately measured for a given experimental system by measuring with that same system, the temporal profile of excitation light scatter.

D. Data analysis

A fluorescence decay obtained *via* TSPC consists of a $1 \times N$ dimensional array of integers, the positions (channels) in the array representing clock times and the

values of the integer representing the number of start-stop events recorded for each of the clock times. The inherent "signal to noise" in a particular of the decay is determined by counting error and follows Poisson statistics:[11] the count $N(t_i)$ in channel i differs from the "true" count with a standard deviation of $\sqrt{N(t_i)}$. Thus, the signal to noise goes as $\sqrt{N(t_i)}$.

In analyzing TSPC decays, it is often useful to fit a measured decay to an assumed molecular decay function with adjustable parameters. The digital form of the data and the well-defined source of noise in the decay allow this to be done quite readily with a small computer (*e.g.*, a PDP 11/23) using a nonlinear least squares fitting algorithm.[12] In such a procedure the sum of the squares of the weighted residuals given by

$$\chi^2 = \sum_i \frac{(N(t_i) - F(t_i))^2}{W(t_i)}, \tag{2.2}$$

(where $N(t_i)$ is the number of measured counts in the i^{th} channel, $F(t_i)$ is the number of counts calculated to be in the i^{th} channel using an assumed decay function, and $W(t_i)$ is the weight[12] for a given data point and is determined by Poisson statistics to be $N(t_i)$) is minimized by adjusting parameters used in the calculation of the $F(t_i)$. The goodness of the fit can be judged by the final value for χ^2.

For many cases in which the temporal response of detection must be accounted for *via* the convolution integral (sum)[13] (2.1) in the calculation of $F(t_i)$ of (2.2), the nonlinear least squares fitting procedure can be rendered more than an order of magnitude faster by using recursion relations in calculating the $F(t_i)$. Such relations are applicable if the true molecular decay $I(t_i)$ that is to be convoluted with the system response function $R(t_i)$ to yield $F(t_i)$ can be expressed as a sum of exponentials of the form e^{Kt_i}, where K does not depend on t_i. This is the case not only for single and multi-exponential decays, but also for decays containing sinusoidal modulation terms, in which case K is imaginary. In these situations, instead of having to calculate the convolution sum

$$F(t_i) = \sum_{t'=0}^{t_i} R(t')I(t_i - t')\Delta t \tag{2.3}$$

every time for all relevant t_i, one notes that

$$f(t_i) \equiv \sum_{t'=0}^{t_i+\Delta t} R(t')e^{K(t_i+\Delta t-t')}\Delta t = e^{K\Delta t}\sum_{t'=0}^{t_i} R(t')e^{K(t_i-t')}\Delta t + R(t_i+\Delta t)\Delta t. \tag{2.3}$$

Thus,

$$f(t_i+\Delta t) = f(t_i)e^{K\Delta t} + R(t_i+\Delta t)\Delta t \tag{2.4}$$

and $F(t_i+\Delta t)$ can be expressed simply in terms of $F(t_i)$. The savings in computational time that this represents is a factor on the order of $N/2$, where N is the number of channels comprising a given decay. Since N is typically greater than 500, this is a significant savings.

Besides fits to measured decays, much of the data analysis in this thesis relies on Fourier transform techniques to extract information from decays. A discussion of this appears in Chapter 4, section II-B. The FORTRAN computer program used in this regard is contained in Appendix IV.

III. EXPERIMENTAL APPARATUS

A. Overview

Excitation source

The experiments described in this thesis were performed using a Spectra-Physics synchronously pumped, cavity dumped dye laser (rhodamine 6G perchlorate—2×10^{-3} M in ethylene glycol, or DCM—5×10^{-3} M in 60/40 volume percent ethylene glycol/ benzyl alcohol as dye). The laser produces $\sim$ 15 psec pulses with frequency bandwidths in the red varying from about 1 cm^{-1} to 3 cm^{-1} depending on the tuning element used (the 1 cm^{-1} value corresponds to the use of a three-plate birefringent filter with ultra-fine tuning etalon, the 3 cm^{-1} value to using just the three-plate filter). The laser pulse train repetition rate is variable from 4 MHz down to 0.4 KHz, although for the work reported herein, it was operated almost exclusively at 4 MHz. At this repetition rate, the average power is $\sim$ 50 mW or about 0.12 erg per pulse.

To obtain excitation light in the ultraviolet with this laser, it was necessary to frequency double the red output. This was done by focusing it into a 1 cm long $LiIO_3$ crystal. The conversion efficiency of red to UV with this set-up was found to be about ten percent.[2a] Frequency doubling has the effect of increasing the bandwidth of the light (and decreasing the temporal pulse width). In the UV, the bandwidth varied from $\sim$ 2 to 5 cm^{-1}, depending on the tuning element used in the laser.

After frequency doubling, the UV was directed through quartz windows into the vacuum chamber where, after focusing, it intersected the free-jet expansion at right angles to the expansion axis.

Free-jet apparatus and fluorescence collection

The detailed design of the free-jet apparatus has been dealt with elsewhere.[2] Briefly, the continuous free-jet expansion was formed by applying a high pressure of carrier gas (typically He, Ne, or N_2) to a heated pyrex nozzle containing the compound of interest. The high pressure gas expanded into an evacuated region ($< 10^{-3}$ Torr) through a $100-150$ μm orifice in the tip of the nozzle. The evacuated

region was maintained at low pressure by a ring-jet booster pump (Edwards 18B4A) backed by a mechanical pump (Kinney KT150). The nozzle apparatus has flexibility for alignment in three directions, which flexibility is extremely useful in the course of doing experiments. Fluorescence was collected and collimated by an $f = 1$ quartz lens through a quartz window parallel to and about 1.5 inches from the expansion axis. A second quartz lens with a focal length of 50 cm focused the collimated fluorescence onto the slit of 0.5 M Spex monochromator (dispersion 16 Å per mm) located about 50 cm away.

Photon counting equipment

The measurement of fluorescence decays was done by time-correlated single photon counting (see section II and Fig. 2 above). The fast photodiode used was a Hewlett-Packard 5082-4203 modified as in Ref. 14. Typically, +100 mV pulses ($\sim$ 1 nsec FWHM) are obtained from it. These pulses were amplified by a Hewlett-Packard 8447E inverting amplifier, directed through a delay line and into a constant fraction discriminator (either an Ortec 473A or, more recently, a Tennelec 455) which produces a uniform output timing pulse for every suitable input pulse. The output pulse served to trigger the *stop* channel of a time-to-amplitude converter (TAC, Ortec 457). The reverse configuration TSPC scheme was used because this enhances the overall detection efficiency. Fluorescence photons were detected (typically with about twenty percent quantum efficiency) by a Hamamatsu R1564U multichannel plate photomultiplier run at -3300 V. The output pulses from the detector (250 psec FWHM, 80 psec transit time jitter) were amplified in one or two stages with Comlin CDC100 noninverting video amplifiers. The pulses then went to a constant fraction discriminator (Ortec 473A, or Tennelec 455), the output of which triggered the start channel of the TAC. Finally, the output of the TAC was read by a multichannel analyzer (MCA, Tracor-Northern TN-1706) run in the pulse height analysis mode. A typical system response function was 80 psec FWHM. In general, such a narrow response can be obtained only by raising the lower limit voltage level of the discriminator in the photomultiplier channel to $>$ 50 mV for the

Tennelec 455. Thus, a narrow response function is obtained at the cost of losing some signal. The data stored by the MCA is ultimately read, stored, and analyzed by a DEC PDP 11/23 computer system.

The measurement of dispersed fluorescence spectra is similar to the measurement of fluorescence decays except that the MCA is used in multichannel scalar mode wherein it counts the number of pulses reaching it for a given interval of time, stores this number, and then steps on to the next channel and does the same thing, *etc.* The stepping of the MCA is controlled by the same microprocessor (Spex CD2) used to drive the monochromator grating. Thus the wavelength setting of the monochromator and the channel setting of the MCA step in synchrony. The pulses counted by the MCA can be from either the TAC or the discriminator in the photomultiplier channel. Using each has its own advantage (a lower baseline when the TAC is used, a greater overall signal when the discriminator output is used), but both methods yield essentially the same spectra.

B. Sensitivity of the method

As a final point of this chapter, it is pertinent to derive an expression for the signal level to be expected in a picosecond-jet experiment utilizing photon counting as the detection scheme. To do this, it is useful to start with several definitions:

$E_0 \equiv$ the energy per pulse of excitation light

$\nu_0 \equiv$ the frequency of the light

$\epsilon \equiv$ the molar extinction coefficient (in liter/(mole-cm)) of the molecular sample for light of frequency ν_0 (multipying ϵ by a constant factor of 1.7×10^{-20}, which is 1000 divided by Avogadro's number, gives the absorption cross-section in cm^2)

$b \equiv$ the path length of the light through the free-jet (in cm)

$C \equiv$ the concentration of the molecular species in the jet (in moles/liter)

$\Phi_f \equiv$ the quantum yield of fluorescence of the molecule excited with light at frequency ν_0.

Upon impinging upon the free-jet sample, a pulse of excitation light will excite

a total of n^* molecules. Assuming (1) the absence of stimulated emission, (2) that spontaneous emission is negligible during the pulse, and (3) that the number of excited molecules equals the number of photons absorbed by the sample, then using the Beer-Lambert law

$$n^* = \frac{E_0}{h\nu_0}(1 - e^{-\epsilon bC}), \tag{2.5}$$

which in the weak absorption limit becomes

$$n^* = \frac{E_0}{h\nu_0}(\epsilon bC), \tag{2.6}$$

where we have assumed that the frequency bandwidth of the laser is on the order of, or less than, the rotational bandwidth characterizing the jet-cooled sample. Of the n^* excited molecules, only $\Phi_f n^*$ will fluoresce. The total number of fluorescence photons is simply this number.

In most experimental set–ups there is a geometrical constraint to the collection of fluorescence photons. Let us assume that the fluorescing sample is located at the focal point of a lens with a focal length-to-aperture ratio of f, and that fluorescence is collected *via* this lens. Such an arrangement samples a fraction ($\equiv g_1$) of the total fluorescence

$$g_1 = \frac{1}{2}(1 - \frac{f}{(f^2+1)^{\frac{1}{2}}}). \tag{2.7}$$

Further fluorescence is lost for geometrical reasons if a monochromator is used in detection. Let us assume that a second lens focuses the fluorescence onto the slit of a monochromator (we also assume that the slit of the monochromator is parallel to the beam of the excitation light). The image of the sample fluorescence on the slit will have a width equal to wM, where w is the width of the excitation light beam at the free-jet, and M is the overall magnification of the detection optics. If the slit of the monochromator has a width s, then the fraction ($\equiv g_2$) of fluorescence which is focused onto the slit and actually enters the monochromator is

$$g_2 = \frac{s}{wM}. \tag{2.8}$$

The total number of fluorescence photons (n_m) getting into the monochromator is

$$n_m = g_1 g_2 \Phi_f n^*. \tag{2.9}$$

Now the use of a monochromator in detection also implies that only fluorescence photons of the proper wavelength will be detected. Thus, the photon counting signal will ultimately depend on the spectral characteristics of the fluorescence and the detection resolution used. Let us lump these together into one factor ($\equiv g_3$), representing the fraction of photons entering the monochromator *and* having the proper wavelength to make it to the detector. Finally, the detection quantum efficiency Φ_d of the photomultiplier must be taken into account.

The total number of electrical pulses (signal counts) produced by fluorescence photons can now be expressed as

$$n_t = g_1 g_2 g_3 \Phi_d \Phi_f n^* \tag{2.10}$$

or

$$n_t = \frac{s g_3 \Phi_d \Phi_f}{2wM}\left(1 - \frac{f}{(f^2+1)^{\frac{1}{2}}}\right)\frac{E_0}{h\nu_0}(\epsilon b C). \tag{2.11}$$

It is instructive to calculate a typical value of n_t for the experimental apparatus described in III-A. For this system and assuming UV excitation ($\nu_0/c = 30000$ cm^{-1}): $f = 1$, $w \simeq 1$ mm, $M \simeq 5$, $\Phi_d \simeq 0.2$, $E_0 \simeq 0.01$ erg, $h\nu_0 = 6 \times 10^{-12}$ erg, and $b \simeq 0.5$ cm. Thus,

$$n_t \simeq 5 \times 10^5 \epsilon s g_3 \Phi_f C, \tag{2.12}$$

with s in mm. C can be calculated by (1.2) of section I-A (averaging over θ), if one assumes a partial pressure (P_0) for the sample in the nozzle. Let us assume $P_0 = 1$ Torr. Then ρ_0 of (1.2), which is equivalent to the concentration of sample molecules in the nozzle, is

$$\rho_0 = \frac{1}{760(22.5)} = 5.7 \times 10^{-5} \quad \text{moles/liter}, \tag{2.13}$$

and by (1.2)

$$\rho = C \simeq \frac{5.7 \times 10^{-5}(0.16)}{2}\left(\frac{D}{x}\right)^2, \tag{2.14}$$

which for $\frac{z}{d} = 30$ gives

$$C \simeq 5.1 \times 10^{-9} \text{moles/liter} \quad (\text{or} \quad 3 \times 10^{12} \text{molecules/cm}^3). \tag{2.15}$$

Using (2.12),

$$n_t \simeq 2.5 \times 10^{-3} \epsilon s g_3 \Phi_f \tag{2.16}$$

with s in mm. This expression is relatively sample-independent, since C can be adjusted by changing the temperature of the nozzle. If now one assumes reasonable values for ϵ and Φ_f of 10^5 liter/mole and 0.1, respectively, and also assumes a moderate detection resolution of 1.6 Å so that $s = 0.1$ mm and $g_3 \sim 10^{-2}$, then

$$n_t = 2.5 \times 10^{-4} \quad \text{counts/laser pulse.} \tag{2.17}$$

Given that the laser pulse repetition rate is 4×10^6 Hz, the photon counting signal is 10^3 counts per second. Such a signal is more than enough to collect a decay in a reasonable amount of time (< 1 hr). For example, for a 1 KHz count rate, a one-hour collection time, and for collection over 1000 channels spanning the fluorescence lifetime, one obtains an average number of counts per channel of about 2000, and a corresponding signal to noise of about 45.

REFERENCES

1. (a) A. Zewail, Faraday Discussions Chem. Soc. **75**, 315 (1983); (b) P. M. Felker and A. H. Zewail, in *Applications of Picosecond Spectroscopy to Chemistry*, edited by K. B. Eisenthal (Reidel, Dortrecht, 1984), p. 273.

2. (a) W. R. Lambert, Ph. D. thesis, California Institute of Technology (1982); (b) W. R. Lambert, P. M. Felker, and A. H. Zewail, J. Chem. Phys. **81**, 2217 (1984).

3. A. Kantrowitz and J. Grey, Rev. Sci. Instrum. **22**, 328 (1951).

4. R. E. Smalley, L. Wharton, and D. H. Levy, Accts. Chem. Res. **10**, 139 (1977); and references therein.

5. D. H. Levy, L. Wharton, and R. E. Smalley in *Chemical and Biological Applications of Lasers, Vol. II*, edited C. B. Moore (Academic, San Francisco, 1977); and references therein.

6. J. B. Anderson and J. B. Fenn, Phys. Fluids **8**, 780 (1965).

7. D. M. Lubman, C. T. Rettner, and R. N. Zare, J. Phys. Chem. **86**, 1129 (1982).

8. J. P. Toennies and Klaus Winklemann, J. Chem. Phys. **66**, 3965 (1977).

9. For example, C. C. Lo, B. Leskover, P. R. Harteg, and K. Sauer, Rev. Sci. Instrum. **47**, 1113 (1976).

10. For a simple discussion of mode-locking by synchronous pumping see: C. K. Chan, Laser Technical Bulletin no. 8, Spectra-Physics Laser Products Division, Feb. 1978.

11. For example, C. Lewis, W. R. Ware, L. J. Doemeny, and T. L Nemzek, Rev. Sci. Instrum. **44**, 107 (1973).

12. P. R. Bevington, *Data Reduction and Error Analysis for the Physical Sciences* (McGraw-Hill, New York, 1969).

13. We use the terms convolution integral and convolution sum interchangably. Obviously, in treating real data, the convolution sum is that which is evaluated.

14. G. H. McCall, Rev. Sci. Instrum. **43**, 865 (1972).

FIGURE CAPTIONS

1. Schematic illustrating the collision of two hard spheres in their center of mass frame of reference. The axes are defined such that the centers of the two spheres are always in a plane parallel to the $z' = 0$ plane. a) shows the two spheres approaching each other with relative velocity $|\vec{v}_r|$ along the x' direction and with impact parameter b. b) shows the moment of impact and the angle $\theta \equiv \cos^{-1}(b/2a)$.

2. Schematic of the TSPC scheme for detection of fluorescence decays. The filled pulses denote light pulses and the empty pulses denote electrical ones. PD stands for photodiode, PMT for photomultiplier tube, S for sample, PSE for pulse shaping electronics (discriminator), TAC for time to amplitude converter, and MCA for multichannel analyzer.

Figure 1

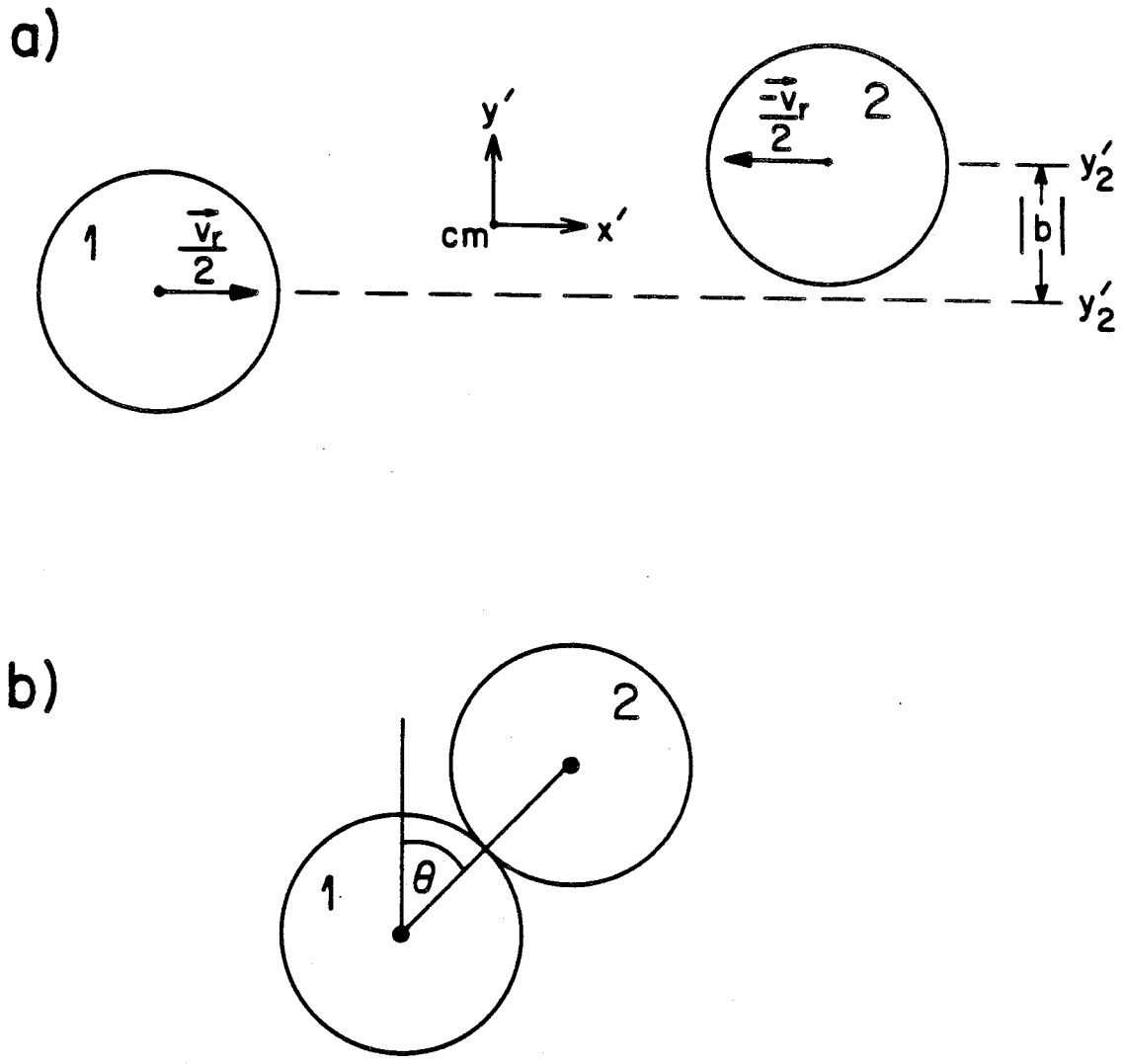

Figure 2

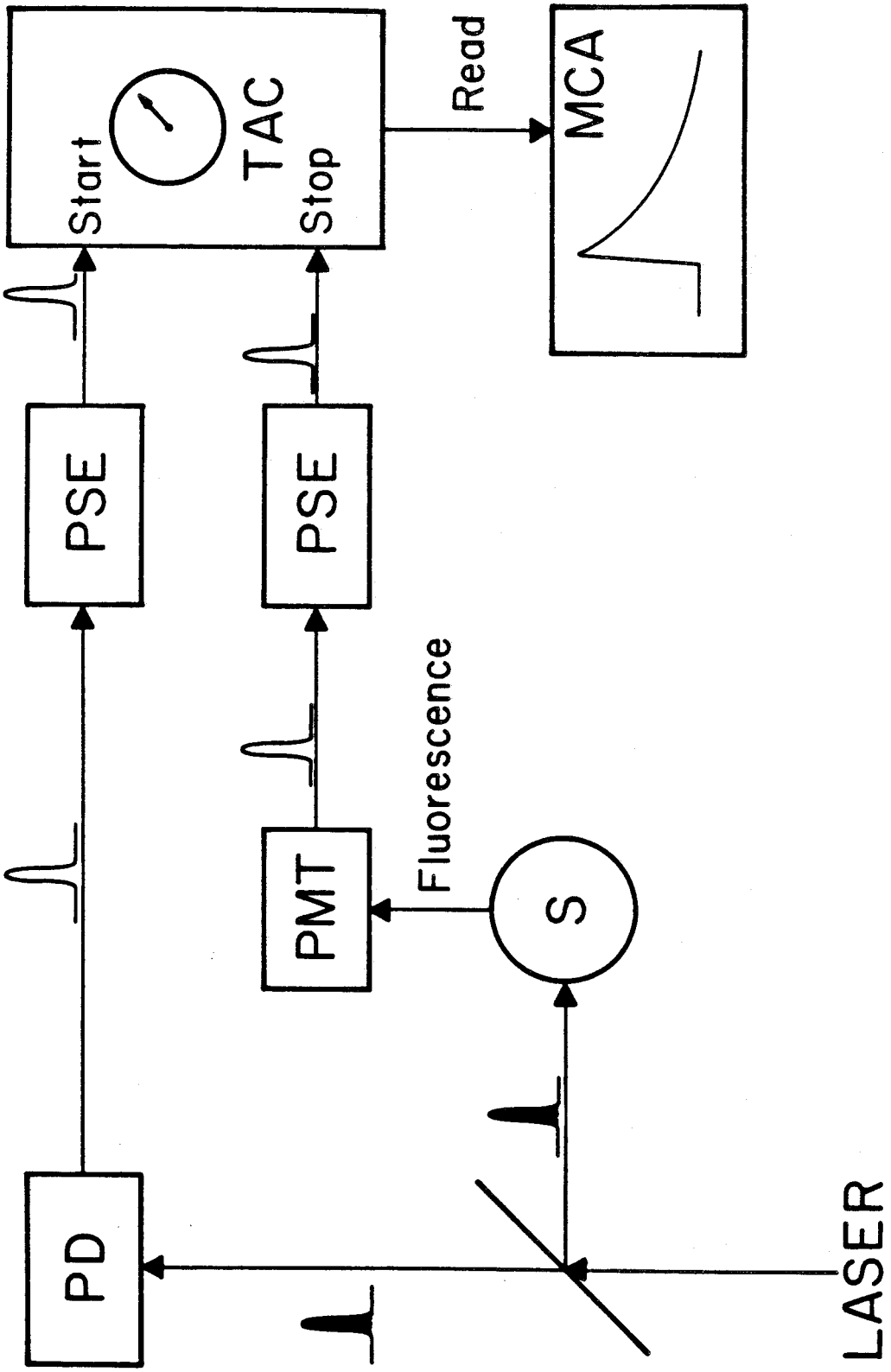

CHAPTER 3

COHERENCE EFFECTS AND IVR*

* Submitted to the Journal of Chemical Physics, as
"Dynamics of intramolecular vibrational-energy redistribution (IVR).
I Coherence Effects," by Peter M. Felker and Ahmed H. Zewail

I. INTRODUCTION

The fundamental process of intramolecular vibrational energy redistribution (IVR) in isolated molecules involves the transfer of energy from a prepared initial state to other isoenergetic states. This *collisionless* redistribution of energy is the result of intramolecular couplings (anharmonic and/or Coriolis interactions) between rovibrational states. Spectral manifestations of IVR have been discussed previously and will not be addressed extensively here[1]. That which is of concern in this work involves the temporal characteristics of dispersed fluorescence on the picosecond timescale[2]. Our interest in these characteristics derives from the fact that the temporal behavior of a given fluorescence band is a direct view of the evolution of vibrational energy in the excited state vibrational manifold; from time- and frequency-resolved fluorescence measurements one can obtain information relating to the timescale of IVR, the nature (restricted or dissipative) of the process, and the coupling matrix elements involved.[3–5]

Recently, we have presented experimental results[3–5] on anthracene which illustrate the use of the picosecond technique in revealing IVR dynamics. There are, however, several relevant points that have not been addressed in detail concerning the dynamics of IVR in general, and its manifestations in the fluorescence decays of large molecules in particular. Firstly, there has been no comprehensive consideration of the consequences of *multilevel* vibrational coupling in IVR. Such consideration is especially essential to the understanding of restricted IVR (*i.e.*, IVR amongst a few vibrational levels), as manifested in fluorescence decays as phase-shifted quantum beats.[3,4] Secondly, one would like to understand more about the changes in the nature of IVR as a function of vibrational energy in such multilevel systems. The parameters governing transitions from absent to restricted to dissipative IVR, as well as the sharpness of these transitions, are of interest. Thirdly, one might legitimately ask how it is possible to observe vibrational coherence effects (phase-shifted quantum beats) even though any given coupled vibrational level has associated with it a rotational level structure. With the large number of rovi-

brational states involved in the coupling between just two vibrational levels, one might think it likely that the superposition of the many different resulting beat frequencies would give rise to fluorescence decays with coherence effects completely smeared out. This is clearly not always the case. Thus, it remains to consider why this is so and what manifestations of the rotational level structure *are* present in a beat-modulated decay. Finally, it would be desirable to assess the generality of the concepts of IVR, which have been derived from the experimental observations made first on anthracene, to other molecules.

Elsewhere,[3,4] we have presented initial theoretical and experimental studies of IVR in what we have termed the restricted limit. In particular, the dynamics of vibrational coupling amongst two or three vibrational levels has been considered. For these cases the manifestations of IVR in the temporal behavior of spectrally resolved fluorescence is relatively easy to recognize and interpret. In view of the expectation that vibrational coupling in molecules may involve any number of levels (especially at high energies) and that many such physical situations are amenable to study by picosecond spectroscopy, it would be useful to have some theoretical guidelines of the dynamical manifestations which a general system of N coupled vibrational levels might exhibit. In this chapter we derive and present such guidelines, discuss some possible deviations from the predicted behavior, and, finally, discuss the physical significance of the results. The results presented herein will be used in accompanying publications to interpret experimental observations made in this laboratory on the molecules anthracene (Chapters 4 and 5)[6,7] and *trans*-stilbene (Chapter 6)[8] in the restricted and dissipative limits of IVR.

II. THEORY

A. General framework

We consider the case of N coupled vibrational levels in the S_1 manifold (Fig. 1). (Here we ignore the presence of the rotational level structure, the effects of which are discussed in Chapter 5.[7]) These zero-order states, which we take to be products of one-dimensional harmonic oscillator wavefunctions, are denoted as $|a\rangle$, $|b\rangle$, $|c\rangle$,... (In denoting a generic zero-order state, $|\gamma\rangle$ shall be used.) The molecular Hamiltonian matrix H, when expressed in this zero-order basis, is not diagonal because of coupling terms involving anharmonicity, *etc.* Diagonalization of H yields the molecular eigenstates $|1\rangle$, $|2\rangle$, $|3\rangle$,..., (with energies E_1, E_2, E_3,..., respectively), which are linear combinations of the zero-order states:

$$|I\rangle = \sum_{\gamma=a,b,\ldots} \alpha_{I\gamma}|\gamma\rangle, \qquad I = 1,\ldots,N; \tag{2.1}$$

where the $\alpha_{I\gamma}$ form a real,[9] orthonormal $N \times N$ matrix of the form :

$$\mathbf{C} = \begin{pmatrix} \alpha_{1a} & \alpha_{2a} & \cdots & \alpha_{Na} \\ \alpha_{1b} & \alpha_{2b} & \cdots & \alpha_{Nb} \\ \vdots & \vdots & \ddots & \vdots \end{pmatrix}. \tag{2.2}$$

Now consider that a molecule in vibrational state $|g\rangle$ of the S_0 manifold is excited by a linearly polarized δ-function laser pulse (polarization vector $\hat{\varepsilon}$) at the proper wavelength to create a coherent superposition of the molecular eigenstates $|I\rangle$, $I = 1,\ldots N$. Such a coherent superposition of states will fluoresce to the levels $\{|f\rangle\}$ in the S_0 manifold. The fluorescence intensity *vs.* time to one of these S_0 levels $|f_\gamma\rangle$ (assuming no analysis of fluorescence polarization) is given by[10]

$$I_\gamma(t) = K \sum_{I,J=1}^{N} \sum_{m=1}^{2} P_x(g,I)P_x(J,g)P_d^m(f_\gamma,J)P_d^m(I,f_\gamma)e^{-(i\omega_{IJ}+\Gamma)t}; \tag{2.3}$$

where K is a constant, $P_x(g,I) \equiv \langle g|\hat{\varepsilon}\cdot\vec{\mu}|I\rangle$ is the excitation transition matrix element connecting $|g\rangle$ and $|I\rangle$, $P_d^m(f_\gamma,I) \equiv \langle f_\gamma|\hat{\varepsilon}_m\cdot\vec{\mu}|I\rangle$ is a fluorescence transition matrix element connecting $|I\rangle$ and $|f_\gamma\rangle$, $\hat{\varepsilon}_1$ and $\hat{\varepsilon}_2$ are the two perpendicular fluorescence detection polarizations, $\omega_{IJ} \equiv (E_J - E_I)/\hbar$, and Γ is the decay rate of

the excited eigenstates (taken for simplicity to be equal for all I[11]). *We call such a fluorescence band a γ-type band.*

In general, because of Franck-Condon factors and symmetry restrictions, only a limited number of the entire manifold of S_1 vibrational levels will have absorption strength from $|g\rangle$, as evidenced by the sharp and uncongested absorption and fluorescence excitation spectra of large jet-cooled molecules.[12] Thus, it is reasonable to take only one of the coupled zero-order levels as having any appreciable absorption strength from $|g\rangle$. *We take this level to be* $|a\rangle$. This leads to the following expression for $P_x(g,I)$:

$$P_x(g,I) = \alpha_{Ia} P_x(g,a) \qquad \text{for } I = 1,\ldots,N. \tag{2.4}$$

Similarly, one expects the Franck-Condon overlap for emission to the S_0 level $|f_\gamma\rangle$ to be dominated by one zero-order level $|\gamma\rangle$. In other words,

$$P_d^m(f_\gamma,I) = \alpha_{I\gamma} P_d^m(f_\gamma,\gamma) \qquad \text{for } I = 1,\ldots,N. \tag{2.5}$$

Substituting these expressions into (2.3) yields the following for the intensity *vs.* time of a γ-type band:

$$I_\gamma(t) = K \sum_{I,J=1}^{N} \sum_{m=1}^{2} \alpha_{Ia}\alpha_{Ja}\alpha_{I\gamma}\alpha_{J\gamma}\{P_x(g,a)P_d^m(f_\gamma,\gamma)\}^2 e^{-(i\omega_{IJ}+\Gamma)t} \tag{2.6a}$$

$$I_\gamma(t) = K'[\sum_{I=1}^{N} \alpha_{Ia}^2\alpha_{I\gamma}^2 + 2\sum_{I>J}^{N} \alpha_{Ia}\alpha_{Ja}\alpha_{I\gamma}\alpha_{J\gamma}\cos\omega_{IJ}t]e^{-\Gamma t}, \tag{2.6b}$$

where K' is a constant. (Note that if the fluorescence *were* analyzed for polarization, *i.e.*, the sum over m were restricted in (2.6a), exactly the same time dependence as (2.6b) would obtain for $I_\gamma(t)$. Only K' would change.[13])

Now $|\gamma\rangle$ represents a generic zero-order state. Thus, one expects N different types of fluorescence bands in the fluorescence spectrum, each distinguished by the zero-order level which contributes to the emission transition moment. The time-integrated intensity of a given band type will scale with the quantity $\sum_{I=1}^{N} \alpha_{Ia}^2\alpha_{I\gamma}^2$. Moreover, from (2.6b) each of these bands will be modulated by the same $N(N-$

1)/2 cosine modulation terms (quantum beats), the frequencies of which will be determined by the energy differences between eigenstates, and the phases of which are determined by the particular band type *via* the coupling coefficients α. (One may further note that $\omega_{IJ} + \omega_{JK} = \omega_{IK}$. In general, $N(N-1)(N-2)/6$ such triplets of Fourier components are present for an N-level system when $N \geq 3$.) In what follows, we shall be interested in making generalizations concerning the amplitudes and the phases (*i.e.*, signs) of quantities of the form

$$M_\gamma(\omega_{IJ}) \equiv \frac{2\alpha_{Ia}\alpha_{Ja}\alpha_{I\gamma}\alpha_{J\gamma}}{\sum_{I=1}^{N}\alpha_{Ia}^2\alpha_{I\gamma}^2}, \tag{2.7}$$

which from (2.6b) represents the modulation depth (normalized Fourier amplitude), for a γ-type band, of the Fourier component at frequency ω_{IJ}.

B. Quantum beat modulation depths

There are several generalizations that can be made about the amplitudes of the modulation depths for a given band type. In making them it is necessary to distinguish between two types of fluorescence bands. The first type is the a-type band, which, using the conventions and nomenclature outlined above, represents a fluorescence band that derives its absorption and emission strength from the same zero-order state ($|a\rangle$). The second type of band is the non-a-type band, which by definition derives its absorption and emission strength from two different zero-order states ($|a\rangle$ and $|\gamma\rangle$, respectively).

For an a-type band (2.7) reduces to

$$M_a(\omega_{IJ}) = \frac{2\alpha_{Ia}^2\alpha_{Ja}^2}{\sum_{I=1}^{N}\alpha_{Ia}^4}. \tag{2.8}$$

Since the α's are real, then $0 \leq 2\alpha_{Ia}^2\alpha_{Ja}^2 \leq \alpha_{Ia}^4 + \alpha_{Ja}^4$. This places a restriction on the magnitude of each Fourier component contributing to an a-type band :

$$0 \leq M_a(\omega_{IJ}) \leq 1 \qquad \text{for all } \omega_{IJ}. \tag{2.9}$$

In addition to restrictions on individual components, it is also possible to place bounds on the sum of the modulation depths of an a-type band :

$$\sum_{I>J=1}^{N} M_a(\omega_{IJ}) = \frac{2\sum_{I>J=1}^{N}\alpha_{Ia}^2\alpha_{Ja}^2}{\sum_{I=1}^{N}\alpha_{Ia}^4}. \tag{2.10}$$

Such bounds derive from

$$(\sum_{I=1}^{N} \alpha_{Ia}^2)^2 = \sum_{I=1}^{N} \alpha_{Ia}^4 + 2 \sum_{I>J=1}^{N} \alpha_{Ia}^2 \alpha_{Ja}^2 = 1, \tag{2.11}$$

which yields

$$\sum_{I>J=1}^{N} M_a(\omega_{IJ}) = \frac{1}{\sum_{I=1}^{N} \alpha_{Ia}^4} - 1. \tag{2.12}$$

And, since $\sum_{I=1}^{N} \alpha_{Ia}^4$ is fixed by normalization such that $1/N \leq \sum_{I=1}^{N} \alpha_{Ia}^4 \leq 1$, then

$$0 \leq \sum_{I>J=1}^{N} M_a(\omega_{IJ}) \leq N - 1. \tag{2.13}$$

For non-a-type bands one must treat the general form for $M_\gamma(\omega_{IJ})$ given by (2.7). Similar to a-type bands, one can place bounds on the magnitudes of individual modulation depths by noting that $|2\alpha_{Ia}\alpha_{Ja}\alpha_{I\gamma}\alpha_{J\gamma}| \leq \alpha_{Ia}^2\alpha_{I\gamma}^2 + \alpha_{Ja}^2\alpha_{J\gamma}^2$ (this follows from $[\alpha_{Ia}\alpha_{I\gamma} \pm \alpha_{Ja}\alpha_{J\gamma}]^2 \geq 0$). Therefore, from (2.7)

$$0 \leq |M_\gamma(\omega_{IJ})| \leq 1 \qquad \text{for all } \omega_{IJ},\ \gamma \neq a. \tag{2.14}$$

Also, since

$$\sum_{I>J=1}^{N} M_\gamma(\omega_{IJ}) = \frac{2\sum_{I>J=1}^{N} \alpha_{Ia}\alpha_{Ja}\alpha_{I\gamma}\alpha_{J\gamma}}{\sum_{I=1}^{N} \alpha_{Ia}^2\alpha_{I\gamma}^2} \tag{2.15}$$

and

$$(\sum_{I=1}^{N} \alpha_{Ia}\alpha_{I\gamma})^2 = \sum_{I=1}^{N} \alpha_{Ia}^2\alpha_{I\gamma}^2 + 2 \sum_{I>J=1} \alpha_{Ia}\alpha_{Ja}\alpha_{I\gamma}\alpha_{J\gamma} = 0, \tag{2.16}$$

then

$$\sum_{I>J=1}^{N} M_\gamma(\omega_{IJ}) = -1, \qquad \text{if } \gamma \neq a. \tag{2.17}$$

That is, the sum of the modulation depths for any non-a-type band must equal -1.

C. Quantum beat phase distributions

Having considered some general restrictions on the magnitudes of the modulation depths of the Fourier components modulating the decay of a given band type, it is now useful to consider the phases of these components, or, equivalently, to

consider the signs of the modulation coefficients. In particular, we are interested in generalizations that can be made concerning the possible distributions of quantum beat phases that can occur in a given decay. To address this task succinctly it is convenient to start with several definitions. Firstly, we define $s_{I\gamma}$ to represent the sign of a given element of the orthonormal **C** matrix:

$$s_{I\gamma} \equiv \text{sign}(\alpha_{I\gamma}) = \pm 1. \tag{2.18}$$

Secondly, we define $\vec{\sigma}_\gamma$ to be an array of such quantities representing the signs of the γ^{th} row of **C** :

$$\vec{\sigma}_\gamma \equiv (s_{1\gamma}, s_{2\gamma}, \ldots, s_{N\gamma}) = \text{sign}(\alpha_{1\gamma}, \alpha_{2\gamma}, \ldots, \alpha_{N\gamma}). \tag{2.19}$$

In similar fashion we define $\vec{\sigma}^I$ to be a column array of signs of the I^{th} column of **C**. Fourthly, we define $s_\gamma(\omega_{IJ})$ to be the phase of the Fourier component at frequency ω_{IJ} which modulates a γ-type band:

$$s_\gamma(\omega_{IJ}) \equiv \text{sign}[M_\gamma(\omega_{IJ})] = \pm 1. \tag{2.20}$$

Finally, we define $\vec{\Delta}_\gamma$ to be the $1 \times [N(N-1)/2]$ dimensional array of quantum beat phases characterizing a γ-type band :

$$\vec{\Delta}_\gamma \equiv (s_\gamma(\omega_{12}), s_\gamma(\omega_{13}), \ldots, s_\gamma(\omega_{1N}), s_\gamma(\omega_{23}), \ldots, s_\gamma(\omega_{N-1,N})). \tag{2.21}$$

Next it is useful to make three observations concerning the arrays $\vec{\sigma}_\gamma$ and $\vec{\sigma}^I$. The first observation is that one is free to choose all the values for one and only one of the arrays $\vec{\sigma}_\gamma$. This freedom derives from the freedom to choose the phases of the eigenvectors composing the columns of **C**. It is convenient to use this to choose

$$\vec{\sigma}_a = (+1, +1, +1, \ldots, +1). \tag{2.22}$$

Secondly and thirdly, we note that

$$\vec{\sigma}_\gamma \neq \pm\vec{\sigma}_{\gamma'} \qquad \text{if } \gamma \neq \gamma', \tag{2.23}$$

and that

$$\vec{\sigma}^I \neq \pm\vec{\sigma}^J \qquad \text{if } I \neq J. \tag{2.24}$$

These conditions follow from the orthogonality of the rows and columns of **C**, respectively.

We are now ready to consider the possible values of $\vec{\Delta}_a$ for an N-level system. Clearly,

$$\vec{\Delta}_a = (+1, +1, +1, \ldots, +1), \tag{2.25}$$

for any system, since by (2.10)

$$s_a(\omega_{IJ}) = \text{sign}(\alpha_{Ia}^2 \alpha_{Ja}^2) = +1 \qquad \text{for all } I, J. \tag{2.26}$$

In other words, a-types bands are modulated only by positive cosine terms (*c.f.*, (2.9)).

For non-a-type bands

$$s_\gamma(\omega_{IJ}) = \text{sign}(\alpha_{Ia}\alpha_{Ja}\alpha_{I\gamma}\alpha_{J\gamma}) = \text{sign}(\alpha_{I\gamma}\alpha_{J\gamma}) = s_{I\gamma}s_{J\gamma} \tag{2.27}$$

by our choice of eigenvector phases. Thus, the distribution $\vec{\Delta}_\gamma$ is entirely determined by $\vec{\sigma}_\gamma$ for this choice of phases. One can now derive several conditions on the non-a-type phase distributions. Firstly, it is evident that all the values occurring in the quantum beat phase distribution array $\vec{\Delta}_\gamma$ are not independent. If the values $s_\gamma(\omega_{1J})$, $J = 2, 3, \ldots, N$ are known, then since

$$s_\gamma(\omega_{1I})s_\gamma(\omega_{1J}) = (s_{1\gamma})^2 s_{I\gamma}s_{J\gamma} = s_\gamma(\omega_{IJ}), \tag{2.28}$$

it is clear that all other values in the array can be found, too. Thus, there are $N-1$ independent phases for a given band of an N-level system, and one can specify a phase distribution just by specifying the $1 \times (N-1)$ dimensional array:

$$\vec{\delta}_\gamma \equiv (s_\gamma(\omega_{12}), s_\gamma(\omega_{13}), \ldots, s_\gamma(\omega_{1N})). \tag{2.29}$$

Instead of working with the larger arrays $\vec{\Delta}_\gamma$, we shall equivalently consider the $\vec{\delta}_\gamma$ arrays henceforth.

Secondly, it is evident from (2.27) that if $\vec{\sigma}_\gamma$ is nontrivially different from $\vec{\sigma}_{\gamma'}$ then $\vec{\delta}_\gamma$ is different from $\vec{\delta}_{\gamma'}$, and *vice versa*. That is,

$$\vec{\sigma}_\gamma \neq \pm\vec{\sigma}_{\gamma'} \longleftrightarrow \vec{\delta}_\gamma \neq \vec{\delta}_{\gamma'}. \tag{2.30}$$

Thirdly, this one-to-one correspondence between nontrivially different $\vec{\sigma}_\gamma$ and the resulting quantum beat phase distributions $\vec{\delta}_\gamma$, can be used along with (2.23) to show that for a given N-level system

$$\vec{\delta}_\gamma \neq \vec{\delta}_{\gamma'} \qquad \text{if } \gamma \neq \gamma'. \tag{2.31}$$

That is, each type of the N possible types of fluorescence bands that arise from an N-level system will have a unique quantum beat phase distribution.

Fourthly, one can use the correspondence between $\vec{\sigma}_\gamma$ and $\vec{\delta}_\gamma$ to calculate the total possible number of different phase distributions for an N-level system. This can be done by calculating the number of nontrivially different $\vec{\sigma}_\gamma$, which is

$$\frac{1}{2}(1 + N + \frac{N(N-1)}{2} + \frac{N(N-1)(N-2)}{6} + \cdots) = \frac{1}{2}(1+1)^N = 2^{N-1}. \tag{2.32}$$

Thus, there are 2^{N-1} possible values of $\vec{\delta}_\gamma$ for N coupled levels. (We enumerate these possibilities for $N \leq 5$ below.) Note that not all these possibilities are realized for a given N-level system ($N \geq 3$), since only N bands occur in any given spectrum. Note also that we have not considered the restriction of (2.24) on the $\vec{\sigma}^I$. It will be shown below that, although this does not restrict the possible values of $\vec{\delta}_\gamma$, it can restrict the possible combinations of $\vec{\delta}_\gamma$ that can occur together in any given spectrum.

Fifthly, if one notes that the total number of distinct ways of distributing two values over $N-1$ variables is simply 2^{N-1}, then it is clear that the 2^{N-1} allowed $\vec{\delta}_\gamma$ for an N level system represent *all the conceivable ways in which $+1$ and -1 can be distributed in these $1 \times (N-1)$ dimensional arrays.* As a consequence of this, it is very easy to write down all the possible $\vec{\delta}_\gamma$ for a given system.

Finally, one can derive a general restriction on the distribution of quantum beat phases over the triplet of beat frequencies ω_{IJ}, ω_{JK}, $\omega_{IK}(=\omega_{IJ}+\omega_{JK})$. We define $\vec{\delta}_\gamma^{IJK}$ to be such a distribution :

$$\vec{\delta}_\gamma^{IJK} \equiv (s_\gamma(\omega_{IJ}), s_\gamma(\omega_{JK}), s_\gamma(\omega_{IK})), \tag{2.33}$$

and recall the expression for the $s_\gamma(\omega)$ (2.27). Now either $s_{I\gamma} = s_{J\gamma} = s_{K\gamma}$, or one of these three signs is different from the other two. The first possibility gives $\delta_\gamma^{IJK} = (+1,+1,+1)$, while the second can result in one of the three distributions $(+1,-1,-1)$, $(-1,+1,-1)$, or $(-1,-1,+1)$. Thus, out of the eight conceivable distributions, only the one with all positive phases and the three with two negative-one positive phase are actually possible.

III. SPECIFIC RESULTS FOR $N \leq 5$

As an illustration of the general concepts derived above, and as a source of information on the coupling cases most amenable to study by quantum beat spectroscopy, we present in this section specific results for $N \leq 5$.

A. $N = 2$

This case has been treated previously in part[3,4]. We include the results here for the sake of completeness. According to the theory presented above, one expects two types of bands (a-type and b-type), and one beat frequency (ω_{12}) modulating both types of bands. The phase of the modulation of the a-type band will be $+1$ (*i.e.*, $s_a(\omega_{12}) = +1$), while that of the b-type band will be -1 (*i.e.*, $s_b(\omega_{12}) = -1$). Furthermore, while by (2.17) $M_b(\omega_{12}) = -1$ and is coupling independent, $M_a(\omega_{12})$ is dependent on the coupling between the zero-order states. In fact, it is a simple matter, given the following definition for the Hamiltonian matrix in the zero-order basis :

$$\mathbf{H}_0 \equiv \begin{pmatrix} E_a & V_{ab} \\ V_{ab} & E_b \end{pmatrix}, \tag{3.1}$$

to show that the a-type modulation depth is

$$M_a(\omega_{12}) = \frac{1}{2R^2+1}, \tag{3.2}$$

where $R \equiv |(E_a - E_b)/2V_{ab}|$. Because

$$\hbar\omega_{12} = 2|V_{ab}|(R^2+1)^{.5}, \tag{3.3}$$

then the measurement of ω_{12} and $M_a(\omega_{12})$ allows one to obtain the zero-order energy difference $|E_a - E_b|$ and the magnitude of the coupling matrix element $|V_{ab}|$.

B. $N = 3$

For $N = 3$ one expects three types of bands (a- ,b-, and c-type) in the dispersed fluorescence spectrum. Each will be modulated by the three beat frequencies ω_{12}, ω_{23}, and $\omega_{13}(= \omega_{12} + \omega_{23})$. One also expects four possible quantum beat phase distributions for these bands. Unlike the case of $N = 2$, all $M_\gamma(\omega_{IJ})$ values are coupling dependent (*i.e.*, $\alpha_{I\gamma}$ dependent) for $N = 3$ (and for $N > 3$). It is only the sum of modulation depths for any given non-a-type band which is coupling independent (*c.f.*, (2.17)). A summary of results for $N = 3$ appears in Table 1. (Note that in Tables 1, 2, and 3 we have labelled specific phase distributions. Note also that in Tables 1 and 2 we have included the dependent quantum beat phases as well as the independent part $\vec{\delta}_\gamma$.)

C. $N = 4$

A summary of information for $N = 4$, including possible beat phase distributions, is contained in Table 2. For this case and for $N > 4$ there are additional restrictions on the phase distributions, which do not appear for $N \leq 3$ and which were not addressed in the general treatment of section II-C. These restrictions derive from the condition that $\vec{\sigma}^I \neq \vec{\sigma}^J$, for $I \neq J$, and they limit the combinations of $\vec{\delta}_\gamma$ which can appear in a given spectrum. As an example, consider the phase distributions $\vec{\delta}^1_\gamma$, $\vec{\delta}^2_\gamma$, $\vec{\delta}^7_\gamma$, and $\vec{\delta}^8_\gamma$ from Table 2, and assume that they correspond to the a-, b-, c-, and d-type bands, respectively, in the spectrum of a 4-level system. Using these distributions and (2.17), one obtains

$$\text{sign}(\mathbf{C}) = \begin{pmatrix} 1 & 1 & 1 & 1 \\ 1 & 1 & -1 & -1 \\ 1 & -1 & 1 & 1 \\ -1 & 1 & 1 & 1 \end{pmatrix}, \tag{3.4}$$

where each row of the matrix is determined up to an overall sign. Now, although $\vec{\sigma}_\gamma \neq \vec{\sigma}_{\gamma'}$ in (3.4), $\vec{\sigma}^3 = \vec{\sigma}^4$, contrary to the restrictions on the $\vec{\sigma}^I$'s (2.24). Thus, the combination of $\vec{\delta}^1_\gamma$, $\vec{\delta}^2_\gamma$, $\vec{\delta}^7_\gamma$, and $\vec{\delta}^8_\gamma$, cannot correspond to bands in the same spectrum. Five other such forbidden combinations of phase distributions exist for $N = 4$. We shall not deal any further with the specifics of these forbidden combinations except to note, again, that they are present for all N greater than three.

D. $N = 5$

A summary of results for $N = 5$ is presented in Table 3.

IV. QUANTUM BEAT PARAMETERS AND THE DETERMINATION OF $\mathbf{H}_0$

Just as observed quantum beat parameters for $N = 2$ can be used to calculate parameters associated with the Hamiltonian matrix expressed in the zero-order basis (*i.e.*, $\mathbf{H}_0$), so too can this be done for $N \geq 3$. Unlike $N = 2$, however, expressions for the parameters of $\mathbf{H}_0$ cannot be conveniently presented for $N \geq 3$. Nevertheless, a general method can be outlined by which a calculation of $\mathbf{H}_0$ can be performed given measured beat frequencies and modulation depths. We present here such an outline for $N = 3$. Extension of the method to larger values of N is straightforward. The calculation of $\mathbf{H}_0$ using real data taken on anthracene will be presented in the following chapter.

The basis of the method of calculation is the relation

$$\mathbf{CEC}^t = \mathbf{H}_0, \tag{4.1}$$

which relates the eigenvalue matrix $\mathbf{E}$, the eigenvector matrix $\mathbf{C}$, and the transpose of the eigenvector matrix $\mathbf{C}^t$, to $\mathbf{H}_0$. Now the eigenvalue matrix is partially determined by the beat frequencies. If one labels the frequencies such that $|\omega_{12}| + |\omega_{23}| = |\omega_{13}|$, then the following possibilities exist for $\mathbf{E}$:

$$\mathbf{E} = E_0\mathbf{I} \pm \begin{pmatrix} 0 & 0 & 0 \\ 0 & |\omega_{12}| & 0 \\ 0 & 0 & |\omega_{13}| \end{pmatrix}, \tag{4.2}$$

where E_0 is an unknown constant and $\mathbf{I}$ is the unit matrix.

The matrix $\mathbf{C}$ can be determined from relative values of the $M_\gamma(\omega_{IJ})$'s and from the orthonormality of its rows and columns. Firstly, it is convenient to calculate the α_{Ia} via the relations

$$\alpha_{2a}^2 = \frac{M_a(\omega_{23})}{M_a(\omega_{13})}\alpha_{1a}^2 \tag{4.3a}$$

$$\alpha_{3a}^2 = \frac{M_a(\omega_{23})}{M_a(\omega_{12})}\alpha_{1a}^2 \tag{4.3b}$$

and the normalization relation $\sum_{I=1}^{3} \alpha_{Ia}^2 = 1$. The signs of the α_{Ia} can be arbitrarily chosen to be positive. Next, the values α_{Ib} can be calculated by the relations

$$\alpha_{2b} = \frac{M_b(\omega_{23})\alpha_{1a}}{M_b(\omega_{13})\alpha_{2a}}\alpha_{1b} \tag{4.4a}$$

$$\alpha_{3b} = \frac{M_b(\omega_{23})\alpha_{1a}}{M_b(\omega_{12})\alpha_{3a}}\alpha_{1b} \tag{4.4b}$$

and the normalization condition $\sum_{I=1}^{3} \alpha_{Ib}^2 = 1$. Note that the *relative* signs of the α_{Ib} are fixed by the beat phases of the b-type band (*e.g.*, if $\vec{\delta}_b = (-1, +1)$, then $\vec{\sigma}_b = \pm(+1, -1, +1)$). Thus, the second row of $\mathbf{C}$ is determined up to an overall sign. Finally, the values α_{Ic} can be calculated up to an overall sign by using several relations, including the normality of the columns of $\mathbf{C}$ and the orthogonality of its rows.

One may note that the values of the elements of $\mathbf{C}$ are overspecified if one has experimental knowledge of all the quantum beat modulation depths for all three types of bands. The extra parameters can be used as self-consistency checks on the calculated $\mathbf{C}$. For instance, absolute modulation depths were not used at all in the calculation outlined above, nor were the modulations depths and phases of the c-type band. These experimental values should, however, be reproduced if one calculates them starting with the derived $\mathbf{C}$. Similarly, a number of orthogonality and normality relations (*e.g.*, $\sum_{I=1}^{3} \alpha_{Ia}\alpha_{Ib} = 0$) need not figure in the calculation of $\mathbf{C}$. These relations should, nevertheless, obtain if the calculated matrix accurately represents the physical situation.

Now, its being clear that one can determine $\mathbf{C}$ and $\mathbf{E}$ up to various additive and multiplicative constants, what can be determined for $\mathbf{H}_0$? Firstly, by (4.1), (4.2), and the orthonormality of $\mathbf{C}$

$$\mathbf{H}_0 = E_0\mathbf{I} \pm \mathbf{C}\begin{pmatrix} 0 & 0 & 0 \\ 0 & |\omega_{12}| & 0 \\ 0 & 0 & |\omega_{13}| \end{pmatrix}\mathbf{C}^t. \tag{4.5}$$

Next, the effect of the ambiguities in the overall signs of the rows of $\mathbf{C}$ must be

considered. Since $h_{\gamma\gamma'}$, a general matrix element of the second term on the right-hand side of (4.5) is

$$h_{\gamma\gamma'} = h_{\gamma'\gamma} = \alpha_{2\gamma}\alpha_{2\gamma'}|\omega_{12}| + \alpha_{3\gamma}\alpha_{3\gamma'}|\omega_{13}|, \tag{4.6}$$

it is clear that changing the overall signs of the γ^{th} row of $\mathbf{C}$ will leave the diagonal element $h_{\gamma\gamma}$ unchanged, but will change the signs of those off-diagonal elements involving γ. From this fact and (4.5), it is evident that by using quantum beat parameters, one can obtain

$$\mathbf{H}_0 = E_0\mathbf{I} \pm \begin{pmatrix} E_a & V_{ab} & V_{ac} \\ V_{ab} & E_b & V_{bc} \\ V_{ac} & V_{bc} & E_c \end{pmatrix}, \tag{4.7}$$

where E_0 and the signs of the $V_{\gamma\gamma'}$ are unknown, but everything else is known.

V. EXPERIMENTAL RESULTS VS. THEORETICAL PREDICTIONS

To handle real data it is useful to have some idea of the way in which the theoretical results, which have been derived using a set of ideal assumptions, can be modified by less than ideal conditions. In this section we discuss effects which the experimental excitation bandwidth, the temporal response of detection, the spectral resolution of detection, the excitation of more than one optically active level, and the presence of sequence congestion can have on experimental observations. Since in many cases these deviations can lead to errors in interpretation, especially in the interpretation of the number of levels involved in the coupling, we suggest ways to avoid such errors. No attempt will be made to be exhaustive in the enumeration of all the causes of possible deviations. Instead, several cases will be presented in the expectation that they represent a significant fraction of those cases likely to be encountered in practice, and in the hope that they will illustrate methods of analysis by which other cases may be treated. Reference to a number of the cases presented here is made in the following chapters in discussing real experimental results.

A. Case 1: Narrow excitation bandwidth and state preparation

In this case we assume that the bandwidth of the experimental source is not large enough to coherently excite all the N eigenstates which arise from the coupling of the N zero-order levels (Fig. 3). This situation is likely to occur in real molecules, since anharmonic coupling matrix elements may be expected to be as high as several wavenumbers and therefore to give rise to significantly coupled states with splittings on this order.

For simplicity, let us say that one state, $|N\rangle$, lies outside the laser bandwidth. In such a case, N band types are still possible, but the temporal behavior of a γ-type band will be given by

$$I_\gamma(t) \sim \sum_{I,J=1}^{N-1} \alpha_{Ia}\alpha_{Ja}\alpha_{I\gamma}\alpha_{J\gamma}e^{-(i\omega_{IJ}+\Gamma)t} \tag{5.1}$$

instead of by (2.6). Thus, although the system involves N coupled zero-order levels, each band will be modulated by the number of beat frequencies expected for an

$(N-1)$-level system. (In the general case wherein n eigenstates lie outside the laser bandwidth, the number of band types will still be N, but the number of beat frequencies will correspond to that expected for an $N-n$ level system.) Fortunately, another deviation from theoretical predictions can be used to give one an idea of the actual number of coupled zero-order levels. If one calculates the total modulation depth of a γ-type band (non-a-type) from (5.1), one obtains

$$\sum_{I>J=1}^{N-1} M_\gamma(\omega_{IJ}) = \frac{2\sum_{I>J=1}^{N-1} \alpha_{Ia}\alpha_{Ja}\alpha_{I\gamma}\alpha_{J\gamma}}{\sum_{I=1}^{N-1} \alpha_{Ia}^2\alpha_{I\gamma}^2}. \tag{5.2}$$

Given that $\sum_{I=1}^{N-1} \alpha_{Ia}\alpha_{I\gamma} \neq 0$, then clearly,

$$(\sum_{I=1}^{N-1} \alpha_{Ia}\alpha_{I\gamma})^2 = \sum_{I=1}^{N-1} \alpha_{Ia}^2\alpha_{I\gamma}^2 + 2\sum_{I>J=1}^{N-1} \alpha_{Ia}\alpha_{Ja}\alpha_{I\gamma}\alpha_{J\gamma} > 0, \tag{5.3}$$

and, therefore,

$$\sum_{I>J=1}^{N-1} M_\gamma(\omega_{IJ}) = \frac{2\sum_{I>J=1}^{N-1} \alpha_{Ia}\alpha_{Ja}\alpha_{I\gamma}\alpha_{J\gamma}}{\sum_{I=1}^{N-1} \alpha_{Ia}^2\alpha_{I\gamma}^2} > -1. \tag{5.4}$$

(Note that the relation $\sum_{I>J=1}^{N_0} M_\gamma(\omega_{IJ}) > -1$, for $N_0 < N$, holds in general.) Equation (5.4) contrasts with the rule given by (2.17). Thus, the measured total modulation depth of a non-a-type band provides a measure by which one can decide if the number of levels indicated by the number of beat frequencies is, in fact, the total number of coupled levels. (This, of course, assumes the ability to accurately measure modulation depths.) This same information would also be obtained if the beat phase distributions indicated that more than $N-1$ types of bands occurred in the spectrum.

In terms of the physics of IVR, case 1 corresponds to the incomplete preparation of the $|a\rangle$ state at $t = 0$. In other words, the initially prepared state is not purely $|a\rangle$ as it would be if the bandwidth of the laser spanned all the eigenstates arising from the coupled system of zero-order states (see section VI-A), but it contains contributions from the other zero-order states, as well. The deviations resulting

from the case 1-type situation are therefore fundamental in nature and underscore the fact that the IVR process is intimately dependent on the preparation of the initial state.

B. Case 2: Finite temporal resolution

In this case we assume that the temporal resolution of the detection system is not sufficient to resolve some of the beat frequencies present in the decays. Obviously, under all circumstances the inability to resolve some beat components reduces the number of observed beat frequencies from the $N(N-1)/2$ expected for N coupled levels. In many cases this will not lead to an incorrect assignment of the number of coupled levels involved. For instance, if for a four-level system only five beat frequencies were resolvable, then despite the missing component, one would not be led to assign the behavior to a three-level system, since in that case there would be only three beat components. Similarly, if one observed three beat components at say 5, 7, and 8 GHz, it would be immediately apparent that the number of coupled levels involved would have to exceed three, since $5+7 \neq 8$ GHz. On the other hand, errors in interpretation *can* be made if the only beat frequencies that are unresolvable are all those involving one of the eigenstates. For example, say all ω_{IN}, for $I = 1, \ldots, N-1$, are too large. In such a case each band will be apparently modulated as if it arose from an $(N-1)$-level system :

$$I_\gamma(t) \sim [\sum_{I=1}^{N} \alpha_{Ia}^2 \alpha_{I\gamma}^2 + 2 \sum_{I>J=1}^{N-1} \alpha_{Ia}\alpha_{Ja}\alpha_{I\gamma}\alpha_{J\gamma} \cos\omega_{IJ}t]e^{-\Gamma t}. \qquad (5.5)$$

Nevertheless, here as with case 1, errors in interpretation can, in principle, be avoided by consideration of the total modulation depths of non-a-type bands

$$\sum_{I>J=1}^{N-1} M_\gamma(\omega_{IJ}) = \frac{2\sum_{I>J=1}^{N-1} \alpha_{Ia}\alpha_{Ja}\alpha_{I\gamma}\alpha_{J\gamma}}{\sum_{I=1}^{N} \alpha_{Ia}^2\alpha_{I\gamma}^2}. \qquad (5.6)$$

Since (5.6) is the same as (5.2) except for one extra positive term in the denominator, then the sum of modulation depths in (5.6) is ≥ -1. Thus, this experimentally measurable quantity can again be used to ascertain whether the apparent number of coupled levels is, in fact, the actual number of coupled levels.

C. Case 3: Finite spectral resolution

Similarly to effects found due to finite temporal resolution, one might expect spectral detection resolution problems to be an especially prevalent source of experimental deviations from the theoretical predictions of sections II and III. Even single, nonvibrationally coupled S_1 vibrational levels of large molecules (for instance, the S_1 vibrationless level) have rich spectra with many bands. Since an N-level system is a superposition of such spectra, there is bound to be some spectral overlap of bands, even for N as small as three. This overlap can result in a number of apparent deviations from theoretical predictions. For example, if an a-type band overlaps with a non-a-type band, then the measured decay may appear to be non-a-type because of Fourier components with -1 phases, yet the total modulation depth of the decay will be found to be ≥ -1. Or, if two different non-a-type bands overlap, then it is possible that the measured decay may exhibit forbidden phase behavior; *e.g.*, a quantum beat triplet may appear to have a phase distribution

$$\vec{\delta}_\gamma^{IJK} = (+1, +1, -1).$$

Clearly, spectral overlap can also be an especially serious hindrance if one wishes to obtain accurate modulation depths for a calculation of $\mathbf{H}_0$. This must be kept in mind in choosing the experimental results to be used in making such a calculation.

D. Case 4: More than one optically active level, uncoupled

As a fourth case, consider the situation wherein the eigenstates formed by the coupling of the M zero-order states $|a\rangle, |b\rangle, \ldots$ ***and*** the eigenstates formed by the coupling of the $N - M$ zero-order states $|a'\rangle, |b'\rangle, \ldots$ are all spanned by the finite bandwidth of the laser pulse. Assume that the unprimed zero-order states are only coupled to other unprimed states and give rise to the eigenstates $|I\rangle$, $I = 1, \ldots, M$, while the primed states are only coupled to primed states and in so doing give rise to the eigenstates $|I\rangle$, $I = M + 1, \ldots, N$; (see Fig. 4). In such a situation $\mathbf{C}$ is block-diagonalized into two blocks such that all the elements $\alpha_{I\gamma}$ are zero if 1) γ is unprimed and $I = M + 1, \ldots, N$; or 2) γ is primed and $I = 1, \ldots, M$. Now,

further assume that only one zero-order state in each set (say $|a\rangle$ and $|a'\rangle$) has any absorption strength from the populated S_0 level. Using (2.3) one can obtain the following for the temporal behavior of the fluorescence band associated with the transition to the S_0 level $|f_\gamma\rangle$:

$$I_\gamma(t) = I_\gamma^1 + I_\gamma^2 + I_\gamma^3, \tag{5.7a}$$

where

$$I_\gamma^1 \sim \sum_{I,J=1}^{M} \sum_{m=1}^{2} \alpha_{Ia}\alpha_{Ja} P_d^m(f_\gamma, J) P_d^m(f_\gamma, I) e^{-(i\omega_{IJ}+\Gamma)t}, \tag{5.7b}$$

$$I_\gamma^2 \sim \sum_{I,J=M+1}^{N} \sum_{m=1}^{2} \alpha_{Ia'}\alpha_{Ja'} P_d^m(f_\gamma, J) P_d^m(f_\gamma, I) e^{-(i\omega_{IJ}+\Gamma)t}, \tag{5.7c}$$

and

$$I_\gamma^3 \sim 2\sum_{I=1}^{M} \sum_{J=M+1}^{N} \sum_{m=1}^{2} \alpha_{Ia}\alpha_{Ja'} P_d^m(f_\gamma, J) P_d^m(f_\gamma, I) \cos(\omega_{IJ}t) e^{-\Gamma t}. \tag{5.7d}$$

As before, we assume that the transition to $|f_\gamma\rangle$ gains its emission strength from only one of the zero-order levels. Unlike before, however, one sees from (5.7) that not all N band types are modulated by all the same beat frequencies. In fact, three different classes of band types can be distinguished based on the frequencies which modulate the bands. Firstly, if the band gains its emission strength from one of the unprimed zero-order states, then $S_\gamma^2 = S_\gamma^3 = 0$ and S_γ^1 reduces to what one would expect for a band of an M-level system. One expects as many as M types of bands exhibiting such behavior. Similarly, if the band gains its emission strength from one of the primed zero-order states, then $S_\gamma^1 = S_\gamma^3 = 0$ and S_γ^2 reduces to what one would expect for a band arising from an $(N-M)$-level system. As many as $N-M$ bands of this type may occur. Finally, there will be at least one band (*i.e.*, the resonance fluorescence band) which gains its emission strength from $|a\rangle$ and $|a'\rangle$. $I_\gamma(t)$ for such a band will have contributions from S_γ^1, S_γ^2, and S_γ^3. Thus, all $N(N-1)/2$ beat frequencies of the N-level system may modulate the band.

Moreover, all these Fourier components will have +1 phases since α_{Ia} and/or $\alpha_{Ia'}$ only enter as squared terms in S_γ^1, S_γ^2, and S_γ^3.

The situation corresponding to case 4 is not particularly unlikely to occur. For example, one can easily imagine two sets of states at the same energy having different symmetry transformation properties. While inter-set anharmonic coupling in such a case would be symmetry forbidden, absorption could still occur to states in both of the sets (*e.g.*, in anthracene, S_1 vibrational levels of both a_g and b_{1g} symmetry have been observed to be optically active[12]).

E. Case 5: More than optically active level, coupled

Here, we consider a situation which gives rise to deviations from theory, not because of any experimental limitations, but because the physical situation does not correspond to the basic assumptions of the theory. In particular, we consider the case wherein there are no restrictions on the absorption transition matrix elements $P_x(g,I)$ or on the emission transition matrix elements $P_d^m(f_\gamma,I)$ in (2.3); that is, (2.4) and (2.5) do not hold. Since this general case is difficult to treat for any but the simplest systems, we only present results for $N = 2$.

As in section II-A, it is useful here to express the transition matrix elements in terms of the zero-order states $|a\rangle$ and $|b\rangle$. We also neglect the effects of detection polarization. Thus,

$$P_x(g,I) = \alpha_{Ia}P_x(g,a) + \alpha_{Ib}P_x(g,b), \tag{5.8}$$

and

$$P_d(f_\gamma,I) = \alpha_{Ia}P_d(f_\gamma,a) + \alpha_{Ib}P_d(f_\gamma,b). \tag{5.9}$$

For the sake of clarity we define $X_\gamma \equiv P_x(g,\gamma)$ and $D_\gamma \equiv P_d(f_\gamma,\gamma)$. Using the facts[15] that $\alpha_{1a} = -\alpha_{2b} = \alpha$ and $\alpha_{2a} = \alpha_{1b} = \beta$ along with (2.3) to find the decay of the fluorescence band with final state $|f\rangle$, one obtains the following for the modulation depth of the beat component ω_{12}:

$$M(\omega_{12}) = \frac{2(\alpha X_a + \beta X_b)(\beta X_a - \alpha X_b)(\alpha D_a + \beta D_b)(\beta D_a - \alpha D_b)}{(\alpha X_a + \beta X_b)^2(\alpha D_a + \beta D_b)^2 + (\beta X_a - \alpha X_b)^2(\beta D_a - \alpha D_b)^2}. \tag{5.10}$$

It is apparent from (5.10) that the general case differs from that of section II in that modulation depths do not depend solely on the coupling coefficients but are dependent on zero-order transition matrix elements, as well. Even in a two-level system, one might therefore expect many different fluorescence bands, each with different $M(\omega_{12})$ depending on the particular values of D_a and D_b for the band. In addition, the possibility exists, despite strong coupling between $|a\rangle$ and $|b\rangle$, that no modulations will appear in any decays if X_a and X_b, or D_a and D_b take on certain values.

It is instructive to consider two limiting cases of (5.10). In particular, one wonders what happens if either D_a or D_b is equal to zero, but both the X_γ have nonzero values. This corresponds to the case of two ***coupled*** optically active levels which have different fluorescence spectra. If one detects the band for which D_b equals zero, one has what is analogous to an a-type band, the modulation depth of which is

$$M_a(\omega_{12}) = \frac{2(\alpha X_a + \beta X_b)(\beta X_a - \alpha X_b)\alpha\beta}{(\alpha X_a + \beta X_b)^2\alpha^2 + (\beta X_a - \alpha X_b)^2\beta^2}. \tag{5.11}$$

With D_a equal to zero one obtains

$$M_b(\omega_{12}) = \frac{-2(\alpha X_a + \beta X_b)(\beta X_a - \alpha X_b)\alpha\beta}{(\alpha X_a + \beta X_b)^2\beta^2 + (\beta X_a - \alpha X_b)^2\alpha^2}. \tag{5.12}$$

Comparing (5.11) and (5.12), one can see that the decays of the two types of bands have opposite quantum beat phases ($+1$ *vs.* -1) just as in the two-level case of section III-A. Now, however, that decay which has the -1 phase cannot be ascertained without specific knowledge of the coupling coefficients ***and*** the X_γ. The same holds true for the magnitudes of $M_a(\omega_{12})$ and $M_b(\omega_{12})$. In general, one expects the modulation depths to decrease with both weaker coupling and with $|X_a|$ more nearly equal to $|X_b|$. One also expects no decay for which the modulation depth equals -1 (in contrast to (2.17)).

It is implicit to the relevance of this chapter that in many real situations the approximations of (2.4) and (2.5) be good ones and that case 5 be an overcomplication. As we have argued, theoretical considerations and experimental results

support this. Given cases for which (2.4) and (2.5) are not valid, one sees from (5.10)-(5.12) that even for $N = 2$ significant deviations from the results of sections II and III can occur.

F. Case 6: Thermal congestion

A primary assumption made in the treatment of section III involves the presence of only one initially populated S_0 state ($|g\rangle$). However, even in jet-cooled samples there exists a distribution of initial states due to incomplete cooling of both rotational and vibrational degrees of freedom. This distribution of initial states can in turn give rise to a distribution of excited states upon laser excitation. The effects that a distribution of excited state rotational levels has on beat-modulated decays are dealt with in Chapter 5.[7] The influence of the vibrational distribution, although not as pervasive as that of the rotational distribution, nevertheless can be substantial. For instance, consider a vibrational distribution characterized by some molecules in the S_0 level $|g_1\rangle$ and all others in the level $|g_2\rangle$. Excitation will project the two types of molecules up into entirely different regions of the excited state level structure given that $|g_1\rangle$ and $|g_2\rangle$ are well separated in energy relative to the bandwidth of the laser pulse. Spectrally, the effect this has is to introduce more congestion in the observed fluorescence spectrum than would otherwise be present if all molecules were initially in $|g_1\rangle$ or $|g_2\rangle$. Temporally, if excitation from $|g_1\rangle$ coherently prepares an N_1-level system and excitation from $|g_2\rangle$ prepares an N_2-level system, then there will be bands in the observed fluorescence spectrum reflecting coupling amongst N_1 levels, and different bands reflecting coupling amongst N_2 levels. The point is that two different and independent dynamical processes arising from two incoherently related excitations are manifested in the observed spectrum and fluorescence decays. Thus, in cases where observations indicate deviations from theoretical predictions regarding the number of beat components and the number of beat triplets, it is possible that the reason for this is vibrational thermal congestion. In the extreme situations where many S_0 vibrational states are initially populated, thermal congestion can completely mask any coherence effects that may be present.

Of course, this is at the heart of the rationale to use jet-cooled molecular samples in the study of large molecule vibrational dynamics. Experimental results pertaining to the effects of thermal congestion are presented in Chapter 5.[7]

VI. PHASE-SHIFTED QUANTUM BEATS AND IVR

A. Direct view of IVR

Being that phase-shifted quantum beats occur as one of the dynamical manifestations of S_1 vibrational coupling in molecules and that the specific characteristics of observed beats can be used to obtain specific vibrational coupling information about a molecule, then the study of phase-shifted vibrational beats amounts to the study of IVR. However, the connection between beats and IVR is even closer than this might lead one to believe. Far from being simple dynamical manifestations of vibrational coupling, beat-modulated fluorescence decays are direct pictures of the distribution in time of vibrational energy in a molecule. This point may be seen by considering the contribution ($\wp_\gamma(t)$) of the zero-order state $|\gamma\rangle$ to the excited state $|\Psi(t)\rangle$ created by the laser pulse:

$$\wp_\gamma(t) = |\langle\gamma|\Psi(t)\rangle|^2. \tag{6.1}$$

Using the assumptions of δ-function excitation and the exclusive absorption strength of $|a\rangle$ one obtains for the normalized excited state

$$|\Psi(t)\rangle = \sum_{I=1}^{N} \alpha_{Ia}|I\rangle e^{-(i\omega_I+\Gamma/2)t} = \sum_{I=1}^{N} \sum_{\gamma=a,b,\ldots} \alpha_{Ia}\alpha_{I\gamma}|\gamma\rangle e^{-(i\omega_I+\Gamma/2)t}. \tag{6.2}$$

And using (6.2),

$$\wp_\gamma(t) = |\sum_{I=1}^{N} \alpha_{Ia}\alpha_{I\gamma}e^{-(i\omega_I+\Gamma/2)t}|^2 = \sum_{I,J=1}^{N} \alpha_{Ia}\alpha_{Ja}\alpha_{I\gamma}\alpha_{J\gamma}e^{-(i\omega_{IJ}+\Gamma)t}. \tag{6.3}$$

(Actually, the requirement of a δ-function excitation pulse is somewhat restrictive. A more realistic condition is that the inverse correlation time of the excitation source—the coherence width—be much greater than the maximum value of ω_{IJ}. This same condition, which ensures that all of the relevant eigenstates are excited and locked in phase at $t = 0$, also applies to (2.6). Comprehensive discussions on the question of initial state preparation can be found in Refs. 10 and 16.)

By comparison of (6.3) with (2.6), it is evident that

$$\wp_\gamma(t) \sim I_\gamma(t). \tag{6.4}$$

The temporal behavior of a γ-type band is exactly the same as the temporal behavior of the $|\gamma\rangle$ content of the excited state. In another manner of speaking, a γ-type decay provides a direct picture of the oscillatory flow of energy into and out of the vibrational motion described by $|\gamma\rangle$. Thus, the two fundamental aspects of the IVR process can be addressed by time- and frequency-resolved fluorescence. The ***extent*** of IVR (the number of coupled vibrational levels) is given by the number of beat frequencies which modulate the decays of the bands in a spectrum, and the ***timescale*** for energy redistribution is given by the inverses of the beat frequencies.

There are other ways in which the correspondence between $I_\gamma(t)$ and $\wp_\gamma(t)$ can be useful in the study of IVR processes. For example, (6.4) allows one to carry all the theoretical results on the modulation phases and modulation depths of fluorescence decays (sections II and III) over to the behavior of $\wp_\gamma(t)$. Conversely, if one first considers the behavior of $\wp_\gamma(t)$, which has a ready interpretation in terms of IVR, then it is possible to come to a fuller appreciation of the physical significance of some of the results derived for $I_\gamma(t)$. One example of this point is (2.17), which holds that the total modulation depth of a non-a-type decay is -1. What does this mean physically ? To answer this note from (6.3) that for $\gamma \neq a$,

$$\wp_\gamma(0) = \sum_{I,J=1}^{N} \alpha_{Ia}\alpha_{Ja}\alpha_{I\gamma}\alpha_{J\gamma} = \sum_{I=1}^{N}\Big(\sum_{J=1}^{N} \alpha_{Ja}\alpha_{J\gamma}\Big)\alpha_{Ia}\alpha_{I\gamma} = 0 \tag{6.5}$$

by orthogonality. That is, $|\gamma\rangle$ does not contribute to the initially prepared excited state. Now by (6.4) this implies that $I_\gamma(0) = 0$, which in turn, by (2.6) and (2.7) implies that the total modulation depth of the γ-type band must be -1. Thus, the modulation depth sum rule (2.17) for non-a-type bands is a reflection of the vibrational content of the initially prepared excited state. Similarly, the fact that an a-type band is modulated exclusively by beats with positive phases is a reflection

of the vibrational content of $|\Psi(t)\rangle$ at $t = 0$. By (6.3) and the normalization of the α_{Ia},

$$\wp_a(0) = \sum_{I,J=1}^{N} \alpha_{Ia}^2 \alpha_{Ja}^2 = \sum_{I=1}^{N} (\sum_{J=1}^{N} \alpha_{Ja}^2) \alpha_{Ia}^2 = 1. \tag{6.6}$$

That is, $|\Psi(0)\rangle = |a\rangle$. Therefore, $\wp_a(t) \leq \wp_a(0)$ and $I_a(t) \leq I_a(0)$. But this can only be true in general if all the a-type phases are $+1$. Thus, the qualitative difference in phase behavior between a-type and non-a-type bands has clear meaning in terms of IVR. The presence of -1 phases in the decays of γ-type ($\gamma \neq a$) bands reflects the fact that vibrational energy will redistribute into the $|\gamma\rangle$ states as time increases. On the other hand, the fact that the amount of vibrational energy in $|a\rangle$ is at a maximum at $t = 0$ (by virtue of the exclusive absorption strength of $|a\rangle$) is reflected in the entirely positive phases of a-type decays.

A final utility of the correspondence between $I_\gamma(t)$ and $\wp_\gamma(t)$ is that it provides a means by which one can experimentally search for quasi-periodic and chaotic vibrational behavior in molecules. Being that such behaviors have been shown to be manifested in characteristically different ways in $\wp_\gamma(t)$,[17] then measurement of $I_\gamma(t)$ would be expected to provide information on the nature (*i.e.*, quasi-periodic or chaotic) of the vibrational dynamics of a given molecule at a given energy.

B. Dependence of decay behavior on total vibrational energy

A number of published accounts[1,14,18] have dealt with the effects of excess vibrational energy on large molecule IVR, as manifested in dispersed fluorescence spectra. From these studies, trends toward increasing spectral congestion and decreasing intensity in the unrelaxed region of the fluorescence spectra were observed as the vibrational energy was increased. These have been interpreted as being manifestations of faster and more extensive IVR at higher energies. Physically, this is reasonable since the average spacing of vibrational states decreases, and, thus, the opportunity for coupling increases with energy. However, the information available from purely spectral results is limited and can be misleading[5]. On the other hand, we have seen that fluorescence decay measurements can directly reveal

a large amount of information about IVR. Thus, it is of interest to consider how time-resolved results might be expected to be dependent on excess vibrational energy and how they might correlate with the trends in dispersed fluorescence spectra.

As mentioned above, the principal expected modification of vibrational coupling with increasing vibrational energy is an average increase in the number of levels coupled to one another. The consideration of the changes in decay behavior with excess energy is, therefore, tantamount to the consideration of the changing nature of decays as N increases. Guided by experimental results[6], we have found it useful to classify decays according to three ranges of N: (1) $N = 1$, (2) $N = 2$ to ~ 10, and (3) $N \geq 10$. These ranges of N may be identified with *low, intermediate,* and ***high*** vibrational energy regimes, respectively, in real molecules.

No IVR

The $N = 1$ case obviously corresponds to no IVR. The spectral manifestations of this are uncluttered spectra consisting of sharp vibronic bands assignable in terms of optically active vibrational intervals.[14] The decays of all the bands in such a spectrum are ***identical*** and in most situations (*i.e.*, barring any unusual nonradiative channels such as small energy gap intersystem crossing) will be single exponential and unmodulated.

Restricted IVR

The $N = 2$ to ~ 10 case corresponds to ***restricted*** IVR. A dispersed fluorescence spectrum belonging to this case consists of an uncongested, vibrationally unrelaxed region (see section II-D) composed of weak intensity a-type bands, and a congested, vibrationally relaxed region consisting primarily of non-a-type bands. The decays of the various bands in the spectra adhere to the characteristics presented in sections II and III. They differ from the $N = 1$ case in that the decay behavior depends on detection wavelength, and that modulations are always present. The feature that distinguishes the decays of this case from those arising from systems of greater N is the presence of a number of essentially full recurrences on the timescale of the fluorescence lifetime. That is, each intensity $I_\gamma(t)$ (and each $\wp_\gamma(t)$) has a number

of maxima, all of which approach the global maximum of that intensity. IVR is restricted in the sense that energy does not irreversibly flow from one vibration into others, but instead oscillates between a small number of levels.

Dissipative IVR

Finally, the case where N is large corresponds to ***dissipative*** IVR. Spectrally, this case is characterized by very weak a-type fluorescence bands in the unrelaxed region, and very congested, predominantly non-a-type fluorescence in the relaxed spectral region. Due to the large number of interference terms modulating fluorescence decays belonging to this case, the overall contribution of these terms is at a maximum at $t = 0$, after which a dephasing occurs which renders the contribution small for all subsequent times. For a-type decays, in which all the interference terms have +1 phases, this dephasing gives rise to a rapid initial decay component[5,19] followed by a long component of comparatively small intensity. For non-a-type decays, in which the initial intensity of zero arises from the -1 value for the sum of the modulation depths, the dephasing results in a risetime followed by a long decay. In both cases the possibility exists that some small modulations may occur on the long decay components; *i.e.*, some partial recurrences may occur on the timescale of the fluorescence lifetime. However, the dephasing is sufficiently complete to exclude anything close to a full recurrence ***on this timescale.*** This type of decay behavior represents the irreversible flow of energy out of the initially prepared $|a\rangle$ excited state into the other coupled zero-order states.

Lahmani, *et al.*[19] have shown (in the context of singlet-triplet coupling) that the decays corresponding to large N may be reproduced by assuming a kinetic rate equation model for the values $\wp_\gamma(t)$. For an a-type decay this model predicts a double exponential decay of the form

$$I_a(t) \sim \wp_a(t) = \frac{1}{N}\{(N-1)e^{-(\Gamma+\Delta)t} + e^{-\Gamma t}\}, \tag{6.7}$$

where Γ is the same as in section II, and Δ is a measure of the width of the distribution of beat frequencies and corresponds to the dephasing contribution to

the decay. For non-a-type decays taken together the model gives

$$\sum_{\gamma \neq a} I_\gamma(t) \sim \sum_{\gamma \neq a} \wp_\gamma(t) = \frac{N-1}{N}\{e^{-\Gamma t} - e^{-(\Gamma+\Delta)t}\}. \tag{6.8}$$

These equations, by virtue of their very simplicity, serve several useful purposes. Firstly, they provide at a glance the general temporal behavior of IVR in the dissipative regime. Secondly, they serve as convenient functions with which one can fit experimental decays and thereby obtain IVR parameters. Thirdly, they relate in a simple way the parameter Δ to the rate of dissipative IVR. Δ, in turn, can be related[20] to molecular parameters such as the vibrational density of states and vibrational coupling matrix elements. Finally, their derivation by means of a kinetic model makes apparent the close analogy between IVR and kinetic behavior. In particular, one can meaningfully speak of $1/\Delta$ as an equilibration time during which a molecule, initially jarred out of equilibrium by the laser, evolves to a "steady-state" in which no further evolution in the distribution of vibrational energy occurs.

One must, however, beware of taking (6.7) and (6.8) too literally. Firstly, as pointed out in Ref. 19, the equations exclude the possibility of quantum beats. Secondly, (6.7) predicts that the ratio of the pre-exponential factors of fast to slow fluorescence for an a-type decay will be equal to $N-1$, the number of states coupled to $|a\rangle$. However, by (2.13) one can see that the value $N-1$ is actually an upper limit to this ratio, and it holds only if $|\alpha_{Ia}| = 1/N$, for all I.

VII SUMMARY AND CONCLUSIONS

In this chapter we have considered the dynamics of molecular vibrational energy flow between an arbitrary number of coupled vibrational levels. In particular, the concern has been centered on the dynamical manifestations of vibrational coupling in the temporal characteristics of spectrally resolved fluorescence. These manifestations take the form of coherence (phase-shifted quantum beats) in fluorescence decays, whose number of beat frequencies is related to the number of coupled levels, and whose beat phases and modulation depths are dependent on the fluorescence band detected. It has been shown that these phases and modulation depths are functions of the coefficients that connect the the basis set of the zero-order, coupled vibrational wavefunctions to the molecular eigenstate basis set. As such, they are not arbitrary, but adhere to certain rules and restrictions ultimately based in the orthonormality of the mixing coefficients. Conversely, it has been shown that with knowledge of beat phases and modulation depths, it is possible to determine these coefficients, which, when so determined, can then be used along with the beat frequencies to construct the Hamiltonian matrix describing the coupling between the zero-order vibrational states. Thus, the measurement of time- and frequency-resolved fluorescence can 1) indicate the presence of vibrational coupling in a molecule, 2) indicate the number of coupled levels, and 3) provide information leading to the determination of the details of the coupling.

It has also been shown in this chapter that, more than just providing parameters pertinent to vibrational coupling, the temporal behavior of dispersed fluorescence has an immediate and simple interpretation in terms of IVR. The intensity *vs.* time of a given band in a fluorescence spectrum is a direct picture of the evolution of vibrational energy in the excited state. Quantum beat frequencies are related to the IVR timescale. Beat phases and modulation depths have straightforward interpretations in terms of the vibrational energy content of the excited state. And, most important, the nature of IVR at a particular vibrational energy is apparent from the decays of fluorescence bands. Thus, one can readily assess the transition

from absent to restricted to dissipative IVR in a given molecule.

The results presented in this chapter have been derived to facilitate the interpretation of real experimental data. In the following chapters these theoretical results will be applied to observations made on the molecules anthracene[6] and *trans*-stilbene.[8]

REFERENCES

1. For a review see: C. S. Parmenter, Faraday Discuss. Chem. Soc. **75**, 7(1983).

2. P. M. Felker and A. H. Zewail, in *Applications of Picosecond Spectroscopy to Chemistry*, edited by K. B. Eisenthal (D. Reidel, Dortrecht, 1984), p. 273.

3. P. M. Felker and A. H. Zewail, Chem. Phys. Lett. **102**, 113(1984).

4. P. M. Felker and A. H. Zewail, Phys. Rev. Lett. **53**, 501(1984).

5. P. M. Felker and A. H. Zewail, Chem. Phys. Lett. **108**, 303(1984).

6. P. M. Felker and A. H. Zewail, J. Chem. Phys. - submitted.

7. P. M. Felker and A. H. Zewail, J. Chem. Phys. - submitted.

8. P. M. Felker, W. R. Lambert, and A. H. Zewail, J. Chem. Phys. - submitted.

9. We assume here that all of the matrix elements of $\mathbf{H}_0$, the Hamiltonian matrix in the zero-order basis, can be expressed as real numbers, in which case all the elements of $\mathbf{C}$ can be taken as real.

10. See, for example: S. Haroche, in *High Resolution Laser Spectroscopy*, edited by K. Shimoda (Springer, New York, 1976), p. 254.

11. Since all the excited eigenstates are S_1 levels of about the same energy, one does not expect Γ to vary much from level to level. Taking Γ to be equal for all levels is therefore a reasonable approximation. It is pertinent to note that even if Γ were not the same for all eigenstates, this would not affect the beat phases or modulation depths in a given decay.

12. Examples are the spectra of anthracene appearing in: W. R. Lambert, P. M. Felker, J. A. Syage, and A. H. Zewail, J. Chem. Phys. **81**, 2195(1984).

13. This is a different situation from that which obtains in, for example, Zeeman quantum beats, where beat phases and modulations depend on the polarizations of the excitation source and detection analyser, as well as on the magnetic field direction. A discussion of polarization effects on molecular quantum beats may be found in: M. Bixon, J. Jortner, and Y. Dothan, Mol. Phys. **17**, 109(1969). For experimental results on Zeeman quantum beats see, for example, Ref. 10; and R. Wallenstein, J. A. Paisner, and A. L. Schawlow, Phys. Rev. Lett. **32**, 1333(1974).

14. For example, S. M. Beck, J. B. Hopkins, D. E. Powers, and R. E. Smalley, J. Chem. Phys. **74**, 43(1981).

15. G. Herzberg, *Infrared and Raman Spectra of Polyatomic Molecules* (Van Nostrand, Princeton, 1945), p. 216.

16. W. Rhodes, in *Radiationless Transitions*, edited by S. H. Lin (Academic, New York, 1980), p. 219.

17. See, for example: (a) G. Hose and H. S. Taylor, Chem. Phys. **84**, 375(1984); (b) M. D. Feit and J. A. Fleck, Jr., J. Chem. Phys. **80**, 2578(1984).

18. For example, (a) P. S. H. Fitch, L. Wharton, D. Levy, J. Chem. Phys. **70**, 2018(1979); (b) A. Amirav, U. Even, and J. Jortner, *ibid.* **74**, 3475(1981); (c) C. Bouzou, C. Jouvet, J. B. Leblond, Ph. Millie, A. Tramer, and M. Sulkes, Chem. Phys. Lett. **97**, 61(1983); (d) M. Fujii, T. Ebata, N. Mikami, M. Ito, S. H. Kable, W. D. Lawrance, T. B. Parsons, and A. E. W. Knight, J. Phys. Chem. **81**, 2209(1984).

19. F. Lahmani, A. Tramer, and C. Tric, J. Chem. Phys. **60**, 4431(1974).

20. C. Tric, Chem. Phys. **14**, 189(1976).

Table 1. A summary of results for $N = 3$.

No. of band-types	No. of beat frequencies	No. of beat triplets
3	3	1

Four possible quantum beat phase distributions:

Distribution	Independent phases		Dependent phase
	$S_\gamma(\omega_{12})$	$S_\gamma(\omega_{13})$	$S_\gamma(\omega_{23})$
$\vec{\delta}_\gamma^1$	+1	+1	+1
$\vec{\delta}_\gamma^2$	+1	−1	−1
$\vec{\delta}_\gamma^3$	−1	+1	−1
$\vec{\delta}_\gamma^4$	−1	−1	+1

Table 2. A summary of results for $N = 4$.

No. of band-types	No. of beat frequencies	No. of beat triplets
4	6	4

Eight possible quantum beat phase distributions:

Distribution	Independent phases			Dependent phases		
	$S_\gamma(\omega_{12})$	$S_\gamma(\omega_{13})$	$S_\gamma(\omega_{14})$	$S_\gamma(\omega_{23})$	$S_\gamma(\omega_{24})$	$S_\gamma(\omega_{34})$
$\vec{\delta}_\gamma^1$	+1	+1	+1	+1	+1	+1
$\vec{\delta}_\gamma^2$	+1	−1	−1	−1	−1	+1
$\vec{\delta}_\gamma^3$	−1	+1	−1	−1	+1	−1
$\vec{\delta}_\gamma^4$	−1	−1	+1	+1	−1	−1
$\vec{\delta}_\gamma^5$	+1	−1	+1	−1	+1	−1
$\vec{\delta}_\gamma^6$	+1	+1	−1	+1	−1	−1
$\vec{\delta}_\gamma^7$	−1	+1	+1	−1	−1	+1
$\vec{\delta}_\gamma^8$	−1	−1	−1	+1	+1	+1

Table 3. A summary of results for $N = 5$.

No. of band-types	No. of beat frequencies	No. of beat triplets
5	10	10

Sixteen possible quantum beat phase distributions:

Distribution	Independent Phases			
	$S_\gamma(\omega_{12})$	$S_\gamma(\omega_{13})$	$S_\gamma(\omega_{14})$	$S_\gamma(\omega_{15})$
1	+1	+1	+1	+1
2	+1	+1	+1	−1
3	+1	+1	−1	+1
4	+1	−1	+1	+1
5	−1	+1	+1	+1
6	+1	+1	−1	−1
7	+1	−1	+1	−1
8	−1	+1	+1	−1
9	+1	−1	−1	+1
10	−1	+1	−1	+1
11	−1	−1	+1	+1
12	+1	−1	−1	−1
13	−1	+1	−1	−1
14	−1	−1	+1	−1
15	−1	−1	−1	+1
16	−1	−1	−1	−1

FIGURE CAPTIONS

1. Level diagram illustrating the general situation to be treated herein. The zero-order harmonic vibrational states on the left are coupled by anharmonic interactions. Only one of these states, the optically active $|a\rangle$ level, can be reached from the ground state via the excitation process. All of the other levels are optically inactive (dark). On the right are pictured the vibrational eigenstates that result from the interactions among the zero-order states. The different lengths of the lines representing these levels are meant to indicate that each eigenstate has a different contribution from $|a\rangle$, and hence has a different absorption strength from the ground state.
2. Level diagram and fluorescence spectrum representing the dispersed fluorescence characteristics to be expected from a set of coupled vibrational levels in S_1. Excitation prepares the zero-order $|a\rangle$ state (indicated by the asterisk) which then undergoes IVR. Emission gaining its strength from $|a\rangle$ is termed vibrationally unrelaxed and tends to occur in the blue region of the spectrum. Emission gaining its strength from $|b\rangle$, $|c\rangle, \ldots$, is termed vibrationally relaxed and occurs near and to the red of the 0_0^0 transition energy of the molecule.
3. Schematic diagram of the situation treated as case 1 (section V-A), wherein it is assumed that the bandwidth ($\Delta\omega_c$) of the excitation source is not large enough to span all the eigenstates ($|1\rangle, \ldots, |N\rangle$) resulting from the coupling of a set of N zero-order states.
4. Schematic diagram of the situation treated as case 4 (section V-D), wherein it is assumed that the laser bandwidth is large enough to excite the eigenstates (right) corresponding to two independent (noninteracting) sets of coupled zero-order levels (left). Only two zero-order levels are assumed to have absorption strength from the ground state—the $|a\rangle$ and $|a'\rangle$ states.

Figure 1

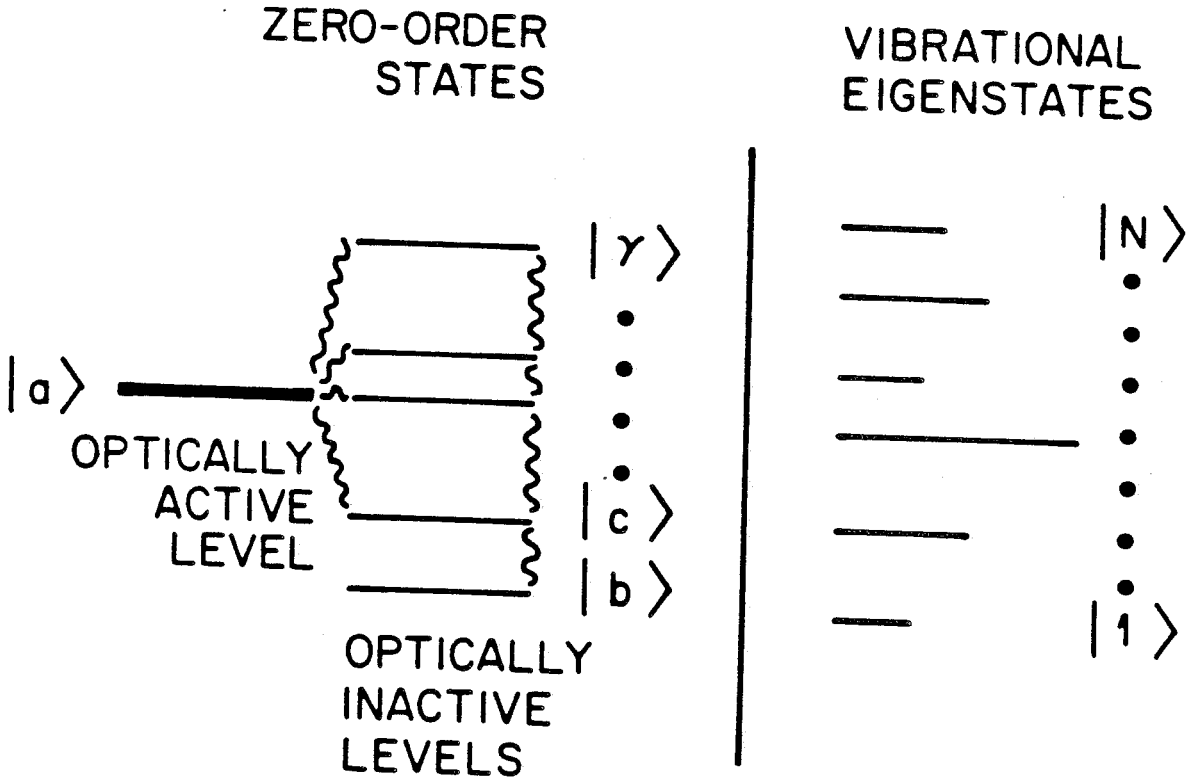
ZERO-ORDER
STATES
VIBRATIONAL
EIGENSTATES
|γ⟩
|N⟩
|a⟩
OPTICALLY
ACTIVE
LEVEL
|c⟩
|b⟩
|1⟩
OPTICALLY
INACTIVE
LEVELS

Figure 2

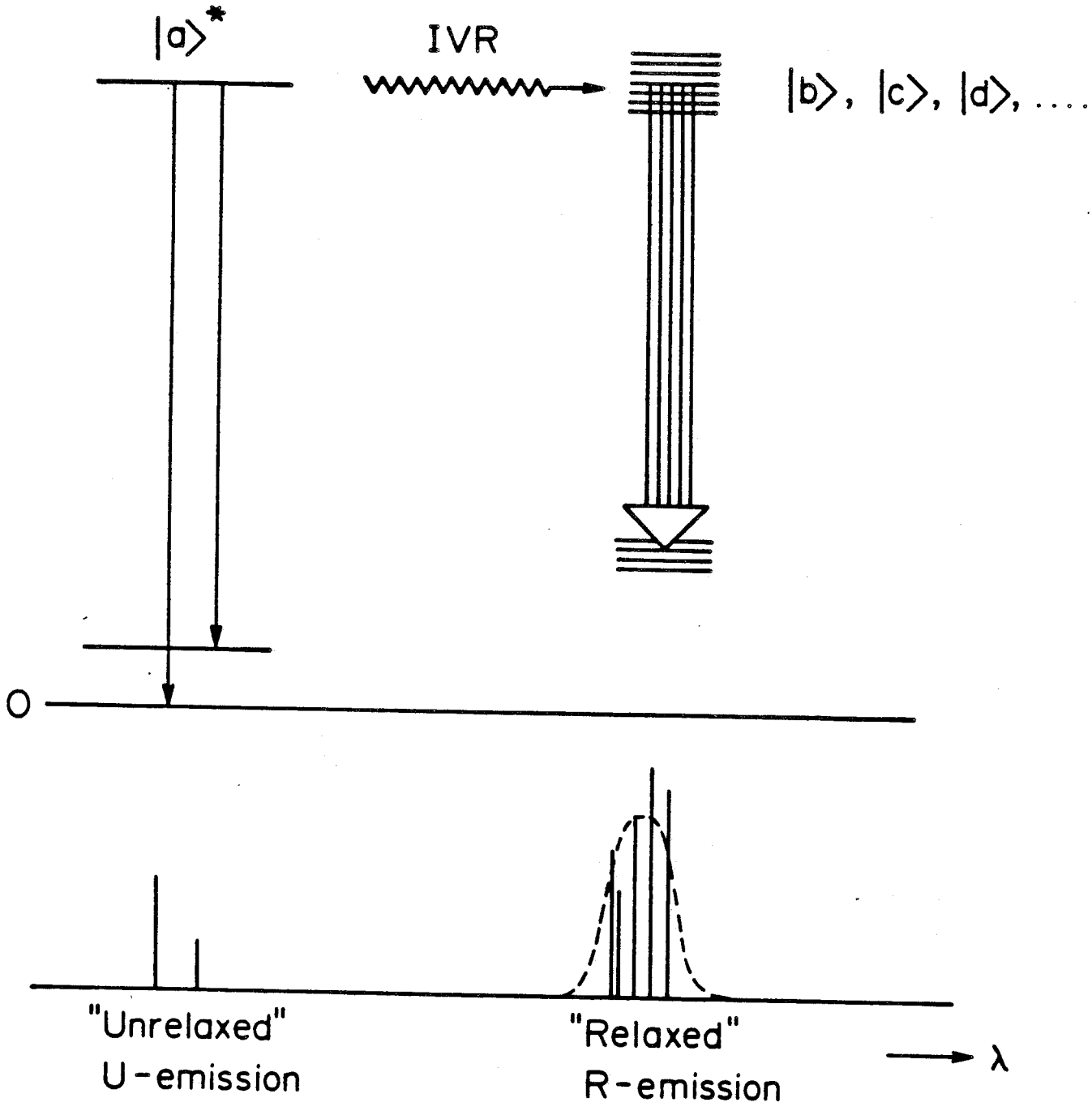

Figure 3

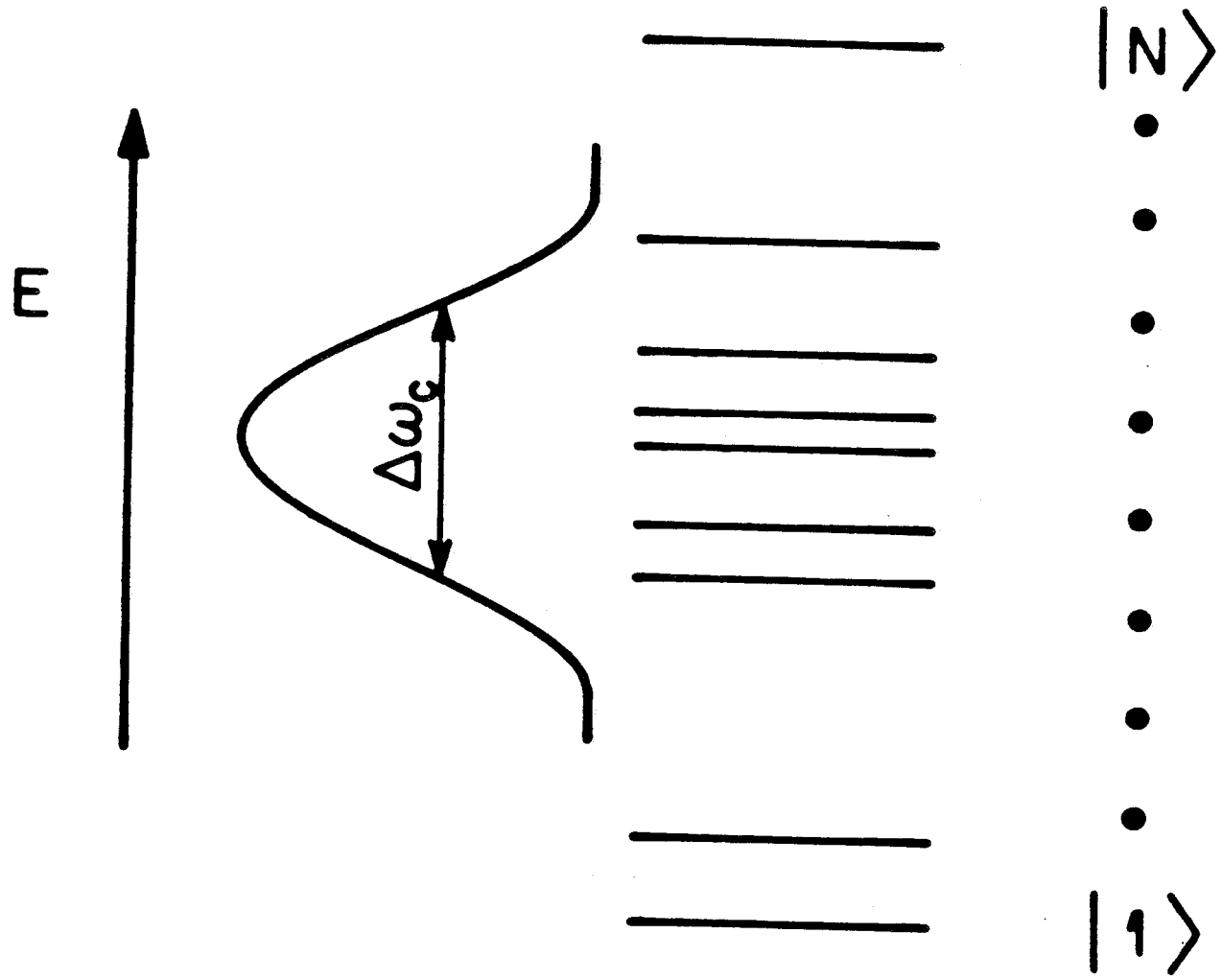

Figure 4

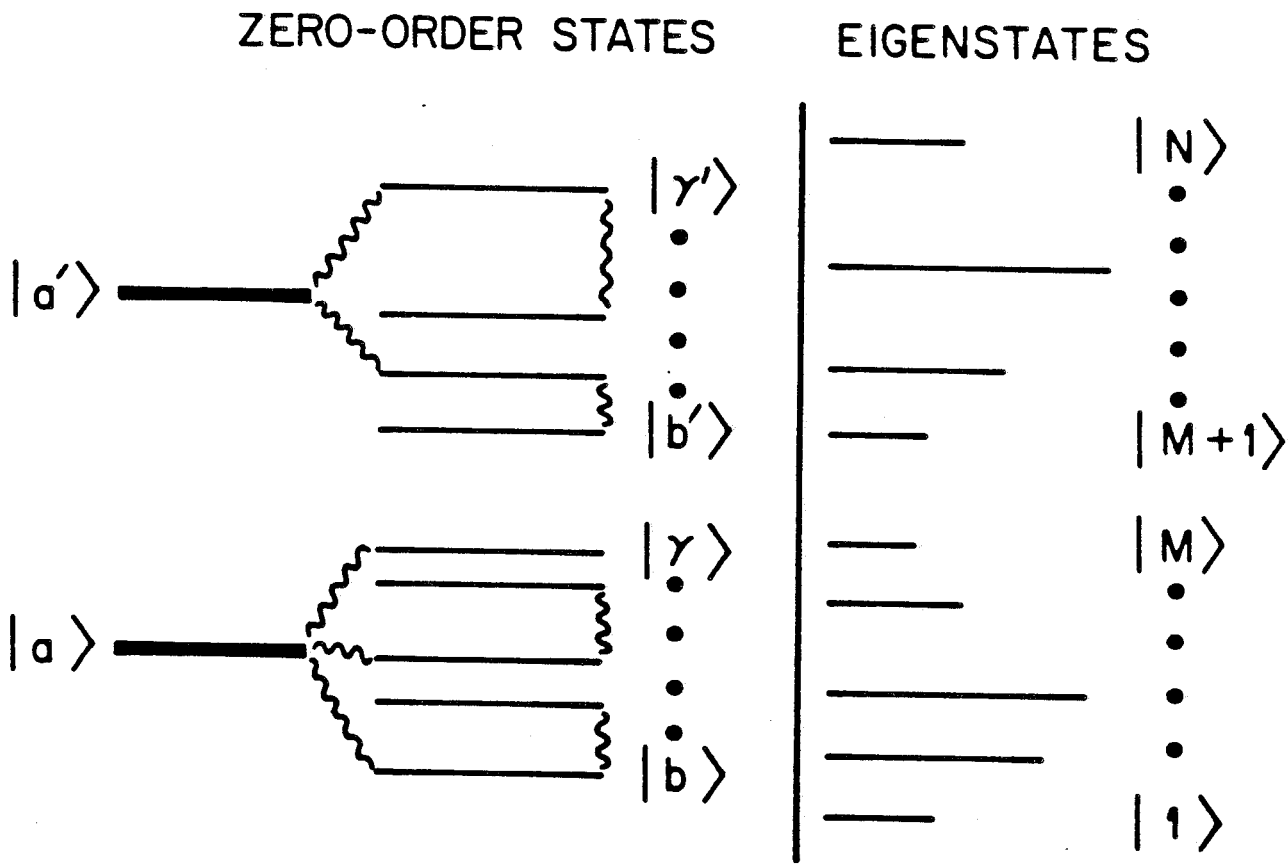

CHAPTER 4

ENERGY DEPENDENCE OF IVR IN ANTHRACENE*

* Submitted to the Journal of Chemical Physics, as
"Dynamics of intramolecular vibrational-energy redistribution (IVR).
II Excess energy dependence," by Peter M. Felker and Ahmed H. Zewail

I. INTRODUCTION

In the context of the theory presented in the previous chapter this chapter provides an account of experimental results pertaining to IVR in anthracene. The results were obtained with temporal resolution five times better than that used in previous studies.[1-3] This has allowed the resolution of beat frequencies up to $\sim$ 12 GHz, and the resolution of decays with time constants on the order of 10 psec. A primary emphasis of the work is on elucidating the changes which take place in IVR processes as the vibrational energy of the molecule increases. In addition, using the theoretical results of Chapter 3 on multilevel systems we show the utility of using quantum beat spectroscopy to reveal parameters associated with vibrational coupling in anthracene for excess vibrational energies ranging from 0 to $\sim 2000\ cm^{-1}$.

The organization of the chapter is as follows. Firstly, the experimental techniques and data analysis are discussed. Of principal importance in this section is the presentation of the Fourier analysis methods which allow one to extract quantum beat frequencies, phases, and modulation depths from fluorescence decays. Secondly, the results for various single vibronic levels (SVL's) in S_1 anthracene are presented in the order of increasing SVL energy. These results are analyzed to determine the number of coupled levels giving rise to the observed behavior and, where possible, to determine elements of the Hamiltonian matrix in the zero-order vibrational basis set. Finally, the overall trends of the results and the timescales for IVR in the molecule are discussed.

II. EXPERIMENTAL

A. Apparatus

The picosecond-jet apparatus used in the experiments reported herein is described in detail elsewhere[2]. The nozzle conditions were much the same as for previous work on anthracene[1-5]. The anthracene sample (Aldrich gold label, 99.9%) was heated to $\sim 180^{o}$ C and expanded through a ~ 100 μm pinhole with $30-40$ psi helium. The laser-to-nozzle distance was typically 3 mm. The excitation source consisted of the frequency-doubled ($LiIO_3$) output of a synchronously pumped, cavity-dumped dye laser (DCM as dye), the bandwidth of which was ~ 2 cm^{-1} FWHM and the temporal pulse width of which was 15 ps FWHM. Fluorescence was collected with right angle geometry and directed through a 0.5 M monochromator. The dispersed fluorescence spectral resolution varied with the particular measurement being made and is noted with the data. Fluorescence photons were detected with a Hamamatsu R1564U multichannel plate photomultiplier, the output of which was amplified before encountering the timing electronics. Decays were measured using time-correlated single photon counting. The total temporal response of detection (response function) was typically 80 ps FWHM as measured by scattering laser pulses off of the nozzle. Care was taken to monitor any major temporal shifts in the peak of the response function since such shifts affect the apparent phases of quantum beat components. Generally, large shifts were not a problem and are not relevant to any of the results included herein.

B. Extraction of beat parameters by Fourier analysis

It is well known that a measured fluorescence decay $F(t)$ may be related to a true molecular decay $I(t)$ by the convolution integral[6]

$$F(t) = \int_0^t R(t')I(t-t')\mathrm{d}t', \tag{2.1}$$

where $R(t)$ is the response function of the experimental apparatus. From theoretical considerations[7] pertaining to vibrational quantum beats the molecular decays are

expected to be of the form

$$I_\gamma(t) = \mathrm{Re}[Ae^{-\Gamma t}(1 + \sum_{I>J=1}^{N} M(\omega_{IJ})e^{-i\omega_{IJ}t})], \tag{2.2}$$

where A is a constant, Γ is the excited state decay rate, N is the number of coupled vibrational levels, and $M(\omega_{IJ})$ is the modulation depth of the beat frequency ω_{IJ}. Now, since one is interested in extracting the values for ω_{IJ} and $M(\omega_{IJ})$ from a measured decay, Fourier analysis is the natural method by which to accomplish this. In particular, one can make use of the theorem[8] for the Fourier transform of a convolution integral to obtain

$$F(\omega) = I(\omega)R(\omega) \tag{2.3}$$

or

$$I(\omega) = F(\omega)/R(\omega), \tag{2.4}$$

where $F(\omega)$, $I(\omega)$, and $R(\omega)$ are the Fourier transforms of $F(t)$, $I(t)$, and $R(t)$, respectively. This procedure of dividing the transform of the measured decay by the transform of the response function automatically compensates for two defects in $F(\omega)$: (1) it enhances the amplitudes of the higher frequency components which tend to be washed out by the finite response function width and (2) it establishes the proper phases for the beat components. By measuring $F(t)$ and $R(t)$, and then calculating $F(\omega)$ and $R(\omega)$, one can obtain $I(\omega)$ by (2.4). For this paper we have calculated $F(\omega)$ and $R(\omega)$ by using the Cooley-Tukey fast Fourier transform algorithm[9] to transform data zero-filled[10] to 4096 points.

After finding $I(\omega)$, the ω_{IJ} are easily obtained by the positions of the bands in the Fourier spectrum. The values of the beat frequencies reported herein are actually the values $\omega_{IJ}/2\pi$. The accuracy of these numbers is ultimately limited by the resolution of the Fourier spectra and the accuracy of the time base. A conservative estimate of the error in quoted beat frequencies is $\pm 5\%$.

The $M(\omega_{IJ})$ are available from the Fourier amplitudes of components in $I(\omega)$, as is evident from

$$\mathrm{Re}(I(\omega)) = K[\frac{\Gamma}{\Gamma^2+\omega^2} + \sum_{I>J=1}^{N} \frac{\Gamma M(\omega_{IJ})}{\Gamma^2+(\omega_{IJ}-\omega)^2}]. \tag{2.5}$$

In principle, the heights of the bands of $\mathrm{Re}(I(\omega))$ normalized to the zero frequency band height should give the various absolute modulation depths $M(\omega_{IJ})$. In practice, it is more accurate to integrate over the individual band shapes in $I(\omega)$ and then to normalize these sums to the integrated intensity of the zero frequency band. This is better for two reasons. Firstly, small variations in vibrational coupling with rotational level[11] tend to broaden the nonzero frequency bands in $I(\omega)$ relative to the breadth Γ of the zero frequency band. That which is pertinent, therefore, are not the heights but the integrated intensities of the bands. Secondly, it is often necessary to collect data in such a manner that decays are truncated at a significant fraction of their initial intensities. This has the effect of introducing sinusoidal oscillations about zero into the derived $I(\omega)$. Summing over a band averages out these oscillations and, by so doing, gives a more accurate value for the Fourier amplitude.

A number of factors contribute to errors in the derived values for the modulation depths (see section V of Chapter 3). The first is noise in the Fourier spectra. The second factor arises from the inability to completely spectrally isolate bands in the fluorescence spectrum. The influence of this factor varies from band to band. It can be significant even for detection resolution better than 1 Å. Thirdly, small drifts in the response function during the course of the measurement of a decay can make a large difference in the values derived for the modulation depths of high frequency beat components. This is the case because the width of the measured response function $R(t)$ will, in general, be narrower than the effective response function $R_{eff}(t)$ corresponding to the decay. (Typically, the time needed to measure a response function is a small fraction of the time needed to measure a decay. This is why one expects $R(t)$ to be narrower than $R_{eff}(t)$.) Thus, in (2.4) $R(\omega)$ will be larger than it should be. A specific example assuming a Gaussian response

function will illustrate the point. If the measured $R(t)$ is 77 psec FWHM, while $R_{eff}(t)$ is 85 psec FWHM (only a drift of one channel under typical experimental conditions) then $R(\omega) \simeq R_{eff}(\omega) = 0.975$ for $\omega/2\pi = 1$ GHz, but $R(\omega) = 0.218$ while $R_{eff}(\omega) = 0.158$ for $\omega/2\pi = 8.5$ GHz. By using $R(\omega)$ in (2.4) essentially no error will be introduced for the 1 GHz modulation depth, but the modulation depth derived for the 8.5 GHz component will be only $\frac{0.158}{0.218} = 72\%$ of its actual value. One expects this source of error in modulation depths to increase in influence as the time needed to measure a decay increase. It is likely that it is the major source of error in the quoted modulation depths of high frequency components.

Despite the value that $I(\omega)$ has in the analysis of a beat-modulated fluorescence decay, the large zero-frequency component and the marked, truncation-induced oscillations of a typical $I(\omega)$ spectrum render it relatively unattractive for display purposes. On the other hand, the Fourier spectrum $I_m(\omega)$ derived solely from the transformation of the modulated portion of a decay multiplied by a suitable shaping function provides almost as much information, as the corresponding $I(\omega)$ (absolute modulation depths are not available from $I(\omega)$), but is rid of the zero-frequency peak and the spurious oscillations. For this reason most of the Fourier spectra which appear as figures in this chapter are $I_m(\omega)$ and not $I(\omega)$ spectra.

To obtain $I_m(\omega)$ for a given decay, the decay is first fit to a single exponential function by using a nonlinear least-squares fitting algorithm.[12] Convolution effects are not considered in this initial portion of the analysis since, in general, $1/\Gamma$ is much greater than the width of $R(t)$. The fitted function is then subtracted from $F(t)$ and the residual $F_m(t)$ is multiplied by the function[13] $(t_f - t)^{\cdot 5}$, which causes it to go to zero smoothly as $t \rightarrow t_f$, t_f corresponding to the point in time at which $F(t)$ is truncated. This manipulation substantially eliminates any spurious oscillations in the Fourier spectrum. The function $(t_f - t)^{\cdot 5} F_m(t)$ is then Fourier transformed and divided by $R(\omega)$ to give $I_m(\omega)$. Now, as we have stated, $\mathrm{Re}(I_m(\omega))$ preserves the phase behavior and the relative values of the $M(\omega_{IJ})$ of a given decay. One should, however, note two points about the spectra. Firstly, the application of

the shaping function $(t_f - t)^{.5}$ to $F_m(t)$ results in artificial widths for the Fourier bands in $I_m(\omega)$. Secondly, the shape of the bands appearing in $I_m(\omega)$ depend on that portion of $F(t)$ which is chosen initially to be fit to the exponential function. The band shape distortions that arise from this second cause become more serious, the farther a decay is fit from its peak. For all practical purposes neither of the above artifacts is important enough to substantially modify the values for the beat frequencies, phase behavior, or relative modulation depths derived for a given decay.

C. Analysis of fluorescence decays in the dissipative regime

In the limit where the number of coupled vibrational levels is large enough to give rise to dissipative IVR,[5] the utility of Fourier transform techniques is limited due to the large number of beat components in any given decay. For such cases, the extraction of IVR parameters from decay measurements can be accomplished by using equations (6.7) and (6.8) of Chapter 3[7] to fit observed decays. Experimentally, it is easier to obtain a "pure" a-type (vibrationally unrelaxed) decay than it is to obtain vibrationally relaxed fluorescence that is uncontaminated by a-type emission. Thus, only fits to a-type (*i.e.*, (6.7) of Chapter 3) dissipative decays are reported herein. These fits were accomplished by the method of nonlinear least squares.[12] The convolution of the true molecular decay with the temporal response of the detection system was taken into account.

III. LOW ENERGY REGION

The fluorescence spectroscopy of anthracene SVL's having energies from E_{vib} = 0 to 1200 cm^{-1} has already been reported on[14,15]. Almost all of the spectra consist of distinct bands which can be assigned exclusively in terms of transitions arising from an optically active SVL (see section II-D of Chapter 3 for what we mean by an optically active level). These spectral characteristics are consistent with the manifestations of uncoupled vibrational levels. Previous studies in this laboratory have corroborated this interpretation in that the fluorescence decays of each of the bands in a given spectrum have been found to be identical single exponentials. These former studies, however, were done with a detection temporal resolution that only allowed beat frequencies of less than $\sim$ 2 GHz to be resolved. It is now apparent that in most cases beats arising from vibrational couplings in anthracene are of frequencies greater than this[4]. Thus, we have remeasured with better time resolution some decays corresponding to excitation of SVL's in the low energy regime. Fig. 1 provides an example of the fluorescence spectrum and decay upon excitation of the 12^2 (766cm^{-1}) SVL. The spectrum is analyzed in Ref. 14. The decay, which corresponds to detection of the 390 cm^{-1} fluorescence band, is clearly unmodulated, and is the same as the decays of the other bands in the spectrum. (The apparent risetime of the decay is a convolution effect, as has been verified by calculating the convolution of an 18 nsec exponential with our measured system response function. Such apparent risetimes become longer, the longer the fluorescence lifetime becomes.) Decays have also been measured for other excitation bands in this low energy regime. No beats have been observed despite the temporal resolution. Both the spectral[14,15] and decay results indicate, therefore, that vibrational coupling leading to IVR does not occur to an appreciable extent in anthracene SVL's up to $\sim$ 1200 cm^{-1}. In saying this we do not exclude the possibility that strong Fermi resonances, resulting in splittings of several wavenumbers or more, are not present in this energy regime. Indeed, other results[15,16] have provided evidence for such coupling in the higher energy portion of the region. The difficulty in preparing such

coupled systems coherently, however, argues against considering them in terms of dynamical energy flow. More discussion on this point is presented in section VI-C to follow.

IV. INTERMEDIATE ENERGY REGION

Without exception, the excitation of jet-cooled anthracene at each of the five prominent vibronic bands in its excitation spectrum[14,15] between $S_1 + 1380$ cm^{-1} and $S_1 + 1514$ cm^{-1} results in quantum beat-modulated fluorescence decays, the beat patterns of which depend on the particular fluorescence band being detected. We have already reported[4] preliminary results for two of these excitation bands: $E_{vib} = 1380$ cm^{-1} and 1420 cm^{-1}. In this section we analyze in detail the results for these two bands in terms of the theory presented in Chapter 3, and obtain parameters pertaining to IVR and vibrational coupling at these energies. For the three other bands, we present representative decays, but do not provide any extensive analysis of the results.

A. $E_{vib} = 1380$ cm^{-1}: The $a_g(6)$ mode

We have previously reported results[1,2] pertaining to the characteristics of the quantum beats which arise from excitation of this prominent band in the excitation spectrum. (The nature of the vibrational level has been assigned in Ref. 14.) In fact, it is this excitation which gives rise to those beats which we reported on three years ago and which represent the first example of a quantum interference effect in a large molecule. It turns out that these "old" results actually represent manifestations of only a minor aspect of the vibrational dynamics associated with this excitation energy; increased temporal resolution has revealed that fast beats[4] modulate many of the dispersed fluorescence bands which appear to be unmodulated under 400 psec resolution. As shall be seen below, the new data lend themselves to a relatively straightforward interpretation in terms of IVR.

Results

The fluorescence spectrum resulting from excitation to $S_1 + 1380$ cm^{-1} is shown in Fig. 2 along with a higher resolution scan of a portion of the spectrum. A previous attempt[15] at assigning this spectrum made note of the fact that while a number of the bands are assignable in terms of optically active intervals (most notably those bands at shifts of 390, 755, 780, 1168, and 1408 cm^{-1} from the excitation energy),

most of the bands, including some of the most intense ones, are not. This mix of assignable (vibrationally unrelaxed) and unassignable (vibrationally relaxed) bands, and the congestion in and to the red of the S_1 origin region indicate (see section II-D of Chapter 3) that the spectrum arises from a relatively small number of coupled vibrational levels.

Confirmation of this is provided by time-resolved results, which reveal beat-modulated fluorescence decays that depend on detection wavelength. It is convenient to consider the decays of various groups of these bands separately.

Fig. 3 presents typical decays of some of those bands (group I) in the spectrum that can be readily assigned. All of the decays have a similar appearance and have roughly the same Fourier spectra. Fig. 4-top, which is the Fourier spectrum that results from transformation of the decay of the 390 cm^{-1} band, is representative of these spectra. In this spectrum, eight beat components are evident at 0.2, 1.8, 2.1, 2.6, 3.5, 4.3, 4.9, and 8.4 GHz. Note that all of these components have positive phases. The Fourier spectra of Figs. 4-middle and 4-bottom illustrate the changes that take place in the 390 cm^{-1} decay as the excitation source is tuned ~ 2 cm^{-1} to the red and to the blue of the excitation peak, respectively. Clearly, there is an enhancement in the components at 1.8, 2.6, and 4.3 GHz for the red excitation relative to the blue. On the other hand, the blue excitation results in a decay which is almost exclusively modulated by the 3.5, 4.9, and 8.4 GHz components (with some contribution from the 2.1 GHz component). For blue excitation one obtains absolute modulation depths of 0.12, 0.16, and 0.75 for the 3.5, 4.9, and 8.4 GHz components, respectively.

The decays of the bands at 1460, $1460+390$, and $1460+1408$ cm^{-1} (group II) are presented in Fig. 5. All three decays look similar, as is confirmed by Fourier analysis. The apparently decreased modulation depths in the lower two decays are attributable to congestion in the spectral regions in which their corresponding fluorescence bands occur. Fig. 6 presents the Fourier spectrum which results from transforming the modulated residual of the 1460 cm^{-1} decay. Only three prominent

beat components at 3.5, 4.9, and 8.4 GHz appear. Note that the phases of the 4.9 and 8.4 GHz components are negative, while the 3.5 GHz component has a positive phase. The absolute modulation depths of the three components, in order of increasing frequency, are found from Fourier analysis to be 0.14, −0.63, and −0.26.

The decays of the bands at 1429, 1528, 1528 + 390, and 1528 + 1408 cm^{-1} (group III) are presented in Fig. 7. Note the similar appearance of the decays. The Fourier transform spectrum of the 1528 cm^{-1} decay is presented in Fig. 8 and is representative of the other Fourier spectra. Again, the 3.5, 4.9, and 8.4 GHz components are the only discernible components. Now, however, the phase of the 4.9 GHz component is positive, while the other two components have negative phases. The derived absolute modulation depths for the decay of this band are quite sensitive to detection wavelength and resolution, as is reasonable considering its position in the spectrum (Fig. 2). The values for the absolute modulation depths derived from the decay of the 1528 cm^{-1} band are −0.45, 0.16, and −0.41, for the three components in order of increasing frequency.

The fourth group of bands which shall be considered (group IV) are the three which occur in the congested 1480 to 1520 cm^{-1} region of the spectrum. In this region the ability to spectrally isolate the various bands to measure a decay, while still maintaining a reasonable signal level, was limited. Nevertheless, modulated decays were observed, as shown in Fig. 9. For some of these decays, Fourier analysis (not shown) reveals some contribution from the 3.5, 4.9, 8.4 GHz triplet of beat components. Also present, however, unlike for the decays of groups II and III, are some of the other beat components that appear in the group I decays. In particular, all or some of the components at 1.8, 2.6, and 4.3 GHz appear prominently in these decays. Moreover, they exhibit phase behaviors that are different from that of the 390 cm^{-1} decay: the 1490 cm^{-1} decay has the 1.8 and 4.3 GHz components with negative phases and the 2.6 GHz component with positive, while the 1505 cm^{-1} decay has the 4.3 GHz component with positive phase and the other two with

negative phases.

Finally, we consider the decay of the band at 1125 cm^{-1}, which has been extensively studied previously[1,2] using $\sim$ 400 ps temporal resolution. The decay of this band using 80 ps temporal resolution is presented in Fig 10. The decay was taken under expansion conditions[2] which favor the appearance of the 0.2 GHz beat component (a 0.5 GHz component predominates under less efficient rotational cooling conditions[2]). This component is clearly present in the decay. Moreover, Fourier analysis confirms our earlier assertion[2] that the component has a negative phase. While higher frequency components also appear to modulate the 1125 cm^{-1} decay, the difficulty in obtaining relatively noiseless data for this weak fluorescence band has precluded any detailed consideration of these components.

Interpretation

As we have stated above, the characteristics of the dispersed fluorescence spectrum and the spectral dependence of the fluorescence decays corresponding to excitation at E_{vib} = 1380 cm^{-1} in anthracene both indicate that the experimental results are the dynamical manifestations of vibrational coupling in the S_1 state. One would, however, like to characterize this coupling more fully. The major problem is to determine the number of levels involved. According to Chapter 3 this can be done if the number of beat components and the number of beat triplets is known. (By a beat triplet[7] we mean the three beat components ω_{IJ}, ω_{JK}, and ω_{IK}. Note that two of the frequencies of such a triplet sum to the third.) The number of components (8) and the number of triplets (2) evident from the 390 cm^{-1} decay do not correspond to the theoretical expectations for any number of coupled levels. This could be due to at least two causes, as pointed out in sections V-B and V-D of the Chapter 3. Either some beat components are too weak or of too high a frequency to be observed, or the finite excitation bandwidth spans at least two independent sets of coupled levels. Here, there is strong reason to believe that the latter situation is the one that obtains. This conclusion arises from the fact that the relative Fourier amplitudes of the various beat components are dependent on excitation energy; the

triplet of frequencies at 1.8, 2.6, and 4.3 GHz is enhanced relative to the triplet at 3.5, 4.9, and 8.4 GHz when the excitation is detuned to the red and *vice versa* when the excitation is detuned to the blue (Fig. 4). Moreover, the other groups of bands in the dispersed fluorescence spectrum have decays in which one or the other beat triplet dominates. This is consistent with the manifestations of two sets of three coupled levels, the energy separation of the two sets being small enough to be within the excitation bandwidth, but large enough to preclude the observation of any beat frequencies corresponding to energy differences between two states belonging to two different sets[17]. In the nomenclature of section V-D (case 4) of Chapter 3, the bands of group I would correspond to overlapping a- and a'-type bands. The bands of groups II and III would then correspond to b-type and c-type bands, respectively, since the phase behaviors of the two types of decays are consistent with theoretical expectations for the two non-a-type bands of a three-level system: two -1 phases and one $+1$ phase for each decay. The 1487 and 1502 cm^{-1} bands would be assigned as b'- and c'-type bands. For these, too, the beat phase behaviors of the decays are consistent with the expectations of theory for the two non-a-type bands of a three-level system.

The sums of the modulation depths for the non-a-type bands, by (2.17) of the previous chapter, should be equal to -1. However, the b-type 1460 cm^{-1} decay gives a value of -0.75, and the c-type 1528 cm^{-1} decay gives a value of -0.70. As was pointed out in section II-B, this could be due to a number of sources of experimental error, particularly problems with spectral resolution and with response function drifts. Alternatively, this could be due to unobserved eigenstates (see sections V-A and V-B of Chapter 3). For example, the $|a\rangle$, $|b\rangle$, and $|c\rangle$ zero-order levels may be just three of four coupled levels, with the coupling being such that three of the eigenstates are closely spaced, and the fourth being widely separated from these three. It is likely that both types of influences play some role in the less than ideal values derived from experiment. In any case, the values -0.75 and -0.70 are close enough to -1 to warrant tentative treatment of the unprimed system in terms of

three coupled levels.

One may also note that two of the beat frequencies modulating the 390 cm^{-1} band remain unexplained by the scheme, presented above, of two sets of three coupled levels; the components at 0.2 and 2.1 GHz. We have previously shown[2] that for the $E_{vib} = 1380$ cm^{-1} excitation there exists a marked rotational level dependence to the coupling which gives rise to the 0.2 GHz component, the coupling only occurring significantly for certain higher energy rotational levels. This combines with the facts that (1) the 0.2 GHz modulation of the 390 cm^{-1} band is relatively weak and (2) any other bands exhibiting decays with significant modulation at this frequency (*e.g.*, the 1125 cm^{-1} band) appear only with weak intensity in the fluorescence spectrum, to indicate that the 0.2 GHz component is a manifestation of a coupling that figures only in a minor way, and at higher rotational energy levels, in the IVR dynamics at this excess vibrational energy. Whether or not this coupling is associated with the $|a\rangle$, $|b\rangle$, and $|c\rangle$ states, the $|a'\rangle$, $|b'\rangle$, and $|c'\rangle$ states, or with neither, cannot be answered without higher resolution excitation contour experiments. As for the beat component at 2.1 GHz, one is handicapped by the fact that no bands have been observed, other than those of group I, which exhibit in their decays a prominent component at this frequency. This suggests that the component does not arise from coupling involving the unprimed or primed set of states. It is possible that it does arise from the same coupling that gives rise to the 0.2 GHz component or that it represents the manifestations of two more coupled levels spanned by the bandwidth of the excitation pulse.

Calculation of H_0

As we have shown in section IV of the preceding chapter, it is possible to use observed quantum beat parameters to calculate the vibrational Hamiltonian matrix in the zero-order basis set (*i.e.*, H_0). In this section we do this for the three-level system composed of the $|a\rangle$, $|b\rangle$, and $|c\rangle$ coupled levels which give rise to the fluorescence bands modulated at 3.5, 4.9, and 8.4 GHz. Our choice of this coupled system is based on the quality of the data associated with it and the fact

that these levels contribute most prominently to the fluorescence arising from the 1380 cm^{-1} excitation band.

We start by labelling the beat frequencies such that $|\omega_{12}/2\pi| = 3.5$, $|\omega_{23}/2\pi| = 4.9$, and $|\omega_{13}/2\pi| = 8.4$ GHz. In so doing, the following is obtained for the diagonal Hamiltonian matrix:

$$\mathbf{E} = E_0\mathbf{I} \pm \begin{pmatrix} 0.0 & 0.0 & 0.0 \\ 0.0 & 3.5 & 0.0 \\ 0.0 & 0.0 & 8.4 \end{pmatrix}, \tag{4.1}$$

where E_0 is an unknown constant, and where the energy values are expressed in GHz.

Next, we calculate the α_{Ia} from the relative modulation depths of the 390 cm^{-1} decay. Using

$$\frac{M_a(\omega_{23})}{M_a(\omega_{13})} = 0.22 \text{ and } \frac{M_a(\omega_{23})}{M_a(\omega_{12})} = 1.31,$$

(4.3a) and (4.3b) of Chapter 3, and the normalization condition, one obtains

$$\alpha_{1a} = .629; \alpha_{2a} = .295; \alpha_{3a} = .720,$$

where we have exercised the freedom to choose all these values to be positive.[7]

Next, we may calculate either the α_{Ib} or the α_{Ic} values. We choose the α_{Ib} because the 1460 cm^{-1} b-type band is very strong and relatively isolated. Therefore, one expects that the values for the relative modulation depths for this band are fairly accurate. Using

$$\frac{M_b(\omega_{23})}{M_b(\omega_{13})} = 2.47 \text{ and } \frac{M_b(\omega_{23})}{M_b(\omega_{12})} = -4.42,$$

(4.4a) and (4.4b) of Chapter 3, and the normalization condition for the α_{Ib} one obtains

$$\alpha_{1b} = 0.152; \alpha_{2b} = 0.799; \alpha_{3b} = -.582,$$

where our choice of α_{1b} as positive fixes the signs of α_{2b} and α_{3b}.

Finally, we calculate the $|\alpha_{Ic}|$ using the relations

$$\sum_{\gamma=a,b,\ldots} \alpha_{I\gamma}^2 = 1 \qquad \text{for } I = 1, 2, 3,$$

and then determine the signs of the coefficients using the quantum phase behavior of the c-type bands (see Fig. 8). This yields

$$\alpha_{1c} = -.762; \alpha_{2c} = 0.525; \alpha_{3c} = 0.378.$$

As a whole, the eigenvector coefficient matrix is

$$\mathbf{C} = \begin{pmatrix} 0.629 & 0.295 & 0.720 \\ 0.152 & 0.799 & -.528 \\ -.762 & 0.525 & 0.378 \end{pmatrix}, \tag{4.2}$$

with the columns labelled by the molecular eigenstates and the rows labelled by the zero-order states. As pointed out in Chapter 3, a number of tests can be made on this calculated matrix. Firstly, the orthogonality of its rows and columns may be checked. Calculating the six possible cross-products, one finds no deviations from orthogonality of over 5.3^o and an average deviation of about 4^o. Secondly, the ***absolute*** modulation depths can be calculated from **C** and compared with experimental values. Such a comparison appears in Table 1. One sees that the calculated magnitudes are generally $\sim 20 - 30\%$ higher than the experimental ones, probably due to experimental limitations or unobserved eigenstates.

Using the values for **C** and **E**, one can calculate $\mathbf{H}_0$ up to various constants by (4.1) of Chapter 3. Doing so, one obtains

$$\mathbf{H}_0^{1380} = E_0 \mathbf{I} \pm \begin{pmatrix} 4.66 & -2.70 & 2.83 \\ -2.70 & 5.08 & -.38 \\ 2.83 & -.38 & 2.16 \end{pmatrix}, \tag{4.3}$$

where the three rows and columns are both labelled by a, b, and c. Note that the relative signs of the off-diagonal elements are not unique[9]. This is because the rows of **C** are only fixed up to an overall sign by the quantum beat results. Thus, instead of the distribution $(-1, +1, -1)$ for the signs of the interaction matrix elements (V_{ab}, V_{ac}, V_{bc}), one also could have obtained $(+1, -1, -1)$, $(+1, +1, +1)$, or $(-1, -1, +1)$ by different choices for the overall signs of the rows of **C**.

B. $E_{vib} = 1420$ cm^{-1}: The $a_g(5)$ mode

The 1420 cm^{-1} excitation band, which has been assigned in Ref. 14, is the one for which phase-shifted quantum beats were first discovered.[3] At that time the beating behavior appeared to arise from a coupled two-level system. Since then, with better time resolution it has become evident that the vibrational dynamics at this energy involve at least three coupled levels.[4] In this section we present and analyze the results for this band in a manner similar to the treatment of the 1380 cm^{-1} band in the previous section.

Results

The fluorescence spectrum resulting from the excitation of the 1420 cm^{-1} band is shown in Fig. 11 together with a high resolution spectrum of the region near the S_1 origin. The general characteristics of the spectrum are quite similar to the 1380 cm^{-1} spectrum; *i.e.*, there is a mix of assignable and unassignable bands, there is some resonance fluorescence, and there is resolvable spectral congestion in and to the red of the S_1 origin region.

Also similar to the 1380 cm^{-1} results, the time-resolved results reveal fluorescence decays which are beat-modulated and which depend on detection wavelength. Again, we shall discuss the various types of decays separately.

Fig. 12-top presents the decay of the 390 cm^{-1} band. Fourier analysis of the decay (Fig. 13-top) reveals three prominent beat components at 1.0, 9.7, and 10.7 GHz, all with positive phases and with absolute modulation depths of 0.55, 0.36, and 0.52, respectively. The 390 cm^{-1} decay is representative of a number of other decays, as well; those of the 0, 780, and 1168 cm^{-1} bands. (Note that all of these bands have counterparts in the group I, *a*-type bands of the 1380 cm^{-1} spectrum and that they are all assignable in terms of intervals associated with optically active modes.[14]) There are also other bands in the congested region of the spectrum near the S_1 origin which appear to exhibit decay behavior similar to the 390 cm^{-1} band (*e.g.*, the 1487 cm^{-1} band).

Fig. 12-middle presents the decay of the 1750 cm^{-1} band in the dispersed

fluorescence. As we have reported,[3,4] this decay shows an obvious 180° phase shift of the 1.0 GHz beat component relative to the +1 phase of the same beat component in the 390 cm^{-1} decay. Fourier analysis (Fig. 13-middle) reveals that besides this beat component, the decay is also modulated by at least four others: the 9.7 and 10.7 GHz components found in the 390 cm^{-1} decay, and two more components at 3.5 and 4.5 GHz. The absolute modulation depths for these components in order of increasing frequency are −0.74, −0.06, 0.04, −0.11, and 0.08. The sum of the modulation depths is −0.79. Although we have not measured the decays of the bands at 1750+390 and 1750+1408 cm^{-1} with 80 ps temporal resolution, previous measurements[3] of the decays showed that the decay behavior of these bands is consistent with that of the 1750 cm^{-1} band (*i.e.*, the 1 GHz component was found to have a large modulation depth and a negative phase).

A third band at 1500 cm^{-1} exhibits different decay behavior than both the 390 and 1750 cm^{-1} bands. Fig. 12-bottom presents the decay of this band and Fig. 13-bottom the Fourier spectrum of the residual. Despite the noise in the Fourier spectrum, three Fourier components are evident at 1.0, 9.7, and 10.7 GHz, with phases of +1, −1, and −1, respectively. Nominal values for the *relative* modulation depths derived from the 1500 cm^{-1} decay are 0.2, −0.9, and −1.0, in order of increasing beat frequency.

Finally, in Fig. 14 the decays for many of the prominent bands that appear in the region of the S_1 origin are presented. We shall not analyze these decays here extensively, since the limitations of spectral and temporal resolution prohibit any very quantitative analysis. It is evident that all of the decays are modulated to some extent by the 1 GHz beat component. Moreover, some, and perhaps all, are modulated prominently with the 9.7 and 10.7 GHz components, as well.

Interpretation

As with the results for the 1380 cm^{-1} band, it is desirable to come to an understanding of the number of coupled levels being manifested in the results for the 1420 cm^{-1} band. Just considering the Fourier spectrum (Fig. 13) for the

390 cm^{-1} decay, which exhibits one triplet of beat components, one would come to the conclusion that only three levels were involved. However, the 1750 cm^{-1} decay, with its five beat components (Fig. 13) is not consistent with this. Instead, the latter decay indicates that the 1.0, 9.7, and 10.7 GHz beat frequencies are just three of the six energy splittings expected for a four-level system. Considering the five beat components of the 1750 cm^{-1} decay as whole, one sees that they are consistent with the manifestations of a four-level system, *if* it is assumed that one beat component, at either 6.2 or 14.2 GHz, is undetectable due to weak modulation or (in the case of the 14.2 GHz component) an unresolvable frequency. In both cases there would be six beat components and four beat triplets, as expected[7] for a four-level system. (The former case would have the triplets (1.0, 3.5, 4.5), (1.0, 9.7, 10.7), (3.5, 6.2, 9.7) and (4.5, 6.2, 10.7), whereas the latter would have the triplets (1.0, 3.5, 4.5), (1.0, 9.7, 10.7), (3.5, 10.7, 14.2), and (4.5, 9.7, 14.2).) Note that no other values for the sixth beat frequency would be consistent with a four-level system. Note also how the 1420 cm^{-1} case differs from the 1380 cm^{-1} case, for which six beat frequencies were assigned to two independent three-level systems: unlike in the 1420 cm^{-1} case, in the 1380 cm^{-1} case the beat frequencies are such that there is no way to form four triplets.

All in all, the results indicate that the 390 cm^{-1} band is an *a*-type band and the 1750 cm^{-1} band is a non-*a*-type band (say *b*-type) of a coupled *four-level* system. The existence of a situation wherein four vibrational levels are coupled implies the existence of four types of fluorescence bands, each with different quantum beat phase behaviors. Obviously, we have observed two of these band types. We can also identify a third one: the band at 1500 cm^{-1}, which we call *c*-type. Our inability to identify a *d*-type band is probably due to problems associated with the spectral overlap of fluorescence bands.

Calculation of H_0

To calculate a four-by-four H_0 matrix for $E_{vib} = 1420$ cm^{-1}, an initial assumption must be made involving the value for the unknown sixth beat frequency.

We shall choose the lower value 6.2 GHz, since using it seems to give values for the elements of **C** which more nearly approximate those of an orthonormal matrix than the values calculated using 14.2 GHz for the sixth beat frequency. Hence we label the beat frequencies such that $|\omega_{12}/2\pi| = 1.0$ GHz, $|\omega_{23}/2\pi| = 3.5$ GHz, $|\omega_{34}/2\pi| = 6.2$ GHz, $|\omega_{13}/2\pi| = 4.5$ GHz, $|\omega_{24}/2\pi| = 9.7$ GHz, and $|\omega_{14}/2\pi| = 10.7$ GHz. This gives an eigenvalue matrix

$$\mathbf{E} = E_0\mathbf{I} \pm \begin{pmatrix} 0.0 & 0.0 & 0.0 & 0.0 \\ 0.0 & 1.0 & 0.0 & 0.0 \\ 0.0 & 0.0 & 4.5 & 0.0 \\ 0.0 & 0.0 & 0.0 & 10.7 \end{pmatrix}. \tag{4.4}$$

Next the eigenvector coefficient matrix **C** must be considered. We start with the calculation of the α_{Ia} from the relative modulation depths of the three detectable Fourier components modulating the 390 cm^{-1} a-type band. These values give

$$\alpha_{2a}^2 = .600\alpha_{1a}^2 \qquad \text{and} \qquad \alpha_{4a}^2 = .609\alpha_{1a}^2.$$

Because the Fourier amplitudes of the ω_{13}, ω_{23}, and ω_{34} components are so weak as to be undetectable, there is no way to calculate α_{3a}. One only knows that the value must be small. Thus, we make an assumption and fix the value of α_{3a} at 0.05. Then, with the normalization condition one finds the following values for the α_{Ia}:

$$\alpha_{1a} = 0.672,\ \alpha_{2a} = 0.521,\ \alpha_{3a} = 0.050,\ \alpha_{4a} = 0.525.$$

The next step is to calculate the α_{Ib}. Using the relative modulation depths of the beat components of the 1750 cm^{-1} b-type band and the normalization condition on the α_{Ib} one obtains

$$\alpha_{1b} = -.503,\ \alpha_{2b} = 0.699,\ \alpha_{3b} = -.498,\ \alpha_{4b} = -.095.$$

The α_{Ic} could conceivably be calculated using the relative modulation depths of the 1500 cm^{-1}, c-type band, but for the fact that some of the beat components are lost in the noise of the pertinent Fourier spectrum. Nevertheless, one can use

$$\frac{M_c(\omega_{14})\alpha_{2a}}{M_c(\omega_{24})\alpha_{1a}}\alpha_{2c} = \alpha_{1c}$$

to obtain $\alpha_{1c} = 0.86\alpha_{2c}$. Then using the orthogonality of the α_{Ic} with the α_{Ib} and the α_{Ia}, and, finally, the normalization of the α_{Ic}, one obtains

$$\alpha_{1c} = 0.316,\ \alpha_{2c} = 0.367,\ \alpha_{3c} = 0.350,\ \alpha_{4c} = -.802.$$

Lastly, the $|\alpha_{Id}|$ can be calculated using the relations

$$\sum_{\gamma=a,b,\ldots} \alpha_{I\gamma}^2 = 1 \qquad \text{for } I = 1, 4.$$

The relative signs of the α_{Id} can then be obtained from orthogonality requirements.

The calculated eigenvector matrix is

$$\mathbf{C} = \begin{pmatrix} 0.672 & 0.521 & 0.050 & 0.525 \\ -.503 & 0.699 & -.498 & -.095 \\ 0.316 & 0.367 & 0.350 & -.802 \\ 0.442 & -.324 & -.792 & -.269 \end{pmatrix}. \tag{4.5}$$

The largest deviation from orthogonality for any of the rows or columns is 3.0^o, with the average being about 1.5^o. In addition, the square root of the sum of the squares of the fourth row, which sum was not fixed by the calculation, is found to be very close to 1 (*i.e.*, 1.003). For each of the four types of the fluorescence bands the absolute modulation depths predicted from the calculated **C** are presented in Table 2 along with the available experimental values. Again the experimental values are consistently lower (by 20−30%) than the calculated ones, which deviation probably arises from the same causes as those which give rise to the less than ideal total modulation depth of the 1750 cm^{-1} band. One may note that the calculated values in Table 2 can serve to aid in the identification of the d−type bands. In particular, the calculated value of −0.73 for $M_d(\omega_{12})$ suggests that perhaps the band at 1521 cm^{-1} is d-type (see the decay in Fig. 14).

Just as for E_{vib} = 1380 cm^{-1}, $\mathbf{H}_0$ for E_{vib} = 1420 cm^{-1} may be calculated using (4.1) of Chapter 3. This results in

$$\mathbf{H}_0^{1420} = E_0\mathbf{I} \pm \begin{pmatrix} 3.23 & -.28 & -4.24 & -1.86 \\ -.28 & 1.70 & 0.29 & 1.82 \\ -4.24 & 0.29 & 7.57 & 0.94 \\ -1.86 & 1.82 & 0.94 & 3.70 \end{pmatrix}. \tag{4.6}$$

Again it must be noted that the distribution of signs for the off-diagonal elements in H_0 is not a unique one[7] and that other distributions are not precluded by the quantum beat results. In any case, the magnitudes of the coupling matrix elements are of the most interest, so this sign ambiguity is not particularly limiting.

C. E_{vib} = 1409, 1501, and 1514 cm^{-1}

The 1380 and 1420 cm^{-1} excitation bands occur in a region of the excitation spectrum which contains a number of other prominent bands,[14] the ones at 1409, 1501, and 1514 cm^{-1}. Given that the former two excitations give rise to dynamical behavior that is characteristic of restricted IVR, one might expect the latter three excitations to do so, as well. Previously published spectral evidence[15] has indeed indicated that restricted IVR influences the molecular dynamics at these energies. However, time-domain evidence has been lacking. Figs. 15, 16, and 17 provide such evidence for the 1409, 1501, and 1514 cm^{-1} excitations, respectively. In each figure the uppermost decay corresponds to detection of the 390 cm^{-1} band, which from spectroscopic considerations[14] and in analogy with the decay behavior of this band for E_{vib} = 1380 and 1420 cm^{-1}, should be a-type. Consistent with this, Fourier analysis of the three 390 cm^{-1} decays reveals that all beat components enter into the decays with +1 phases. On the other hand, each of the spectra arising from the three excitations also contain bands with different decays than the corresponding 390 cm^{-1} decay, the most notable differences being that some of the beat components appear with −1 phases. Examples of such decays are shown in the lower portions of Figs. 15-17. It is pertinent to note that the order of magnitude of the beat frequencies appearing in the decays of these figures is the same as for the beat components associated with 1380 and 1420 cm^{-1} excitations.

It is clear from the experimental results that the decay behaviors of the 1409, 1501, and 1514 cm^{-1} excitations are qualitatively similar to the behaviors of the 1380 and 1420 cm^{-1} excitation bands, and, moreover, are consistent with the manifestations of restricted IVR. Since the vibrational density of states (see section VI-A below) does not change much more than a factor of two in going from E_{vib} = 1380

$E_{vib} = 1380$ to $E_{vib} = 1514$ cm^{-1}, this similarity is not particularly surprising. The significance of the results is that they show the general occurrence of phase-shifted beats in the energy region corresponding to restricted IVR.

V. HIGH ENERGY: $E_{vib} = 1792\ cm^{-1}$

Above $E_{vib} = 1514\ cm^{-1}$ in S_1 anthracene, there are only a small number of excitation energies which yield dispersed fluorescence spectra with resolvable (or partially resolvable) structure[5,15] and which are thereby amenable to the direct study of IVR through the measurement of the temporal evolution of *individual* fluorescence band types. One such excitation corresponds to $E_{vib} = 1792\ cm^{-1}$, which is most likely a combination band of the 385 cm^{-1} (S_1 12) mode[14] with the 1409 cm^{-1} band. As may be seen from Fig. 18, the dispersed fluorescence spectrum which arises from this excitation is quite congested compared with lower energy spectra, but nevertheless has at least two discrete bands of weak intensity in the blue portion of the spectrum (the bands at 390 and 780 cm^{-1}) and also some incompletely resolved structure with overall strong intensity in the region near the S_1 origin. The 390 and 780 cm^{-1} bands (vibrationally unrelaxed or *a*-type bands), being assignable in terms of optically active modes, correspond to transitions from the optically prepared zero-order state. The bands in the congested region near the S_1 origin arise predominantly from zero-order states populated by the IVR process (vibrationally relaxed bands). Given that the two types of bands arise from different zero-order states, one expects differences in their decays to provide a picture of vibrational energy flow at this energy (see section VI-B of Chapter 3).

Fig. 19 presents the decays of the 390 and 780 cm^{-1} bands. It is evident that they are very similar. Fitting each according to the procedure of section II-C gives a short component lifetime of 22 psec and a long component lifetime of 6.4 nsec. Fig. 20 shows a typical fit to the data. We would make two points about the lifetimes obtained from the fits. Firstly, the short lifetime differs significantly from the value of ~75 psec that we have quoted in a preliminary work.[5] This discrepancy arises from the fact that in the previous work we fit only the initial portion of a given decay to a *single* exponential. Evidently, the contribution of the long-time component at early time is substantial enough to render such a procedure inaccurate. One expects the double exponential fitting procedure to yield a much more accurate fast

time constant. Secondly, the long-time component has a lifetime that matches the lifetime[15] of the total fluorescence decay at this energy, as one would expect from (6.7) of Chapter 3. Finally, it is worth noting that Fourier analysis (see Fig. 21) reveals that all of the large number of beat components which contribute to the decays of Fig. 19 have +1 phases as expected for an *a*-type band. (For comparison we include in Fig. 21 the uncluttered Fourier spectrum of the *a*-type 390 cm^{-1} decay corresponding to $S_1 + 1380$ cm^{-1} excitation.)

Since the 390 and 780 cm^{-1} bands are weak in intensity and occur in a region close to the excitation wavelength, several checks were made to ensure that the measured decays of these bands represent molecular decays and not scattered laser light. These checks included measuring decays at a detection wavelength of 3410 Å(Fig. 22a), a wavelength which is spectrally closer to the exciting light but at which there is no fluorescence, and measuring decays without any anthracene in the free-jet expansion (Fig. 22b). These checks yielded no evidence for any significant scatter contribution. Some leakage light was found to contribute to the decays. However, this spurious component was determined to be due to molecular fluorescence and to contribute to the long-time intensity of the decays. This is evident from Fig. 19-bottom, which shows an increased intensity of the long-time component of the 390 cm^{-1} decay for decreased spectral resolution of detection relative to that used to detect the decay of Fig. 19-top. Laser-to-nozzle distance and carrier gas dependences were also checked in order to assess the influence of intermolecular interactions on the observations. No significant effects of this kind were observed (see Fig. 23).

Fig. 24 presents decays corresponding to three fluorescence detection wavelengths in the region of the S_1 origin. There are several notable features of these decays. Firstly, each has a time constant of *ca.* 6 ns. Secondly, all of the decays are modulated, but exhibit different beat patterns. Finally, the decays all have finite risetimes. As may be seen from Fig. 24-bottom, which is a decay measured at the same detection wavelength as used for the decay above but at lower spectral

resolution, there is a pronounced spectral resolution effect on the decays measured in this region. Given a number of different types of fluorescence bands in the same spectral region, this is not surprising[7]. The apparent risetimes of the decays were examined in several ways to determine whether they were real risetimes. For example, all of the decays were compared with decays of the 390 cm^{-1} band measured immediately before or immediately after. In all cases the decays of Fig. 24 peaked after the 390 cm^{-1} decay did and appeared to rise at the same rate at which the short component of the 390 cm^{-1} transient decayed. Also, the smooth decay of Fig. 24-bottom, and others like it, were compared with calculated decays of 6 ns exponentials convoluted with the measured system response function. In all cases a significant difference between the calculated and measured decays was found, with the measured decays rising more slowly than the calculated ones. (Notably, this difference was not found for fluorescence at the same detection wavelength when the excitation was to $E_{vib} = 2750$ cm^{-1}.) Finally, Fourier analysis of the decays reveals Fourier components with negative phases. Such components must be present for a decay with a risetime. Notably, no components with negative phases modulate the 390 or 780 cm^{-1} decays.

We interpret the results for $E_{vib} = 1792$ cm^{-1} in terms of dissipative vibrational energy flow. The 390 and 780 cm^{-1} a-type decays, being direct representations of the $|a\rangle$ content of the excited state (see section VI of Chapter 3), show that vibrational energy redistributes dissipatively from $|a\rangle$ to the states coupled to $|a\rangle$ on a timescale of 22 psec. This initial redistribution of energy is also reflected in the risetimes of the decays of the bands near the S_1 origin, decays which are direct representations of the contributions of the states other than $|a\rangle$ to the excited state[7]. The presence of beats in the fluorescence decays is a manifestation of the fact that although the initial energy flow is substantially irreversible, it does not reach a steady state on the 22 ps timescale. Rather, the vibrational content of the excited state continues to evolve to some extent throughout the timescale of the fluorescence lifetime.

Regarding the number N of coupled vibrational levels being manifested in the fluorescence behavior of the $S_1 + 1792$ cm^{-1} excitation, it is more difficult to determine an accurate value than it is in the lower energy regime. This is a result of the large number of beat components in, and complicated Fourier spectra of, the 1792 cm^{-1} decays. Nevertheless, it is reasonably certain from the Fourier transform of the 390 cm^{-1} decay (Fig. 21) that greater than ten coupled levels give rise to the observed results. This is supported by the parameters derived from the fits to the decays of Fig. 19, since from these it is found that the ratio of fast to slow fluorescence in the decays is ~ 17. This ratio represents a lower limit to the number of coupled states in the dissipative regime (see section VI-B of Chapter 3). It is notable that if one assumes that the number of coupled levels at a particular E_{vib} scales with the vibrational density of states (see section VI-A below), then the roughly fivefold increase in this density in going from 1400 to 1800 cm^{-1}, along with the values of N at 1380 and 1420 cm^{-1}, would suggest that there are fifteen to twenty states coupled at $E_{vib} = 1792$ cm^{-1}.

The results for $E_{vib} = 1792$ cm^{-1} are also interpretable in terms of the dense intermediate case of radiationless transitions.[18] The vibrational coupling at this energy is such that the number of effectively coupled zero-order states N is larger than in the lower energy regime of restricted IVR (sparse intermediate case), but smaller than would be the case if the intrinsic linewidths of the states exceeded their energy spacings (statistical limit). This conclusion is reached by consideration of two facets of the fluorescence decays. Firstly, the short-time component of the 390 and 780 cm^{-1} decays and the rise times of the other decays are indicative of an intramolecular dephasing between the eigenstates composing the optically prepared state. Secondly, the presence in all of the decays of a long-time component with beats indicates that the dephasing does not preclude partial recurrences on the timescale of the fluorescence lifetime. The short-time behavior distinguishes the dense from the sparse intermediate case, while the presence of long-lived intramolecular coherence distinguishes the intermediate case from the statisical limit.[18]

VI. DISCUSSION AND CONCLUSIONS

A. IVR vs. vibrational energy

The experimental results presented above allow one to make a number of different conclusions concerning IVR in anthracene. The first pertain to the nature of the process as a function of vibrational energy in the molecule. It is clear in light of the discussion in section VI-B of Chapter 3 that the low, intermediate, and high energy results for anthracene represent manifestations of absent, restricted, and dissipative IVR, respectively. In the low energy regime ($\leq$ 1200 cm^{-1}), vibrational mixing is not extensive, if present at all. The excitation process prepares just one vibrational eigenstate which undergoes no further vibrational evolution. For somewhat higher energies (*i.e.*, 1380 to 1520 cm^{-1}) the vibrational coupling becomes appreciable; systems of coupled states involving two to approximately ten levels characterize the regime. Upon preparation of an optically active zero-order state, IVR occurs but is restricted in the sense that essentially full recurrences in the vibrational energy distribution occur on the timescale of the fluorescence lifetime. The timescale of IVR in the restricted regime is given by the order of magnitude of the inverses of the beat frequencies which modulate dispersed fluorescence decays. For anthracene the beat frequencies are on the order of 5 GHz, leading to a timescale for restricted IVR of several hundreds of picoseconds. Finally, at high energies (*e.g.*, E_{vib} = 1792 cm^{-1}) the extent of vibrational coupling is great enough (systems of $\geq$ 10 levels) that dissipative IVR occurs. In these cases, IVR is such that nothing close to a full recurrence occurs on the fluorescence timescale. The timescale of IVR in the dissipative regime is given by that of the initial, approximately exponential dephasing of the optically prepared state. For the E_{vib} = 1792 cm^{-1} band, $\tau_{ivr} \simeq$ 22 psec.

It is of interest to correlate changes in the nature of IVR in anthracene with the vibrational density of states (ρ_{vib}) in the S_1 manifold. We have calculated ρ_{vib} at various energies using a direct count procedure and the calculated frequencies of Refs. 19. The results are shown in Fig. 25. In the region of no IVR, ρ_{vib} is less than $\simeq$ 10 per wavenumber. For E_{vib} = 1380 to 1520 cm^{-1}, ρ_{vib} goes from $\sim$ 25

to 40 per cm^{-1}. And for $E_{vib} = 1800$ cm^{-1}, $\rho_{vib} \simeq 120$ per cm^{-1}. These values of ρ_{vib} for the different regimes of IVR in anthracene are useful for two reasons. Firstly, they suggest that vibrational coupling in the molecule is selective. For instance, at $E_{vib} = 1380$ cm^{-1} there are three strongly coupled vibrational states within an 8.4 GHz energy interval. But, if there were mixing between all the states in this interval, then since $\rho_{vib} = 25$ per cm^{-1} one would expect at least twice as many coupled levels. A similar point can be made for the $E_{vib} = 1420$ and 1792 cm^{-1} excitations; the number of coupled levels is less than would be expected from consideration of the total density of vibrational states. This selectivity in coupling is not unreasonable. For vibrational states to be coupled by anharmonic interactions, they must have the same vibrational symmetry. In D_{2h} anthracene this means that a given vibrational state can couple anharmonically with at most one-eighth of the total number of other states in the molecule. Thus, selectivity in coupling is expected on the basis of symmetry considerations. Secondly, the specific values for ρ_{vib} are useful for their predictive value. Using these values, symmetry considerations, and knowledge of ρ_{vib} *vs.* energy one can make predictions of the nature of IVR as a function of energy for other molecules.

A last point of interest concerning IVR as a function of energy in anthracene derives from the connection between IVR behavior and quasi-periodic or ergodic vibrational dynamics in molecules.[20] For a model Hamiltonian (Henon-Heiles), the transition with increasing energy from classical mechanical quasi-periodic to ergodic vibrational dynamics has been found[21] to be correlated with quantum mechanical quantities derived from the same Hamiltonian. Regular, periodic behavior of the quantity

$$\wp_\gamma(t) \equiv |\langle \Psi(t)|\gamma\rangle|^2, \tag{6.1}$$

which is the contribution of the harmonic state $|\gamma\rangle$ to the time dependent vibrational wavefunction $|\Psi(t)\rangle$, correlates with classical quasi-periodic behavior. On the other

hand, irregular behavior of $\wp_\gamma(t)$ correlates with classical chaotic behavior. Since

$$\wp_\gamma(t) \sim I_\gamma(t), \tag{6.2}$$

where $I_\gamma(t)$ is the intensity *vs.* time of a γ-type fluorescence band (see section VI-A, Chapter 3), then the decays of fluorescence bands are indicators of quasi-periodic or ergodic vibrational dynamics. The upshot is that the regular, periodic decays characterizing the restricted IVR regime in anthracene suggest quasi-periodic quantum dynamics, while the less regular, high energy dissipative decays suggest quantum chaotic behavior. Thus, time-resolved measurements of dispersed fluorescence promise to be very useful in the study of the nature and onset of quantum chaos.

B. Coupling matrix elements

Besides providing information concerning the nature and timescale of IVR in anthracene, the experimental results also provide information pertaining to the details of the couplings which give rise to IVR. Thus, for the restricted IVR that occurs for $E_{vib} = 1380$ and $1420\ \mathrm{cm}^{-1}$, one can see from (4.3) and (4.6) that the magnitudes of the coupling matrix elements between zero-order states range from 0.3 to 4.2 GHz. For the dissipative $1792\ \mathrm{cm}^{-1}$ case, the variance in coupling matrix elements, $\bar{V}$, can be calculated[22] by using the golden rule-type expression $\frac{1}{\tau_{ivr}} \simeq 2\pi\bar{V}^2\rho$ and by assuming that because of symmetry selectivity in coupling, $\rho = \frac{\rho_{vib}}{8} = 15$ per cm^{-1} (0.5 per GHz). This gives $|\bar{V}| = 3.8$ GHz. It is clear therefore that coupling matrix elements on the order of several GHz heavily influence both restricted and dissipative IVR in the molecule.

Another point concerning the vibrational coupling elements in anthracene pertains to the distribution of the coupling between zero-order states. One can see from (4.3) and (4.6) that significant coupling occurs between all the coupled zero-order states. Thus, for instance, one would be mistaken in viewing the IVR process as arising from the coupling of an optically active state with a manifold of uncoupled bath states. There *is* coupling within the bath manifold, and this coupling affects the IVR dynamics.

C. The purity of optically prepared states

As we have discussed in section V of Chapter 3, various experimental limitations can prevent the complete characterization of IVR processes by time-resolved spectroscopy. One limitation of a fundamental nature involves the inability to optically prepare *all* the eigenstates that arise from the coupling of a given set of zero-order states. In cases where this limitation applies, the optically prepared state is not a pure zero-order harmonic vibrational state. At the very outset the vibrational energy is distributed amongst a number of vibrational motions.

Under the conditions of our experiments, we are able to coherently prepare eigenstates within a range of approximately 2 cm^{-1}. Therefore, any coupling interactions on this order will prevent the preparation of a pure zero-order state. There is experimental evidence that vibrational couplings of this magnitude are present in anthracene. Firstly, the sums of the absolute quantum beat modulation depths of the non-a-type fluorescence bands for $E_{vib} = 1380$ and 1420 cm^{-1} are not -1. This kind of behavior can be the result of the inability to prepare a pure zero-order state (see section V-A of Chapter 3). A second point related to the first is that the absolute modulation depths calculated from the eigenvector matrices (4.2) and (4.5) are consistently greater in magnitude than observed modulation depths. This, too, can be due to an impure initial state. Finally, evidence from excitation spectra indicates that Fermi resonances that give rise to splittings on the order of several cm^{-1} are prevalent in anthracene.

All of this evidence points to the fact that one must be somewhat cautious in determining the purity of the $|a\rangle$ state. For anthracene, it probably is the case in the restricted regime that impure initial states are prepared by the laser, although the sums of absolute modulation depths for non-a-type bands are close enough to -1 to suggest that the degree of impurity is not particularly great.

D. Spectral vs. temporal measurements

In light of the previous section, it is pertinent to discuss the merits of time-resolved *vs.* time-integrated approaches to the experimental study of IVR and

vibrational coupling. On the one hand, we have seen that the limitations of finite excitation bandwidth and finite temporal resolution can restrict the utility of time-resolved techniques to the regime of relatively small magnitude matrix elements. In the cases of large magnitude matrix elements, time-integrated fluorescence excitation spectra can provide valuable information about long range coupling that is unavailable from fluorescence decays. On the other hand, time-resolved measurements have many advantages over fluorescence excitation and dispersed fluorescence studies. Medium resolution (~ 0.05 cm^{-1}) excitation spectra are only useful for the study of couplings with matrix elements on the order of, or greater than, rotational contour widths (one to several wavenumbers for jet-cooled large molecules). For smaller couplings, rotational congestion necessitates taking Doppler-free excitation spectra to obtain the number and distribution of the eigenstates resulting from the coupled system of zero-order levels. Whatever the magnitudes of the matrix elements, it is never certain from excitation spectra alone that the structure in them arises from a coupled system of levels. This is in contrast to time-resolved measurements which, by virtue of quantum beat phases behavior, can differentiate between the manifestations of coupled *vs.* uncoupled states.

Time-integrated dispersed fluorescence measurements also have limited utility in the study of IVR. Such measurements cannot provide detailed information pertaining to the evolution of vibrational energy in a molecule. For instance, the dispersed fluorescence spectra arising from excitations into the restricted IVR regime look very much the same as the spectra resulting from excitation into the dissipative IVR regime. It is only with knowledge from time-resolved studies that one can confidently make conclusions about the nature of IVR behavior. Also, in determining timescales for IVR, dispersed fluorescence measurements are limited. There is no way by such measurements to determine the recurrence times characterizing vibrational energy flow in the restricted regime. In the dissipative regime, one can in principle determine the timescale for IVR by measurements of the relative intensities of vibrationally relaxed and unrelaxed bands in a given spectrum. The

problem with such measurements is that both types of fluorescence occur together in the congested region at and to the red of the 0_0^0 energy. There is no accurate way to separate out the two types of contributions in this region unless one has precise knowledge of the emission Frank-Condon factors for the optically prepared state.

E. Future directions

The results and conclusions of this chapter point to several areas wherein further work could add significantly to the understanding of IVR in anthracene in particular, and large molecules in general. One such area is the role of rotations. Herein and in Chapter 3, we have neglected rotations and, thereby, have assumed implicitly the prevalence of anharmonic coupling interactions in IVR. In the following chapter we show how the rotational level structure can affect anharmonic interactions. More detailed work, both experimentally and theoretically, is needed, however, to assess the influence and manifestations of Coriolis coupling.

A second area involves the question of the significance of large magnitude matrix elements in the vibrational coupling of large molecules. As we have mentioned earlier, work directed toward this problem is in progress.[16]

A final area involves the determination of the S_1 vibrational normal modes of anthracene, with the aim of ultimately trying to make the connection between observed coupling matrix elements and the natures of the vibrational states that are coupled. One wonders if *all* zero-order states of a given symmetry within a given energy interval are significantly coupled, or if, on the other hand, there are propensity rules governing the magnitudes of the couplings between various types of vibrations. Such knowledge is of obvious importance to the understanding of both IVR and vibrational level-specific dynamics.

REFERENCES

1. W. R. Lambert, P. M. Felker, and A. H. Zewail, J. Chem. Phys. **75**, 5958(1981).
2. W. R. Lambert, P. M. Felker, and A. H. Zewail, J. Chem. Phys. **81**, 2217(1984).
3. P. M. Felker and A. H. Zewail, Chem. Phys. Lett. **102**, 113(1983).
4. P. M. Felker and A. H. Zewail, Phys. Rev. Lett. **53**, 501(1984).
5. P. M. Felker and A. H. Zewail, Chem. Phys. Lett. **108**, 303(1984).
6. See, for example: C. Lewis, W. R. Ware, L. J. Doemeny, and T. L. Nemzek, Rev. Sci. Instr. **44**, 107(1973).
7. P. M. Felker and A. H. Zewail, J. Chem. Phys. - submitted.
8. W. Kaplan, *Advanced Calculus* (Addison-Wesley, Reading, Mass., 1973), pp. 512-14.
9. (a) J. W. Cooley and J. W. Tukey, Math. Comput. **19**, 297(1965); (b) E. O. Brigham, *The Fast Fourier Transform* (Prentice-Hall, Englewood Cliffs, NJ, 1974).
10. E. Bartholdi and R. R. Ernst, J. Magn. Reson. **2**, 9(1973).
11. P. M. Felker and A. H. Zewail, J. Chem. Phys. - submitted.
12. P. R. Bevington, *Data Reduction and Error Analysis for the Physical Sciences* (McGraw-Hill, New York, 1969).
13. J. Chaiken, M. Gurnick, and J. D. McDonald, J. Chem. Phys. **74**, 106(1981).
14. W. R. Lambert, P. M. Felker, J. A. Syage, and A. H. Zewail, J. Chem. Phys. **81**, 2195(1984).
15. W. R. Lambert, P. M. Felker, and A. H. Zewail, J. Chem. Phys. **81**, 2209(1984).
16. B. W. Keelan and A. H. Zewail - submitted.
17. This interpretation is further supported by results reported in Ref. 16, which show that there are indeed two overlapping rotational band contours separated by about one wavenumber in the 1380 cm^{-1} region of the anthracene excitation spectrum.
18. K. F. Freed and A. Nitzan, J. Chem. Phys. **73**, 4765(1980).
19. (a) D. J. Evans and D. B. Scully, Spectrochim. Acta **20**, 891(1964); (b) B. N. Cyvin and S. J. Cyvin, J. Phys. Chem. **73**, 1430(1969). Note that the values reported in these papers represent those calculated for S_0 modes. One expects that the S_1 values are lower on the average than these. Therefore, in reality the ρ_{vib} *vs.* E_{vib} curve of Fig. 25 probably is shifted somewhat toward lower energies.

20. For a review see: D. W. Noid, M. L. Koszykowski, and R. A. Marcus, Ann. Rev. Phys. Chem. **32**, 267(1981).

21. For example, (a) G. Hose and H. S. Taylor, Chem. Phys. **84**, 375(1984); (b) M. D. Feit and J. A. Fleck, Jr., J. Chem. Phys. **80**, 2578(1984).

22. C. Tric, Chem. Phys. **14**, 189(1976).

Table 1. Calculated and observed absolute modulation depths for bands in the $E_{vib} = 1380\ cm^{-1}$ spectrum of anthracene.

Band-type	Individual modulation depths			Sum of modulations
	3.5 GHz	4.9 GHz	8.4 GHz	
a-type:				
calculated	+0.16	+0.21	+0.95	+1.26
observed	+0.12	+0.16	+0.75	+1.03
b-type:				
calculated	+0.22	−0.86	−0.35	−0.99
observed	+0.14	−0.63	−0.26	−0.75
c-type:				
calculated	−0.45	+0.26	−0.80	−0.99
observed	−0.45	+0.16	−0.41	−0.70

Table 2. Calculated and observed absolute modulation depths for bands in the $E_{vib} = 1420$ cm^{-1} spectrum of anthracene.

Band-type	Individual modulation depths						Sum of
	1.0	3.5	4.5	6.2	9.7	10.7 GHz	modulations
a-type:							
calculated	+0.69	+0.004	+0.006	+0.004	+0.42	+0.70	+1.82
observed	0.55	—	—	—	+0.36	+0.52	+1.43
b-type:							
calculated	−0.98	−0.07	+0.07	+0.01	−0.15	+0.13	−0.99
observed	−0.74	−0.06	+0.04	—	−0.11	+0.08	−0.79
c-type:							
calculated	+0.31	+0.03	+0.03	−0.06	−0.62	−0.68	−0.99
d-type:							
calculated	−0.73	+0.10	−0.17	+0.08	+0.34	−0.61	−0.99

FIGURE CAPTIONS

1. Dispersed fluorescence spectrum and fluorescence decay resulting from excitation of jet-cooled anthracene to $S_1 + 766\ cm^{-1}$ (12^2). The fluorescence spectrum was obtained with 1.6 Å monochromator resolution ($\equiv R$). An arrow marks the excitation wavelength. The decay corresponds to detection of the 390 cm^{-1} band in the spectrum with $R = 3.2$ Å.

2. Dispersed fluorescence spectra resulting excitation of jet-cooled anthracene to $S_1 + 1380\ cm^{-1}$. The upper portion is a high resolution ($R = 0.5$ Å) trace of the region in and about the wavelength of the 0_0^0 transition of the molecule. The lower portion taken with $R = 1.6$ Å covers a wider range and includes the excitation wavelength (arrow). Various bands in the spectra are marked with their shifts in cm^{-1} from the excitation energy.

3. Fluorescence decays of group I bands (see text) in the $E_{vib} = 1380\ cm^{-1}$ spectrum of anthracene. The shifts of the bands from the excitation energy are given in the figure. Since these bands are relatively isolated spectrally, low detection resolution was used to maximize the signal. From top to bottom $R = 24$, 16, and 5 Å.

4. Fourier spectra of decay residuals (see section II-B) for the 390 cm^{-1} band in the $E_{vib} = 1380\ cm^{-1}$ spectrum of anthracene for three slightly different excitation energies. All other experimental conditions were the same for the decays. The top spectrum corresponds to excitation at the band maximum, the middle spectrum to excitation about 2 cm^{-1} to the red of this, and the bottom spectrum about 2 cm^{-1} to the blue of the maximum. Prominent Fourier bands are labelled with their frequencies in GHz. Note that some bands change in relative intensity from spectrum to spectrum. Note also that all bands have positive amplitudes (+1 phases).

5. Fluorescence decays of group II bands in the $E_{vib} = 1380\ cm^{-1}$ spectrum of anthracene. The shifts of the bands from the excitation energy are given in the figure. From top to bottom $R = 0.5$, 1.0, and 1.6 Å.

6. Fourier spectrum of the residual of the decay of Fig. 5-top. Fourier bands are labelled with their frequency values in GHz. Note that two of these bands have -1 phases and one has a $+1$ phase.

7. Fluorescence decays of group III bands in the $E_{vib} = 1380$ cm^{-1} spectrum of anthracene. The shifts of the bands from the excitation energy are given in the figure. From top to bottom $R = 0.8$, 1.0, 1.0, and 1.3 Å.

8. Fourier spectrum of the residual of the decay of Fig. 7-top. Bands are labelled with their frequency values in GHz. Note that two of the bands have -1 phases and one has a $+1$ phase. Note also, however, that the phase behavior is different from that in Fig. 6.

9. Fluorescence decays of group IV bands in the $E_{vib} = 1380$ cm^{-1} spectrum of anthracene. The shifts of the bands from the excitation energy are given in the figure. For all decays $R = 1.6$ Å.

10. Fluorescence decays of the 1125 cm^{-1} band in the $E_{vib} = 1380$ cm^{-1} spectrum of anthracene on long (top) and short (bottom) timescales. The decays are modulated principally at 0.2 GHz. The top decay was taken with $R = 1.6$ Å and the bottom with $R = 3.2$ Å.

11. Dispersed fluorescence resulting from excitation of jet-cooled anthracene to $S_1 + 1420$ cm^{-1}. The upper portion was taken with $R = 0.6$ Å and the lower with $R = 1.6$ Å. Various bands in the spectra are marked with their shifts in cm^{-1} from the excitation energy.

12. Representative decay types for fluorescence bands in the $E_{vib} = 1420$ cm^{-1} spectrum of anthracene. The wavenumber shifts of the bands from the excitation energy are given in the figure. From top to bottom $R = 16.0$, 1.6, and 1.6 Å.

13. Fourier spectra of the residuals of the decays of Fig. 12. Bands in the middle spectrum are labelled with values in GHz. Although there appear to be more than three components in the lower spectrum, only the ones at 1.0, 9.7, and 10.7 GHz are reproducible. Any other apparent bands in this spectrum are

therefore probably noise.

14. Fluorescence decays of bands in the $E_{vib} = 1420$ cm^{-1} spectrum of anthracene that occur near the 0_0^0 transition energy of the molecule (see the spectrum of Fig. 11-top). The wavenumber shifts of the bands from the excitation energy are given in the figure. From top to bottom $R = 1.6$, 1.6, 0.8, 1.6, and 1.6 Å.

15. Fluorescence decays of two bands in the $E_{vib} = 1409$ cm^{-1} spectrum of jet-cooled anthracene. The wavenumber shifts of the bands from the excitation energy are given in the figure. For the upper decay $R = 16$ Å, for the lower $R = 1.6$ Å. Note that the 390 cm^{-1} band is very isolated spectrally compared with the 1640 cm^{-1} band (see Ref. 15). Thus it was possible to use a relatively large value of R in measuring the 390 cm^{-1} decay. The same holds true for the 390 cm^{-1} decays in Figs. 16 and 17.

16. Fluorescence decays of two bands in the $E_{vib} = 1501$ cm^{-1} spectrum of anthracene. The wavenumber shifts of the bands from the excitation energy are given in the figure. For the upper decay $R = 24$ Å, and for the lower one $R = 1.6$ Å.

17. Fluorescence decays of two bands in the $E_{vib} = 1514$ cm^{-1} spectrum of anthracene. The wavenumber shifts of the bands from the excitation energy are given in the figure. For the upper decay $R = 32$ Å, and for the lower one $R = 2.4$ Å.

18. Dispersed fluorescence resulting from excitation of jet-cooled anthracene to $S_1 + 1792$ cm^{-1}. The upper portion was taken with $R = 0.5$ Å. For the lower portion $R = 1.6$ Å for the main spectrum and $R = 3.2$ Å for the inset, which corresponds to the vibrationally unrelaxed region. Various bands in the spectra are labelled with their wavenumber shifts from the excitation energy.

19. Fluorescence decays for the 390 and 780 cm^{-1} bands in the spectrum of anthracene excited to $S_1 + 1792$ cm^{-1}. The top two decays were taken with $R = 3.2$ Å. For the bottom decay $R = 32$ Å. A slight increase in the relative intensity of the long-time component is apparent in the lower decay compared

with the upper two.

20. Double exponential fit (line) to the measured decay of Fig. 19-bottom. The weighted difference (residual) between the observed decay and the fitted curve appears at the top of the figure. Best fit values of the two lifetimes and the ratio of fast to slow fluorescence are given in the figure. One notes that the best fit fast to slow ratio is greater than what one would judge by eye from the decay because the finite temporal response of detection tends to reduce the apparent magnitude of the fast component.

21. Top and middle: Fourier spectra ($I(\omega)$—section II-B) of the decay of Fig. 19-bottom. The top spectrum is the same as the middle one but is expanded along the ordinate. Bottom: The Fourier spectrum of the decay of the 390 cm^{-1} band in the E_{vib} = 1380 cm^{-1} spectrum (see Fig. 4-bottom), presented to provide an idea of the kind of Fourier "structure" (note the oscillations) to be expected as a result of the truncation of measured decays.

22. (a) Decays measured for similar collection for on-resonance (top) and off-resonance (bottom) detection, and for excitation of anthracene to E_{vib} = 1792 cm^{-1}. Conditions for both decays (R = 3.2 Å) were identical except for detection wavelength. (b) Decays measured for similar collection times and under the same experimental conditions (excitation to E_{vib} = 1792 cm^{-1}, detection of the 390 cm^{-1} band with R = 3.2 Å) except that the bottom decay corresponds to a situation wherein the free-jet expansion was devoid of anthracene.

23. Fluorescence decays of the 390 cm^{-1} band in the E_{vib} = 1792 cm^{-1} spectrum of anthracene for (a) different carrier gas conditions and (b) different laser to nozzle distances. For the decays in (a), R = 32 Å. In (b), R = 16 Å.

24. Fluorescence decays of bands in the vibrationally relaxed region of the E_{vib} = 1792 cm^{-1} spectrum of anthracene (see Fig. 18-top). Wavenumber shifts of the detected bands from the excitation energy are given in the figure. From top to bottom, R = 1.6, 3.2, 1.6, and 16 Å.

25. Vibrational density of states (ρ_{vib}) *vs.* vibrational energy (E_{vib}) in anthracene calculated using a direct count method and the frequencies of Refs. 19. Given in the figure are characteristic times for IVR in the absent, restricted, and dissipative regimes.

Figure 1

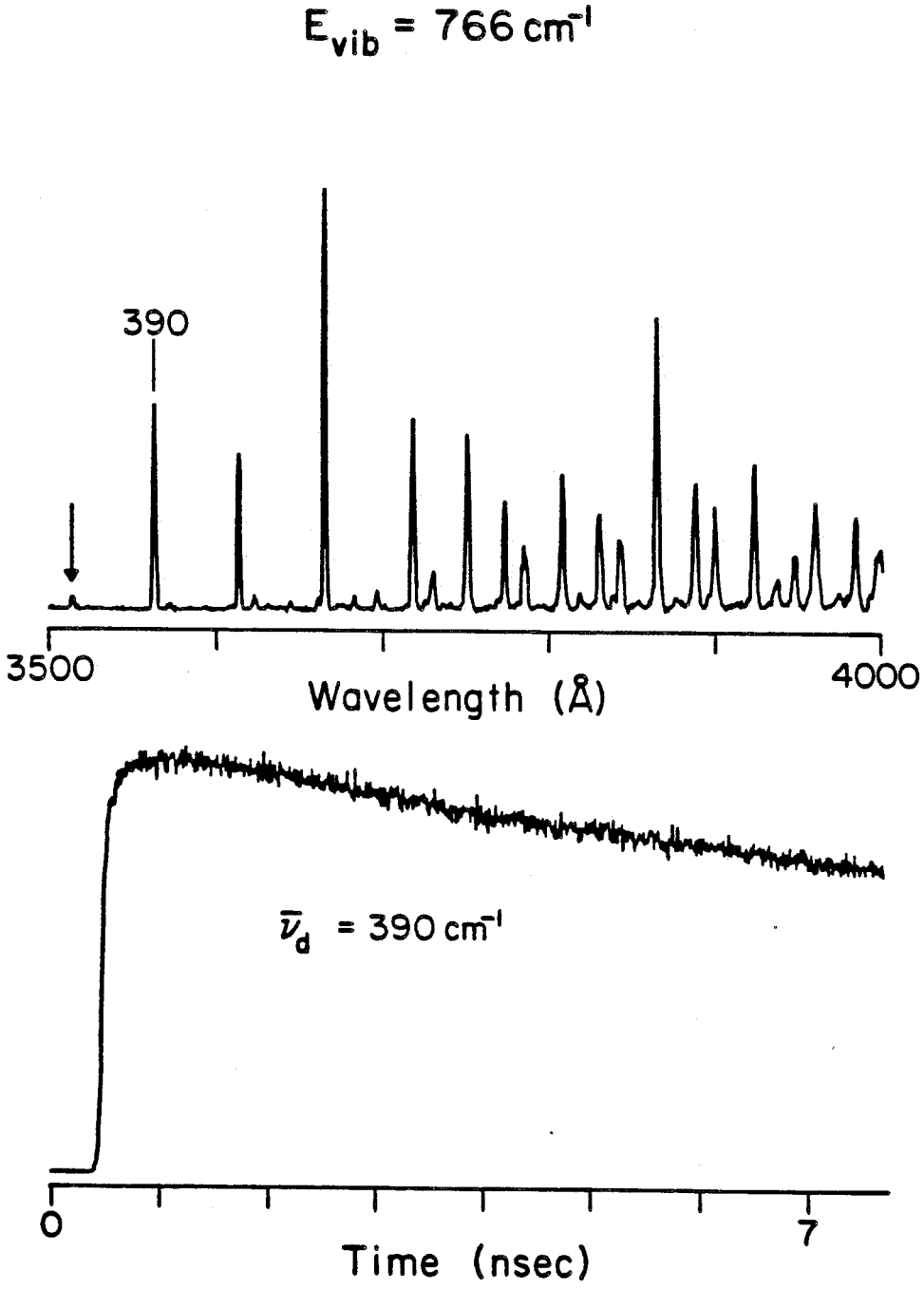
E_{vib} = 766 cm^{-1}
390
3500
4000
Wavelength (Å)
$\bar{\nu}_d$ = 390 cm^{-1}
0
7
Time (nsec)

Figure 2

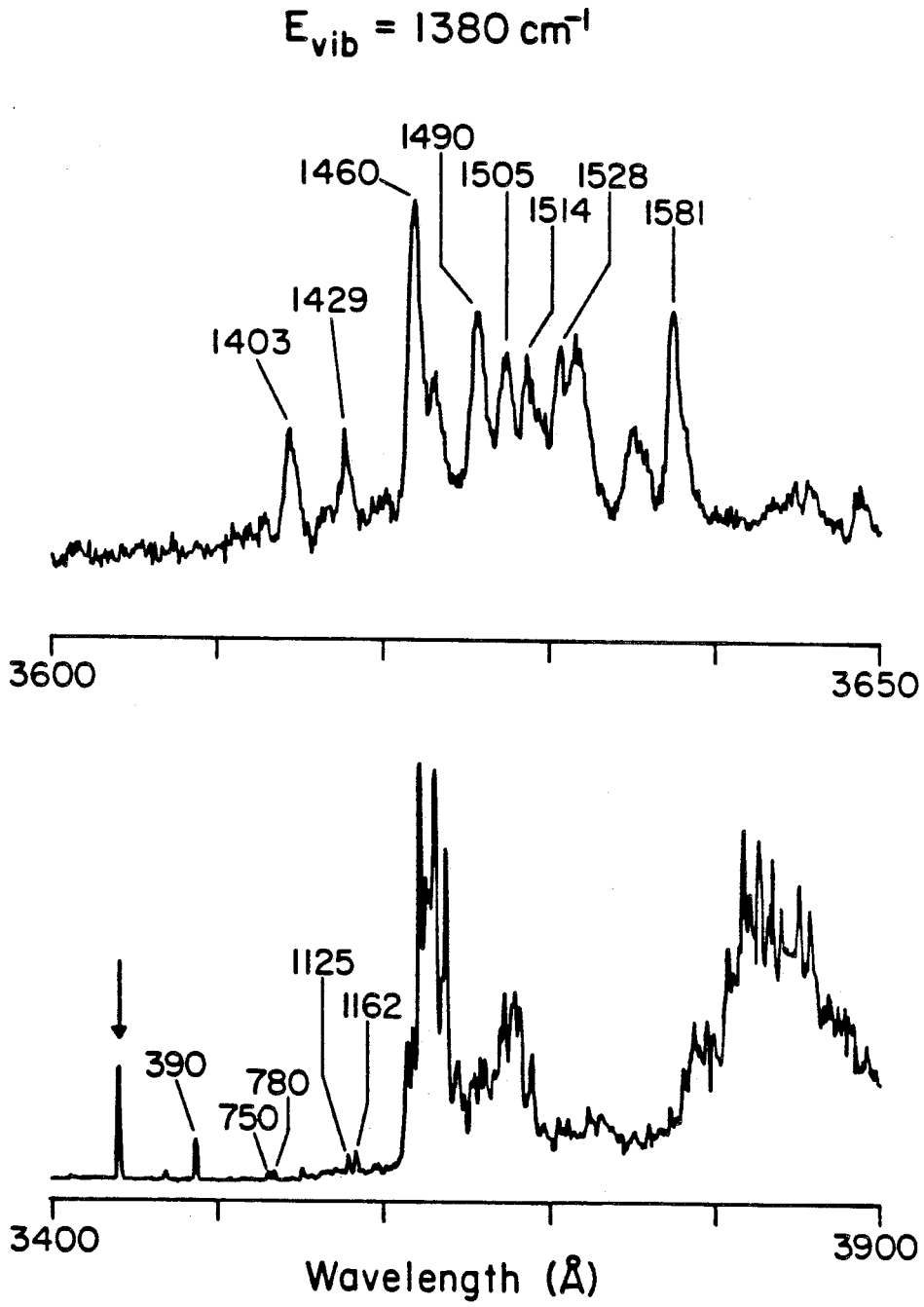
E_{vib} = 1380 cm^{-1}
1490
1460
1505
1528
1514
1581
1429
1403
3600
3650
1125
1162
390
780
750
3400
3900
Wavelength (Å)

Figure 3

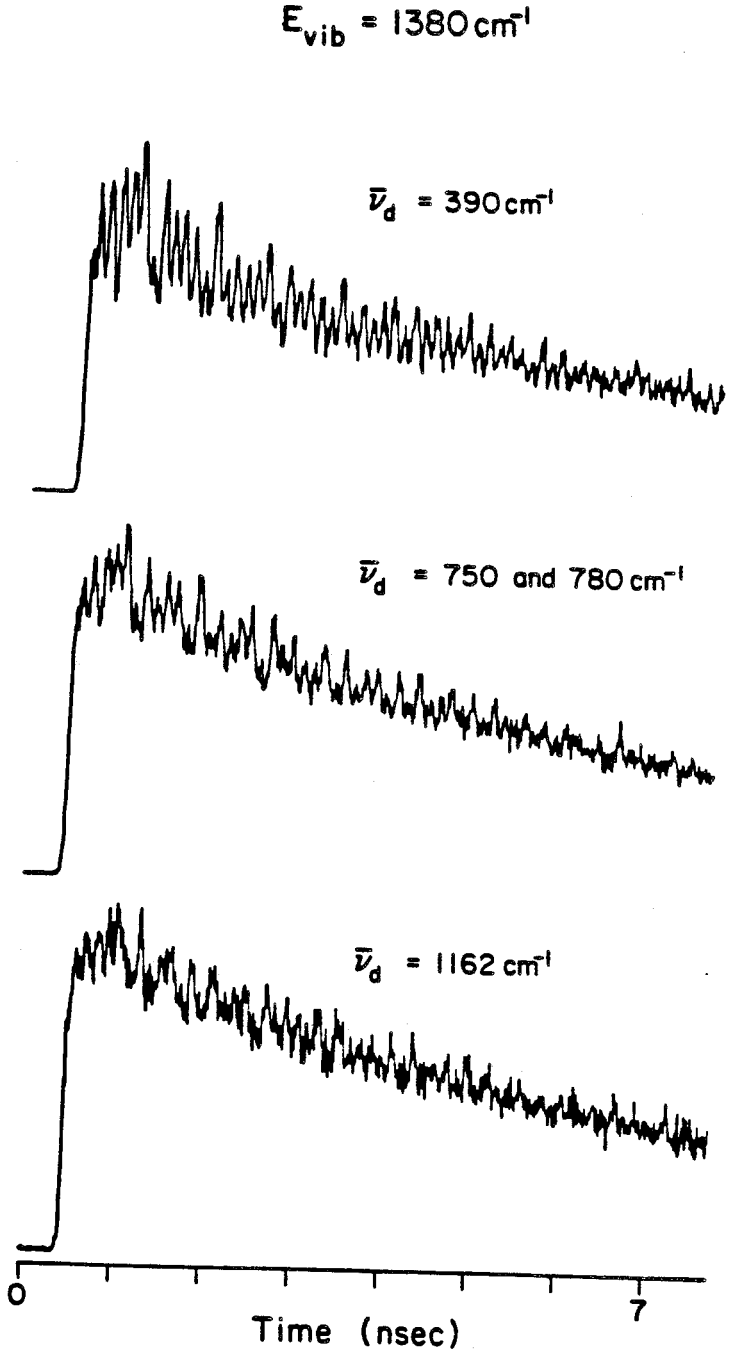
E_{vib} = 1380 cm^{-1}
$\bar{\nu}_d$ = 390 cm^{-1}
$\bar{\nu}_d$ = 750 and 780 cm^{-1}
$\bar{\nu}_d$ = 1162 cm^{-1}
0
7
Time (nsec)

Figure 4

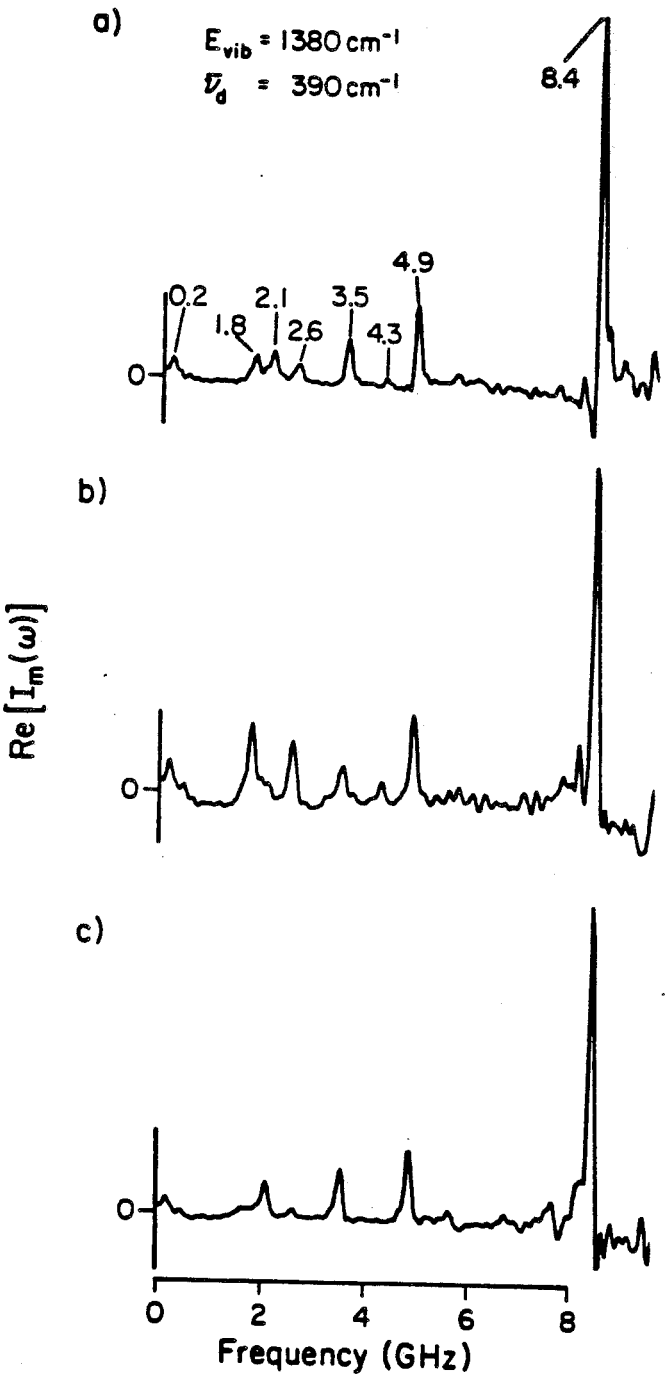
a)
E_{vib} = 1380 cm^{-1}
ν_d = 390 cm^{-1}
8.4
4.9
0.2
2.1
3.5
1.8
2.6
4.3
0
b)
Re [$I_m(\omega)$]
0
c)
0
0
2
4
6
8
Frequency (GHz)

Figure 5

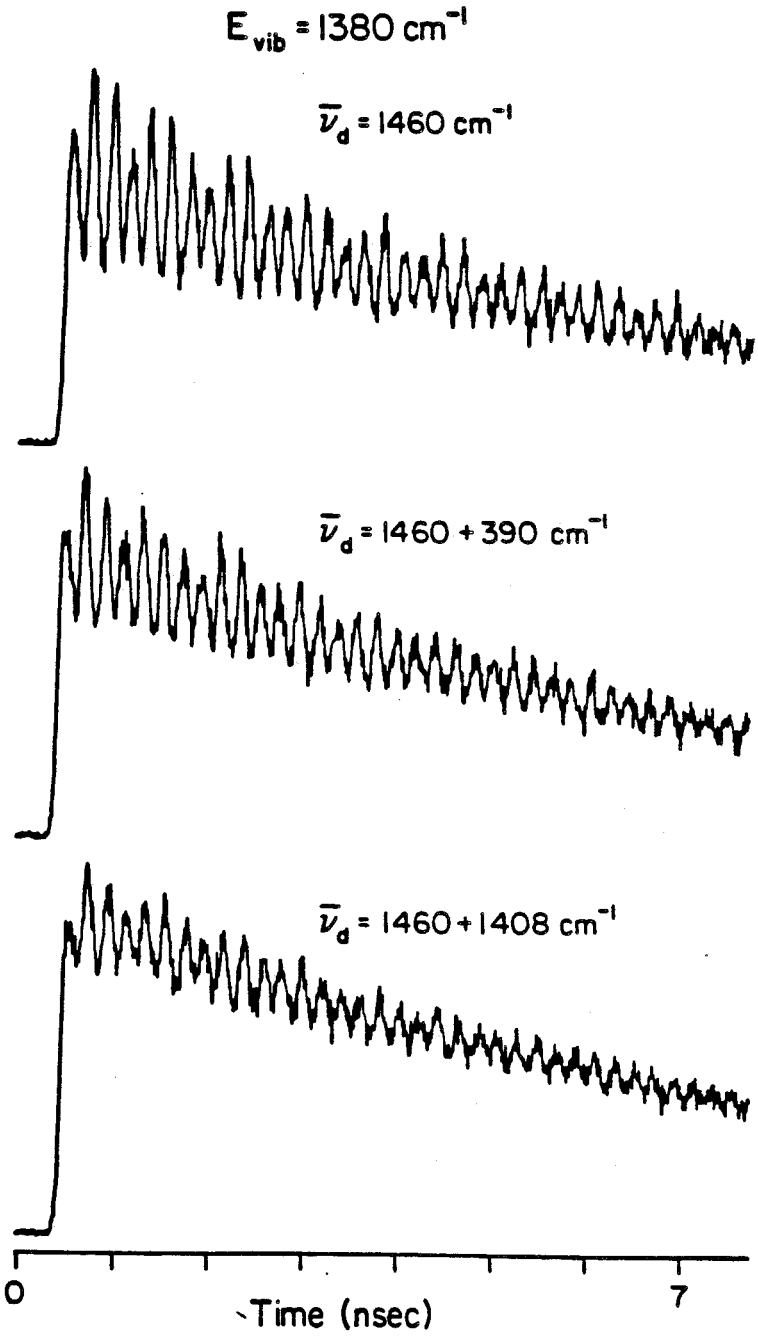
E_{vib} = 1380 cm^{-1}
$\bar{\nu}_d$ = 1460 cm^{-1}
$\bar{\nu}_d$ = 1460 + 390 cm^{-1}
$\bar{\nu}_d$ = 1460 + 1408 cm^{-1}
0
7
Time (nsec)

Figure 6

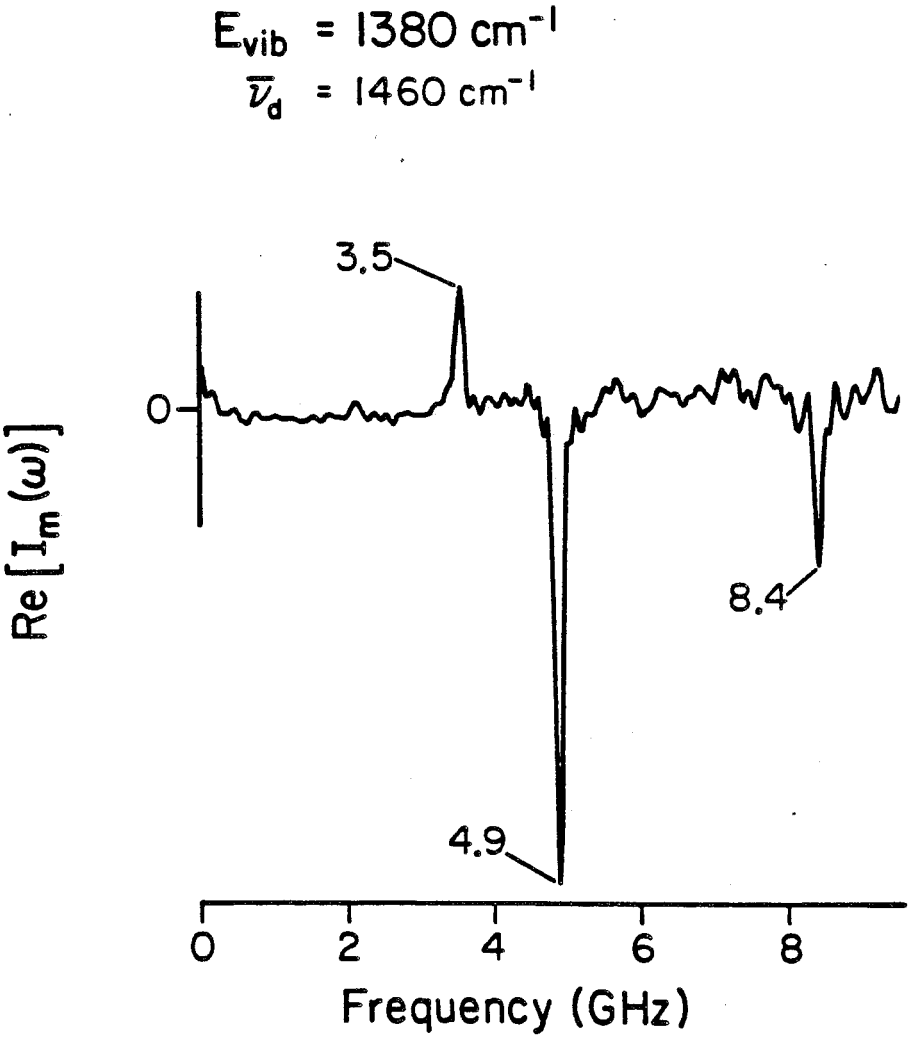
E_{vib} = 1380 cm^{-1}
$\bar{\nu}_d$ = 1460 cm^{-1}
3.5
0
8.4
4.9
Re [I_m (ω)]
0
2
4
6
8
Frequency (GHz)

Figure 7

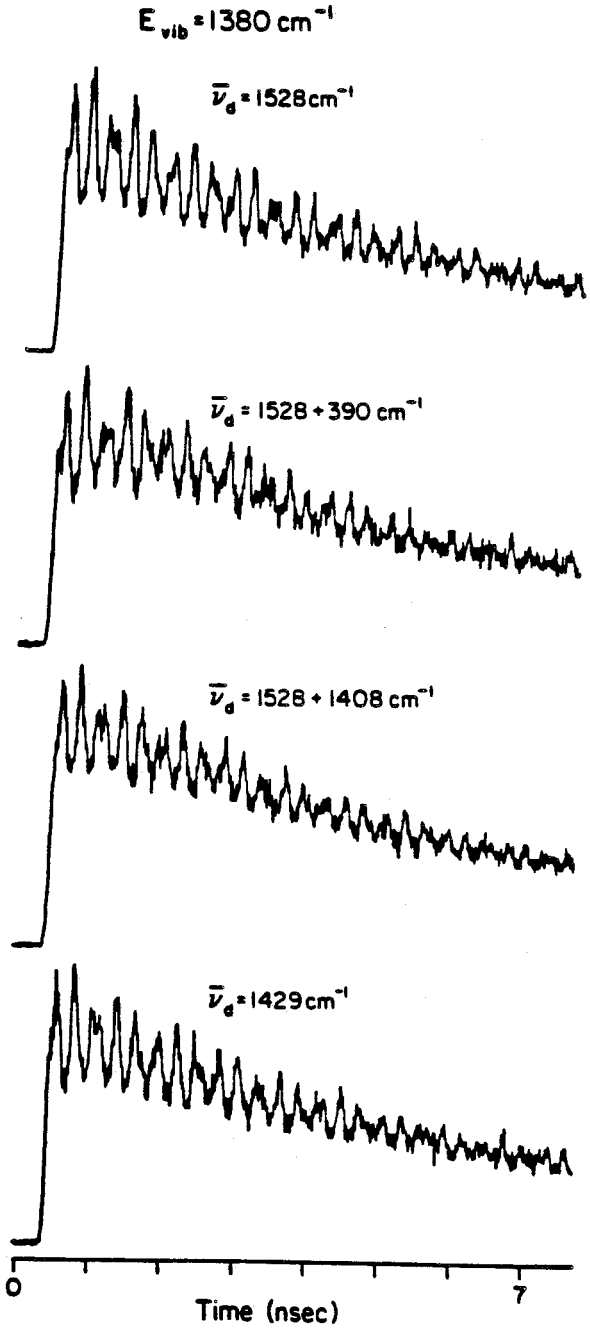
E vib = 1380 cm⁻¹
ν̄d = 1528cm⁻¹
ν̄d = 1528 + 390 cm⁻¹
ν̄d = 1528 + 1408 cm⁻¹
ν̄d = 1429cm⁻¹
0
7
Time (nsec)

Figure 8

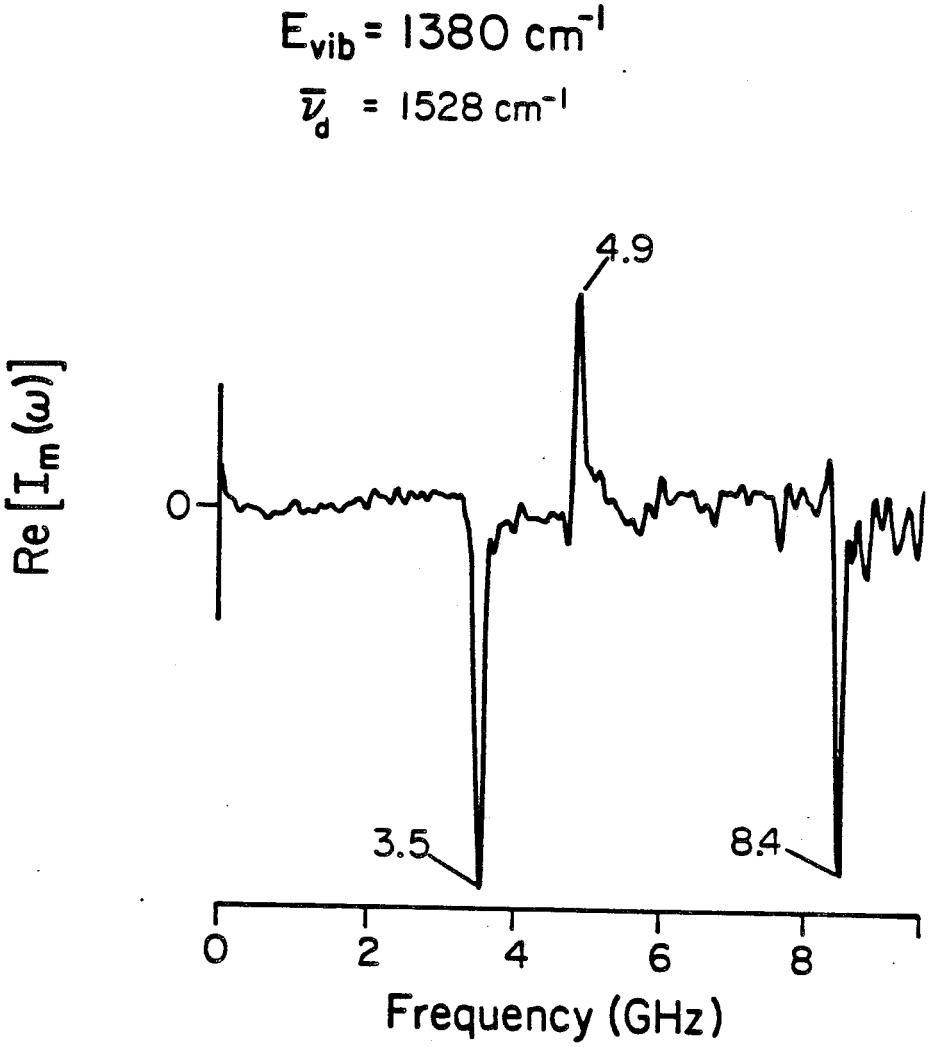
E_{vib} = 1380 cm^{-1}
$\bar{\nu}_d$ = 1528 cm^{-1}
4.9
Re [I_m (ω)]
0
3.5
8.4
0
2
4
6
8
Frequency (GHz)

Figure 9

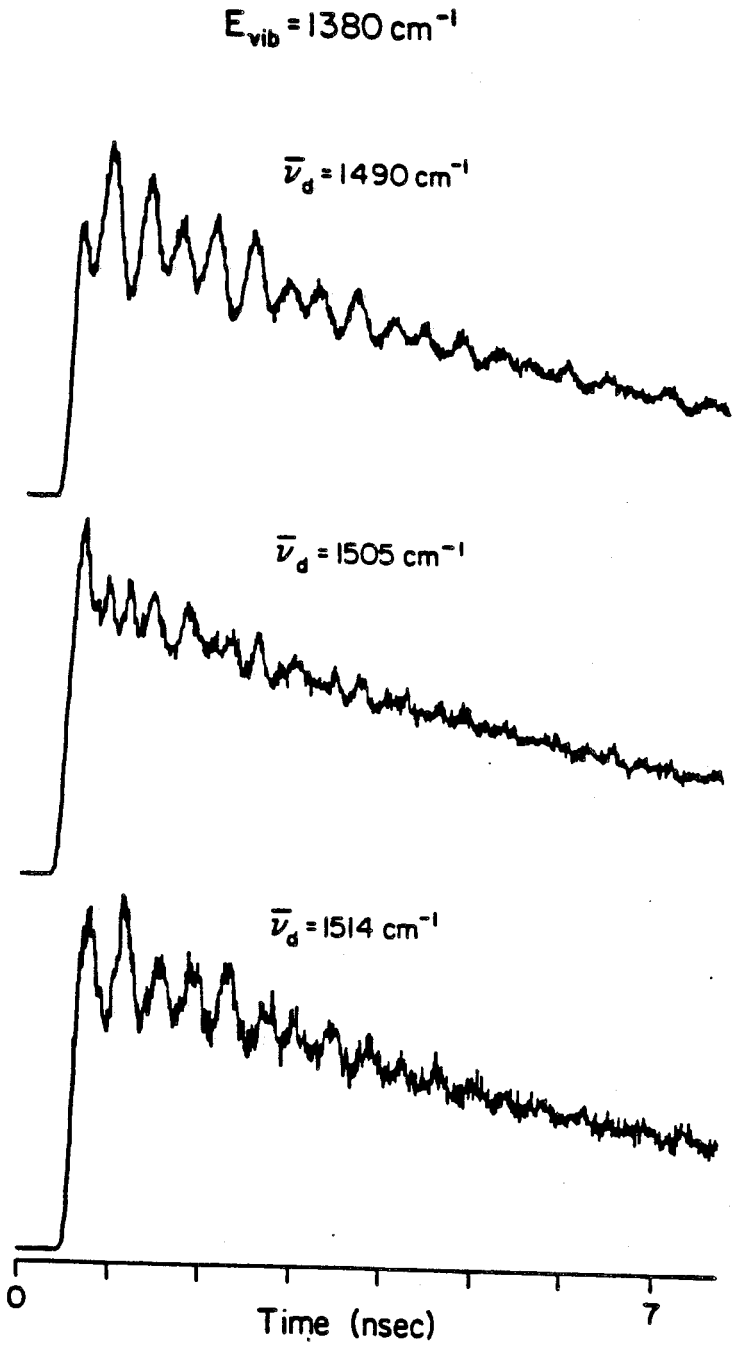
$E_{vib} = 1380\ cm^{-1}$
$\bar{\nu}_d = 1490\ cm^{-1}$
$\bar{\nu}_d = 1505\ cm^{-1}$
$\bar{\nu}_d = 1514\ cm^{-1}$
0
Time (nsec)
7

Figure 10

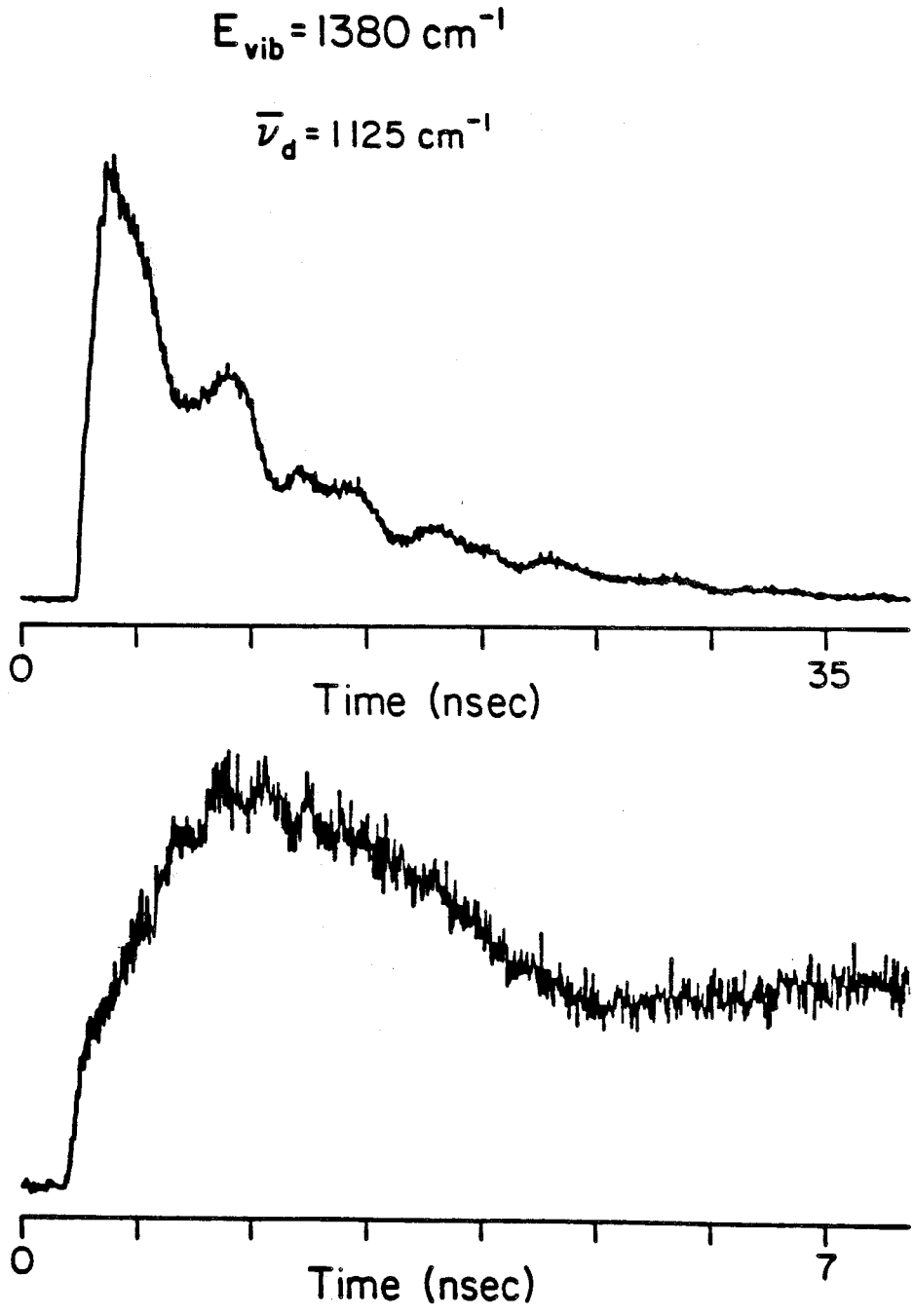

Figure 11

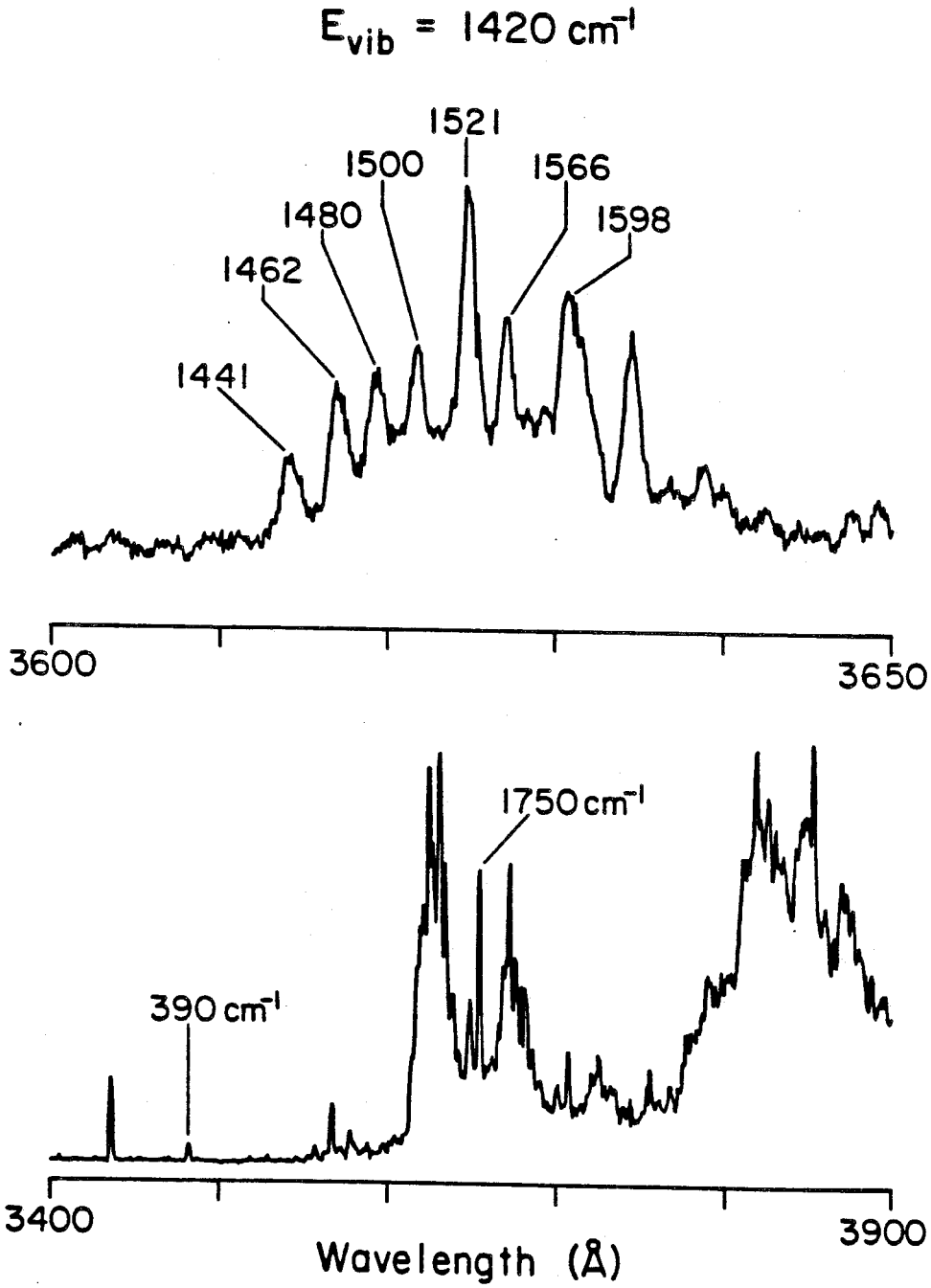
E_{vib} = 1420 cm^{-1}
1521
1500
1566
1480
1598
1462
1441
3600
3650
1750 cm^{-1}
390 cm^{-1}
3400
3900
Wavelength (Å)

Figure 12

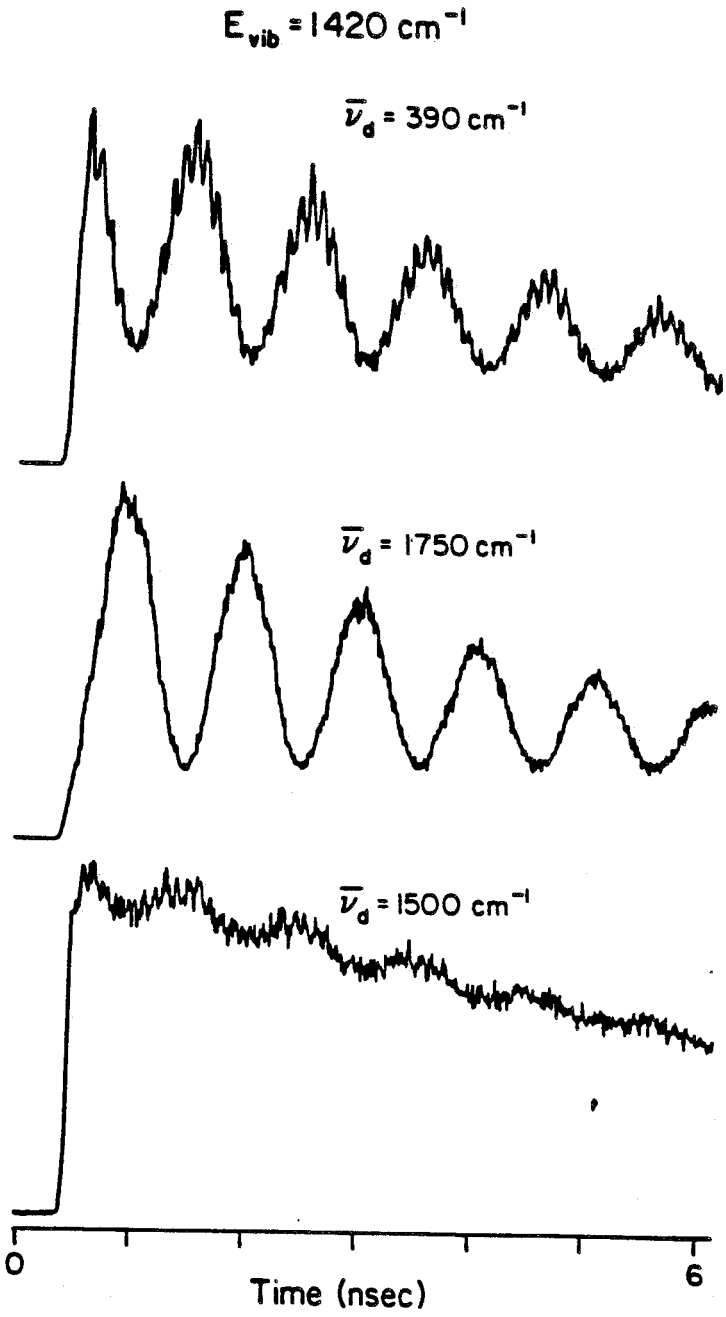
E_{vib} = 1420 cm^{-1}
$\bar{\nu}_d$ = 390 cm^{-1}
$\bar{\nu}_d$ = 1750 cm^{-1}
$\bar{\nu}_d$ = 1500 cm^{-1}
0
6
Time (nsec)

Figure 13

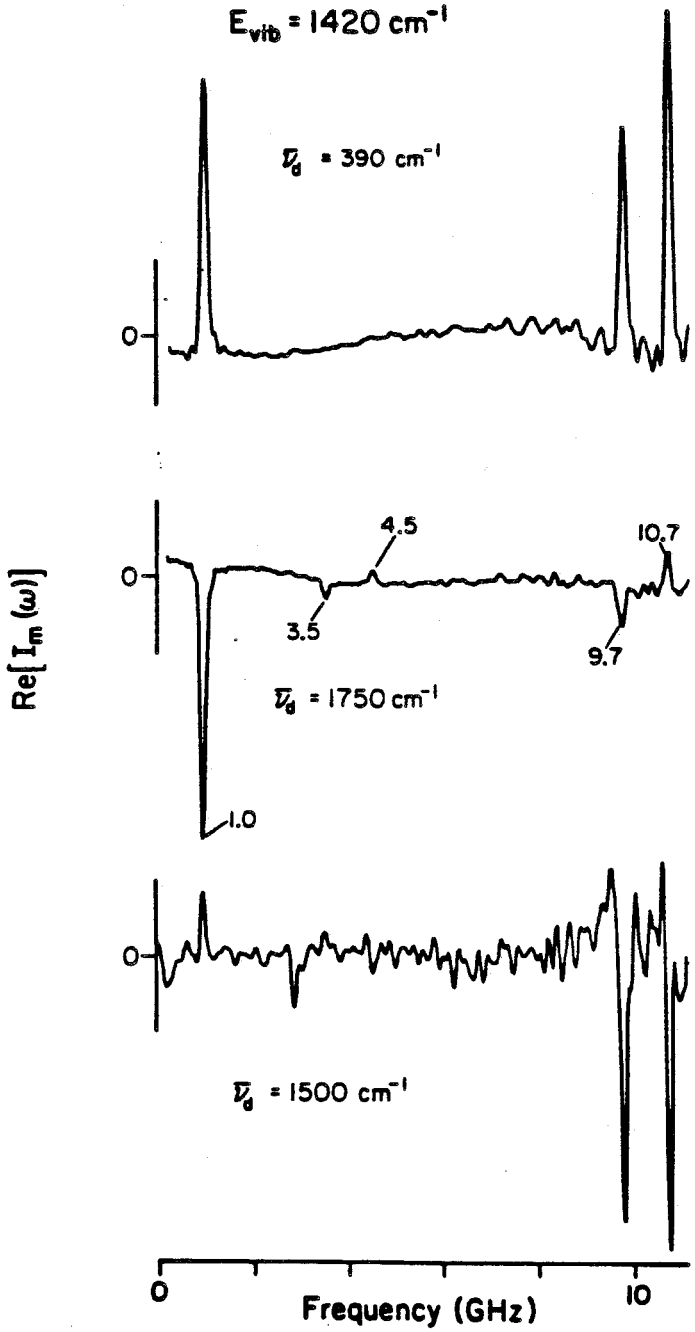
E_{vib} = 1420 cm^{-1}
Γ_d = 390 cm^{-1}
0
4.5
10.7
3.5
9.7
Γ_d = 1750 cm^{-1}
1.0
0
Γ_d = 1500 cm^{-1}
Re[I_m (ω)]
0
Frequency (GHz)
10

Figure 14

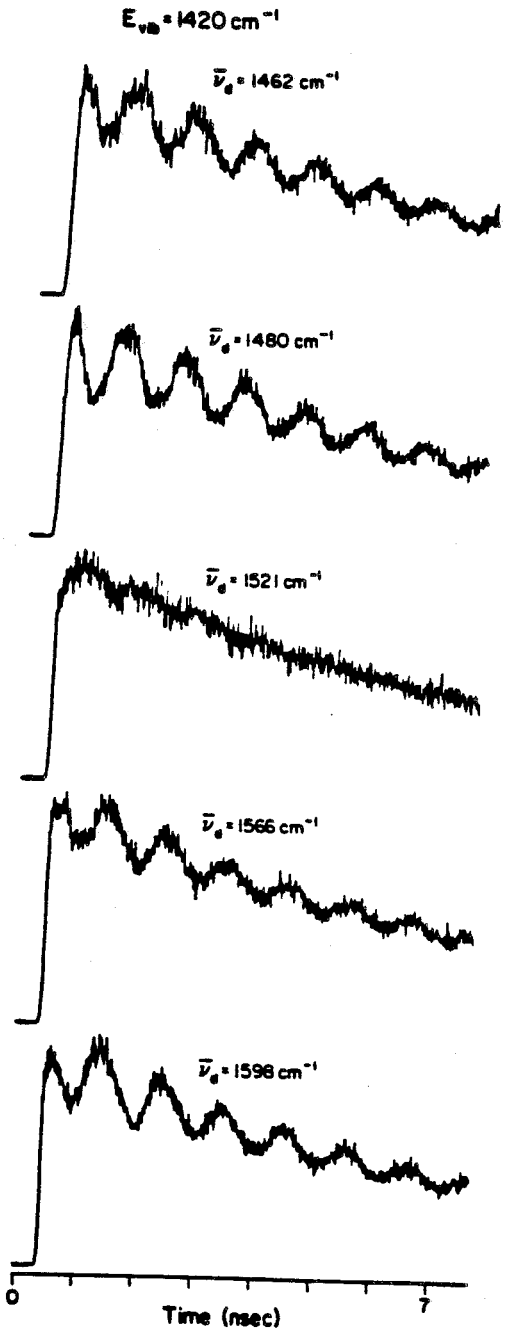
E_{vib} = 1420 cm^{-1}
$\bar{\nu}_d$ = 1462 cm^{-1}
$\bar{\nu}_d$ = 1480 cm^{-1}
$\bar{\nu}_d$ = 1521 cm^{-1}
$\bar{\nu}_d$ = 1566 cm^{-1}
$\bar{\nu}_d$ = 1598 cm^{-1}
0
7
Time (nsec)

Figure 15

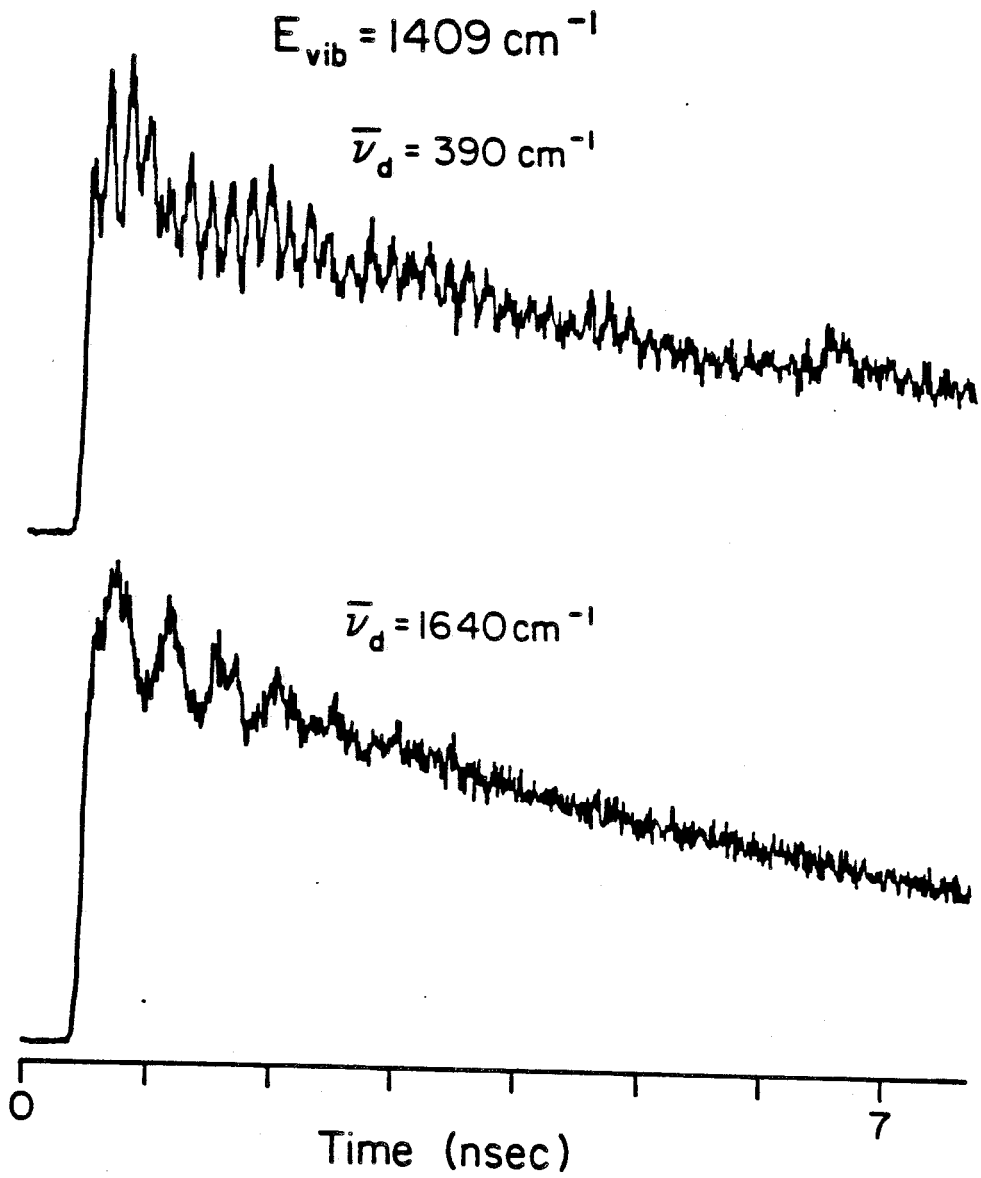

Figure 16

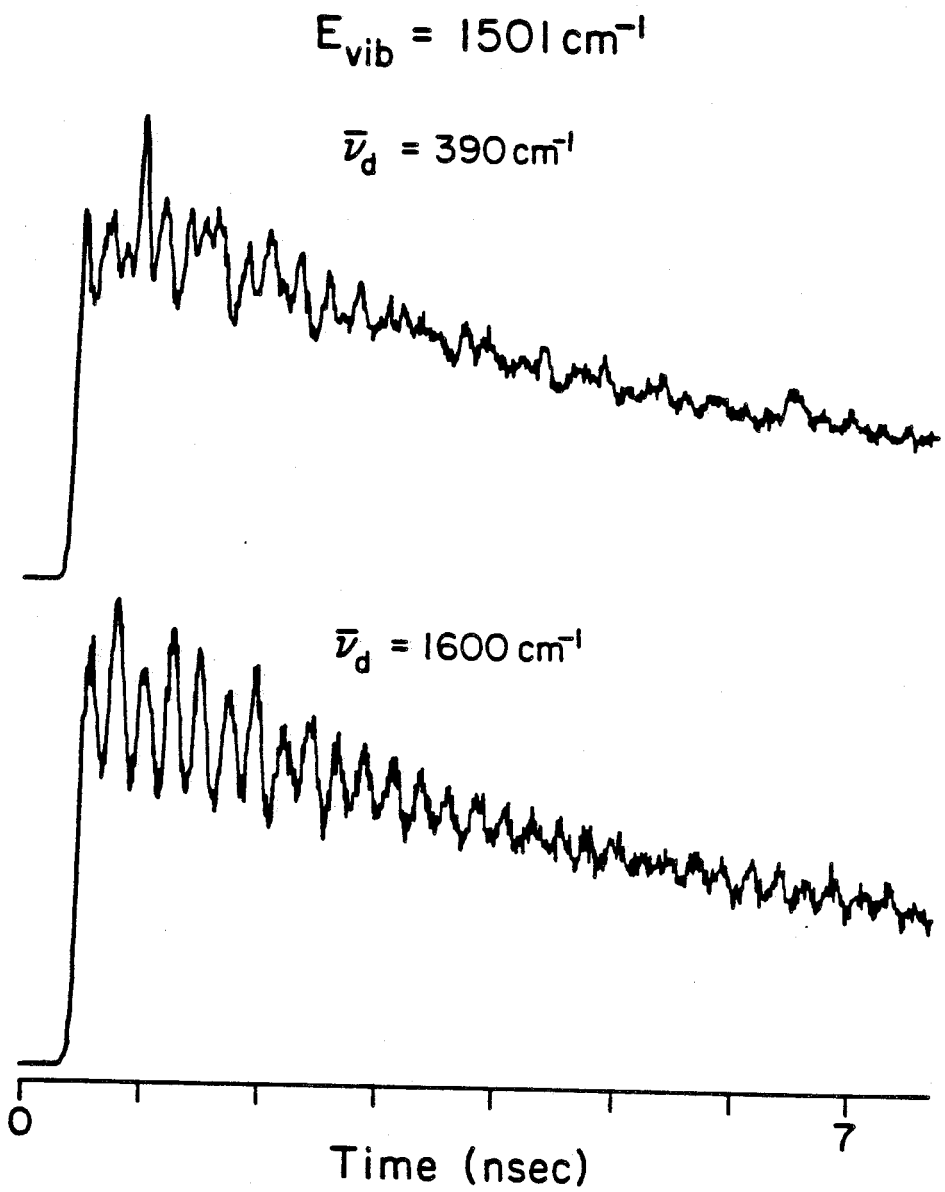

Figure 17

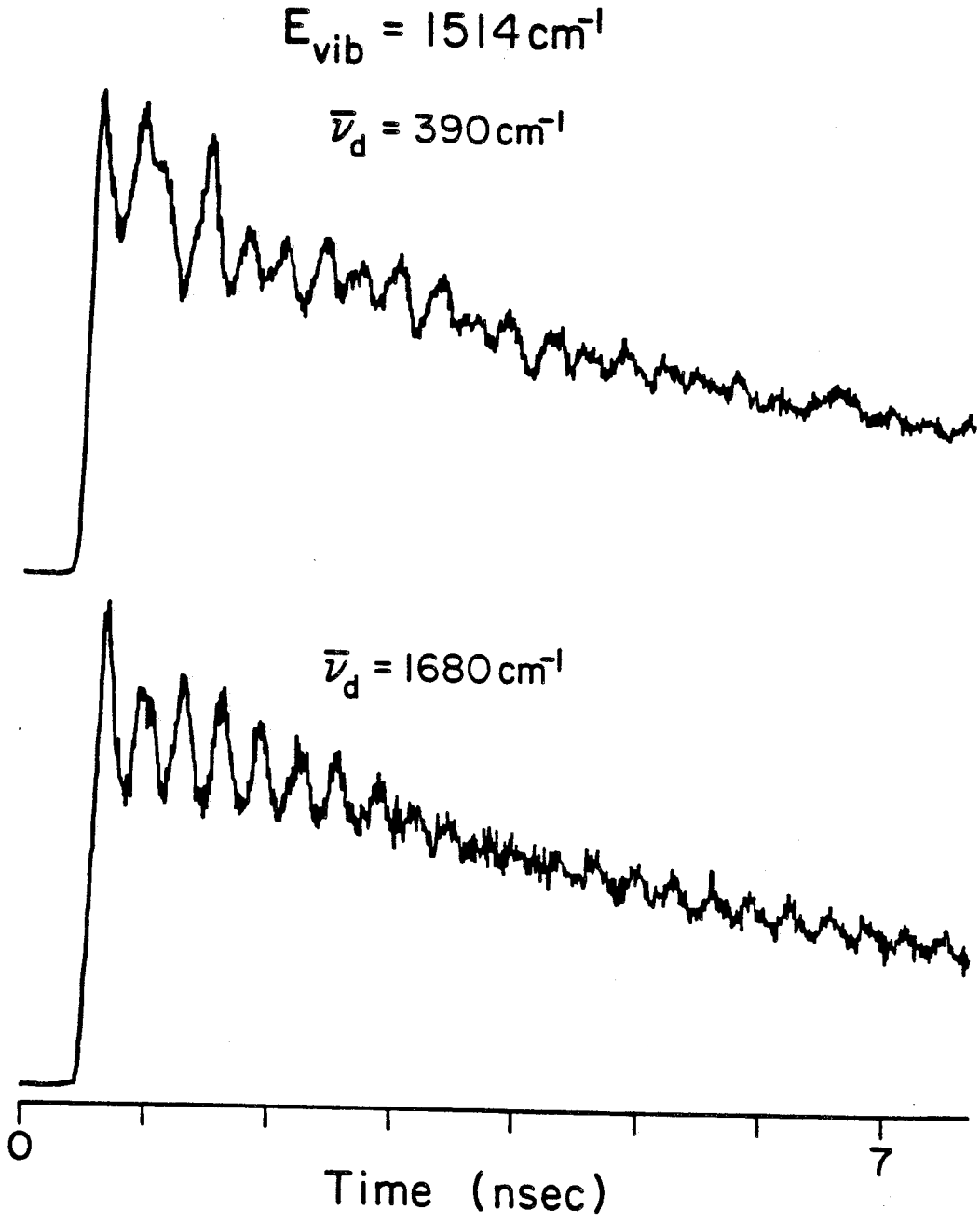

Figure 18

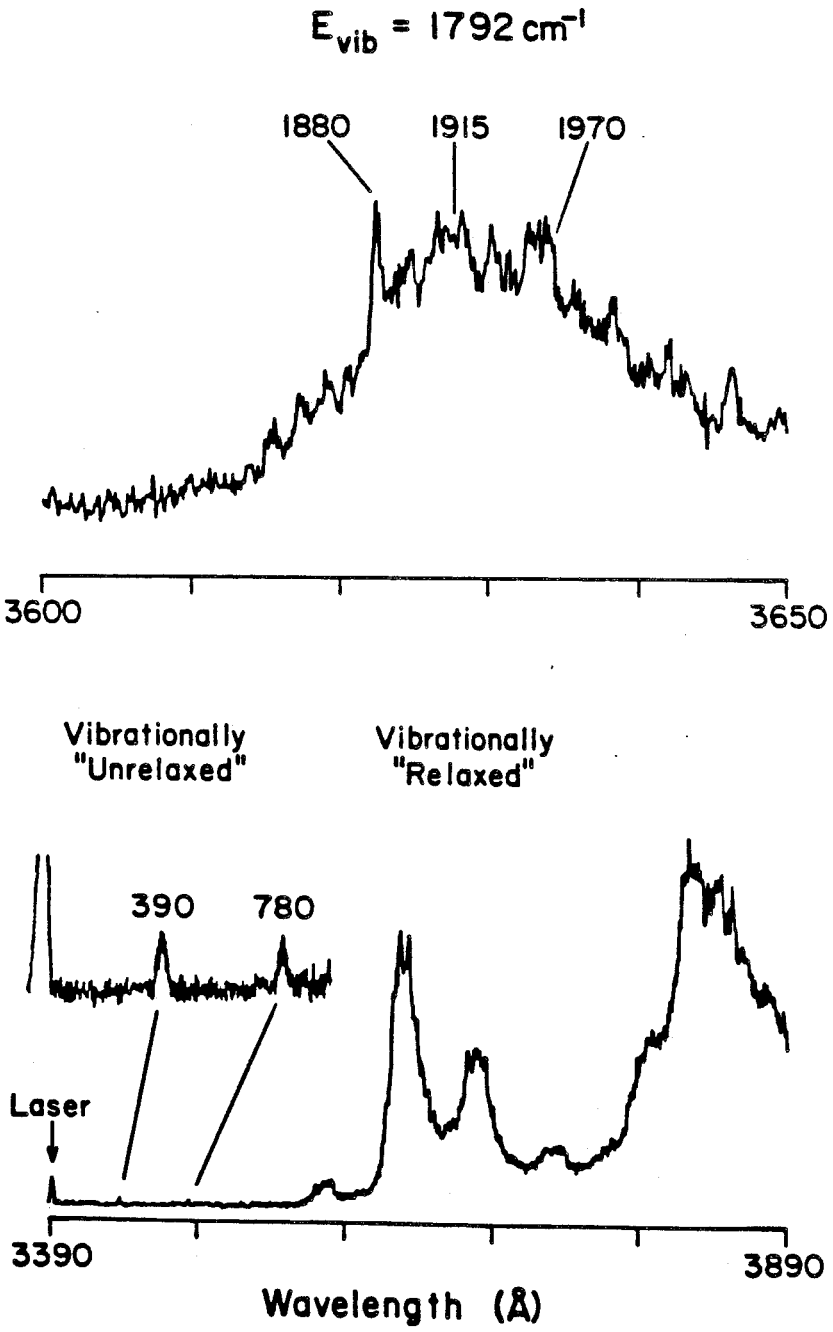
E_{vib} = 1792 cm^{-1}
1880
1915
1970
3600
3650
Vibrationally "Unrelaxed"
Vibrationally "Relaxed"
390
780
Laser
3390
3890
Wavelength (Å)

Figure 19

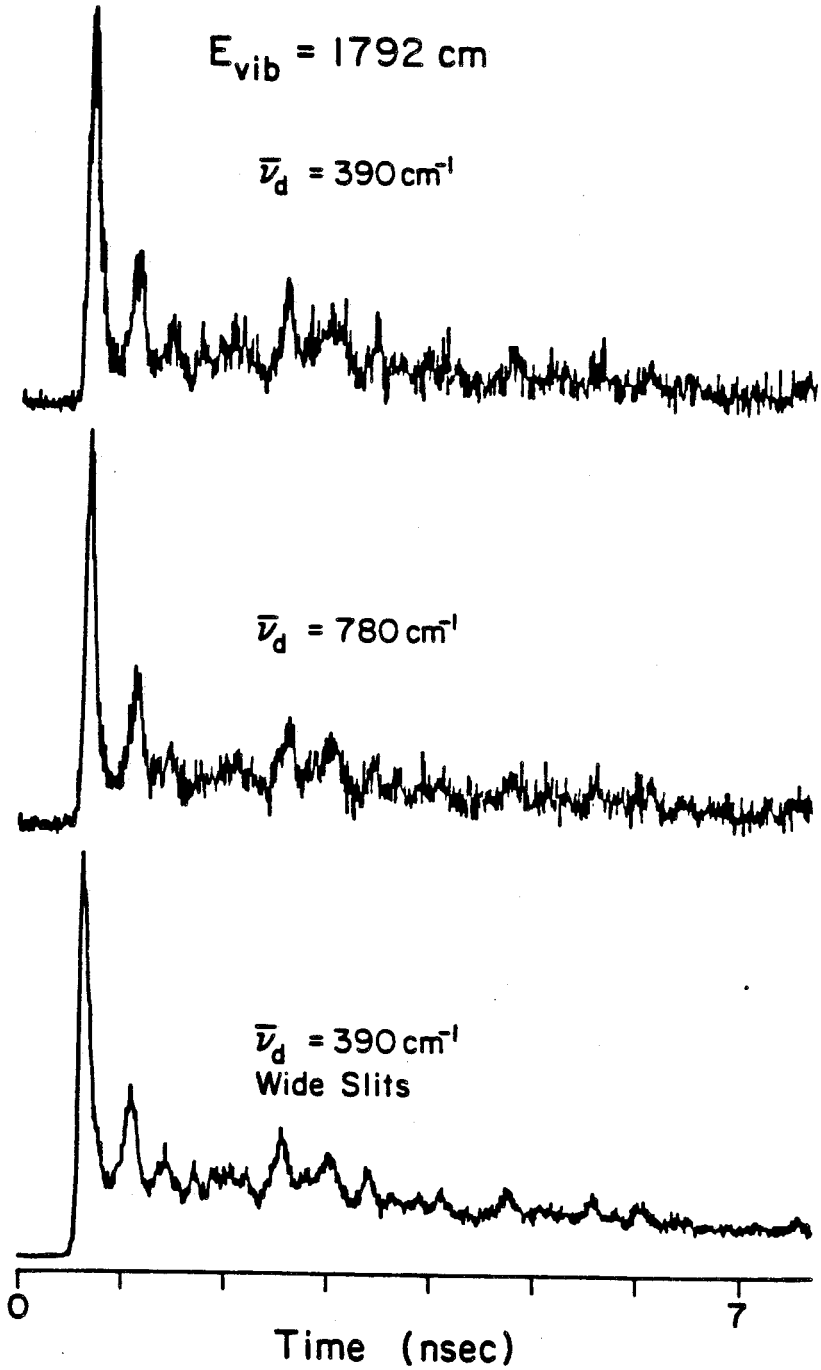
E_{vib} = 1792 cm
$\bar{\nu}_d$ = 390 cm^{-1}
$\bar{\nu}_d$ = 780 cm^{-1}
$\bar{\nu}_d$ = 390 cm^{-1}
Wide Slits
0
7
Time (nsec)

Figure 20

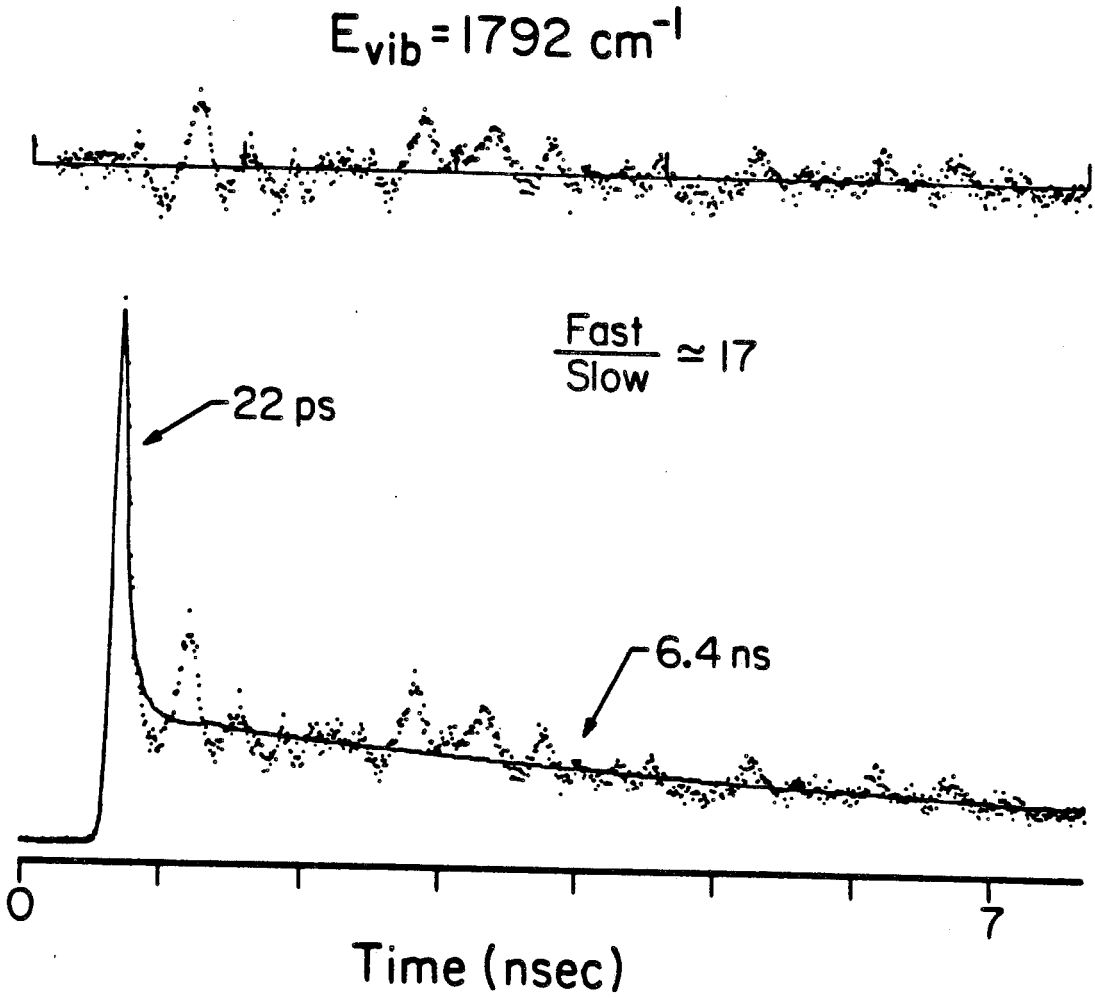

Figure 21

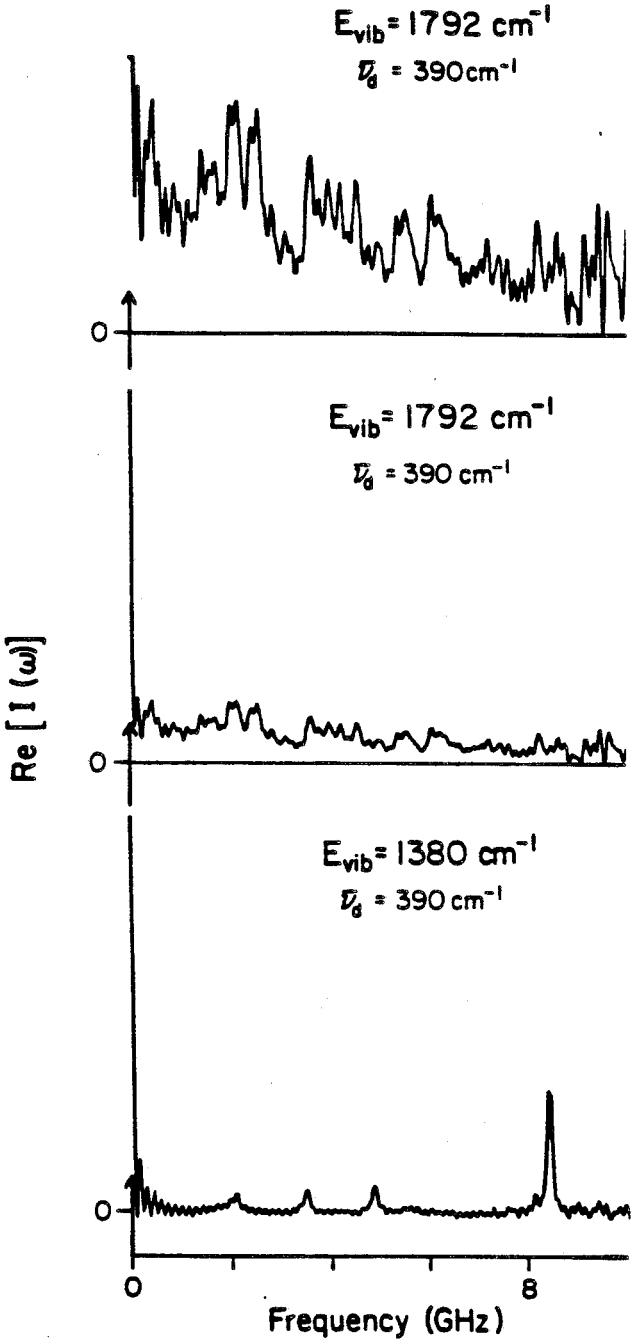
E_vib = 1792 cm⁻¹
Γ_d = 390 cm⁻¹
0
E_vib = 1792 cm⁻¹
Γ_d = 390 cm⁻¹
Re [I (ω)]
0
E_vib = 1380 cm⁻¹
Γ_d = 390 cm⁻¹
0
0
8
Frequency (GHz)

Figure 22

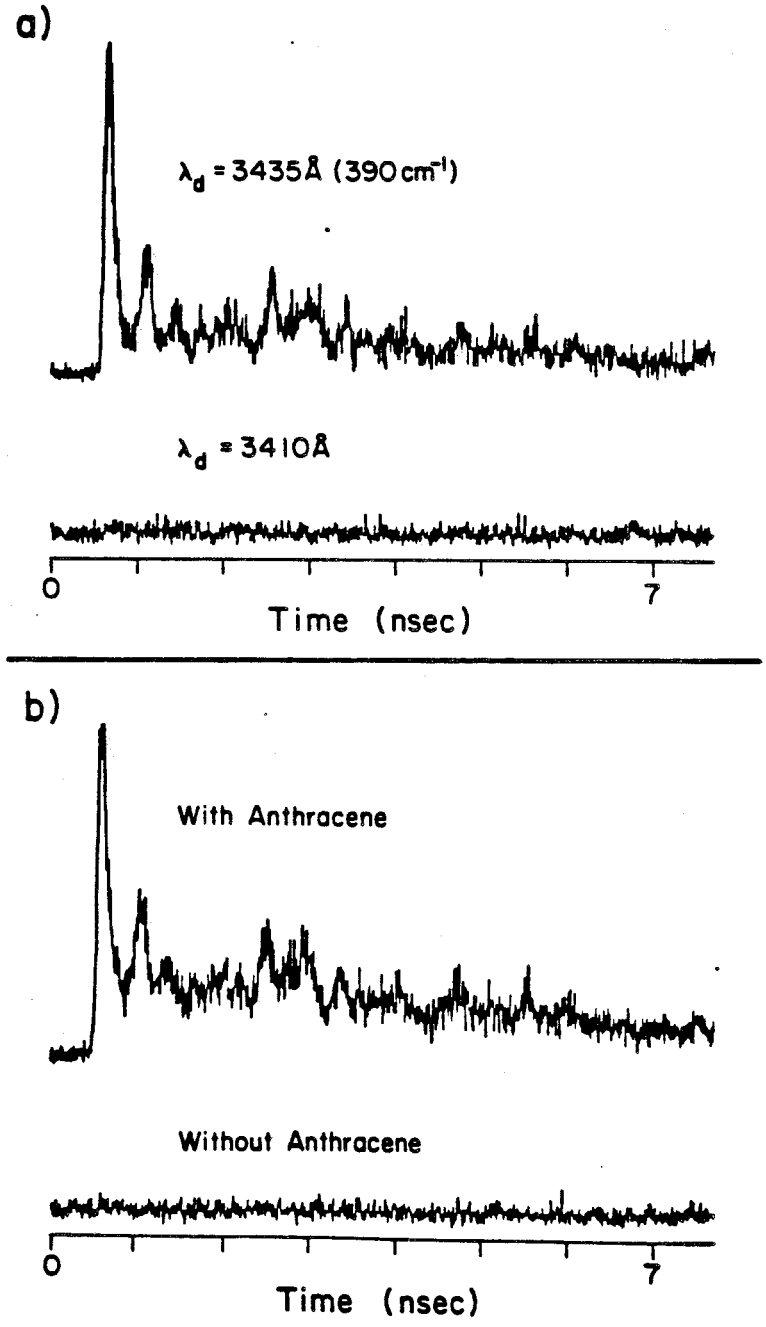
a)
λ_d = 3435Å (390cm^{-1})
λ_d = 3410Å
0
7
Time (nsec)
b)
With Anthracene
Without Anthracene
0
7
Time (nsec)

Figure 23

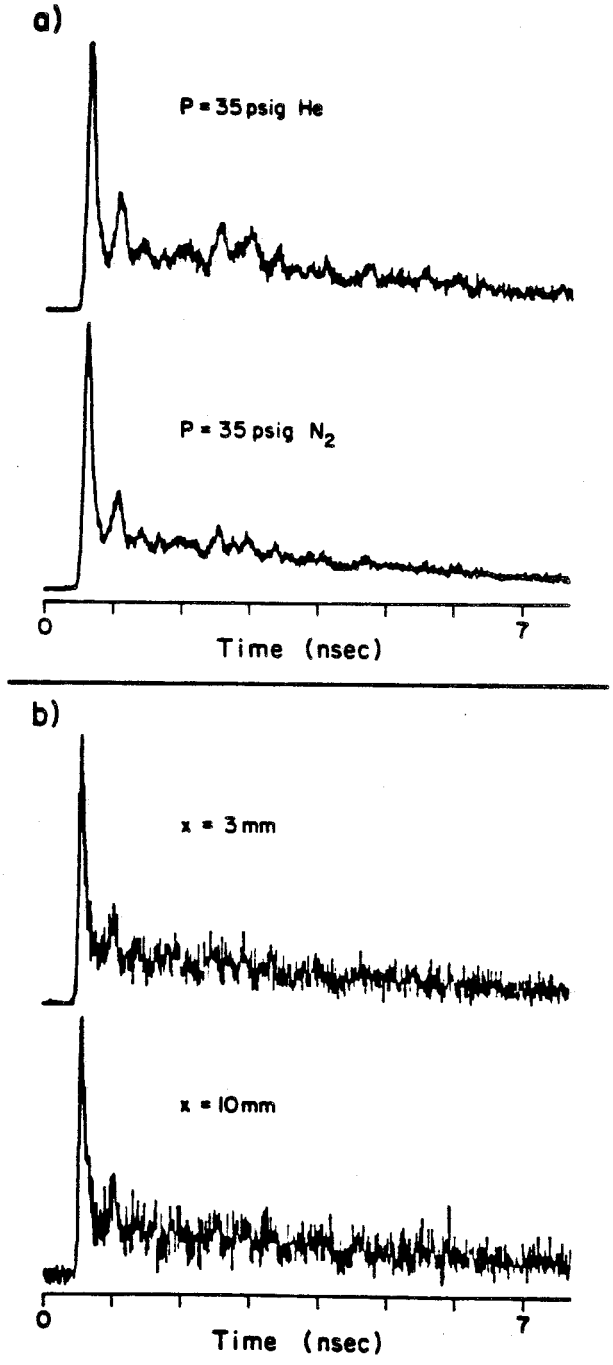

Figure 24

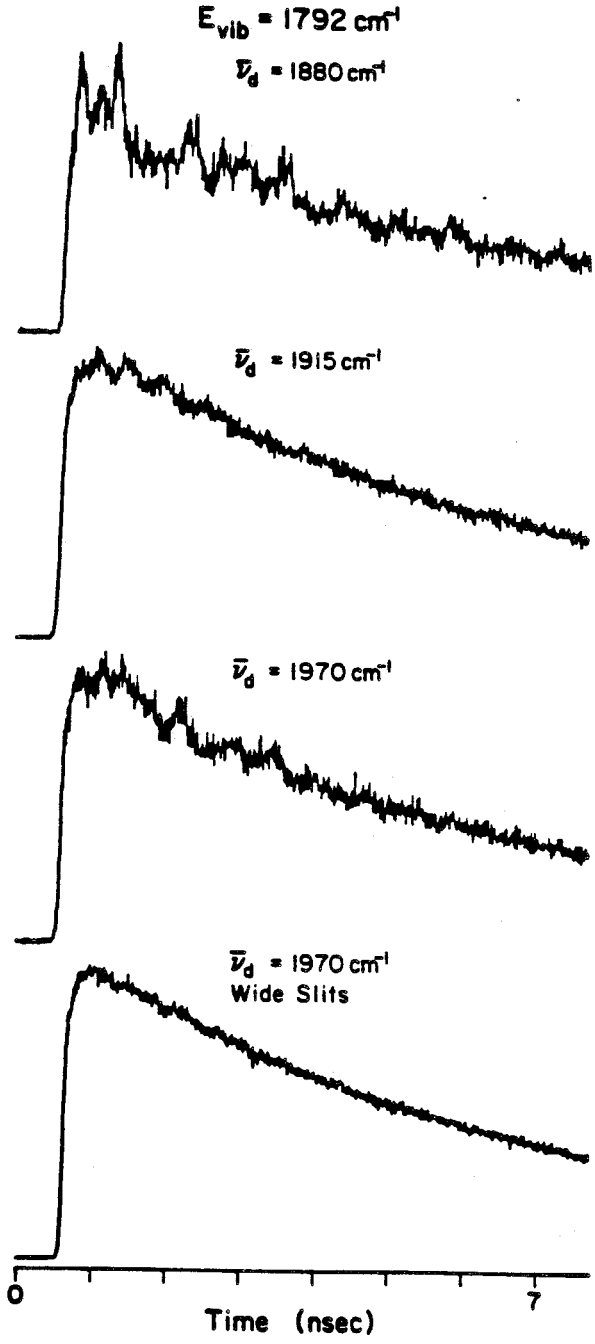
E_{vib} = 1792 cm^{-1}
$\bar{\nu}_d$ = 1880 cm^{-1}
$\bar{\nu}_d$ = 1915 cm^{-1}
$\bar{\nu}_d$ = 1970 cm^{-1}
$\bar{\nu}_d$ = 1970 cm^{-1}
Wide Slits
0
7
Time (nsec)

Figure 25

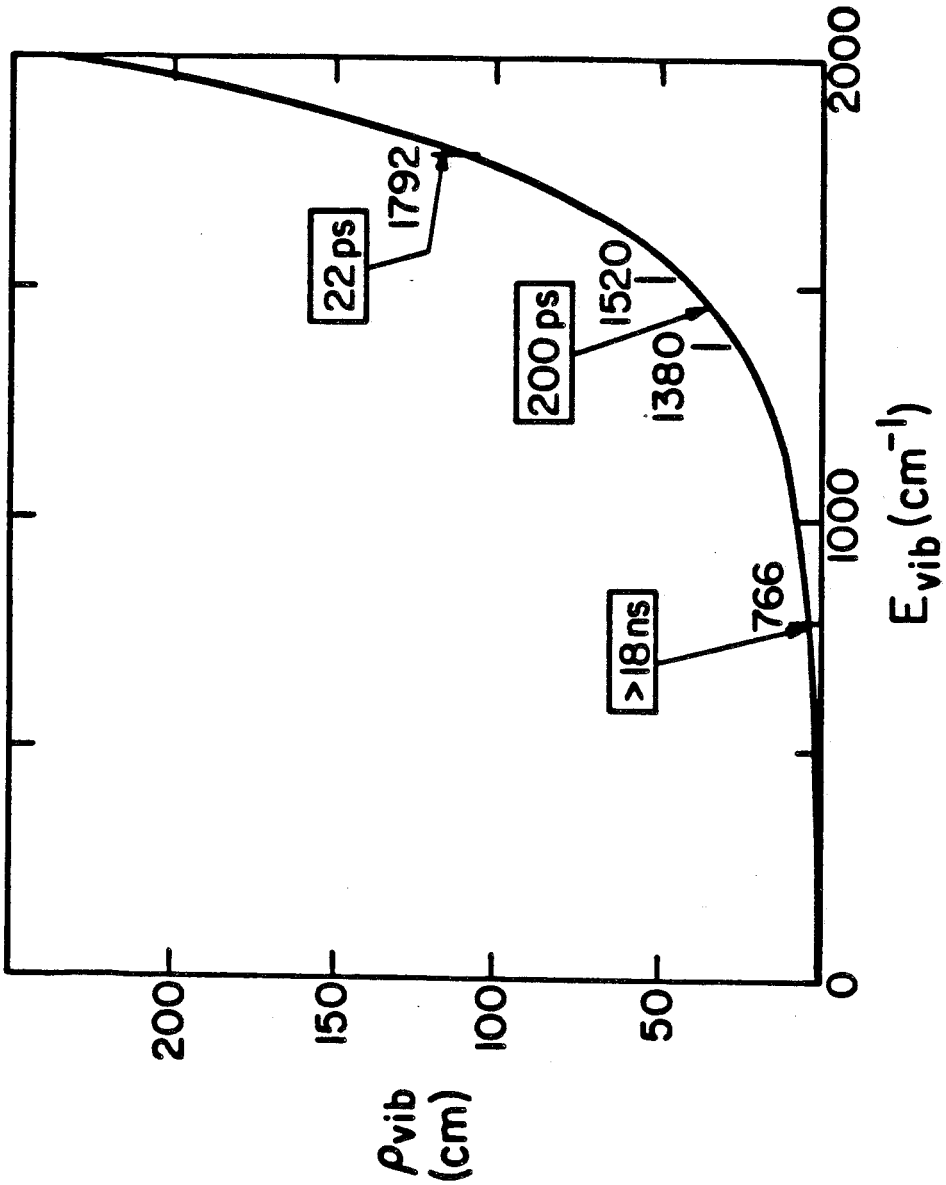
22 ps
1792
200 ps
1520
1380
>18 ns
766
0
1000
2000
E_{vib} (cm^{-1})
50
100
150
200
ρ_{vib} (cm)

CHAPTER 5

ROTATIONAL EFFECTS ON IVR*

* Submitted to the Journal of Chemical Physics, as
"Dynamics of intramolecular vibrational-energy redistribution (IVR).
III Role of rotations," by Peter M. Felker and Ahmed H. Zewail

I. INTRODUCTION

In the theoretical treatment of vibrational quantum beats (Chapter 3[1]) and in the interpretations of experimental results[2-6] pertaining to this phenomenon that have been reported on by this laboratory, little attention has been directed toward one molecular characteristic that might be expected to play a large role in influencing the observed consequences of vibrational coupling: the fact that each vibrational level is actually an entire manifold of rotational levels. In some sense, our neglect of this aspect of molecular level structure can be justified by the close correspondence between the theory constructed without its inclusion and experimental results[2-4,6]. This argues that the observed results are, on the whole, manifestations of vibrational couplings which are weakly dependent on rotational level. On the other hand, we have reported[5] some results which can only be interpreted by taking into account the rotational level structure. Morever, a comprehensive description of vibrational quantum beats should come to terms with the manifestations that can arise from rotational effects on vibrational coupling. This is a particularly pertinent task since it has been widely believed that such effects preclude the possibility of observing vibrational quantum beats in the fluorescence of large molecules, even molecules cooled by supersonic expansion; the number of populated ground state rotational levels and the variation in vibrational coupling with rotational level in the excited state are thought to be large enough that any coherence effects due to rovibration-rovibration coupling will be washed out. In actual fact, the number of superimposed incoherent excitations due to rotational level structure *is* large for large molecules (like anthracene), even at very low rotational temperatures (*e.g.*, 2 K). It is clear, however, that vibrational quantum beats can be observed for such molecules. Therefore, it must be that rotational effects on vibrational coupling need not be so marked as to render quantum beats unobservable. Yet, it may also be true that such effects are large enough to manifest themselves more subtly in beat-modulated decays.

Since the first observation[2] of phase-shifted quantum beats in anthracene, one

characteristic has been noted which cannot be reconciled with theoretical predictions. While theory[1] predicts essentially equal decay rates for the amplitudes of the modulated and unmodulated portions of a given decay, it has been observed in general that the amplitude of the modulated portion of an experimental decay (*i.e.*, the quantum beat envelope) decays faster than that of the unmodulated portion (*i.e.*, the lifetime-type decay). Two aspects of this discrepancy point toward a rotational involvement in vibrational coupling. Firstly, the theory in question does not account for rotations, and it is plausible to attribute the errors in theoretical predictions to the neglect of such a factor. Secondly, and more significantly, an increased beat decay rate implies that the widths of the beat components in the frequency domain are greater than the width of the zero frequency component corresponding to the unmodulated exponential. An increased width is just what one would expect, given vibrational couplings which are dependent on rotational level.

In an effort to establish a firmer link between quantum beat envelope decays and rotational influences we have performed a number of experiments and theoretical simulations. At the heart of both the experimental and theoretical approaches is the fact that, if vibrational coupling is dependent on rotational level, then this will be manifested as a dependence of beat-modulated fluorescence decays on the rotational temperature of the sample. By varying this temperature and observing the changes in decays, one can assess the rotational influences on beats.

In this chapter, we present experimental results which show that the decay rates of quantum beat envelopes of jet-cooled anthracene increase significantly as the rotational temperature of the sample increases. This behavior is found to be consistent with the results of theoretical simulations for which it is assumed that 1) vibrational levels are coupled by anharmonic coupling and 2) rotational effects on this coupling arise solely from the differences in rotational constants between coupled vibrational levels. The results lead us to conclude that rotational effects on vibrational coupling need not wash out the manifestations of vibrational coherence in large molecules, but may be subtly manifest in observed beat-modulated decays.

II. THEORETICAL SIMULATIONS

A. Outline of calculations

In this section the results of calculations designed to elucidate the effects which rotational temperature may have on vibrational quantum beats in anthracene will be presented. First, however, it is pertinent to outline these calculations and point out the various approximations inherent in them. A basic assumption involved in the computations is that any coherence effects due to the coherent excitation of rotational levels within the *same* vibrational state are negligible. This assumption, which can be justified on experimental and theoretical grounds[7], has the consequence of allowing one to calculate a fluorescence decay simply by summing the individual decays associated with individual rotational levels. In particular, if one adopts the definitions and nomenclature of the previous two chapters[1,6], and considers the fluorescence intensity $I_\gamma(t)$ of a γ-type fluorescence band, then

$$I_\gamma(t) = \sum_{J=0}^{\infty} \sum_{K_a=-J}^{J} W(J, K_a, T) I_\gamma(J, K_a, t), \tag{2.1}$$

where J and K_a are the usual rotational quantum numbers of an approximate prolate symmetric top[8] and refer to rotational levels in the manifold of the $|a\rangle$ (optically active) zero-order vibrational level, T is the rotational temperature of the sample, $W(J, K_a, T)$ is a weighting factor for each rovibrational level $|a, J, K_a\rangle$, and $I_\gamma(J, K_a, t)$ is the γ-type fluorescence decay which arises from the coupling of $|a, J, K_a\rangle$ with the rotational levels of the other zero-order vibrational states.

To calculate $I_\gamma(t)$ from (2.1) it is very useful to make several simplifying approximations. The first has already been mentioned; the molecule is treated as an approximate symmetric top. This allows one to calculate the rotational energy of a given rotational level $|J, K_a\rangle$ as[8]

$$E(J, K_a) = \frac{1}{2}(B + C)J(J + 1) + (A - \frac{1}{2}(B + C))K_a^2, \tag{2.2}$$

where A, B, and C are the rotational constants of the molecule and for anthracene are taken to have mean values[9] of 2155, 453, and 375 MHz, respectively. A second

useful approximation is the assumption that the thermal distribution of ground state rotational levels that exists prior to the excitation of the sample is projected into the excited state upon excitation. One then obtains the following expression[8] for the weighting factor in (2.1):

$$W(J,K_a,T) = g_N(J,K_a)(2J+1)\exp(-E(J,K_a)/k_BT), \tag{2.3}$$

where $g_N(J,K_a)$ is the nuclear spin statistical weight (which shall henceforth be taken equal to 1 for all rotational levels[10]), and k_B is Boltzmann's constant. A third approximation involves limiting the sum over J in (2.1). This is justified by the expectation that $W(J,K_a,T)$ will become small for high enough J,K_a. The calculations reported here for anthracene were made for $J \leq 30$. No significant qualitative deviations from the results of these calculations were noted when the J range was increased to $J = 60$ and beyond.

The factors $I_\gamma(J,K_a,t)$ in (2.1) represent the effects of rovibrational coupling in the decay. The form which these terms take depends wholly on the assumptions made concerning the coupling. Once these assumptions are made, $I_\gamma(J,K_a,t)$ can be calculated by first diagonalizing the rovibrational Hamiltonian for $|a,J,K_a\rangle$ and all the levels coupled to it, and then by using the eigenvalues obtained to get the beat frequencies and the eigenvectors obtained to get the modulation depths (magnitudes and phases) of the beat components.[11]

Knowing both $W(J,K_a,T)$ and $I_\gamma(J,K_a,t)$ for all pertinent rotational levels, $I_\gamma(t)$ can be calculated. The calculations of $I_\gamma(t)$ presented in this chapter have been performed in such a way as to allow direct comparison with experimental decays. In particular, it is not actually the $I_\gamma(t)$ which are shown in the figures but convolutions of typical temporal response functions with $I_\gamma(t)$ (see eqn. (2.1) of Chapter 4). Also, the simulated decays have been calculated for one thousand discrete points in time to match the number of channels that were used for collecting experimental decays.

B. Anharmonic coupling

Anharmonic coupling between zero-order rovibrational levels is characterized by two general features (see Fig. 1). Firstly, angular momentum selection rules and symmetry restrictions[8] limit this type of coupling to rovibrational levels of $|a\rangle$, $|b\rangle$, $|c\rangle$,... having the same J, K_a values. Thus, for a coupling between N vibrational states, one need only consider an $N \times N$ Hamiltonian matrix for each value of J, K_a, the rows and columns of such a matrix being labelled by the zero-order states $|a, J, K_a\rangle$, $|b, J, K_a\rangle$, $|c, J, K_a\rangle$.... Secondly, the off-diagonal elements of the Hamiltonian matrices do not change with rotational level[8] (to first order). As a consequence of this, $I_\gamma(J, K_a, t)$ only depends on J, K_a through variations in the energy spacings of the zero-order levels; *i.e.,* variations in the differences between diagonal elements of the Hamiltonian matrix. Such variations with rotational level can occur if some of the coupled vibrational states have different rotational constants, in which case the zero-order energy differences between states $|\gamma\rangle$ and $|\gamma'\rangle$ can be expressed as

$$E_{\gamma\gamma'}(J, K_a) = E_{\gamma\gamma'}(0,0) + \Delta_{\gamma\gamma'}(\frac{B+C}{2})J(J+1) + \Delta_{\gamma\gamma'}(A - \frac{B+C}{2})K_a^2, \quad (2.4)$$

where $\Delta_{\gamma\gamma'}(\frac{B+C}{2})$ and $\Delta_{\gamma\gamma'}(A - (\frac{B+C}{2}))$ represent the mismatches in rotational constants between $|\gamma\rangle$ and $|\gamma'\rangle$.

The perturbations which contribute to rotational constant mismatches between vibrational states are small ones[8]. Thus, these mismatches are expected to be small fractions of the mean rotational constants. Since data pertaining to the rotational constants of vibrational states of aromatics are hard to come by, an order of magnitude for the effect has been assumed after consideration of more readily available measurements of the changes in constants between *electronic* states[8]. Such changes are on the order of several parts in a thousand. For the results presented herein it has been assumed that rotational mismatches between vibrational states are roughly one part in one thousand. For anthracene, this means that $\Delta_{\gamma\gamma'}(\frac{B+C}{2}) \sim 0.4$ MHz and $\Delta_{\gamma\gamma'}(A - \frac{B+C}{2}) \sim 1.7$ MHz. Actual values for mismatches for a given cal-

culation were generated by a random number generator constrained to produce rotational constants within a set range.

Two-level coupling is conceptually the easiest case since there are only pairwise interactions up the rotational level structure of the coupled vibrational states (see Fig. 1). One expects the overall coupling between manifolds to give rise to a large number of different beat frequencies, each corresponding to the interaction of a pair of rovibrational levels, but all being fairly close to some average value. At finite rotational temperatures one expects that the superposition of all of these different fluorescence decays will result in a total fluorescence decay in which only one beat component appears to be present and in which the rate of decay of the beat envelope will be greater than the decay rate of the unmodulated portion of the transient. Moreover, this envelope decay rate should increase with increasing rotational temperature. In Fig. 2 we show calculated results of both a-type and b-type decays for a model two-level system. For these calculations $E_{ab}(0,0)$ of (2.4) and V_{ab}, the anharmonic coupling matrix element, have been chosen to be 2.24 and 1.0, respectively, to give typical values for both the beat frequencies (3 GHz) and the modulation depth (0.28) of the a-type band. The other calculational parameters are included in the figure caption. One can clearly see from the figure that the beat envelope decay rate and its behavior as a function of temperature match our intuitive expectations of this behavior.

To aid direct comparison with experimental data, calculations have also been performed using the 4×4 and 3×3 Hamiltonians which were derived from experimental beat data, and which correspond to the $S_1 + 1420$ cm^{-1} and $S_1 + 1380$ cm^{-1} excitations of anthracene, respectively. These two Hamiltonians appear in the previous chapter[6]. Fig. 3 presents calculated decays of the b-type bands of the $S_1 + 1420$ cm^{-1} system for different rotational temperatures. The b-type band was chosen because good experimental data for it are relatively easy to obtain and because the decay is dominated by one beat component (1 GHz with a -1 phase). The rotational constants used for the calculation appear in the figure caption. Sets of

other constants yielded qualitatively similar results. The system response function used was 150 psec FWHM (two channels). Clearly, there is a marked rotational temperature effect on the calculated decays. Although all of the decays are modulated similarly at early time, at later times the beats are increasingly washed out as the rotational temperature increases; that is, the apparent decay rate of the beat envelope increases at higher rotational temperatures. Behavior similar to this also occurs in calculated decays of other types of bands in the fluorescence spectrum.

Figs. 4 and 5 present calculated decays of the *b*-type bands in the fluorescence spectrum corresponding to $S_1 + 1380$ cm^{-1} excitation. Such decays[6] are modulated by beat components at 3.5, 4.9, and 8.4 GHz with phases of +1, −1, and −1, respectively. The two figures correspond to two different sets of rotational constants. Both sets of decays were calculated using a response function of about 90 psec FWHM (six channels). Again, and in both figures, one can see an increase in the beat envelope decay rate as the rotational temperature increases. One may notice an additional point from the decays of Fig. 5. Not all beat components decay at the same rate—one component persists at long time, even for T_{rot} = 10 K. Evidently, those components which turn out to be more (or less) sensitive to rotational temperature are determined by the mismatches in rotational constants. As with the $S_1 + 1420$ cm^{-1} case, calculated decays for the other band types in the $S_1 + 1380$ cm^{-1} spectrum show trends similar to the decays of the *b*-type band.

III. EXPERIMENTAL

The experimental apparatus and conditions have been reported in the preceding chapter[6]. The dependence of beat parameters on rotational temperature was assessed by measuring fluorescence decays as a function of carrier gas and carrier gas pressure. The carrier gases used were helium, neon, and nitrogen. A small laser-to-nozzle distance (x) dependence was observed for the beat-modulated decays; the greater x, the slower the decay rate of the beat envelope. Because of this, data for different carrier gas parameters are only compared for the same values of x. An excitation wavelength and bandwidth effect was also observed on the decays. In general, decays collected for excitation slightly off a given band maximum were less modulated than for excitation at a band maximum. Similarly, the greater the bandwidth of excitation, the smaller the observed modulation depths. Again, those decays collected for different carrier gas parameters are compared herein only if they were measured under identical excitation conditions.

Most data were taken for the S_1+1420 cm^{-1} excitation in anthracene, although some are presented for the $S_1 + 1380$ cm^{-1} excitation. There are two reasons for the preponderance of $S_1 + 1420$ cm^{-1} data. Firstly, it is relatively easy to measure decays of the intense, spectrally isolated 1750 cm^{-1} band in the $S_1 + 1420$ cm^{-1} fluorescence spectrum[6]. Secondly, the decays of this band are dominated by one beat component. Thus, they may be fit to functions having a relatively small number of adjustable parameters.

Experimental decays that were dominated by one beat frequency were fit to the convolution of the measured system response function with a function of the form:

$$I(t) = A_1[e^{-\Gamma_1 t} + A_2 e^{-\Gamma_2 t}\cos\omega t] + A_3, \tag{3.1}$$

where A_1, A_2, A_3, Γ_1, and Γ_2 are parameters. Such fits were accomplished *via* a nonlinear least-squares algorithm[12]. The fit parameters obtained in this way are useful indications of the effects which rotational temperature has on modulation depths (A_2) and quantum beat envelope decay rates (Γ_2).

The Fourier analysis of several experimental decays was also undertaken. The method used is the same as that reported on in the preceding chapter. The real parts of the Fourier transforms of entire decays compensated for response function effects are presented. Unlike those in Chapter 4, the decays that were subjected to analysis were truncated at a late enough time to eliminate substantially any truncation artifacts in the transforms.

IV. RESULTS

A. $S_1 + 1420$ cm^{-1}

Fig. 6 presents decays of the 1750 cm^{-1} fluorescence band of anthracene excited to $S_1 + 1420$ cm^{-1} for three different carrier gas conditions. One point which is immediately obvious from the figure is that the amplitude of the 1 GHz component, which modulates all three decays, decays at an increasingly faster rate as the carrier gas changes from 75 psig neon to 40 psig helium to 40 psig nitrogen. A more quantitative measure of this trend can be obtained from the fits of these decays. The fit parameters corresponding to the modulation depth of the 1 GHz component are -0.7, -0.67, and -0.61, and the decay rates of the beat envelopes are 0.13, 0.18, and 0.31 GHz for the three decays from top to bottom. While the values for the three modulation depths do not vary very widely and are close to the values previously reported, the values for Γ_2 change from being very close to the unmodulated decay rate (0.11 GHz) to a value which is a factor of ~ 3 greater than this. This trend is matched by the width of the 1 GHz band in the Fourier spectra of the decays of Fig. 6. These spectra, which appear in Fig. 7, show a clear increase in the bandwidth of this component as the carrier gas changes from Ne to He to N_2.

The changes which occur in Γ_2 as the carrier gas is varied also occur when the carrier gas pressure is varied. In general, as the carrier gas pressure increases, Γ_2 decreases. This effect on Γ_2 is not as marked as that which arises when the gas is changed from N_2 to Ne (for instance, a decay taken under the same conditions as for those corresponding to Fig. 6-top, except that $P = 50$ psig rather than 75 psig Ne, was fit to a function with $\Gamma_2 = 0.15$ GHz) but it is reproducible for all three carrier gases. In the extreme case of *no* carrier gas, the quantum beats are completely washed out, as shown in Fig. 8.

Besides the 1750 cm^{-1} band, the carrier gas dependences of the decays of other fluorescence bands arising from $S_1 + 1420$ cm^{-1} excitation have also been measured. In particular, the 390 and 780 cm^{-1} a-type fluorescence bands[6] have been studied. Fig. 9 shows results for the 780 cm^{-1} band. The overall beat modulation depth

for the decays is less than that of the 1750 cm^{-1} decays for two reasons; (1) the inherent modulation depth for the 1 GHz component is less for the a-type bands in the spectrum than for the non-a-type 1750 cm^{-1} band, and (2) the large detection bandwidth needed to measure decays of the weak 780 cm^{-1} band made it impossible to spectrally isolate the band. The values for Γ_2 derived from fits to the decays of Fig. 9 are in good agreement with those found for the 1750 cm^{-1} decays for similar carrier gas conditions.

B. $S_1 + 1380$ cm^{-1}

Extensive studies of the effects of carrier gas parameters on the decays of the bands in the $S_1 + 1380$ cm^{-1} fluorescence spectrum have not been performed with 80 psec time resolution. Nevertheless, the limited studies which have been performed reveal behavior entirely consistent with that observed for the $S_1 + 1420$ cm^{-1} excitation. Fig. 10 provides an example. The two decays correspond to the detection of the 1460 cm^{-1} (b-type) band[6] in the spectrum for two different carrier gases. Although the presence of three beat frequencies in the decays makes fitting them difficult, it is clear without any fits that the modulations wash out much more quickly in the nitrogen than in the neon decay. Similar behavior has been observed for the 390 (a-type) and 1528 cm^{-1} (c-type) bands[6] in the spectrum.

V. DISCUSSION

It is clear from the simulated decays of Figs. 2–5 that a marked rotational temperature effect on the beat-modulated decays which arise from vibrational states coupled by anharmonic interactions can exist, and that this effect is primarily on the decay rates of quantum beat *envelopes*. One would now like to directly relate this trend to experimental results.

The analysis of the experimental results of section IV in terms of the effects of rotational temperature on beats requires some prior knowledge of the way in which different experimental expansion parameters affect the rotational temperature of the sample. Knowledge of this sort is available from experimental and theoretical sources. Experimentally, we have reported[9] the measurement of 0_0^0 B-type rotational contours of anthracene for a variety of expansion conditions. The band shape was found to change noticeably with changes in expansion conditions (see Fig. 20, Ref. 9). These changes match the changes that occur in calculated B-type contours as a result of variations in the rotational temperature (see Fig. 21, Ref. 9). In particular, the measured contours match the calculated behavior if it is assumed that the rotational temperature follows the trend $T(\mathrm{Ne}) \leq T(\mathrm{He}) < T(\mathrm{N_2})$ for changes in carrier gas. Although no fits to the experimental contours have been performed, rough estimates of the rotational temperature for various expansion conditions can be made by comparison of the experimental and simulated contours. These estimates go from 1 K for 50 psig Ne to 10 K for 20 psig N_2.

Theoretically, an idea of the rotational temperature of a free-jet sample can be obtained if it is assumed that the rotational temperature follows the terminal translational temperature of the expansion. Terminal translational temperatures have been calculated[13] for typical expansion conditions used in this laboratory. The general trend and the absolute magnitudes of these temperatures for different carrier gases and pressures are consistent with the conclusions derived from the contour measurements. For example, for a nozzle temperature of 450 K and a pinhole diameter of 150 μm, 40 psig expansions of Ne, He, and N_2 were calculated

to have terminal translational temperatures of 0.9, 1.2, and 3.9 K, respectively. One expects the rotational temperatures of such expansions seeded with anthracene to be somewhat higher than these values, being that rotational degrees of freedom do not cool as efficiently as translational degrees of freedom.

Having established a semi-quantitative link between expansion parameters and rotational temperature, one can now consider the changes in quantum beat decays with rotational temperature. As was noted in section IV, the major trend which emerges from the experimental results is that the decay rate of quantum beat envelopes increases as the carrier gas is changed from Ne to He to N_2. Interpreting this trend strictly in terms of the changes induced in rotational temperature with changes in carrier gas, one may say that as the rotational temperature increases, the beat decay rate increases, as well. Now, it may be argued that some carrier gas dependent collisional interaction between the carrier gas and anthracene is responsible for the observed trend, instead of changes in rotational temperature. However, if this were the case, the beat decay rate would be expected to increase as the pressure of a given carrier gas were increased. This is the opposite of what is observed. On the other hand, this kind of behavior with pressure is consistent with rotational temperature changes since the temperature would be expected to decrease with increasing pressure[13]. Therefore, one arrives at the conclusion that increasing the rotational temperature of anthracene increases the quantum beat decay rates of the fluorescence decays corresponding to the $S_1 + 1380$ cm^{-1} and $S_1 + 1420$ cm^{-1} excitations. Complementary to this effect of rotational temperature on decay parameters is the effect of temperature on the widths of the beat component in the Fourier spectra (Fig. 7). Just as one might expect, the increase in beat decay rate with increasing rotational temperature is directly linked to an increase in bandwidth in the frequency domain.

The changes with rotational temperature that occur in measured decays are quite similar to those changes which occur in simulated decays calculated assuming anharmonic coupling and rotational constant mismatches. This similarity is readily

seen in a comparison of Figs. 3 and 6, and Figs. 4 and 10. We take this as strong evidence that the observed beat envelope decay behavior arises from some anharmonic coupling-rotational constant mismatch mechanism. The operation of such a mechanism in enhancing beat decay rates is perhaps best explained by reference to what happens in the frequency domain. Given small variations with rotational level in the Hamiltonian matrices ($\mathbf{H}_0(J, K_a)$) describing the coupling of a set of rovibrational levels, one expects similar variations in the eigenvalues of these matrices. Given also a situation wherein $\mathbf{H}_0(J, K_a)$ tends to deviate more from $\mathbf{H}_0(J', K_a')$ when J and K_a differ more from J' and K_a' (*c.f.*, (2.4)), then one expects the eigenvalues of the two matrices to differ more for more widely separated J, K_a and J', K_a'. Now at low rotational temperatures, there is a narrow distribution of populated rotational levels. Thus, the relevant values of J, K_a are all close to one another and the variations in eigenvalues of the relevant $\mathbf{H}_0(J, K_a)$ are small. As T increases, however, more widely varying values of J, K_a become relevant, and the variations in eigenvalues increase. Small variations in eigenvalues translate directly into beat frequency bandwidths. Thus, it is clear that these beat frequency bandwidths will increase with increasing rotational temperature given the hypotheses about $\mathbf{H}_0(J, K_a)$. Moreover, since the rate of decay of a beat component can be directly related to the bandwidth of that component, it is also clear that beat decay rates should increase with increasing rotational temperature.

Note that in the preceding paragraph we have emphasized the smallness of the variations in $\mathbf{H}_0(J, K_a)$. Large variations do not, in general, give rise to the sort of quasi-continous variations in eigenvalues which result in bandwidths for beat components. It is the smallness of the variations in $\mathbf{H}_0(J, K_a)$ that would be expected given anharmonic coupling and rotational constant mismatch that renders such a mechanism a plausible explanation for the observed behavior.

A connection between beat envelope decay rates and the rotational constants of zero-order vibrational states could turn out to have very useful consequences in the study of intramolecular vibrational energy redistribution (IVR). Because

different classes of vibrational motions in a molecule would be expected to have rotational constants with characteristicly different deviations from average values, then knowledge of these deviations could facilitate the assignment of vibrational states in terms of the normal modes of the molecule. The ability to do this for the coupled vibrational states giving rise to an IVR process is of tremendous and obvious value to the full understanding of the process. To help accomplish this with beat envelope decay rates, one would require a more quantitative theoretical connection between these rates and rotational constant mismatches. Experimentally, more precise measurements of rotational temperatures and decay rates (especially for decays modulated by a number of components) would be needed. Such advances are certainly not inconceivable and, indeed, may be at hand.

At this point, a few remarks concerning the uniqueness of the anharmonic coupling–rotational constant mismatch mechanism in explaining the trend of the experimental results should be made. One can certainly envision other coupling mechanisms which would give rise to distributions of beat frequencies dependent on rotational temperature. In particular, one might consider Coriolis coupling[8,14]. Coriolis coupling, however, has matrix elements which are steeply dependent on J, K_a. Given a Hamiltonian matrix with off-diagonal elements solely determined by Coriolis coupling, one would not expect the simple beat patterns and small numbers of beat components observed in the experimental decays[6]. Indeed, even decay simulations done by us using a 2×2 Hamiltonian matrix have been found to produce extremely complicated beat patterns. Nevertheless, this is not proof positive that Coriolis coupling does not bear any influence on the experimental results. We say this because Hamiltonian matrices with interaction matrix elements solely determined by Coriolis coupling are not the only ones in which such coupling may be realized. In fact, it is more probable that most real Hamiltonians consist of some states coupled anharmonically and other ones coupled (probably weakly) by Coriolis interactions. This kind of situation could give rise to subtle rotational temperature effects such as have been reported on herein. And, they may explain

other, less subtle effects reported on elsewhere[5]. The large number of possibilities for such mixed coupling has precluded, however, any detailed consideration here.

The theoretical and experimental results of this chapter on the role of rotations in IVR can be related to temperature effects on intramolecular dephasing. At 0 K rotational temperature, IVR occurs with the rotational "bath" being essentially empty. Γ_2 approaches the fluorescence decay rate Γ_1 in this limit. Or, in the language of the density matrix formalism, T_2 approaches T_1. As the rotational temperature increases, however, rotational dephasing, brought about by the many overlapping incoherent excitations from thermally populated J, K_a levels, is possible. This pure dephasing causes T_2 to become less than T_1. In a sense, the rotational reservoir in this case is similar to the phonon reservoir in solids, for which T_2 has been measured to be less than T_1 at temperatures above ~ 2 K.[15]

VI. CONCLUSIONS

We have considered theoretically the effects which the rotational level structure can have on beat-modulated fluorescence decays that arise from anharmonically coupled vibrational states. For small mismatches in rotational constants between coupled vibrational states, these effects primarily take the form of increased decay rates for quantum beat envelopes relative to the overall fluorescence decay rates. Experimental results of decays as a function of carrier gas parameters reveal behavior in anthracene which is entirely consistent with the theoretical results. Taken together, all the results argue convincingly that 1) vibrational coherence effects need not be washed out by the rotational level structure, 2) anharmonic coupling is the primary coupling interaction giving rise to phase-shifted beats in anthracene, and 3) the effects of rotations on IVR can be assessed by time-resolved experiments.

REFERENCES

1. P. M. Felker and A. H. Zewail, J. Chem. Phys. - submitted.

2. P. M. Felker and A. H. Zewail, Chem. Phys. Lett. **102**, 113(1983).

3. P. M. Felker and A. H. Zewail, Phys. Rev. Lett. **53**, 501(1984).

4. P. M. Felker and A. H. Zewail, Chem. Phys. Lett. **108** 303(1984).

5. W. R. Lambert, P. M. Felker, and A. H. Zewail, J. Chem. Phys. **81**, 2217(1984).

6. P. M. Felker and A. H. Zewail, J. Chem. Phys. - submitted.

7. Experimentally, the justification derives from the fact that no quantum beats have been observed for a large number of low energy ($E_{vib} < 1200\ \mathrm{cm}^{-1}$) excitation bands in anthracene. Given observable coherence effects involving rotational levels in the same vibrational manifold, one would expect to observe beats for excitation of essentially every band. Theoretically, one notes selection rules which limit both the number of levels which can be prepared coherently *via* excitation and which restrict the number of beating fluorescence transitions from these coherently prepared levels. Further, one notes the large distribution of beat frequencies and the large number of high frequency components to be expected from the coherent preparation of rotational levels within the same vibrational state.

8. See G. Herzberg, *Infrared and Raman Spectra of Polyatomic Molecules* (Van Nostrand, Princeton, 1945).

9. W. R. Lambert, P. M. Felker, J. A. Syage, and A. H. Zewail, J. Chem. Phys. **81**, 2195(1984).

10. The actual values for the four types of levels are not all equal (they have relative values of 1.12, 1.00, 0.94, and 0.94). Nevertheless, the number of thermally populated rotational levels is large enough, and the weights near enough to one another, that one expects that the differences in weights do not give rise to any readily observable effects.

11. See section II of Ref. 1 (Chapter 3). Note that $I_\gamma(J, K_a, t)$ used herein corresponds to $I_\gamma(t)$ in Ref. 1 in the sense that both are associated with a single $N \times N$ Hamiltonian matrix. $I_\gamma(t)$ in this chapter, however, is associated with the large number of independent matrices describing the vibrational coupling interactions as a function of rotational level.

12. P. R. Bevington, *Data Reduction and Error Analysis for the Pysical Sciences* (McGraw-Hill, New York, 1969).

13. W. R. Lambert, Ph.D. thesis, California Institute of Technology (1982).

14. E. B. Wilson, J. Chem. Phys. **4**, 313(1936).

15. M. J. Burns, W.-K. Liu, and A. H. Zewail, in: *Spectroscopy and Excitation Dynamics of Condensed Molecular Systems, Vol. 4*, edited by V. M. Agranovich and R. M. Hochstrasser (North-Holland, Amsterdam, 1983), p. 301.

FIGURE CAPTIONS

1. Schematic diagram of the anharmonic coupling between the rotational levels of two zero-order vibrational states—$|a\rangle$ (left) and $|b\rangle$ (right). Only those rotational levels having the same rotational quantum numbers (J, K_a) are coupled. Moreover, the coupling matrix element V is constant for each pair of coupled rovibrational states. Coupling can vary up the rotational manifold only through differences in energy spacings between coupled states. (Such differences are not shown in the figure.) Note that there has been no attempt to draw the spacings between levels to scale.
2. Simulated decays as a function of rotational temperature for the a-type and b-type decays of a coupled two-level system. The lowest rotational states of the two zero-order levels were taken to be spaced by 2.24 GHz (the $|b\rangle$ state being at higher energy) and the coupling matrix element was taken to be 1 GHz. The rotational constants used, $(\frac{B+C}{2})$ and $(A-\frac{B+C}{2})$, were 0.4119 and 1.7396 GHz for the $|a\rangle$ state; and 0.4116 and 1.7385 GHz for the $|b\rangle$ state. For other details see the text.
3. Simulated b-type decays as a function of rotational temperature for the coupled four-level system described by the Hamiltonian matrix of eqn.(4.6), Chapter 4, which represents the coupling situation at $E_{vib} = 1420$ cm^{-1} in S_1 anthracene. The randomly generated rotational constants $(\frac{B+C}{2})$ and $(A-\frac{B+C}{2})$ were for the $|a\rangle$, $|b\rangle$, $|c\rangle$, and $|d\rangle$ states, respectively: 0.4119 and 1.7396; 0.4124 and 1.7417; 0.4120 and 1.7401; and 0.4122 and 1.7407 GHz.
4. Simulated b-type decays as a function of rotational temperature for the coupled three-level system described by the Hamiltonian matrix of eqn.(4.3), Chapter 4, which represents the coupling situation at $E_{vib} = 1380$ cm^{-1} in S_1 anthracene. The rotational constants $(\frac{B+C}{2})$ and $(A-\frac{B+C}{2})$ used were, for the $|a\rangle$. $|b\rangle$, and $|c\rangle$ states, respectively: 0.4127, 1.7428; 0.4119, 1.7395; and 0.4117, 1.7389 GHz.
5. Same as Fig. 4 but using the rotational constants: 0.4116, 1.7383; 0.4119, 1.7397; and 0.4122, 1.7409 GHz for the $|a\rangle$, $|b\rangle$, and $|c\rangle$ states, respectively.

6. Measured fluorescence decays of the 1750 cm^{-1} (b-type) band in the E_{vib} = 1420 cm^{-1} spectrum of jet-cooled anthracene as a function of carrier gas parameters. Decays were measured under identical conditions except for carrier gas. For each decay $x = 6$ mm, the monochromator resolution $R = 3.2$ Å, and the laser bandwidth $BW \simeq 2$ cm^{-1}.
7. Fourier spectra ($I(\omega)$—see section II-B of Chapter 4) of the decays of Fig. 6. The peaks are negative because the 1 GHz component in the decays has a -1 phase.
8. Measured fluorescence decays for detection of the 1750 cm^{-1} band in the E_{vib} = 1420 cm^{-1} spectrum of anthracene for no carrier gas (top) and for 30 psig neon (bottom), all other conditions being the same ($BW \simeq 3$ cm^{-1}, $R = 8.0$ Å, $x = 3$ mm). The relative lack of modulation in the neon decay compared to the decay of Fig. 6-top is primarily due to the poorer detection spectral resolution used in obtaining the former decay.
9. Measured fluorescence decays for detection of the 780 cm^{-1} (a-type) band in the $E_{vib} = 1420$ cm^{-1} spectrum of jet-cooled anthracene as a function of carrier gas parameters. For each decay $x = 3$ mm, $R = 16$ Å, and $BW \simeq 2$ cm^{-1}.
10. Measured fluorescence decays for detection of the 1460 cm^{-1} (b-type) band in the $E_{vib} = 1380$ cm^{-1} spectrum of anthracene as a function of carrier gas parameters. For each decay $x = 3$ mm, $R = 0.8$ Å, and $BW \simeq 2$ cm^{-1}.

Figure 1

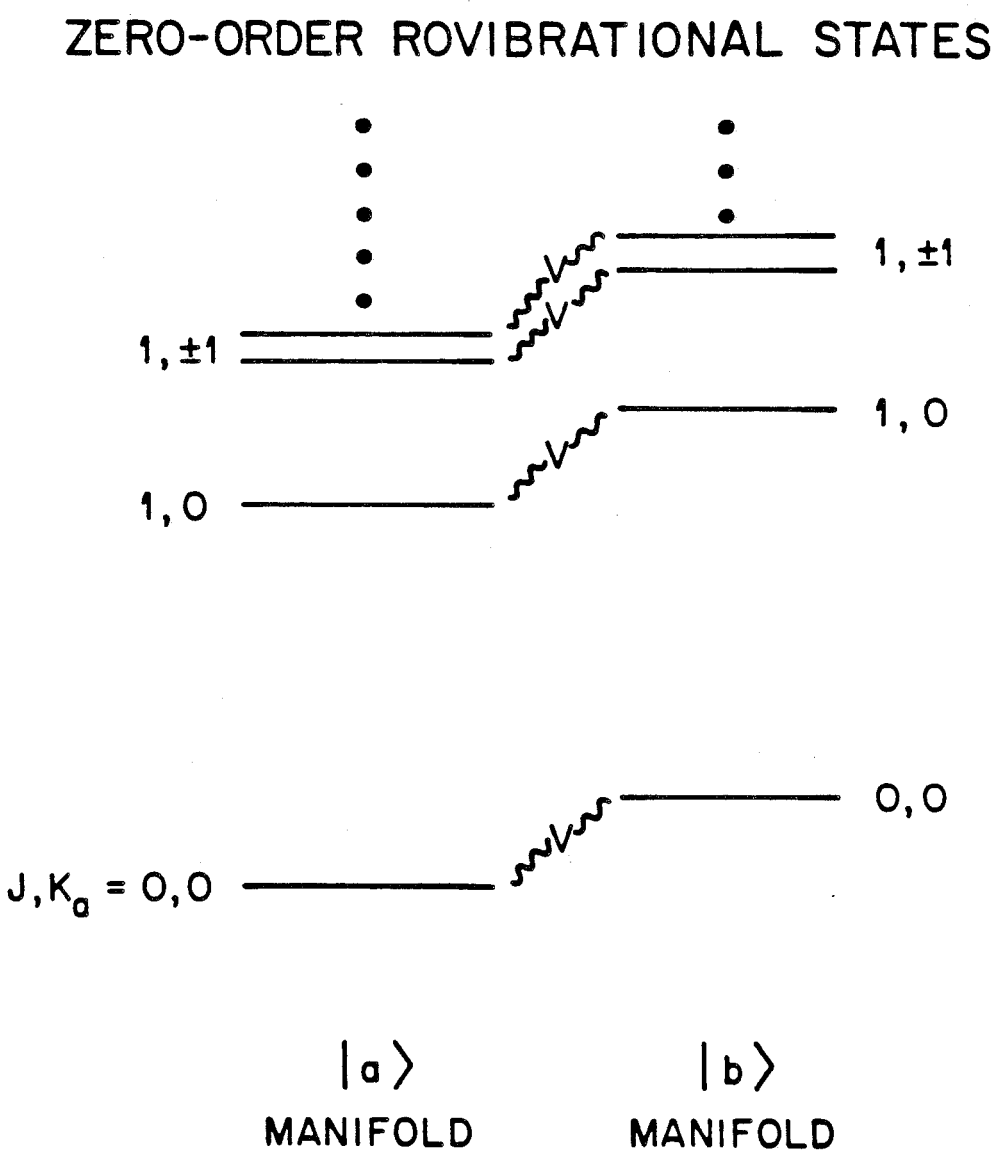
ZERO-ORDER ROVIBRATIONAL STATES
1, ±1
1, 0
J, K_a = 0, 0
1, ±1
1, 0
0, 0
V
V
V
V
|a⟩
MANIFOLD
|b⟩
MANIFOLD

Figure 2

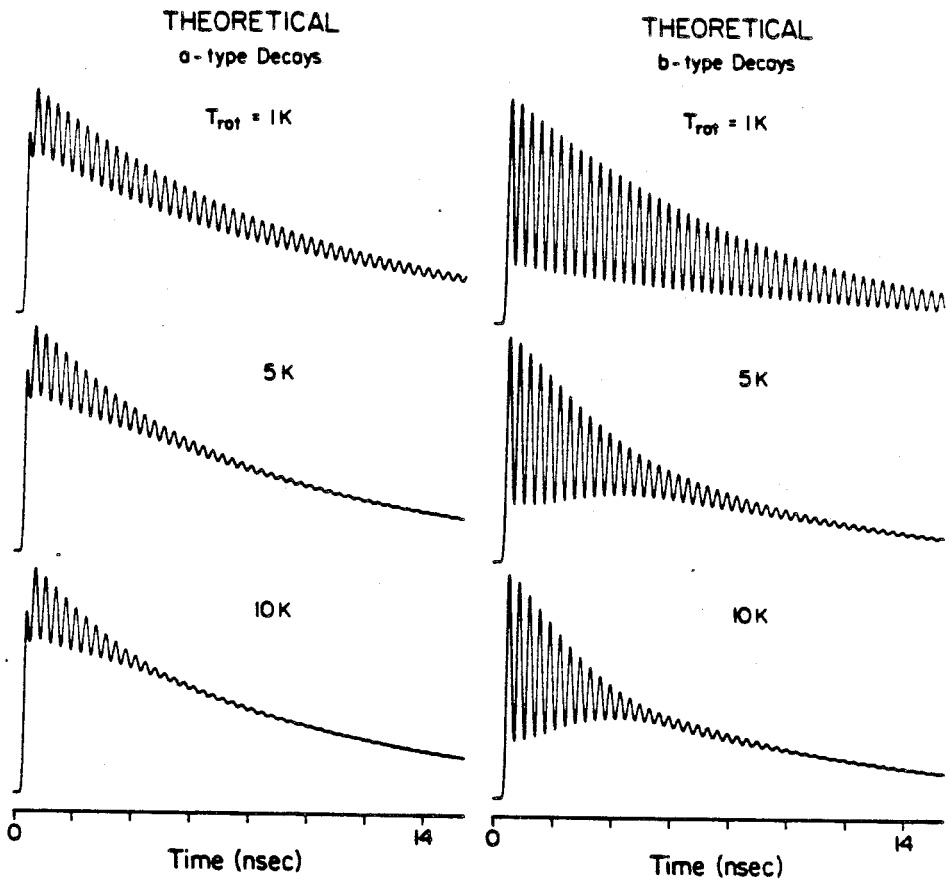
THEORETICAL
a-type Decoys
T_{rot} = 1K
5K
10K
0
14
Time (nsec)
THEORETICAL
b-type Decoys
T_{rot} = 1K
5K
10K
0
14
Time (nsec)

Figure 3

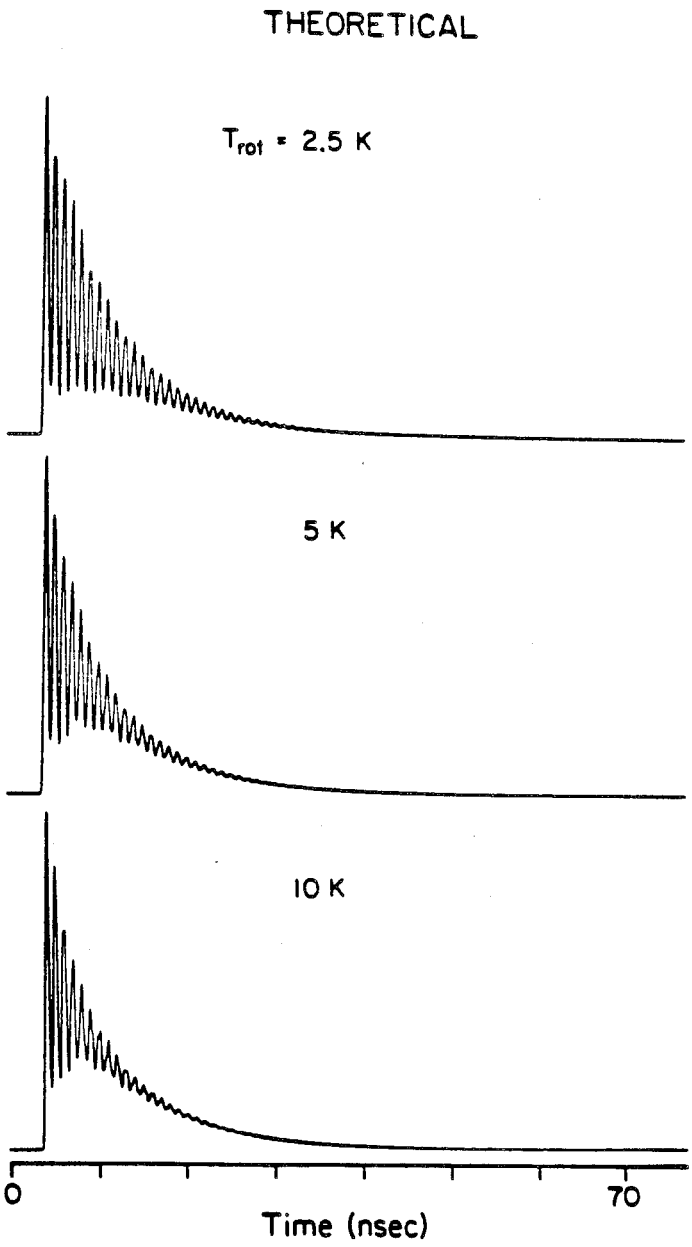

Figure 4

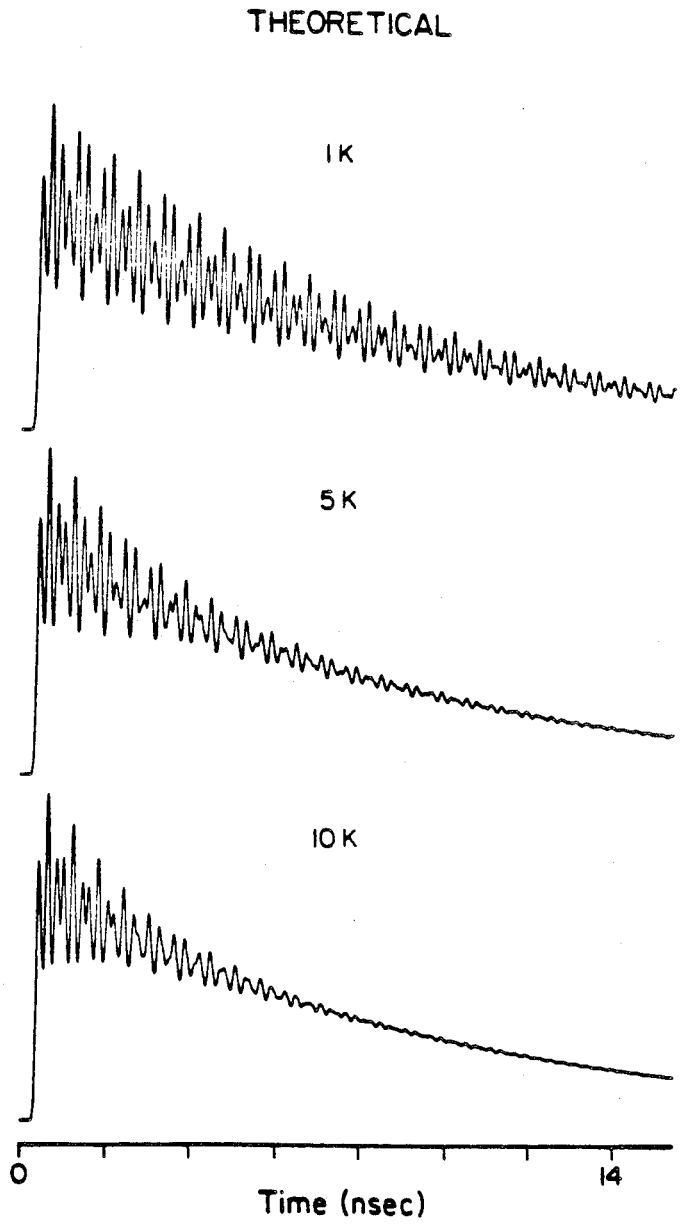

Figure 5

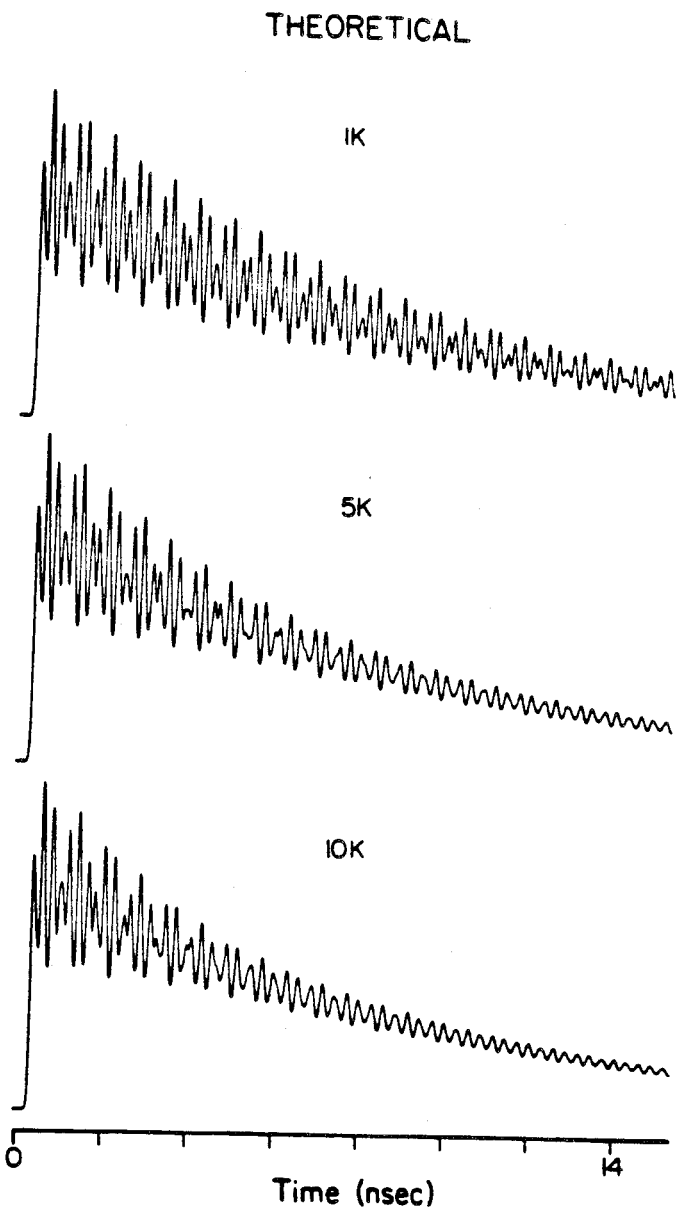

Figure 6

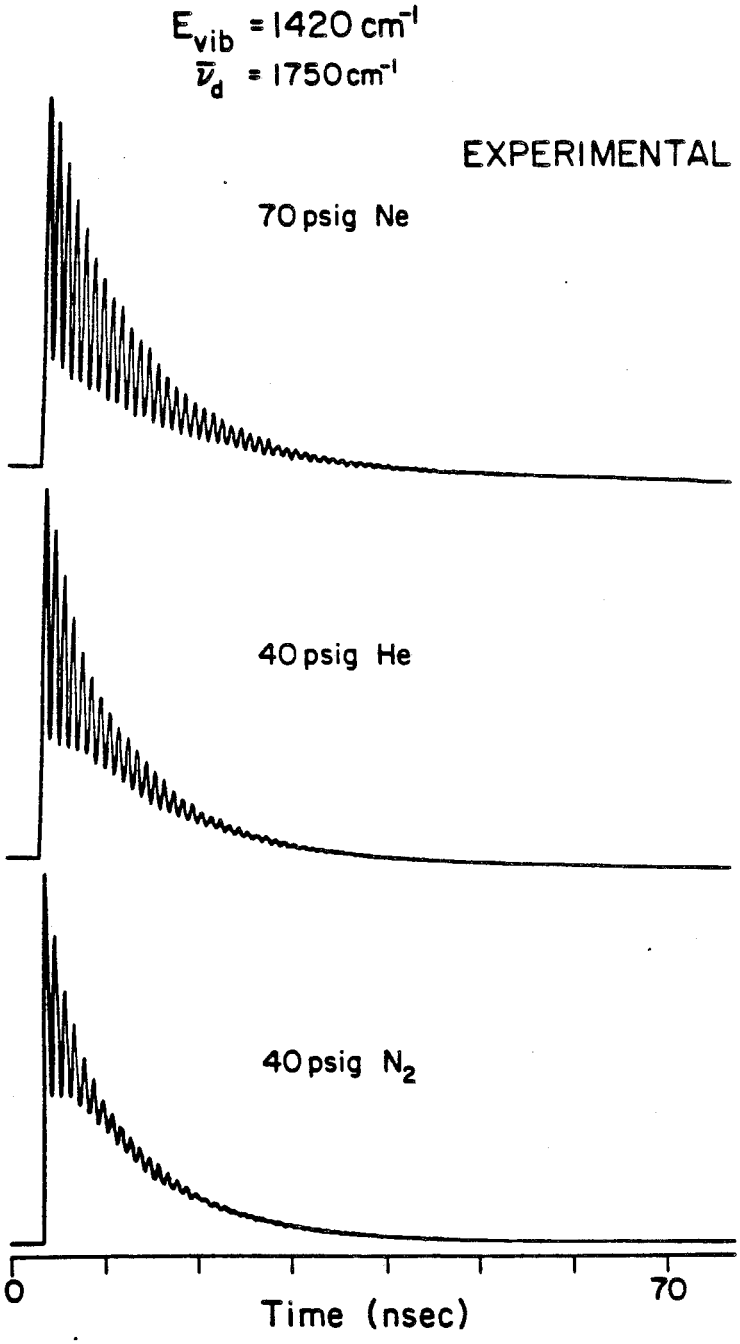
E_{vib} = 1420 cm^{-1}
$\bar{\nu}_d$ = 1750 cm^{-1}
EXPERIMENTAL
70 psig Ne
40 psig He
40 psig N_2
0
70
Time (nsec)

Figure 7

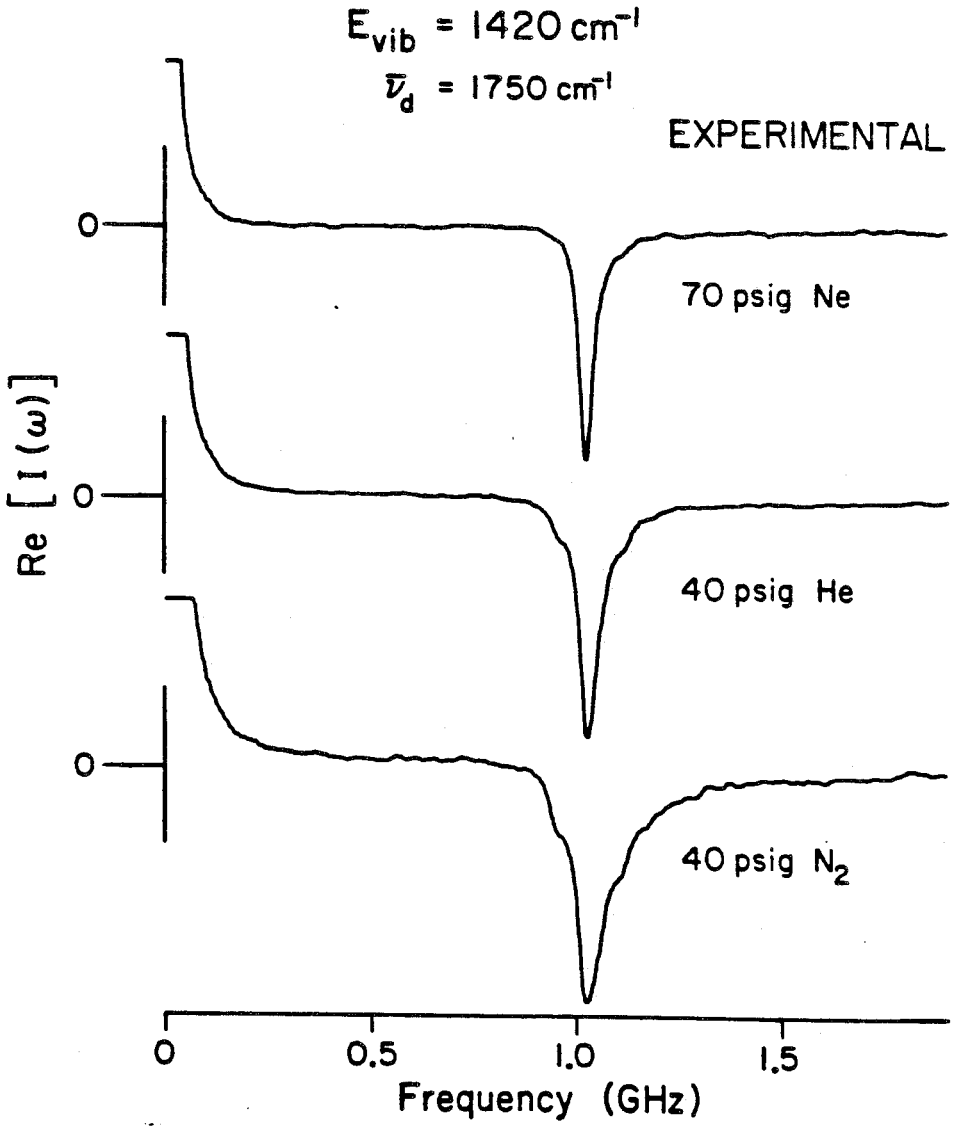
E_{vib} = 1420 cm^{-1}
$\bar{\nu}_d$ = 1750 cm^{-1}
EXPERIMENTAL
70 psig Ne
40 psig He
40 psig N_2
0
0
0
Re [I (ω)]
0
0.5
1.0
1.5
Frequency (GHz)

Figure 8

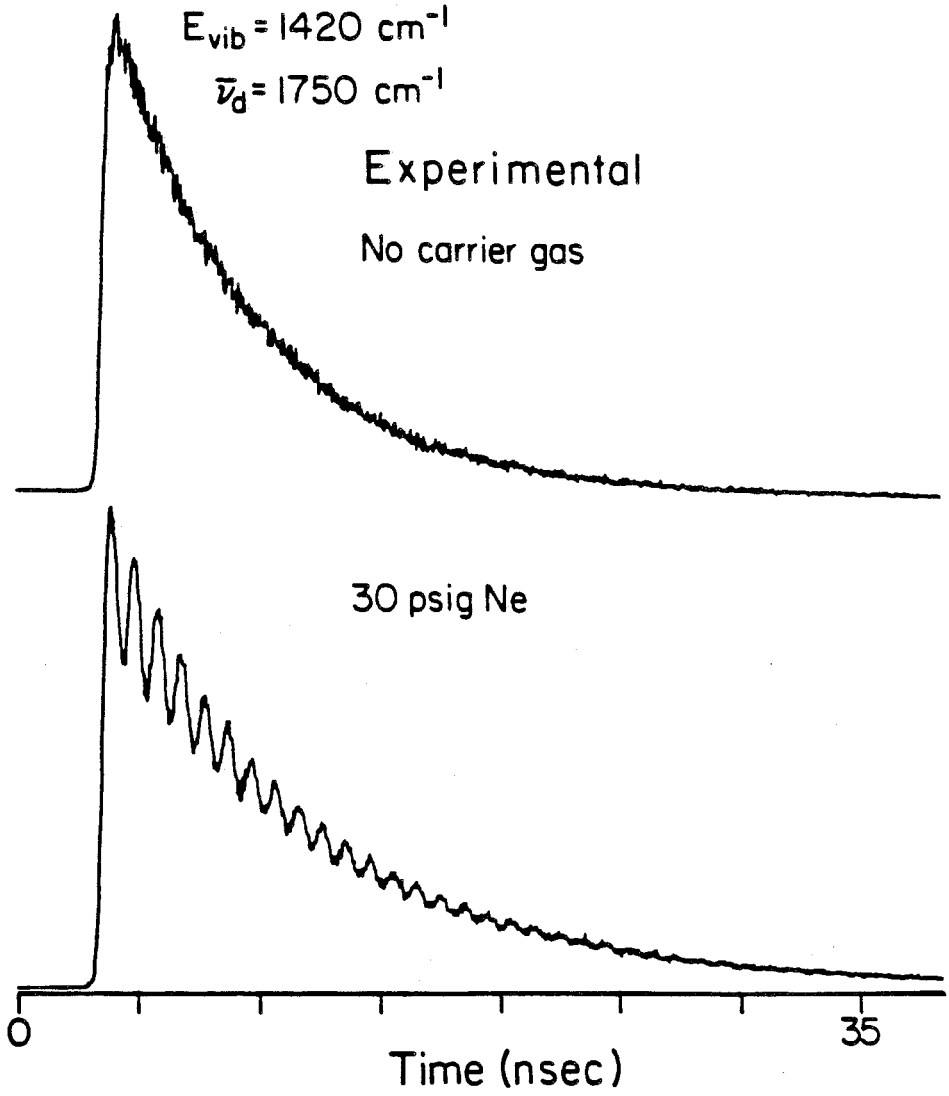
E_{vib} = 1420 cm^{-1}
$\bar{\nu}_d$ = 1750 cm^{-1}
Experimental
No carrier gas
30 psig Ne
0
35
Time (nsec)

Figure 9

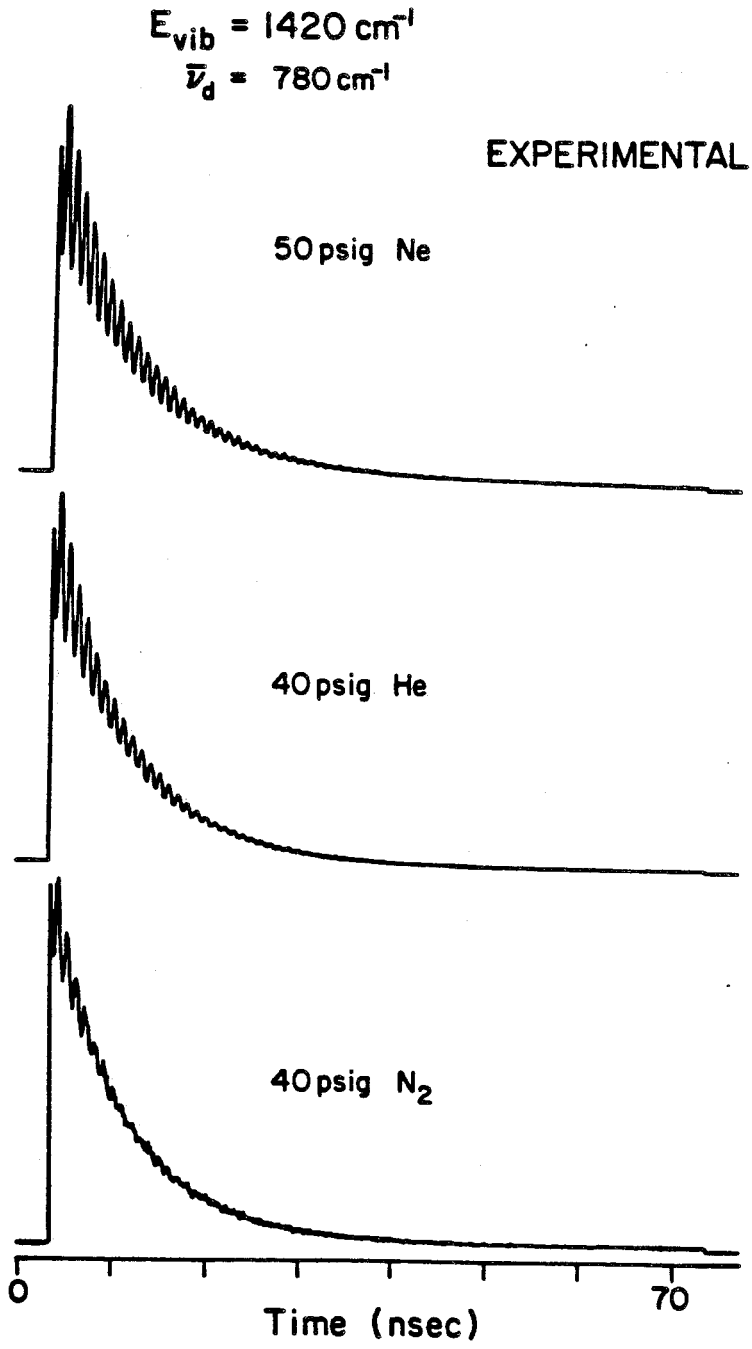
E_{vib} = 1420 cm^{-1}
$\bar{\nu}_d$ = 780 cm^{-1}
EXPERIMENTAL
50 psig Ne
40 psig He
40 psig N_2
0
70
Time (nsec)

Figure 10

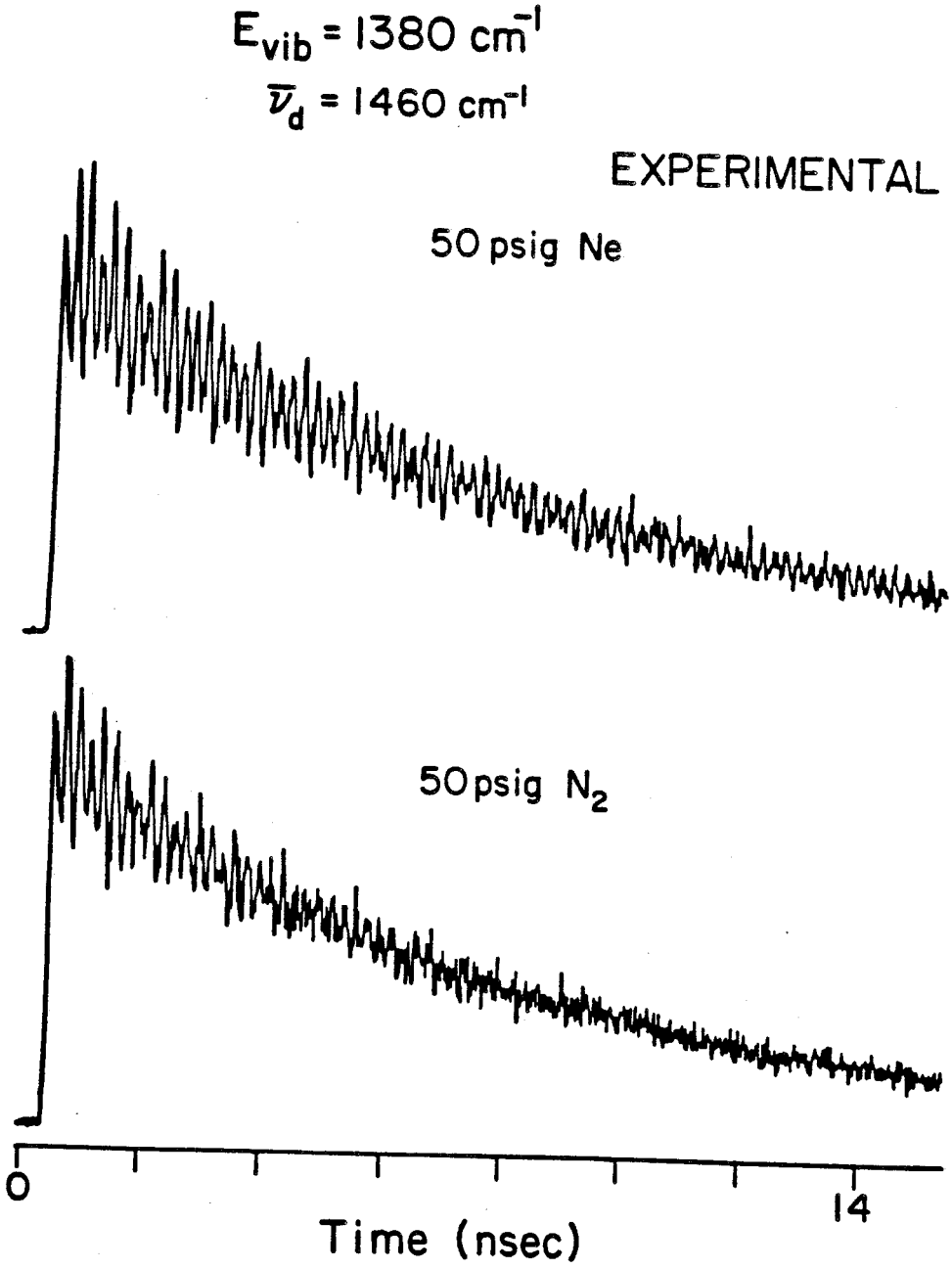
E_{vib} = 1380 cm^{-1}
$\bar{\nu}_d$ = 1460 cm^{-1}
EXPERIMENTAL
50 psig Ne
50 psig N_2
0
14
Time (nsec)

CHAPTER 6

ENERGY DEPENDENCE OF IVR IN *t*-STILBENE*

* Submitted to the Journal of Chemical Physics, as
"Dynamics of intramolecular vibrational-energy redistribution (IVR).
IV Excess energy dependence, *t*-stilbene,"
by P. M. Felker, W. R. Lambert, and A. H. Zewail

I. INTRODUCTION

In this chapter we present experimental studies of IVR in jet-cooled *t*-stilbene. The aim is to assess the generality of the picture of IVR which has emerged from the preceding three chapters.[1-3] For several reasons this picture of IVR might be considered primarily to be representative of "well-behaved" molecular systems such as anthracene. These reasons are rooted in the theoretical treatment of Chapter 3 and the assumptions made therein. It was shown in Chapters 4 and 5 that, for the anthracene molecule, the theory of Chapter 3 applies rather well, especially when account is taken of the possible rotational level dependence of anharmonic vibrational coupling. The uniqueness of the anthracene system arises from several molecular properties: 1) anthracene is a relatively rigid molecule and consequently less vulnerable to vibrational coupling interactions having matrix elements dependent on rotational level, 2) the molecule is of high enough symmetry (D_{2h}) to render the great majority of vibrational modes optically inactive and to effectively limit vibrational interactions, and 3) no ultra-fast radiationless process other than IVR occurs in the pertinent energy region of the S_1 state. IVR in molecules which undergo significant Coriolis vibrational coupling, which have a large fraction of optically active vibrational modes, or which are subject to photophysical or photochemical processes on timescales comparable to or more rapid than IVR, might not be expected to be well described by the theoretical treatment of Chapter 3.

With the above points in mind, one notes that *t*-stilbene has several characteristics that could render it less than well-behaved when compared with anthracene. The molecule has a number of low frequency, presumably large amplitude vibrational modes[4,5] (*e.g*, the phenyl torsions) which could induce large anharmonic coupling matrix elements or couplings with marked rotational level dependences. It has low symmetry (C_{2h}, or less[5,6]), which leads to rich spectral structure and, possibly, to complex coupling interactions. And, for sufficiently great vibrational energy in its S_1 state, it undergoes photoisomerization on a sub-nanosecond timescale.[7] It is possible, therefore, that IVR in the molecule need not be manifested experimen-

tally in the ways that are described in Chapter 3 and have been shown to apply to anthracene.

Herein, we report the results of measurements of the temporal behavior of dispersed fluorescence as a function of excess vibrational energy in S_1 *t*-stilbene. The results show behavior which is qualitatively similar to that observed for anthracene. In the low energy region, decays are predominantly single exponential. In an intermediate energy region, excitations exist which give rise to beat-modulated decays with spectrally dependent quantum beat phases. (The beats are observed at excess energies below the barrier energy for photoisomerization.) At higher energies, decays which show behavior typical of dissipative IVR processes are observed. While close scrutiny of the results reveals some deviations from the theory of Chapter 3 and the anthracene results of Chapter 4, the trend with energy argues for the general nature of the transition, first shown to occur in anthracene, from *absent* to *restricted* to *dissipative* IVR in large molecules.

II. EXPERIMENTAL

The experimental apparatus, procedures, and data handling techniques were primarily the same as used in Chapters 4 and 5. *trans*-Stilbene (Eastman, scintillation grade; or Aldrich, $\geq 96\%$) was heated to $\sim 125^{o}$ C and expanded with 30–50 psi He through a 100 μm pinhole into the vacuum chamber. The frequency doubled output of a synchronously pumped, cavity-dumped dye laser (DCM or R6G as dye) intersected the jet at $x = 3$ mm downstream from the expansion orifice. The determination of the particular absorption bands being excited in any given experiment was made by correlating the monochromator measurement of laser scatter with the normalized excitation spectrum of Ref. 5. The laser source was operated at all times with a three-plate birefringent filter as a tuning element. In many cases a fine or ultra-fine tuning etalon was also used. In the former tuning configuration the excitation bandwidth (BW) in the UV was ~ 5 cm^{-1}, while in the latter configurations it was $2-3$ cm^{-1}. Fluorescence was collected through a 0.5 M monochromator and detected with a fast photomultiplier. Decays were measured using time-correlated single photon counting. Data obtained with both 80 and 300 psec FWHM temporal resolution are presented here. Those decays obtained at the lower temporal resolution are indicated. The data were analyzed using the Fourier transform techniques and fitting procedures outlined in Chapter 4.

III. RESULTS

The UV spectroscopy of jet-cooled *t*-stilbene is quite complex[5,8,9] owing to the large number of optically active and low frequency vibrational modes in the molecule. Nevertheless, the dispersed fluorescence spectra[5] of the molecule as a function of vibrational energy show trends that have come to be regarded as characteristic of jet-cooled large molecules (see Figs. 1 and 2). For low energy excitations the spectra (for example, those of Fig. 1) are structured and contain significant amounts of vibrationally unrelaxed fluorescence (see section II-D of Chapter 3). At higher energies the spectra (Fig. 2) become very congested and consist primarily of vibrational relaxed emission. From the spectral trends one can come to some idea of the energy at which dissipative IVR appears to become significant. In *t*-stilbene this energy is about 1230 cm^{-1} (an energy near the threshold energy for photoisomerization[7] in the molecule). However, the transition from absent to restricted to dissipative IVR cannot be accurately identified without temporally resolved measurements, as discussed in Chapters 3 and 4. In the following, we present results divided into three energy groups, with the divisions based on temporally resolved data.

A. Low energy region

Many bands occur in the excitation spectrum[5,8,9] of *t*-stilbene in the region from $S_1 + 0$ to 752 cm^{-1}. While we cannot claim to have checked the temporal behavior of dispersed fluorescence for all significantly intense excitation bands in this region, we have made such measurements for the most prominent bands below $E_{vib} = 592$ cm^{-1} and for most of the significantly intense excitation bands in the $E_{vib} = 592$ to 752 cm^{-1} region. With one exception, the decays were found to exhibit no quantum beats. (Of course, it must be remembered that the observation of beats relies on sufficient temporal resolution.)

In contrast to the other excitation bands in its vicinity, excitation of the band at $S_1 + 663$ cm^{-1} gives rise to fluorescence bands, the decays of which are beat-modulated. Fig 1-lower left shows the fluorescence spectrum corresponding to this

excitation and Fig 3-lower left the decay of the band (marked by an asterisk in the spectrum of Fig. 1) shifted 800 cm^{-1} from the excitation energy. This decay is representative of the decays of most of the other bands in the spectrum. By Fourier analysis it is found to be modulated by a 780 MHz beat component (FWHM of about 250 MHz) which has a +1 phase (see Chapter 3). In addition to this type of decay, however, at least one weak band (e.g., the one at a $\simeq$ 585 cm^{-1}) was found to exhibit a decay modulated at the 780 MHz frequency but with a -1 phase. (It should be noted that this phase-shifted decay is not particularly well-modulated. This is discussed in section IV.) The presence of quantum beats and the dependence of their phases on detection indicate that, unlike levels of similar energy, the $E_{vib} = 663$ cm^{-1} level undergoes restricted IVR.

B. Intermediate energy region

In the region from E_{vib} = 789 to 1170 cm^{-1} a total of seven excitation bands have been observed to give rise to quantum beat-modulated decays. These bands are the ones at E_{vib} = 789, 821, 852, 860, 987, 1048, and 1170 cm^{-1}. The fluorescence spectra arising from excitation of these bands are given in Fig. 1. These excitations represent roughly one-half of the total number of prominent bands in this region of the excitation spectrum.[5] Dispersed fluorescence decays for the other excitation bands in this region have been measured with 80 psec temporal resolution and have been found to exhibit no obvious beats.

Fig. 3 shows representative decays for the seven beating excitations. The excitation energies are given in the figure. The respective detection wavelengths are given by asterisks in the spectra of Fig. 1. It is important to point out that the degree of detection resolution was found to be critical to the observation of these beat-modulated decays. (Thus, for example, no beats were observed at any excitation energy when the detection resolution was the worst the monochromator would allow, *i.e.*, 50 Å.) This fact implies that there is some dependence of decay behavior on detection wavelength, as is the case for anthracene.[2] Now, Fourier analysis of the decays of Fig. 3 reveals that all of the prominent beat frequencies in each of the decays occur with +1 phases. However, for three of the beating excitations, other dispersed fluorescence bands have been found to exhibit beating decays with components having −1 phases. The best example of phase-shifted behavior is shown in Fig. 4. The two decays arise from excitation to the E_{vib} = 789 cm^{-1} band. The top decay corresponds to detection of the 610 cm^{-1} band in the spectrum, while the bottom decay corresponds to detection of the 700 cm^{-1} band. Clearly, the dominant 1.3 GHz beat component is phase-shifted 180° in the lower decay relative to the upper one. Similar phase-shift behavior has been found for bands in the spectra of the E_{vib} = 860 and 987 cm^{-1} levels as well. For the four other beating excitations at E_{vib} = 821, 852, 1048, and 1170 cm^{-1}, the combination of weak fluorescence intensity and congested fluorescence spectra render very difficult

all but the most cursory experimental surveys of decays *vs.* detection wavelength. Thus, the fact of our not having observed phase-shifted beats for bands in these spectra does not at all mean that they do not exist.

The beat frequencies determined by Fourier analysis to be prominent in the decays of Fig. 3 are given in Table 1. It is pertinent to mention that the resolution in the Fourier spectra was 30 MHz and the typical beat component bandwidths were $\sim$ 250 Mhz. Thus, the values in the table reflect these sources of uncertainty.

C. High energy region

Excitation of *t*-stilbene to energies above $E_{vib} \sim 1230$ cm^{-1} in S_1 gives rise to fluorescence spectra which bear the characteristics of spectra of levels that undergo dissipative IVR, as may be seen from the the spectra of the $E_{vib} = 1246$ and 1249 cm^{-1} vibrational levels shown in Fig. 2. (For details of the excitation spectrum in this region see Ref. 5.) Inset in the figure are the blue portions of these spectra. One notices in the insets the weak band that occurs in each spectrum at a shift of 205 cm^{-1} from the excitation energy. Similar bands are also present in the spectra of the 1237, 1241, and 1332 cm^{-1} vibrational levels. These bands in each spectra can be confidently assigned in terms of transitions from the optically prepared state to the vibrational level in S_0 characterized by one quantum of the optically active ν_{25} vibrational mode.[5] They can therefore be assigned as vibrationally unrelaxed bands (see Chapter 3, section II-D). In turn, the broad, intense emission in the red parts of the spectra has the characteristics of vibrationally relaxed fluorescence.

Fig. 5 shows the decays that are observed when the 205 cm^{-1} bands in the $E_{vib} = 1237$, 1241, 1246, 1249, and 1332 cm^{-1} spectra are detected with 3 Å spectral resolution. Each decay, although being of the same, approximately double exponential form, is different from the others. This is apparent in the different modulation patterns that occur in their long-time components. We emphasize that these individual patterns are reproducible. Double exponential fits with convolution also reveal differences in the decays. Of particular pertinence are the short- and long-time decay constants and the ratios of fast to slow fluorescence, the values of which are given in Fig. 5. The values for the $E_{vib} = 1246$ and 1249 cm^{-1} decays are quoted quite confidently, since they have been reproduced many times. The other three excitations are less well-studied, especially the 1332 cm^{-1} one, and the values for them are quoted primarily to give an idea of approximate magnitudes from decay to decay.

Two experiments were performed to check for possible scatter artifacts in the decays of Fig. 5. The first experiment compared the decays observed (for the same

collection times) upon excitation to the 1249 cm^{-1} band and detection (3 Å resolution) at 3004 (Fig. 6a) and 2999 Å (Fig. 6b). The first detection wavelength corresponds to the 205 cm^{-1} band in the spectrum, while the second corresponds to no emission band and is closer to the laser wavelength. The second experiment involved tuning the excitation source to 10 cm^{-1} to the blue of the E_{vib} = 1249 cm^{-1} band, a region of the excitation spectrum that has little intensity, and detecting at a 205 cm^{-1} red shift from this. The "decay" that was observed is shown in Fig. 6c and should be compared with the decay corresponding to on-resonance 1249 cm^{-1} excitation and detection of the 205 cm^{-1} band (Fig. 6a). Clearly, the results of both experiments represented in Fig. 6 argue against scatter artifacts in the measured decays.

While the double exponential form characterizes the decays of the 205 cm^{-1} in the high energy spectra, similar decays have not been observed when detecting in the vibrationally relaxed region of the spectra. Here, decays devoid of any early time spike and with lifetimes matching those of the long components of the Fig. 5 decays are characteristic of the transients observed for these detection wavelengths. An example is shown in Fig. 7. Given that spectral evidence and the decays of Fig. 5 are indicative of dissipative IVR, one might expect decays such as that shown in Fig. 7 to exhibit finite risetimes matching the initial decay time of the pertinent transient in Fig. 5 (see Chapter 3, section VI-B). In fact, the decay of Fig. 7 does show a risetime. However, it should be noted that this behavior, at least in the best-studied case of excitation to E_{vib} = 1249 cm^{-1}, is not the same for every detection wavelength in the vibrationally relaxed region; the apparent risetimes of decays change with detection wavelength. This is probably the result of underlying vibrationally unrelaxed emission in the vibrationally relaxed region. (We note that this behavior is somewhat different from that observed for dissipative IVR in anthracene,[2] for which risetimes in the relaxed spectral region are less sensitive to detection wavelength and apparently match the initial decay of the unrelaxed emission.)

IV. DISCUSSION

A. IVR vs. vibrational energy

The general trend of the experimental results as a function of vibrational energy in *t*-stilbene is very similar to that of the results of jet-cooled anthracene (Chapter 4). In the low energy regime ($\leq$ 752 cm^{-1}) the data (except for one vibrational level) indicate the absence of IVR on the timescale of the fluorescence lifetime. For intermediate energies (789-1170 cm^{-1}), the presence of phase-shifted quantum beats points to the existence of restricted IVR and vibrational coherence effects. Finally, at high energies ($>$ 1230 cm^{-1}), the decay behavior is consistent with dissipative IVR.

One may note that the onsets of restricted and dissipative IVR in *t*-stilbene occur at vibrational energies significantly lower than the onset energies in anthracene.[2] There are two plausible explanations for this. It is first instructive to consider the vibrational density of states (ρ_{vib}) *vs.* vibrational energy (E_{vib}) for the molecules. A plot of ρ_{vib} *vs.* E_{vib} for *t*-stilbene appears in Fig. 8. (A listing of the frequencies used and an outline of the calculation of ρ_{vib} is given in an appendix to this chapter.) Comparing Fig. 8 to the ρ_{vib} for anthracene (Fig. 25, Chapter 4), one can see that the *t*-stilbene curve is shifted to lower energy. (This is primarily due to the larger number of low frequency vibrational modes[4,5] in the molecule.) It seems likely that this shift of ρ_{vib} to lower energy is responsible for the lower energy IVR onsets in *t*-stilbene. Indeed, if one directly compares the ranges of ρ_{vib} for the restricted and dissipative IVR energy regions, respectively, in the two molecules, it is evident that the values for *t*-stilbene ($\sim$ 10 to 50 per cm^{-1}, and $>$ 160 per cm^{-1}) are very close to those for anthracene ($\sim$ 25 to 40 per cm^{-1} and 120 per cm^{-1}). A second possible reason for the lower energy onsets of IVR in *t*-stilbene involves its reduced symmetry relative to that anthracene. While in anthracene, symmetry restrictions are expected to limit the vibrational states available to couple with one another, these restrictions are significantly reduced in *t*-stilbene. Thus, the effective density of states available for coupling in the latter molecule is a greater fraction

of the total density of states. This factor may be manifest in the fact that even in terms of ρ_{vib}, *t*-stilbene IVR seems to "turn on" sooner than anthracene IVR.

B. IVR timescales and coupling matrix elements

Besides the trend in the nature of IVR as a function of energy, the IVR timescales and vibrational coupling matrix elements manifested in *t*-stilbene decays are similar to those characterizing the process in anthracene.[2] In the restricted regime, recurrence times on the order of several hundreds of picoseconds seem to be the rule. In the dissipative regime, the timescales for initial vibrational dephasing are similar to that of the $E_{vib} = 1792$ cm^{-1} decays in anthracene. One point of interest in this regard, that is dealt with more explicitly in Chapter 7, is that there is a vibrational mode dependence to the dissipative IVR rate in the $E_{vib} \simeq 1240$ cm^{-1} region.[10] Further characterization of this mode specificity awaits work pertaining to the assignment of the vibrational levels involved.

Regarding the vibrational coupling matrix elements manifested in the modulated decays, the data for *t*-stilbene are not as amenable to quantitative analysis as those for anthracene (section IV of Chapter 4). Reasons for this are dealt with in the next section. Nevertheless, the order of magnitude for the coupling matrix elements can be obtained fairly accurately from the beat frequencies. From Table 1, one sees that restricted IVR in *t*-stilbene arises from vibrational couplings of similar magnitude to the couplings in anthracene. In the dissipative regime one can calculate[11] the variance in coupling matrix elements $\bar{V}$, analogous to the 3.8 GHz value calculated for anthracene (see section VI-B of Chapter 4), by making use of a golden rule-type relation: $\frac{1}{\tau_{ivr}} \simeq 2\pi\bar{V}^2\rho$. If one assumes C_2 or C_i symmetry for the molecule and symmetry restrictions on vibrational coupling, then $\rho = \frac{\rho_{vib}}{2} = 80$ cm^{-1} for $E_{vib} \simeq 1240$ cm^{-1}. Using this, $\bar{V}$ is found to range from about 1.1 to 1.7 GHz for the vibrational levels in the 1240 cm^{-1} energy region.

C. Vibrational coherence in *t*-stilbene vs. anthracene

Although there is much about the experimental results on *t*-stilbene which is similar to the anthracene results (Chapter 4) and which is readily interpreted in the context of the theory of Chapter 3, there are also significant points of difference that must be addressed. A first such aspect is the fact that for the observed phase-shifted (non-*a*-type) decays of *t*-stilbene the sum of modulation depths of the beat components are not nearly as large as they are in anthracene or as they are predicted to be (see (2.17) of Chapter 3). This is evident from Fig. 4 for E_{vib} = 789 cm^{-1} and occurs to an even greater degree for the 663, 860, and 987 cm^{-1} excitations. We have treated possible reasons for such behavior in section V of Chapter 3. Aside from "trivial" reasons (*e.g.*, insufficient temporal or spectral resolution) there are at least two other causes which would seem to be plausible given the molecule's characteristics. Firstly, owing to the reduced symmetry of *t*-stilbene, one expects a large fraction (relative to anthracene) of its vibrational modes to be optically active. In turn, the probability of encountering two or more coupled optically active vibrational levels is higher. Such a situation runs counter to the basic assumptions of Chapter 3 and has been shown (section V-E, Chapter 3) to give rise to undermodulated non-*a*-type decays. Secondly, the presumed nonrigidity of the molecule would be expected to lead to some large anharmonic coupling matrix elements which could couple widely separated zero-order vibrational states. As has been shown in section V-A of Chapter 3, this can lead to less than ideal modulation depths.

A second point of difference between the *t*-stilbene and anthracene results is the fact that many prominent excitation bands in the energy region corresponding to restricted IVR in *t*-stilbene are nonbeating excitations, while in anthracene, beating excitations seem to be much more prevalent. Reasons for this could be the same as those given above for the poorly modulated non-*a*-type decays. In addition, one may note that the relative nonrigidity of the molecule might be expected to lead to a large rotational influence in vibrational coupling compared to more rigid

molecules. For instance, vibrational levels involving a large amplitude phenyl torsional motion could conceivably have very different rotational constants than levels involving benzene-type vibrational motions. Now we have shown in Chapter 5 that if vibrational levels with small differences (*i.e.*, one part in a thousand) in rotational constants are coupled, then the vibrational coherence effects arising from the coupling are partially washed out. *Large* differences in rotational constants might be expected to completely mask these effects. Also, it may be that the "nonbeating" excitation bands correspond to S_1 vibrational levels that undergo significant Coriolis interactions. Finally, it is possible that there is some mode selectivity for vibrational coupling in the restricted IVR regime, in which case some of the nonbeating levels may be nonbeating simply because they are not effectively coupled to any other levels. We note that there is evidence[10] for such mode selectivity in the dissipative regime of the molecule.

A third aspect of *t*-stilbene quantum beats which should be addressed is the fact that for four excitation energies, beating decays have been observed to be modulated, at least in part, by a component at about 780 MHz. It seems unlikely that four unrelated vibrational levels would each be coupled to a nearby level such that all four coupled systems would give rise to pairs of eigenstates separated by the 780 MHz energy interval. In response to this we would make several points. Firstly, spectroscopic evidence indicates that two of the pertinent excitations, $E_{vib} = 663$ cm^{-1} and $E_{vib} = 860$ cm^{-1}, *are* related. The 860 cm^{-1} band is a combination band of the 663 cm^{-1} interval and the optically active ν_{25} interval.[5] Since this is so, one can certainly imagine that the vibrational coupling situation (*i.e.*, the zero-order Hamiltonian matrix) at the 663 cm^{-1} energy might be very similar to that at the 860 cm^{-1} energy. In such a case, the resulting beat-modulated decays would also be very similar. A second point is that the resolution in the Fourier spectra and the inherent breadth of the Fourier components in these spectra (probably due to rotational level effects[3]) render it difficult to determine beat frequencies to better than $\pm$100 MHz. Thus, there may be real differences in the beat frequencies which

are not apparent from Fourier analysis. Further, there is other evidence that not all the decays are modulated in the same way, in that the decays corresponding to the levels at $E_{vib} = 987$ and 1170 cm^{-1} have other beat components. Finally, it is possible that the prevalence of the 780 MHz splitting is not fortuitous but instead represents a vibrational splitting of the kind that would arise between eigenstates of a multiple-well potential. The phenyl torsional potential surface in *t*-stilbene is of this kind. This problem, however, is outside the scope of this chapter.

In ending this section it is pertinent to note that the energy corresponding to the onset of dissipative IVR in *t*-stilbene is very similar to the experimentally deduced threshold energy for photoisomerization. It is likely that this is not fortuitous and that there is a strong connection between the two processes. The question is what this connection is. One can certainly see how IVR might be necessary for the photoisomerization to occur. But, it may also be true that the molecular changes associated with isomerization influence the redistribution of vibrational energy. It is notable that IVR at 1250 cm^{-1} is faster than the fastest photisomerization rate that has been measured thus far ($\simeq 7.5 \times 10^9$ sec^{-1} at $E_{vib} = 2950$ cm^{-1}). This is at least partial justification for the treatment of the isomerization rates in terms of a statistical method (*i.e.*, RRKM).[7b]

V. CONCLUSIONS

IVR in S_1 *t*-stilbene follows much the same trend with energy as does the (in many ways) dissimilar molecule, anthracene. At low energies there is no apparent vibrational evolution of optically prepared states on the timescale of the fluorescence lifetime. At intermediate energies ($\sim$ 760 to 1170 cm^{-1}) restricted IVR is manifested as phase-shifted quantum beat-modulated fluorescence decays. At high excitation energies ($>$ 1230 cm^{-1}) IVR becomes dissipative in nature. The occurrence of this trend in more than one molecule suggests its generality and allows for comparison of details of the IVR in different species. Such comparison does, in fact, show differences between vibrational coupling and IVR in *t*-stilbene *vs.* that in anthracene, which differences can be attributed to differences in molecular characteristics.

APPENDIX

The density of states results presented in Fig. 8 were calculated using a direct count procedure.[13] The frequencies used in the count were obtained from three sources: 1) our assignments (Ref. 5) of S_1 modes from the fluorescence excitation spectrum, 2) assignments of modes from IR and Raman work (Ref. 12), and 3) calculated frequencies (Ref. 4). The frequencies used appear in Table 2. Note that only frequencies less than 1500 cm^{-1} are pertinent. This is why all 72 normal modes of the molecule are not represented in the table. We would note that the calculated ρ_{vib} is sensitive to the grouping of the frequencies for the direct count and to the values used for the lowest frequency modes, as illustrated in Ref. 7b.

REFERENCES

1. P. M. Felker and A. H. Zewail, J. Chem. Phys. - submitted.
2. P. M. Felker and A. H. Zewail, J. Chem. Phys. - submitted.
3. P. M. Felker and A. H. Zewail, J. Chem. Phys. - submitted.
4. A. Warshel, J. Chem. Phys. **62**, 214(1975).
5. J. A. Syage, P. M. Felker, and A. H. Zewail, J. Chem. Phys. (in press).
6. M. Traetteberg, E. B. Frantsen, F. C. Mijlhoff, and A. Hoekstra, J. Mol. Struct. **26**, 57(1975).
7. (a) J. A. Syage, W. R. Lambert, P. M. Felker, A. H. Zewail, and R. M. Hochstrasser, Chem. Phys. Lett. **88**, 268(1982); and references therein; (b) J. A. Syage, P. M. Felker, and A. H. Zewail, J. Chem. Phys. (in press).
8. A. Amirav and J. Jortner, Chem. Phys. Lett. **95**, 295(1983).
9. T. S. Zwier, E. Carrasquillo M., and D. H. Levy, J. Chem. Phys. **78**, 5493(1983).
10. P. M. Felker and A. H. Zewail, J. Phys. Chem. - submitted.
11. C. Tric, Chem. Phys. **14**, 189(1976).
12. Z. Meic and H. Gusten, Spectrochim. Acta **34A**, 101(1978).
13. L. R. Khunkar, R. A. Marcus, A. H. Zewail, J. Phys. Chem. **87**, 2473(1983).

Table 1. Prominent beat frequencies modulating the decays of Fig. 3.

E_{vib} in cm^{-1}	Frequencies $(\omega/2\pi)$ in GHz
663	0.78
789	1.3 ; 1.75[a]
821	1.35 ; 6.1 ; 7.0 ; 7.4[b]
852	1.6
860	0.78
987	0.75 ; 1.4
1048	0.55 ; 3.3 ; 3.9
1170	0.75 ; 0.9[c] ; 1.8

[a] This frequency does not appear in the decay of Fig. 3 but does prominently modulate the decays of some of the bands in the $E_{vib} = 789$ cm^{-1} spectrum.

[b] Other higher frequency bands also appear to be present, but noise in the Fourier spectrum obscures them.

[c] The 0.75 and 0.9 GHz components may be parts of one very wide band in the Fourier spectrum.

Table 2. *trans*-Stilbene normal mode frequencies (in cm^{-1}) used in the density of states calculation (Fig. 8).

83[a]	88[b]	95[a]	108	198[a]	233
239	280[a]	338	410	455	467
526	540	591[a]	612	622[a]	675
691	735	763	840	842	845
846[a]	907	916	963	969	969
973[a]	985	995[a]	998	999	1027
1059	1069	1153	1156	1181	1187
1218	1249[a]	1297	1315	1321[b]	1329
1336[a]	1336	1339	1430[a]	1450	1463[a]
1494					

[a] From Ref. 5.

[b] From Ref. 4.

All other values are from Ref. 12.

FIGURE CAPTIONS

1. Dispersed fluorescence spectra of jet-cooled *t*-stilbene for excitation energies that have been observed to give rise to beat-modulated fluorescence decays. Excess energies in S_1 for the excitations are given in cm^{-1} in the figure and the excitation wavelengths are marked with arrows in the spectra. The asterisks refer to detection wavelengths for the decays of Fig. 3. All of the spectra were obtained using similar experimental conditions (see text): *i.e.*, $BW = 2-3$ cm^{-1}; and monochromator resolution $R = 0.5$ Å for most spectra, except $R = 0.65$ Å for the $E_{vib} = 821$ and 860 cm^{-1} spectra and $R = 0.32$ Å for the $E_{vib} = 789$ cm^{-1} spectrum.

2. Dispersed fluorescence spectra of jet-cooled *t*-stilbene for excitation to $S_1 +$ 1246 cm^{-1} (top), and $S_1 + 1249$ cm^{-1} (bottom). Inset are the blue portions of each spectrum. In all spectra the positions of the excitation wavelength and the 205 cm^{-1} band are marked. Both the main spectra were obtained with $BW \simeq 2$ cm^{-1} and $R = 0.64$ Å. For the insets $BW \simeq 2$ cm^{-1} and $R = 3.2$ Å.

3. Quantum beat-modulated fluorescence decays observed for excitation of various bands (the excess S_1 vibrational energies are given in cm^{-1} in the figure) of jet-cooled *t*-stilbene . The particular fluorescence band detected for each decay is given by an asterisk in the appropriate spectrum in Fig. 1. All decays were obtained with 80 psec temporal resolution and $BW \simeq 5$ cm^{-1}, except the ones corresponding to the $S_1 + 852$ and 860 cm^{-1} excitations, which were measured with 300 psec resolution and $BW \simeq 2$ cm^{-1}. R for the decays was 1.6 Å, except the $S_1 + 821$ and 987 cm^{-1} decays for which $R = 3.2$ Å and 16.0 Å, respectively.

4. Fluorescence decays of two bands in the $E_{vib} = 789$ cm^{-1} spectrum of *t*-stilbene. The wavenumber shifts of the bands from the excitation energy are given in the figure. Note the clear phase-shift of the prominent 1.3 GHz beat component in the lower relative to the upper decay. For both decays $BW \simeq 5$ cm^{-1}. For the upper decay $R = 1.6$ Å, and for the lower one $R = 1.2$ Å.

5. Decays and double exponential fits corresponding to the 205 cm^{-1} bands in the (from top to bottom) E_{vib} = 1237, 1241, 1246, 1249, and 1332 cm^{-1} spectra of jet-cooled *t*-stilbene. Given in the figure are the best fit parameters for both the fast and slow lifetimes, and the ratio (F/S) of pre-exponential factors of fast *vs.* slow fluorescence. All decays were obtained using $BW \simeq 2$ cm^{-1} and $R = 3.2$ Å.
6. Comparison of decays observed for similar collection times for: a) on-resonance excitation and detection of the 205 cm^{-1} band in the $E_{vib} = 1249$ cm^{-1} spectrum of *t*-stilbene, b) on-resonance excitation of the $S_1 + 1249$ cm^{-1} band and off-resonance detection ($\lambda_d \simeq 2999$ Å or $\bar{\nu}_d \simeq 150$ cm^{-1}), and c) off-resonance excitation (10 cm^{-1} to the blue of the 1249 cm^{-1} band) and "on-resonance" detection in the region of the 205 cm^{-1} band. All other experimental conditions were the same for all three decays: $BW \simeq 2$ cm^{-1} and $R = 1.6$ Å.
7. Measured fluorescence decay for detection in the blue part of the vibrationally relaxed region of the $E_{vib} = 1249$ cm^{-1} spectrum of *t*-stilbene. The detection wavelength is given in the figure. The decay has a risetime similar to the initial decay time (47 psec) of the 205 cm^{-1} band in the same spectrum, and a long component having the same lifetime (2.0 nsec) as the long component of the 205 cm^{-1} decay. The decay was measured with $BW \simeq 2$ cm^{-1} and $R = 3.2$ Å.
8. Vibrational density of states (ρ_{vib}) *vs.* vibrational energy (E_{vib}) in S_1 *t*-stilbene, calculated as outlined in the appendix to this chapter. In the figure are given the characteristic times for IVR in the absent, resticted, and dissipative regimes.

Figure 1

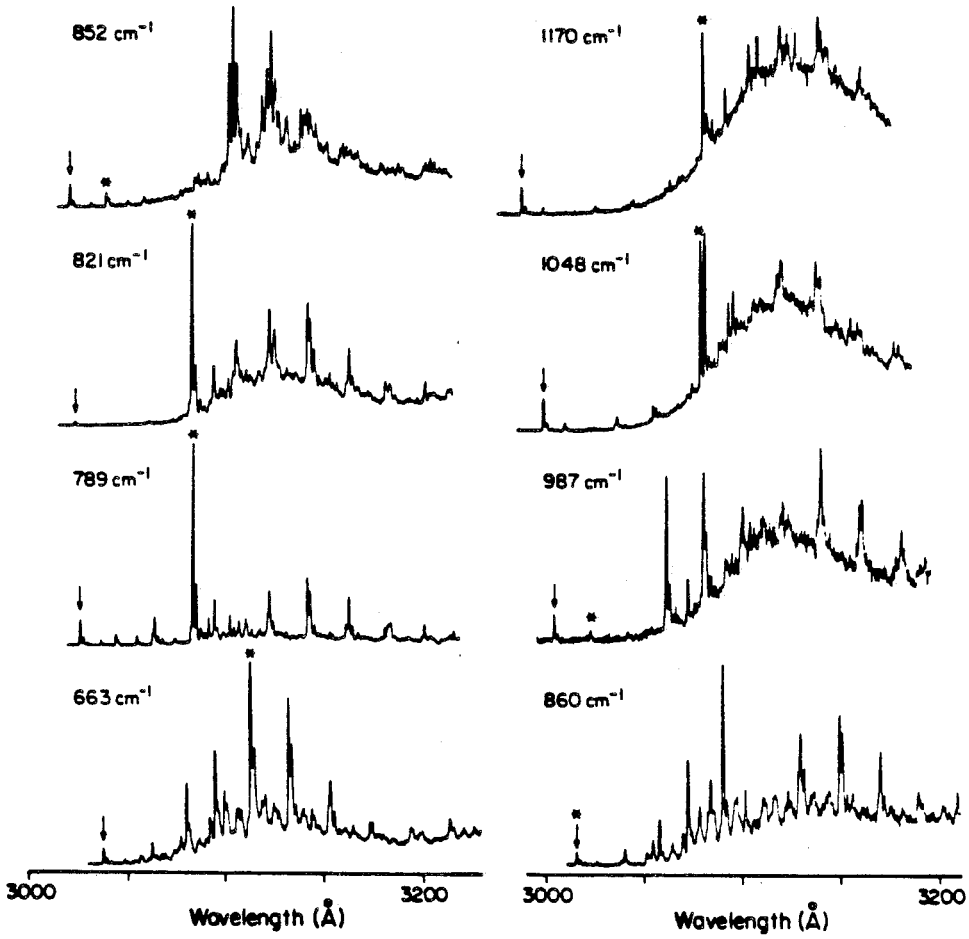
852 cm⁻¹
1170 cm⁻¹
821 cm⁻¹
1048 cm⁻¹
789 cm⁻¹
987 cm⁻¹
663 cm⁻¹
860 cm⁻¹
3000
3200
Wavelength (Å)
3000
3200
Wavelength (Å)

Figure 2

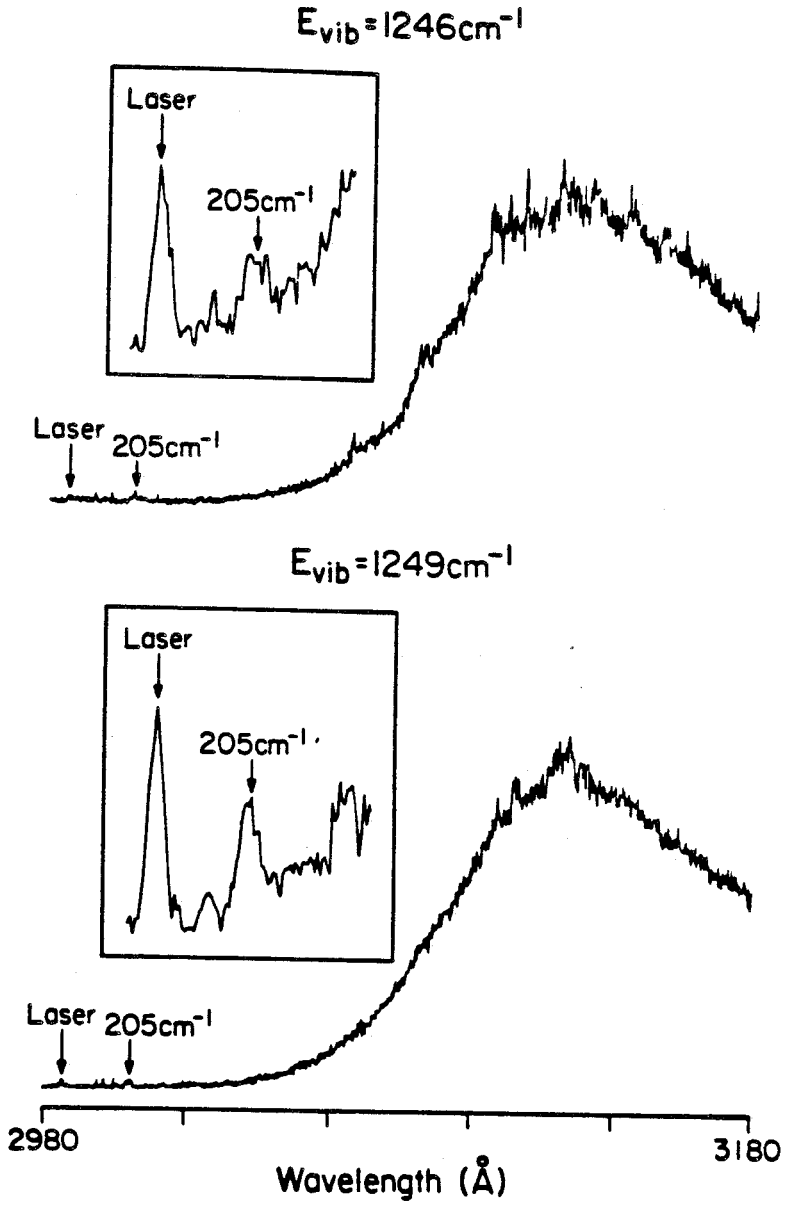
E_{vib}=1246cm^{-1}
Laser
205cm^{-1}
Laser
205cm^{-1}
E_{vib}=1249cm^{-1}
Laser
205cm^{-1}
Laser
205cm^{-1}
2980
3180
Wavelength (Å)

Figure 3

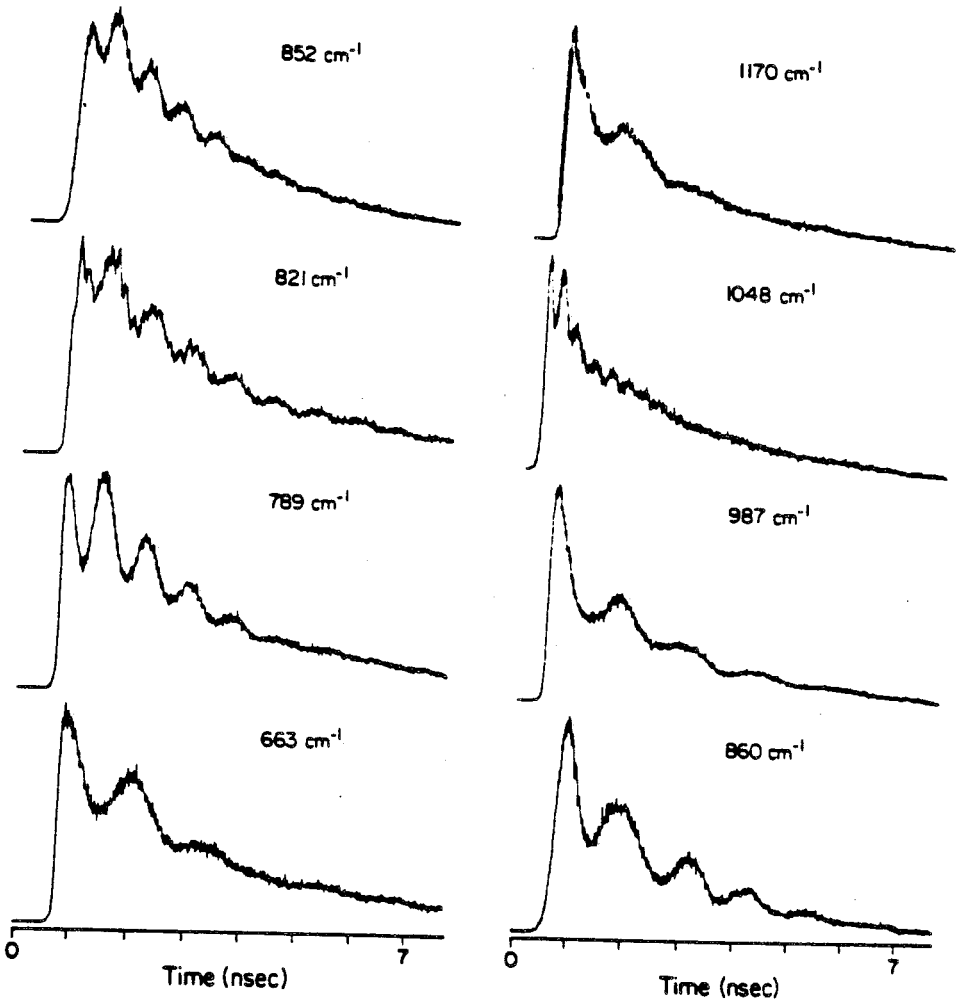
852 cm⁻¹
1170 cm⁻¹
821 cm⁻¹
1048 cm⁻¹
789 cm⁻¹
987 cm⁻¹
663 cm⁻¹
860 cm⁻¹
0
7
Time (nsec)
0
7
Time (nsec)

Figure 4

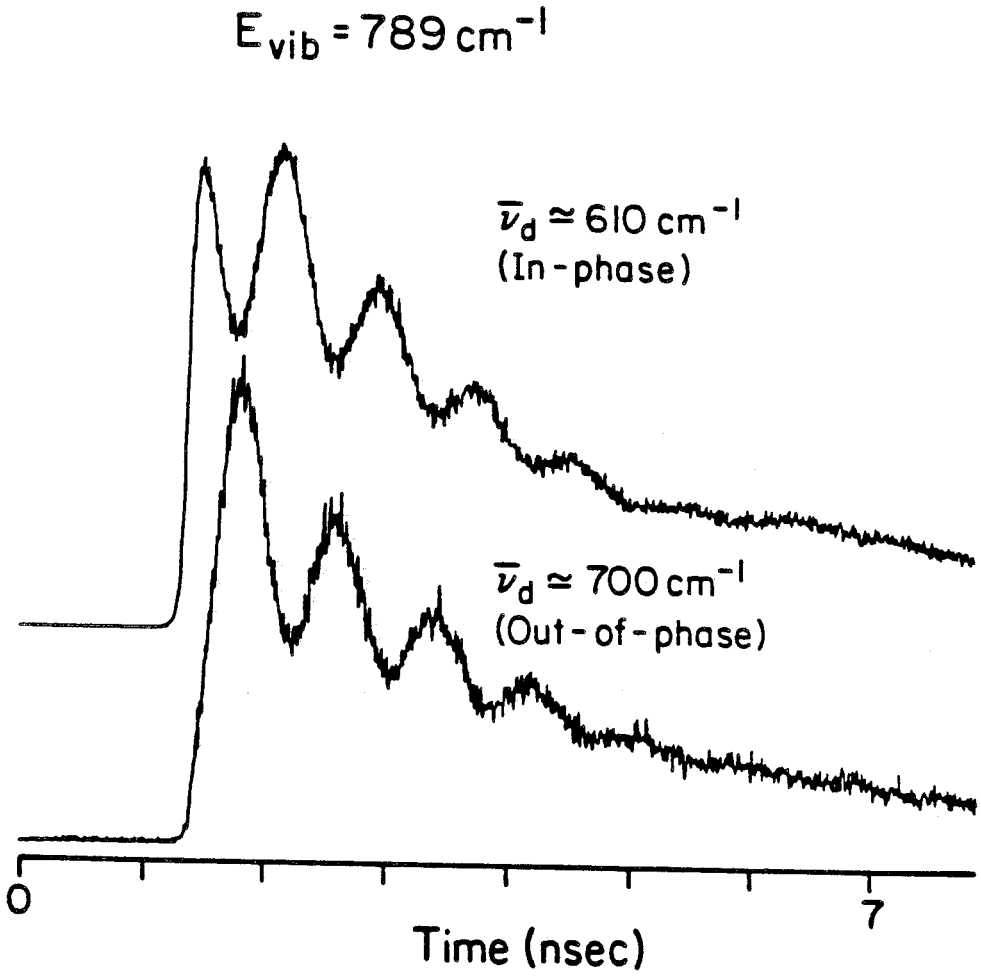
$E_{vib} = 789\ cm^{-1}$
$\bar{\nu}_d \simeq 610\ cm^{-1}$
(In-phase)
$\bar{\nu}_d \simeq 700\ cm^{-1}$
(Out-of-phase)
0
7
Time (nsec)

Figure 5

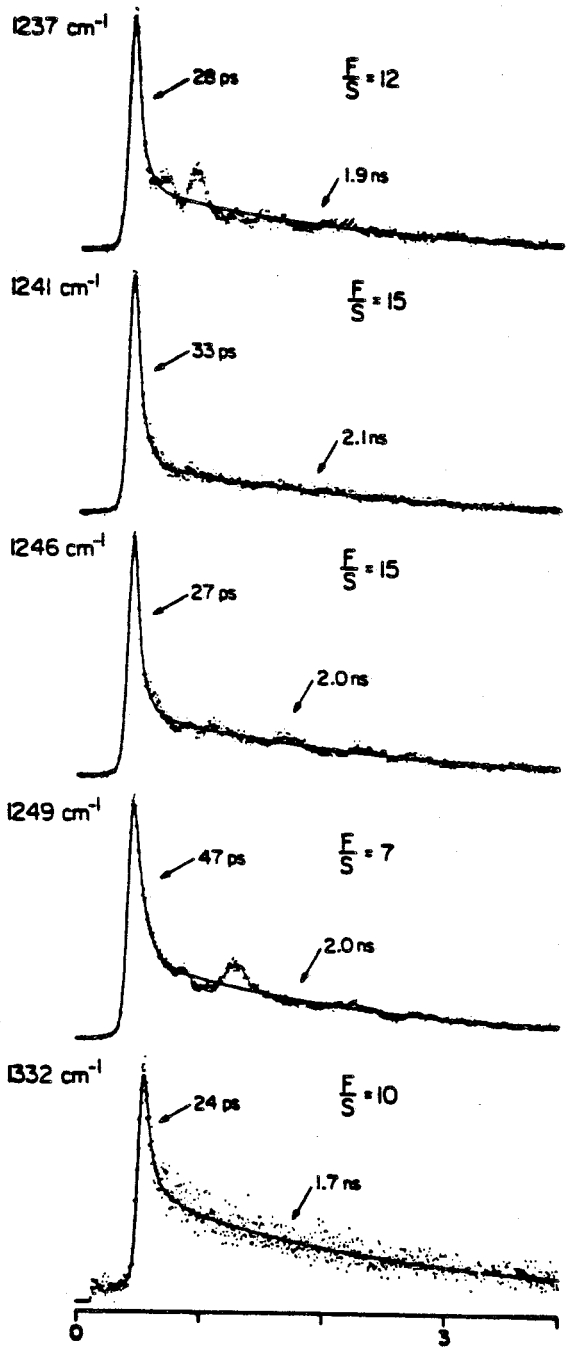
1237 cm⁻¹
28 ps
F/S = 12
1.9 ns
1241 cm⁻¹
F/S = 15
33 ps
2.1 ns
1246 cm⁻¹
F/S = 15
27 ps
2.0 ns
1249 cm⁻¹
47 ps
F/S = 7
2.0 ns
1332 cm⁻¹
24 ps
F/S = 10
1.7 ns
0
3

Figure 6

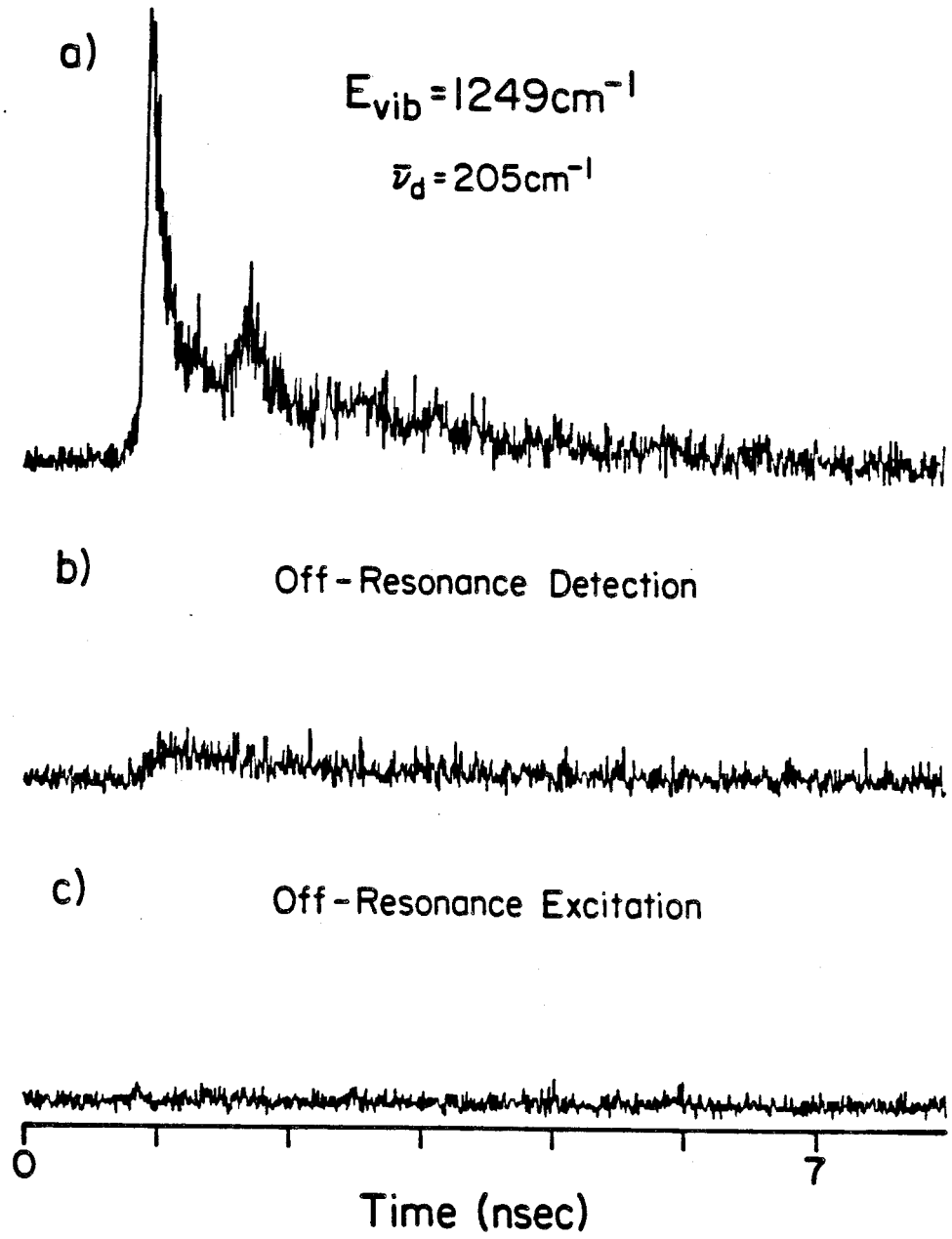
a)
$E_{vib} = 1249 cm^{-1}$
$\bar{\nu}_d = 205 cm^{-1}$
b)
Off-Resonance Detection
c)
Off-Resonance Excitation
0
7
Time (nsec)

Figure 7

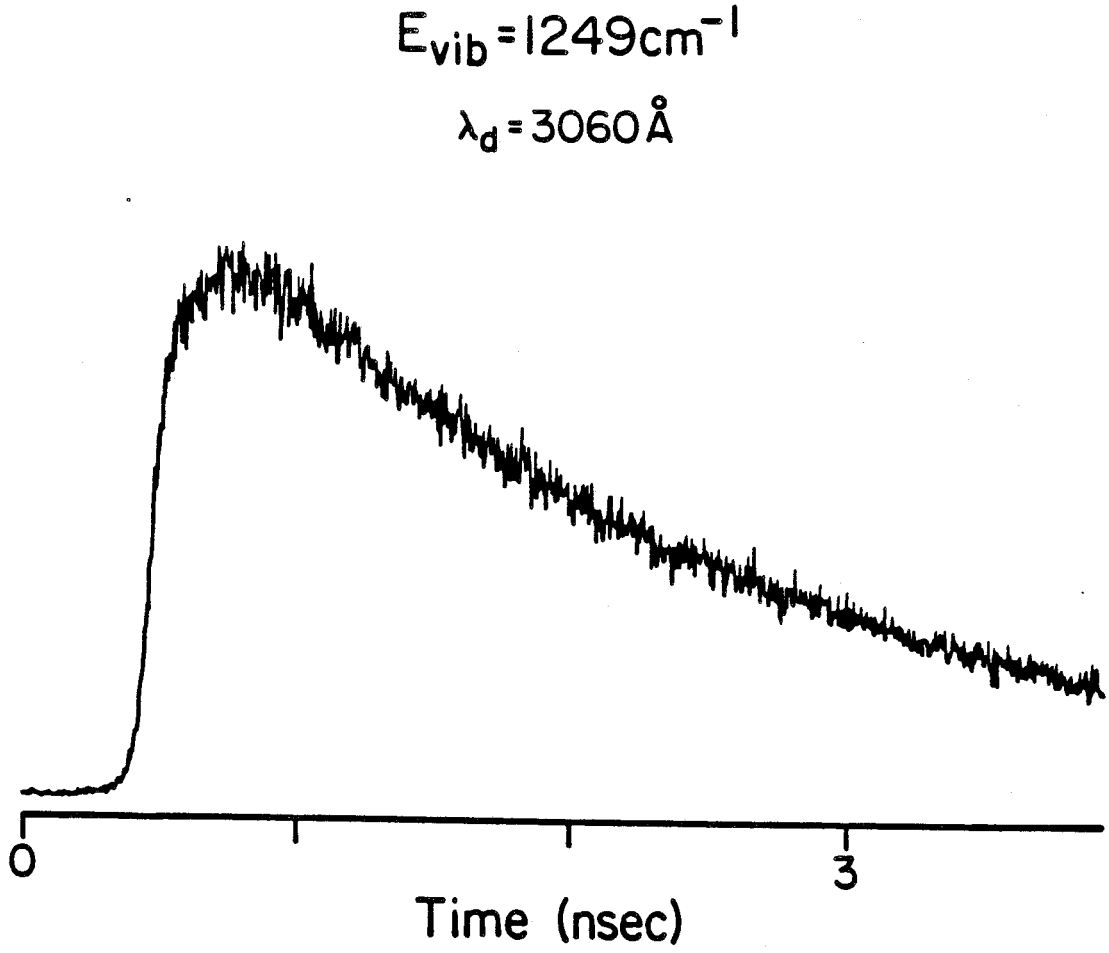

Figure 8

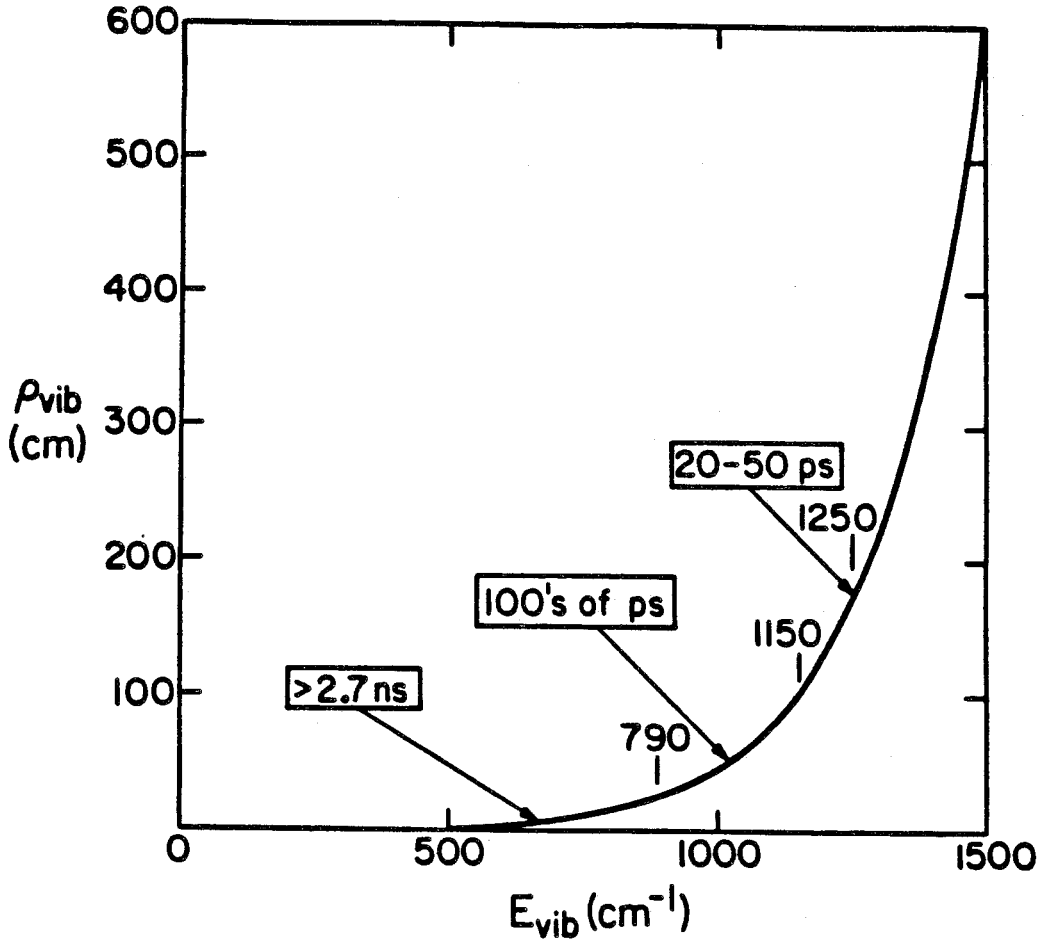
600
500
400
300
200
100
0
500
1000
1500
ρvib (cm)
Evib (cm-1)
20-50 ps
1250
100's of ps
1150
>2.7 ns
790

CHAPTER 7

MODE-SPECIFIC IVR: DIRECT PICOSECOND RESULTS*

* Submitted to the Journal of Physical Chemistry, as
"Mode-specific IVR: Direct picosecond results,"
by Peter M. Felker and Ahmed H. Zewail

The characterization of intramolecular vibrational-energy redistribution (IVR) in the high energy regime is presently one of the most challenging problems in intramolecular dynamics.[1] An issue of particular importance concerns the dependence of IVR dynamics on the *character* of the initially excited vibrational motion. One would like to know whether certain types of levels couple more efficiently than other types to the intramolecular bath of vibrational states. Such dependences, if they were to exist in the high energy regime, would show that dissipative IVR need not be solely governed by excess vibrational energy and would help to pinpoint the molecular parameters influencing the IVR process.

Recently, (time-integrated) dispersed fluorescence measurements have spectroscopic features that are consistent with mode-dependent vibrational coupling in *para*-difluorobenzene.[2] However, the timescales for the selective IVR of different modes have not been reported yet, since this requires direct picosecond temporal resolution of the IVR.

In this chapter, we report on the direct measurement of mode-dependent, dissipative IVR rates in jet-cooled *t*-stilbene. It is found that excitation of different bands in the $S_1 + 1250$ cm^{-1} energy region of the molecule gives rise to different IVR rates, as determined by the temporal evolution of vibrationally unrelaxed fluorescence. The results are discussed in terms of the spectroscopic assignments for the excitation bands.

The experimental system has been described in detail elsewhere.[3] *trans*-Stilbene (Eastman scintillation grade, or Aldrich > 96%) at 125° C was expanded with 30 to 40 psig He through a 100 μm pinhole into an evacuated chamber. The frequency-doubled output ($\Delta\bar{\nu} \simeq 2$ cm^{-1}) of a synchronously pumped, cavity-dumped dye laser (Rhodamine 6G as dye) excited the jet at $x = 3$ mm from the pinhole. Fluorescence was detected at right angles through a monochromator. Decays were measured by time-correlated single photon counting with a system response function of about 80 psec FWHM.[4] The decays of vibrationally unrelaxed fluorescence were fit to a double exponential decay function. Various checks of carrier gas de-

pendences and the effects of off-resonance excitation and detection were made to verify the intramolecular natures of the decays (as opposed to their being the result of intermolecular interactions or laser scatter).

In the $S_1 + 1250$ cm^{-1} region of the *t*-stilbene excitation spectrum,[5] there exist four closely spaced bands at 1236, 1240, 1246, and 1249 cm^{-1}. Here, we are primarily concerned with the two bluest bands. Excitation to these bands gives rise to very similar fluorescence spectra. An example is the spectrum of Fig. 1, which corresponds to the 1249 cm^{-1} band. One notices the weak, structured blue portion of the spectrum near the excitation energy, and the broad, intense portion near and to the red of the $S_1 - 0_0^0$ transition energy of the molecule. Fig 2a shows the decay and double exponential fit of the weak 205 cm^{-1} band in the $E_{vib} = 1246$ cm^{-1} spectrum and Fig. 2b shows that of the same band in the $E_{vib} = 1249$ cm^{-1} spectrum. (Similar (approximately) double exponential decays also occur for detection of the 205 cm^{-1} bands in the $E_{vib} = 1236$ and 1240 cm^{-1} spectra.) For neither excitation have decays like those of Fig. 2 been observed for detection wavelengths greater than 3060 Å (*i.e.*, the broad intense region in Fig. 1). In this region, only decays with long ($\sim$ 2 nsec) components, or long components with risetimes similar to the initial decay times of the Fig. 2 transients[6], have been observed.

Inset in Fig. 2 are the early time portions of the two transients. One can tell from the insets that the initial decay of the 1246 cm^{-1} transient is faster than that of the 1249 cm^{-1} one. This is verified by the double exponential fits, which give lifetimes of 27 psec and 2.0 nsec for the 1246 cm^{-1} decay and 47 psec and 2.0 nsec for the 1249 cm^{-1} decay. While the long lifetimes are similar and match the lifetimes for detection in the red region of the spectrum, the short decays are measurably and reproducibly different.

The fluorescence spectra of the $E_{vib} = 1246$ and 1249 cm^{-1} excitations show the characteristics of spectra which arise from optically prepared levels that undergo significant vibrational state mixing. The blue regions of each consist of weak, readily assignable bands (the 205 cm^{-1} band can be assigned as a transition from the

S_1 optically prepared state to the S_0 level characterized by one quantum of the strongly optically active ν_{25} mode[5]) which represent vibrationally unrelaxed (U) transitions, while the broad, intense region to the red of about 3100 Å corresponds to the superposition of a large number of predominantly vibrationally relaxed (R) bands.

The two decays shown in Fig. 2 are consistent with the two types of decays expected for U and R fluorescence in the dissipative IVR regime. As we have discussed elsewhere,[7] the double exponential decay behavior of U bands can be interpreted in terms of a fast dissipative IVR process (initial decay) that leads to an approximate steady-state in energy flow (long component). The fact that dissipative IVR occurs in the $E_{vib} \simeq 1250\ cm^{-1}$ region of the *t*-stilbene level structure also is consistent with the facts that 1) the density of vibrational states at this energy (~ 160 per cm^{-1}) is similar to the density of states at which dissipative IVR occurs in anthracene (*i.e.*, ~ 120 per cm^{-1}), and 2) the energy region below 1170 cm^{-1} in the molecule has been found[8] to consist of levels, some of which show manifestations (phase-shifted quantum beats) in fluorescence decays of restricted IVR.[9]

That which is novel, however, is that the levels at 1246 and 1249 cm^{-1} have significantly different IVR rates. Moreover, the higher energy level has a slower IVR decay rate than the lower energy one. In a simple golden-rule picture such behavior could be due to either inhomogeneities in the density of "bath" vibrational states (ρ_{vib}) in the 1246-49 cm^{-1} region or to a factor of ~ 1.5 difference in the average coupling matrix elements (V) that connect the optically prepared levels to the bath states. Since ρ_{vib} at this energy is fairly high, one does not expect inhomogeneities of sufficient magnitude to effect a factor of two difference in rates. On the other hand, spectroscopic considerations[5] have led to the assignment of the 1246 cm^{-1} interval as a combination band and the 1249 cm^{-1} interval as a fundamental vibration. Since the two levels are of significantly different vibrational character, one might expect them to be characterized by different V. *Thus the*

mode-dependent dissipative IVR, manifested as different decay rates, seems likely to have origins in the different natures of the vibrational motions initially excited. A full account of this work will be published later when the picosecond IVR dynamics of other levels in *t*-stilbene is characterized.

REFERENCES

1. For a review see: C. S. Parmenter, Faraday Discuss. Chem. Soc. **75**, 7(1983).

2. M. Fujii, T. Ebata, N. Mikami, M. Ito, S. H. Kable, W. D. Lawrance, T. B. Parsons, and A. E. W. Knight, J. Chem. Phys. **88**, 2937(1984).

3. W. R. Lambert, P. M. Felker, and A. H. Zewail, J. Chem. Phys. **81**, 2217(1984).

4. In Ref. 3 the photomultiplier tube that was used was considerably slower than the tube used for the obtaining the results reported in this paper. This is the reason for the much faster response function quoted herein.

5. J. A. Syage, P. M. Felker, and A. H. Zewail. J. Chem. Phys. (in press).

6. It should be noted that apparent risetimes for decays in this region vary with detection wavelength from 50 psec to faster than this. This is probably due to contributions from vibrationally unrelaxed emission.

7. P. M. Felker and A. H. Zewail, Chem. Phys. Lett. **108**, 303(1984).

8. P. M. Felker, W. R. Lambert, A. H. Zewail, J. Chem. Phys. - submitted.

9. P. M. Felker and A. H. Zewail, Chem. Phys. Lett. **102**, 113(1983); P. M. Felker and A. H. Zewail, Phys. Rev. Lett. **53**, 501(1984).

FIGURE CAPTIONS

1. Dispersed fluorescence spectrum of the $S_1 + 1249$ cm^{-1} level of *t*-stilbene. Inset in the figure is that portion of the spectrum (the vibrationally unrelaxed region) near the excitation wavelength. The monochromator resolution R for the inset was 3 Å ($\sim$ 30 cm^{-1}). For the main spectrum $R = 0.6$ Å. Other experimental conditions are given in the text.
2. Measured decays (dots) with double exponential fits (lines) of the 205 cm^{-1} fluorescence bands in the $S_1 + 1246$ cm^{-1} spectrum (top) and the $S_1 + 1249$ cm^{-1} spectrum (bottom) of *t*-stilbene. Inset are the expanded early time portions of the two measured decays, and the fast lifetimes obtained from the double exponential fits (convolution of the system temporal response function was accounted for). Both decays were measured with $R = 3.2$ Å. Other experimental conditions are given in the text.

Figure 1

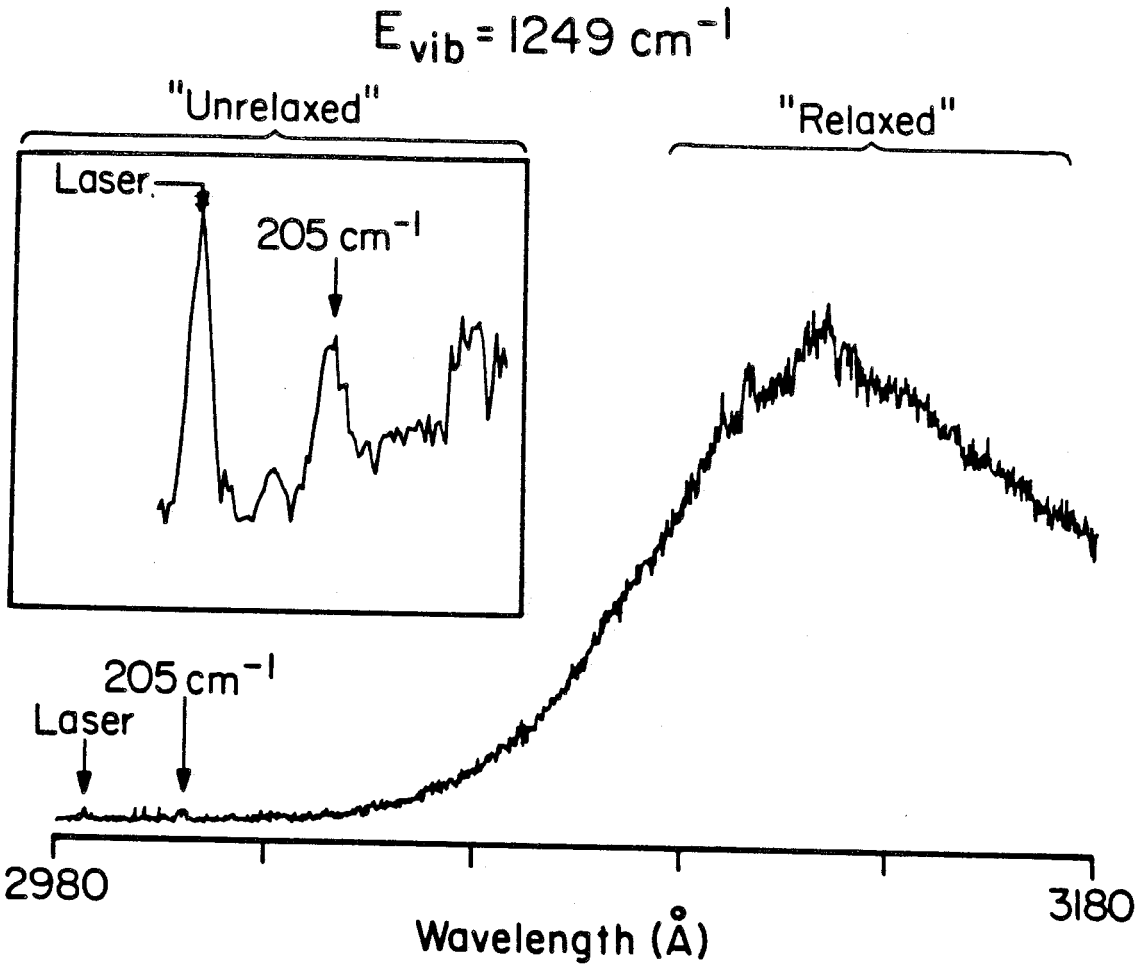
E_{vib} = 1249 cm^{-1}
"Unrelaxed"
"Relaxed"
Laser
205 cm^{-1}
205 cm^{-1}
Laser
2980
3180
Wavelength (Å)

Figure 2

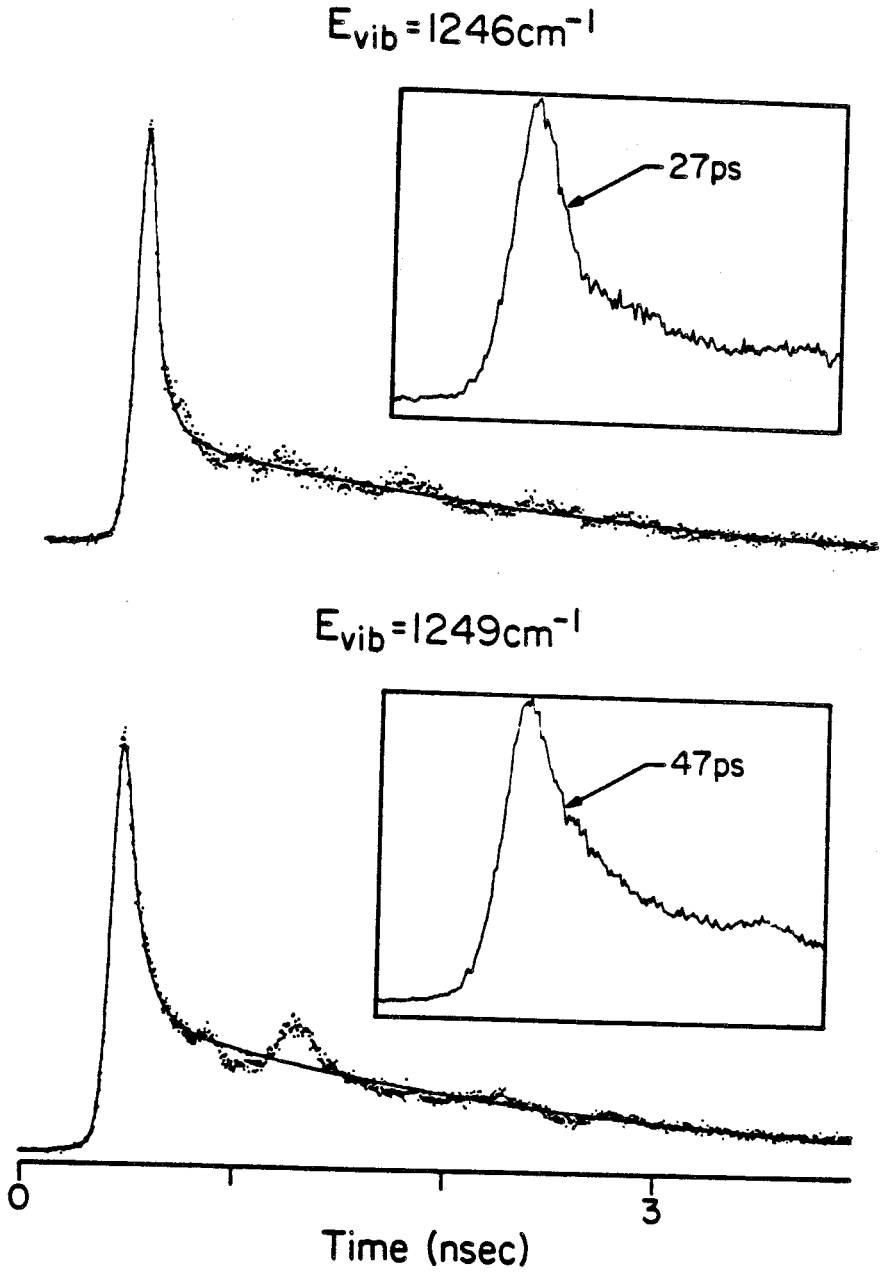

APPENDIX I*

* Published paper: Peter M. Felker and Ahmed H. Zewail, Chem. Phys. Lett. **102**, 113 (1983).

Volume 102, number 2,3 CHEMICAL PHYSICS LETTERS 18 November 1983

OBSERVATION OF RESTRICTED IVR IN LARGE MOLECULES: QUASI-PERIODIC BEHAVIOR, PHASE-SHIFTED AND NON-PHASE-SHIFTED QUANTUM BEATS

Peter M. FELKER * and Ahmed H. ZEWAIL **

Arthur Amos Noyes Laboratory of Chemical Physics ‡, California Institute of Technology, Pasadena, California 91125, USA

Received 19 August 1983; in final form 22 August 1983

The concept of *phase-shifted quantum beats* in large molecules is developed. Measurements are reported for jet-cooled anthracene excited by a 15 ps pulse to S_1 + 1420 cm^{-1}. The results represent the direct observation, in the time domain, of vibrational energy flow within specific sets of modes in the molecule. The importance of the results to intramolecular vibrational-energy redistribution (IVR) and quasi-periodic behavior is discussed.

1. Introduction

Quasi-periodic versus ergodic behavior in large systems with many degrees of freedom has been, and still is, of great current interest [1]. Of particular interest are two questions: (1) At what energy region does a particular molecular system undergo a change between these two limits of behavior, and (2) what are the observable manifestations (e.g. spectroscopic) of the two types of behavior in large isolated molecules, with their complicated level structures and couplings?

Lambert et al. [2] have reported the observation of quantum beats in the fluorescence decay of jet-cooled anthracene excited by picosecond pulses to an excess vibrational energy of 1380 cm^{-1} in S_1. This observation of a coherence phenomenon in a large, isolated molecule led us to examine the role that rovibrational coupling might have in creating this dynamical effect at this excess energy. However, a clear link between the coherence (or the recurrence) and the dynamics of vibrational energy flow was not established. In fact, until this report, a direct view of energy flow between vibrational modes in the time domain has not been seen. Both adequate temporal and spectral resolution are needed to observe the dynamics of *initially prepared* and *redistributed* states.

In this letter, we present experimental evidence for restricted IVR (quasi-periodic behavior) in anthracene. *Temporal* and *spectral* manifestations of this dynamical effect are illustrated by the novel observation of phase-shifted quantum beats and the time evolution of dispersed fluorescence spectra of jet-cooled molecules.

The concept of phase-shifted quantum beats can be illustrated using the scheme of fig. 1, which repre-

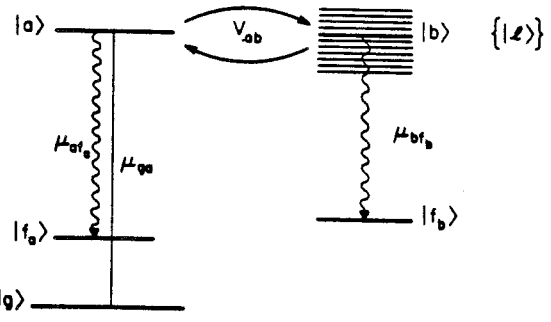

Fig. 1. A schematic level structure diagram pertaining to an experiment involving two zero-order excited state vibrational levels, |a⟩ and |b⟩, coupled by an interaction V_{ab}. |a⟩ is active in absorption from |g⟩ and emission to $|f_a\rangle$, while |b⟩ is not active in absorption but is active in emission to $|f_b\rangle$. See the text (section 2) for further details.

* IBM Research Fellow.

** Camille and Henry Dreyfus Foundation Teacher–Scholar.

‡ Contribution No. 6899.

0 009-2614/83/0000–0000/$ 03.00

sents a fluorescence experiment involving two nearby S_1 vibrational levels; $|a\rangle$ and $|b\rangle$, where $|a\rangle$ is active in absorption and $|b\rangle$ is not. After the laser pulse excites $|a\rangle$, the coupling between $|a\rangle$ and $|b\rangle$ will manifest itself through quantum-beat-modulated fluorescence decays from the coupled levels. But, because of differences in the emission Franck–Condon factors between $|a\rangle$ and $|b\rangle$, there will be two types of emission bands. Those that derive their strength from $|b\rangle$ will exhibit beating decays that are phase-shifted by 180° from the modulated decays of bands that derive their strength from $|a\rangle$. If such behavior is actually observed, one can attribute the phenomenon to a restricted IVR process, obtain the characteristic time constant for this process, and observe a time evolution in the emission spectrum. The experiments presented here on jet-cooled anthracene, excited to $S_1 + 1420$ cm^{-1} by a 15 ps pulse, demonstrate this idea, and provide the abovementioned information concerning IVR.

2. Theoretical

In the following section, we derive the fluorescence signal that arises from the situation represented by fig. 1. First, consider the two zero-order S_1 vibrational levels, $|a\rangle$ and $|b\rangle$, which are separated by energy E_{ab} and coupled via an interaction matrix element V_{ab}. The resulting vibrational eigenstates, $|e_1\rangle$ and $|e_2\rangle$, are separated by an energy $E_{12} = (E_{ab}^2 + 4|V_{ab}|^2)^{1/2}$, and take the form:

$$|e_1\rangle = \alpha_{1a}|a\rangle + \alpha_{1b}|b\rangle \tag{1a}$$

and

$$|e_2\rangle = \alpha_{2a}|a\rangle + \alpha_{2b}|b\rangle, \tag{1b}$$

where

$$\alpha_{1a} = -\alpha_{2b} \ (\equiv \alpha), \tag{2a}$$

$$\alpha_{2a} = \alpha_{1b} \ (\equiv \beta). \tag{2b}$$

α and β are real, and $\alpha^2 + \beta^2 = 1$. Expressions for α and β are well known and involve V_{ab} and E_{ab} [3].

Now consider a process by which $|e_1\rangle$ and $|e_2\rangle$ are, first, prepared coherently by a delta-function light pulse through absorption from the ground-state level $|g\rangle$, and, subsequently, emit to the manifold of levels $|f\rangle$. The resulting fluorescence intensity versus time [4] (assuming the same relaxation rate, Γ, for $|e_1\rangle$ and $|e_2\rangle$, although generalization to the case of different Γ is straightforward) is

$$I(t) = K \sum_f \sum_{i,j=1}^{2} \mu_{ig}\mu_{gj}\mu_{jf}\mu_{fi} \times \exp(-\Gamma t)\exp(-iE_{ij}t/\hbar), \tag{3}$$

where $\mu_{nm} \equiv \langle n|\hat{\mu}|m\rangle$ is the transition electric dipole moment matrix element between $|n\rangle$ and $|m\rangle$ †, and where K is a constant. In terms of the zero-order states

$$I(t) = K \sum_f \sum_{i,j=1}^{2} (\alpha_{ia}\mu_{ag} + \alpha_{ib}\mu_{bg}) \times (\alpha_{ja}\mu_{ga} + \alpha_{jb}\mu_{gb})(\alpha_{ja}\mu_{af} + \alpha_{jb}\mu_{bf}) \times (\alpha_{ia}\mu_{fa} + \alpha_{ib}\mu_{fb})\exp(-\Gamma t)\exp(-iE_{ij}t/\hbar). \tag{4}$$

If one assumes that, because of Franck–Condon factors, only $|a\rangle$ can combine with the initial state $|g\rangle$ (i.e. $|\mu_{ag}| \neq 0$, $|\mu_{bg}| = 0$), then one may see that two limiting types of bands (type a and type b), differentiated by the zero-order state that provides the emission strength, may occur in the dispersed fluorescence spectrum (see fig. 1). Type-a bands are defined as those for which the fluorescence transition involves a final state $|f_a\rangle$, such that $|\mu_{af_a}| \neq 0$ but $|\mu_{bf_a}| = 0$. The decay for type-a bands may be calculated by using eq. (4) and restricting the f summation to just one f_a term:

$$I_a(t) = K|\mu_{af_a}|^2|\mu_{ag}|^2\exp(-\Gamma t) \times [1 - 2\alpha^2\beta^2 + 2\alpha^2\beta^2\cos(E_{12}t/\hbar)], \tag{5}$$

where we have substituted for the α_{mn}. For type-b bands, the fluorescence transition is taken to involve a final state $|f_b\rangle$, for which $|\mu_{bf_b}| \neq 0$ and $|\mu_{af_b}| = 0$. From eq. (4)

† Note that we have suppressed the influences of excitation and detection polarization in eq. (3). This neglect is justified for consideration of our experimental results being that no polarization analysis is made in the experiments reported here, yet beats are still observed. For a full discussion of polarization effects and molecular quantum beats, see ref. [5].

$$I_b(t) = 2K|\mu_{ag}|^2|\mu_{bf_b}|^2$$

$$\times \exp(-\Gamma t)\alpha^2\beta^2[1 - \cos(E_{12}t/\hbar)]. \quad (6)$$

Comparing the decays of the two types of bands, it is evident that both types exhibit beat-modulated decays at an angular frequency of $E_{12}/\hbar$. However, two significant differences occur between the forms of the two types of decays. Firstly, the type-a and type-b beat patterns are 180° out-of-phase. Secondly, the degree of modulation of type-a decays depends on α and β (i.e. depends on the vibrational coupling) and in general is less than 100%, whereas type-b decays are 100% modulated, independent of α and β. Note that eq. (5) and eq. (6) represent observables associated with the dynamics of a limited IVR process: The optically prepared state, $|a\rangle$, evolves in time into some mixture of $|a\rangle$ and $|b\rangle$. The decays of type-a bands probe the $|a\rangle$ content of the excited non-stationary state, those of type-b bands, the $|b\rangle$ content. Hence, phase-shifted and non-phase-shifted beats can sort out the vibrational subsets involved in the IVR.

Significantly, the spectral dependence of beat patterns, which is predicted by the vibrational coupling scheme above, is different for cases where beats arise from coupling wherein $|a\rangle$ is an S_1 level coupled to a triplet or S_0 level [6,7], $|b\rangle$. In such cases $|\mu_{bf}| = 0$ for all f corresponding to optical fluorescence transitions to S_0 levels, and all fluorescence bands in the spectrum decay in exactly the same way, i.e. in a fashion similar to type-a bands.

Eqs. (5) and (6) provide a basis upon which the dynamical manifestations of vibration–vibration coupling within an electronic state manifold may be analyzed. In what follows, we present quantum-beat results for anthracene which, owing to their very close fit to the predictions of this section, provide clear evidence that we have observed the time evolution of a limited intramolecular vibrational energy redistribution (IVR) process.

3. Experimental

A short account of the experimental apparatus has appeared [2]. Full details are published elsewhere [8]. Briefly, He, Ne, or N_2 at 30 psi, seeded with anthracene at ≈180°C, was expanded through a 100 μm pinhole into an evacuated chamber ($<10^{-3}$ Torr). Both anthracene (Aldrich 98%) and purified anthracene (recrystallized from CCl_4) were used. No differences in results were observed between the two. Also, using these materials we reproduced the results for the 1380 cm^{-1} excitation [2] obtained using zone refined anthracene. The 6870 Å output of a synchronously pumped, cavity-dumped picosecond dye laser (DCM as dye, a three-plate birefringent filter and fine-tuning etalon as tuning elements) was frequency-doubled ($LiIO_3$) to produce UV pulses (≈3 cm^{-1} bandwidth) which crossed the jet expansion at distances (≡ X) of 2–8 mm from the nozzle pinhole. No effect on the results reported here was observed as X was varied over this range. Fluorescence was collected with $f/1$ optics, spectrally dispersed and detected by a fast photomultiplier. Fluorescence decays were measured by time-correlated single-photon counting.

The influence of magnetic fields on beat-modulated decays was assessed by using the arrangement described in ref. [7]. To make certain that there was a field under our anthracene experimental conditions, published results [7] for pyrazine were reproduced.

4. Results

Upon excitation of the prominent, jet-cooled anthracene band at S_1 + 1420 cm^{-1} in the excitation spectrum [9] (3435 Å), phase-shifted quantum beats (995 ± 30 MHz) have been observed (fig. 2). The experimental decays that appear in fig. 2 correspond to detection of the dispersed fluorescence bands appearing at 390 and 1750 cm^{-1} shifts, respectively, from the excitation energy (see fig. 3a). The two decays show a clear 180° phase difference between them. As is apparent from the figure, the 390 cm^{-1} decay may be simulated ‡ by convoluting a decay function of the form $A\exp(-\Gamma t)[1 + 0.4\cos(\omega t)]$ with the system response function; where $\omega = 2\pi \times 10^9$ s^{-1} and

‡ Our prime motivation in performing these simulations is not to obtain extremely accurate values for decay parameters, but instead to clearly illustrate that the 390 cm^{-1} decay involves a *plus* cosine term and the 1750 cm^{-1} decay a *minus* cosine term. The decay of the beat envelope and its relation to differences in Γs will be dealt with later.

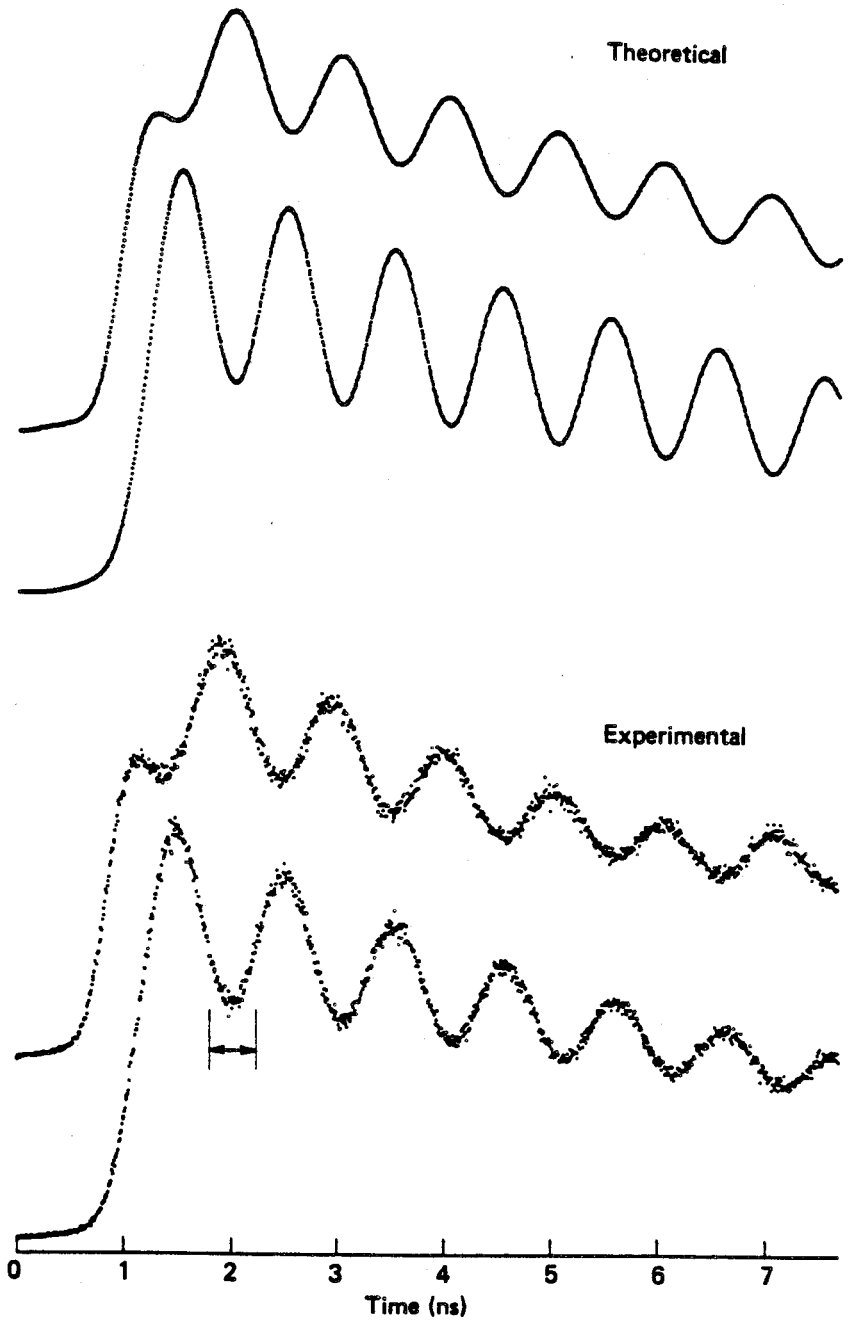

Fig. 2. Experimental and theoretical fluorescence decays. The calculation of the theoretical decays is outlined in the text. The top theoretical decay corresponds to a *plus* cosine modulation term, the bottom decay to a *minus* cosine term. X = 3 mm, and P = 30 psi He (the effect of X and carrier gas are discussed in the text). Beats were observed when X varied from 2 to 8 mm. The top experimental decay corresponds to detection of the 390 cm^{-1} dispersed fluorescence band with detection bandwidth (R) of 16 A. The bottom decay corresponds to detection of the 1750 cm^{-1} fluorescence band with R = 1.6 A (see footnote *). *Note that the peaks in the top experimental decay correspond to the troughs in the bottom decay.* The time window indicated in the figure is pertinent to fig. 3b.

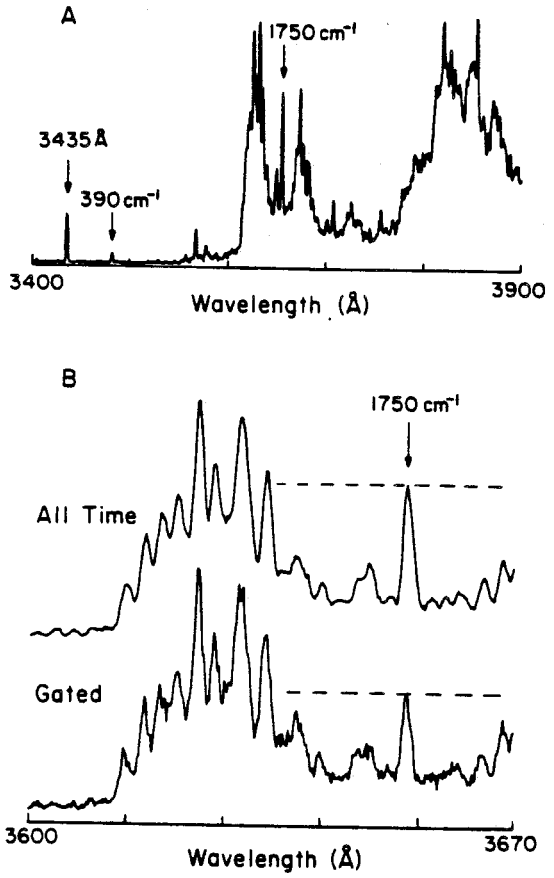

Fig. 3. (a) Dispersed fluorescence spectrum for anthracene excited to S_1 + 1420 cm^{-1}. X = 3 mm, P = 30 psi He, R = 1.6 A. The 390 and 1750 cm^{-1} bands are marked as is the excitation wavelength. (b) Dispersed fluorescence spectra corresponding to anthracene excited to S_1 + 1420 cm^{-1}. The top spectrum detected emission at all times. The detection for the bottom spectrum was time-gated to the window indicated in fig. 2. For both spectra X = 2 mm, P = 30 psi He, R = 1.1 A. The 1750 cm^{-1} band is marked. The line drawn across the top of the 1750 cm^{-1} serves to illustrate the decrease in relative intensity of this band in the time-gated spectrum.

$\Gamma = 1(8.6 \times 10^9\ s^{-1})$. The 1750 cm^{-1} decay is reproduced if a decay function of the form $A \times \exp(-\Gamma t)[1 - 0.9\cos(\omega t)]$ is used to calculate a convoluted decay. The difference in modulation between the 390 and 1750 cm^{-1} decays is very apparent in fig. 4. Clearly, the decay of the 1750 cm^{-1} band is better modulated than that of the 390 cm^{-1} band for the experimental conditions given in the caption of the figure *.

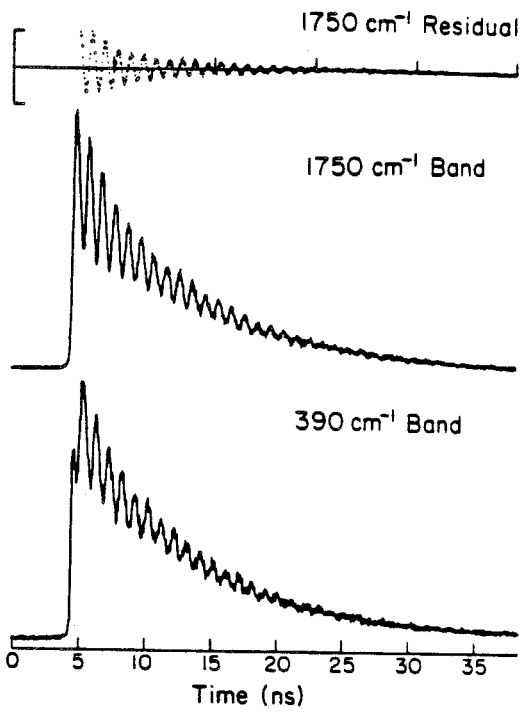

Fig. 4. Beat-modulated fluorescence decays of the 1750 and 390 cm^{-1} bands for excitation of anthracene to S_1 + 1420 cm^{-1}. X = 3 mm, P = 30 psi Ne. For the 1750 cm^{-1} decay R = 0.5 A; for the 390 cm^{-1} decay R = 1.6 A (see footnote *). At the top of the figure is the residual which results from the subtraction of a best fit exponential decay function from the experimental decay. Note the modulation of the 1750 cm^{-1} decay relative to that of the 390 cm^{-1} decay.

In addition to the beating decays of the 390 and 1750 cm^{-1} bands, other bands exhibit modulated decays. The resonance fluorescence band (0 cm^{-1} shift), the band at 1482 cm^{-1}, and others have been found to show beats similar to those of fig. 2a (i.e. $+\cos(\omega t)$ beats, 0° phase), while decays of the bands at 1750 + 390 and 1750 + 1408 cm^{-1}, as well as others, beat in a manner similar to fig. 2b (i.e.

* One may note that the monochromator resolution for the 1750 cm^{-1} decay of fig. 4 is better than that for the 390 cm^{-1} decay. No bandwidth effect on the modulation of the 390 cm^{-1} decay has been observed, consistent with the fact that it appears in a congestion-free region of the spectrum. On the other hand, the modulation of the 1750 cm^{-1} band has been found to be detection bandwidth sensitive (modulation increases with increasing resolution). Thus, if anything the 1750 cm^{-1} may be more modulated than it appears to be in the figure, while the 390 cm^{-1} decay modulation is accurately represented.

$-\cos(\omega t)$ beats, 180° phase). The difference in beat phase between the 1750 cm^{-1} band and other bands that appear in the 3600–3670 Å region of the dispersed fluorescence spectrum is quite apparent in fig. 3b. The top spectrum of fig. 3b corresponds to collection of emission at *all* times. The lower one corresponds to detection of the emission occurring in the narrow time window or *gate* indicated on the experimental decays of fig. 2. Clearly, the relative intensity of the 1750 cm^{-1} band decreases in the gated spectrum. (Although the spectra of fig. 3b are not corrected for laser power drifts, the trend of the spectra regarding the relative intensity of the 1750 cm^{-1} band is quite reproducible.)

A slight carrier gas effect on the beats has been observed. As the gas is changed from Ne or He to N_2, decreases in beat modulation occur. However, no new beat frequencies appear. This behavior contrasts with results for other beats, e.g. those that appear for S_1 + 1380 cm^{-1} excitation in anthracene [8].

No magnetic field effect on the beats was observed for detection of the well-modulated 1750 cm^{-1} band, suggesting that there is no involvement of S_1–triplet coupling in the beats, in contrast to results published on pyrazine [7].

5. Discussion

The experimental results presented above clearly match the theoretical predictions of section 2 pertaining to the manifestations of vibration–vibration coupling in quantum-beat-modulated decays. In the nomenclature of section 2, the zero, 390, and 1482 cm^{-1} bands are "type a". They are not fully modulated and involve a phase of 0°. The 1750, 1750 + 390, and 1750 + 1408 cm^{-1} bands, being more fully modulated and having phases of 180°, are assigned as "type b".

These assignments are quite reasonable in terms of anthracene spectroscopy. The 0, 390, and 1482 cm^{-1} bands can be assigned as $\{A\}_{\{0\}}^{\{n\}}$, $\{A\}_{\{0\}}^{\{n\}}12_1^0$, and $\{A\}_{\{0\}}^{\{n\}}5_1^0$ [9] #§, respectively, and because of this are expected to be type a. In contrast, the 1750 cm^{-1} interval does not correspond to obvious fundamental, overtone, or combination bands of known optically active [9] †† ground-state modes. This suggests that the band is of the form $\{C\}_{\{l\}}^{\{l\}}\{A'\}_{\{m'\}}^{\{m\}}$, where $\{C\}$ is some set of optically inactive modes and $\{A'\}$ some set of optically active ones. Note that the level $\{C\}^{\{l\}}\{A'\}^{\{m\}}$ cannot be populated by absorption from the 0_0 level, and thus must gain absorption strength (under jet conditions) by coupling to some optically active level †† (i.e. $\{A\}^{\{m\}}$). Thus, the 1750 cm^{-1} band is expected to be type b. The 1750 + 390 and 1750 + 1408 cm^{-1} bands are assignable [9] as $\{C\}_{\{l\}}^{\{l\}}\{A'\}_{\{m'\}}^{\{m\}}12_1^0$ and $\{C\}_{\{l\}}^{\{l\}}\{A'\}_{\{m'\}}^{\{m\}}6_1^0$, respectively, and are, therefore, also expected to be type b.

The above results represent the first clear observations in the time domain of vibrational energy flow in a jet-cooled large molecule. They may be expected to yield much new information pertaining to both IVR processes in anthracene and such processes in general.

Regarding the particular characteristics of the vibrational dynamics of anthracene in its S_1 + 1420 cm^{-1} level, it is clear (owing to the close fit of our experimental results to the predictions of a two-level model) that only a very limited vibrational energy redistribution process is being observed, and that it is characterized by a finite recurrence time (1 ns) and a vibrational coupling matrix element of less than 0.5 GHz. The lack of a pronounced carrier gas effect, in contrast to other beats in anthracene [8], implies that rotational levels only minimally influence the IVR dynamics of the optically prepared level at this particular excess energy.

Besides the immediate implications our results have to energy flow in anthracene, it is very important, with regard to the study of IVR processes in general, that the dynamical manifestations of vibrational coupling have now been observed and can be studied in further detail. A first aspect of importance is the establishment of the utility of using the concept

The notation $\{A\}^{\{n\}}$ represents an excited-state vibrational level consisting of a set of vibrational modes (i.e. $\{A\}$) characterized by a set of vibrational quantum numbers $\{n\}$. Similarly, $\{A\}_{\{n\}}$ represents a level of the ground state. $\{A\}_{\{m\}}^{\{n\}}$ represents a fluorescence or absorption transition.

§ Evidence in ref. [9] indicates that the S_1 + 1420 cm^{-1} level is the 5^1 level.

†† By an optically active level we mean a level that can be reached in absorption from the vibrationless level of the ground state. By an optically active mode we mean a mode that can undergo transitions involving a change of vibrational quantum number.

of quantum-beat phase shifts as a diagnostic for limited IVR processes. One may expect quantum beats arising from vibrational couplings to occur in many molecules. The analysis of phase shifts could prove to be essential to a full understanding of IVR dynamics in such cases.

A second implication of our work pertains to the spectral methods widely used to study IVR processes in large molecules [10]. Being that we now are able to assign so-called vibrationally "relaxed" (type-b) and "unrelaxed" (type-a) fluorescence bands via measurements in the time domain, it will be possible to examine the extent of the validity of using the characteristics of dispersed fluorescence spectra (i.e. broadening, red-shifts, etc.) as a means of arriving at IVR parameters. Finally, the limited nature of the IVR process for the S_1 + 1420 cm^{-1} anthracene level, provides a clean example of quasi-periodic behavior in a large system. By further studies of phase-shifted and non-phase-shifted quantum beats in anthracene and other molecules, it may be possible to arrive at some knowledge of the characteristics of the transition between quasi-periodic and ergodic vibrational behavior in this large molecule. We plan to present a full account of this work later.

Acknowledgement

This material is based upon work supported by the National Science Foundation under Grant No. DMR-8105034 and Grnat. No. CHE-8211356. We wish to thank Professor R. Marcus for many enlightening discussions, especially on the quasi-periodic behavior.

References

[1] D.W. Noid, M.L. Koszykowski and R.A. Marcus, Ann. Rev. Phys. Chem. 32 (1981) 267.
[2] W.R. Lambert, P.M. Felker and A.H. Zewail, J. Chem. Phys. 75 (1981) 5958.
[3] G. Herzberg, Infrared and Raman spectra of polyatomic molecules (Van Nostrand, Princeton, 1945).
[4] S. Haroche, in: High resolution laser spectroscopy, ed. K. Shimoda (Springer, Berlin, 1976) pp. 254–313.
[5] M. Bixon, J. Jortner and Y. Dothan, Mol. Phys. 17 (1969) 109.
[6] J. Chaiken, M. Gurnick and J.D. McDonald, J. Chem. Phys. 74 (1981) 106;
H. Henke, H.L. Selzle, T.R. Hays, S.H. Lin and E.W. Schlag, Chem. Phys. Letters 77 (1981) 448;
M. Ivanco, J. Hayes, W. Sharfin and S.C. Wallace, J. Chem. Phys. 78 (1983) 6531;
S. Okajima, H. Sarbusa and E.C. Lim, J. Chem. Phys. 76 (1982) 2096;
B.J. van der Meer, H.Th. Jonkman, G.M. ter Horst and J. Kommandeur, J. Chem. Phys. 76 (1982) 2099.
[7] P.M. Felker, W.R. Lambert and A.H. Zewail, Chem. Phys., submitted for publication.
[8] W.R. Lambert, P.M. Felker and A.H. Zewail, J. Chem. Phys., submitted for publication.
[9] W.R. Lambert, P.M. Felker, J.A. Syage and A.H. Zewail, J. Chem. Phys., submitted for publication.
[10] P.S.H. Fitch, L. Wharton and D. Levy, J. Chem. Phys. 70 (1979) 2018;
S.M. Beck, J.B. Hopkins, D.E. Powers and R.E. Smalley, J. Chem. Phys. 74 (1981) 43;
A. Amirav, U. Even and J. Jortner, J. Chem. Phys. 74 (1981) 3745;
C. Bouzou, C. Jouvet, J.B. Leblond, Ph. Millie, A. Tramer and M. Sulkes, Chem. Phys. Letters 97 (1983) 161.

APPENDIX II*

* Published paper: Peter M. Felker and Ahmed H. Zewail, Phys. Rev. Lett. **53**, 501 (1984).

Direct Observation of Nonchaotic Multilevel Vibrational Energy Flow in Isolated Polyatomic Molecules

Peter M. Felker and Ahmed H. Zewail
Arthur Amos Noyes Laboratory of Chemical Physics, California Institute of Technology, Pasadena, California 92215
(Received 11 May 1984)

With picosecond spectroscopy and molecular beams it is shown that nonchaotic *multilevel* vibrational energy flow is present in large polyatomic molecules. This Letter reports on this novel observation and its probing of the fundamental process of energy redistribution in molecules.

PACS numbers: 82.20.Rp, 33.50.Hv

The fundamental process of collisionless intramolecular vibrational energy redistribution (IVR) in polyatomic molecules has been extensively studied for at least two major reasons. Firstly, IVR plays a central role in a wide variety of molecular processes such as multiphoton dissociation, laser-selective chemistry, radiationless transitions, and unimolecular reactions.[1] Secondly, classical and semiclassical treatments[2] of vibrational dynamics in a coupled two-mode system (Heńon-Heiles Hamiltonian) have revealed interesting changes in vibrational motion (quasiperiodic or chaotic) which depend on total energy and coupling parameters. The results have stimulated research aimed at defining and discovering analogous quantum behavior in molecules. For these reasons two fundamental questions concerning IVR in real molecules are important: Given the impulsive excitation of an isolated molecule to some nonstationary excited state, *how rapidly* does this initial state evolve to encompass other vibrational motions, and *to what extent* do other vibrational motions become involved in the vibrational motion as a whole?

An intuitive feel for the concept of IVR can be gained by consideration of the classical case of coupled oscillators represented in Fig. 1. With pendulum a initially set in motion and pendulum b at rest, the effect of the coupling V_{ab} is to transfer energy from a to b. In the quantum analog to this situation (Fig. 1, middle) a harmonic oscillator zero-order state $|a\rangle$ is assumed to be prepared by a light pulse at $t=0$. Due to the coupling V_{ab} to the zero-order state $|b\rangle$ (via anharmonicity, for instance) this initially prepared state evolves in time to contain some contribution from $|b\rangle$. It is this wave-function evolution which describes the flow of energy from the vibrational motion represented by $|a\rangle$ to that represented by $|b\rangle$. In the situation where the initially prepared $|a\rangle$ is coupled to more than one other level (Fig. 1, bottom) multilevel IVR occurs.

Time-integrated experimental measurements[3] concerning IVR are somewhat indirect in that the observables measured depend on IVR but are removed from the primary process itself. Recently, however, the combination of ultracold, seeded supersonic molecular beams with picosecond laser spectroscopy has been shown to be useful to the study in real time of a number of aspects of isolated-molecule dynamics.[4] In this Letter we report on the direct observation, using these techniques, of nonchaotic *multilevel* IVR in the large molecule, anthracene.

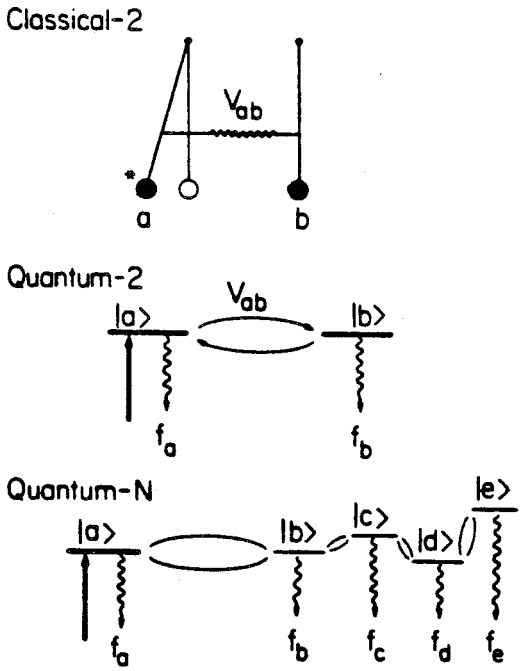

FIG. 1. Schematic representations of coupled oscillators in classical and quantum systems. In the quantum cases the probing of IVR by fluorescence spectroscopy is indicated. Note that other coupling schemes for quantum N are also possible.

We shall be concerned with IVR in anthracene at $\sim 1400\text{-cm}^{-1}$ excess vibrational energy in the first excited singlet electronic state S_1. At these energies the density of S_1 vibrational states is $\sim 25/\text{cm}^{-1}$. Excitation to S_1 from an S_0 level selectively prepares the (ultracold) molecule in one well-defined vibrational state (harmonic state) while the remainder of the states are not excited because of symmetry and/or Franck-Condon restrictions. The scheme of our experiment (Fig. 1) is to prepare such a well-defined optically allowed vibrational state, $|a\rangle$, and then to probe the temporal evolution of the state by temporally and spectrally resolving the fluorescence from the sample. In what follows, we shall show that the flow of vibrational energy from an initially prepared state to other vibrational states is manifested in fluorescence decays as modulations (quantum beats), the *phases* of which are spectrally dependent, and the number of Fourier components of which are dependent on the number of levels involved in the energy flow.

Consider the case of N coupled vibrational levels (Fig. 1, bottom). It is convenient to initially deal with the molecular eigenstates, $|I\rangle$, $I=1,N$, which result from the coupling of these levels:

$$|I\rangle = \sum_{\gamma=a,b,c,\ldots} \alpha_{I\gamma}|\gamma\rangle, \tag{1}$$

where the α's are elements of a real orthogonal matrix.

Delta function excitation of a molecule from the vibrational level $|g\rangle$ of S_0 will prepare these N eigenstates coherently, given that at least one of the zero-order states $|\gamma\rangle$ has a nonzero transition moment with $|g\rangle$. The wavelength-integrated fluorescence versus time to the manifold of S_0 vibrational levels $\{|f\rangle\}$ is given by[5,6]

$$I(t) = C\sum_f \sum_{I,J=1}^{N} \mu(I,g)\mu(g,J)\mu(J,f) \times \mu(f,I)e^{-t(i\omega_{IJ}+\Gamma)}, \tag{2}$$

where C is a constant, the $\mu(I,g)$'s are dipole matrix elements between $\langle I|$ and $|g\rangle$, Γ is the excited-state decay rate (taken for simplicity to be the same for all N excited states), and $\omega_{IJ}=(E_J-E_I)/\hbar$, E_I and E_J being the energies of the eigenstates $|I\rangle$ and $|J\rangle$, respectively. Now, as noted above, usually only one harmonic vibrational level, say $|a\rangle$, within a given small energy region has nonzero absorption from $|g\rangle$. Thus, $\mu(I,g)=\alpha_{Ia}\mu(a,g)$ for all I. Similarly, for fluorescence into state $|f_\gamma\rangle$, $\mu(I,f_\gamma)=\alpha_{I\gamma}\mu(\gamma,f_\gamma)$ for all I. We shall call the corresponding fluorescence band a γ-type band. Given this it is clear from Eq. (2) that the fluorescence spectrum from an N-level system may contain as many as N types of bands, all with different temporal behaviors determined by the zero-order level which contributes to the emission dipole of the band. Furthermore, since the excited state formed by δ-function excitation is

$$\psi(t) \sim \sum_{I=1}^{N} \alpha_{Ia}|I\rangle \exp[-t(iE_I+\Gamma/2)],$$

it is clear with use of Eqs. (1) and (2) [restricting f to f_γ] that the intensity of a γ-type band, which is proportional to

$$\sum_{I,J=1}^{N} \alpha_{Ia}\alpha_{Ja}\alpha_{I\gamma}\alpha_{J\gamma} \exp[-t(i\omega_{IJ}+\Gamma)],$$

is also directly proportional to the contribution of $|\gamma\rangle$ to the excited state: $|\langle\gamma|\psi(t)\rangle|^2$. *Thus the measurement of the decays of different band types provides a direct picture of the vibrational content of the excited state.* In addition, being that the $|\langle\gamma|\psi(t)\rangle|^2$ are measures of vibrational chaos,[7] the fluorescence decays are related to this, too, as we shall discuss later.

The simplest case is for $N=2$. Here, two types of bands can arise, a type and b type.[6] The temporal characteristics of each of the bands can be derived from Eq. (2) by using the eigenstate results for two-level coupling: $|1\rangle=\alpha|a\rangle+\beta|b\rangle$ and $|2\rangle=-\beta|a\rangle+\alpha|b\rangle$. Both types of bands have have fluorescence decays modulated by a $\cos\omega_{12}t$ interference term. However, the cosine term has a *negative* coefficient for the b-type band, whereas for the a-type band is it *positive*. These phase-shifted beats are manifestations of the oscillatory flow of energy between the $|a\rangle$ and $|b\rangle$ vibrational motions. (Note the analogy with the oscillatory distribution of energy that occurs in the coupled pendulums of Fig. 1.)

The spectral dependence of quantum beat phases also applies to $N \geq 3$. Herein, we only consider results for $N=3$. In this case, a-, b-, and c-type bands can arise in the fluorescence spectrum. As is evident from Eq. (2) all three types will have decays modulated at the frequencies ω_{12}, ω_{23}, and $\omega_{12}+\omega_{23}$. The three cosine terms, however, will have different phases depending on the band type. In particular, it can be shown, with use of the orthonormal properties of the α's, that (1) for a-type bands all cosine terms are positive, (2) for b- and c-type bands two of the terms are negative and the third positive, and (3) the cosine term that is positive for the b-type band is different from that

for the *c*-type band. The experiments reported here show that behavior matching these predictions occurs.

Our experimental apparatus is described in detail elsewhere.[4,8] Briefly, an anthracene beam is formed by expanding anthracene vapor at 180 °C with 35–50-psi helium through a 100-μm pinhole into a chamber at $< 10^{-3}$ Torr. A picosecond uv pulse ($\Delta t \sim 15$ ps, $\Delta\bar{\nu} \leq 2$ cm^{-1}) derived from frequency doubling a synchronously pumped, cavity-dumped (4 MHz) dye laser intersects the expansion 3 mm downstream from the pinhole. Fluorescence is collected with right-angle geometry, wavelength analyzed by a 0.5-m monochromator and detected by a fast multichannel plate photomultiplier (Hamamatsu R1564U). Decays are measured with time-correlated single-photon counting. Unlike our previous measurements,[4] the total time response of the detection system is now ~ 80 ps full width at half maximum. Decays are fitted by a single exponential function which is then subtracted from the data to yield the modulated portion (residual) of a given decay. One can analyze the residual for beat frequencies and phases by Fourier transformation of the residual, followed by division by the Fourier transform of the system response function. This automatically establishes the proper phases for the various beat components. Thus, positive cosine components appear as positive peaks in the real part of the Fourier transform and negative cosine ones as negative peaks.

A clear illustration of the concept of the spectral dependence of quantum beat phases is presented in Fig. 2, which consists of two decays taken for vibrational excitation of anthracene to 1420 cm^{-1} in S_1. The upper decay corresponds to detection of the fluorescence band at a red shift of 390 cm^{-1} from the excitation energy, and the lower decay to detection of the band at 1750 cm^{-1}. The slow modulation (~ 1 GHz) is clearly a positive cosine in the upper decay and a negative cosine in the lower decay. Two other prominent beat frequencies at 9.7 and 10.7 GHz also modulate the decays of Fig. 2. Fourier analysis reveals that all three beat components have 0° phases in the upper decay (*a* type), whereas in the lower decay (not *a* type) the 1- and 9.7-GHz components have 180° phases, and the 10.7-GHz components a 0° phase. Moreover, a third type of band has been observed, the decay of which has the 1-GHz component with 0° phase and the two fast components with 180° phases. The quantum beat behavior for this excitation therefore matches that expected for three coupled vibrational levels.

Another anthracene S_1 vibrational level which manifests multilevel coupling through spectrally dependent quantum beat phases is that which is populated by excitation to $E_{vib} = 1380$ cm^{-1}. Figure 3 displays the Fourier transforms of beat patterns for three of the bands that appear prominently in the fluorescence spectrum resulting from this excitation. The phases of the three beat components (3.5, 4.9, and 8.4 GHz) clearly match the predic-

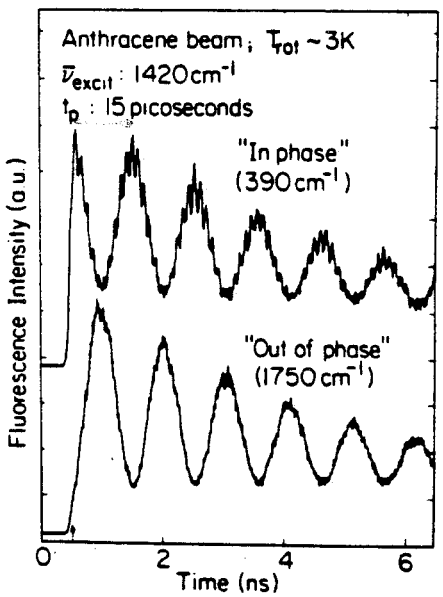

FIG. 2. The fluorescence decays of two bands in the spectrum of jet-cooled anthracene excited to $E_{vib} = 1420$ cm^{-1}. The arrow marks the temporal position of the excitation pulse.

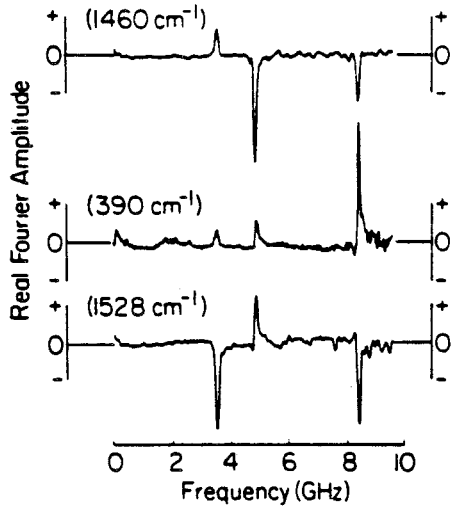

FIG. 3. Fourier-transform spectra of the quantum beat residuals of three bands in the fluorescence spectrum of anthracene excited to $E_{vib} = 1380$ cm^{-1}.

tions for three coupled vibrational levels.

Having directly observed vibrational energy flow in anthracene it is pertinent for one to consider the implications of these results. Firstly, it is evident that for excitations to $E_{vib} \cong 1400$ cm^{-1}, vibrational couplings from 1 to 10 GHz (~ 0.3 cm^{-1}) figure prominently in IVR processes. Secondly, it is meaningful that at these energies, energy flow involves approximately three levels spaced within 10 GHz. From direct counts of S_1 vibrational levels using calculated frequencies one would expect approximately ten levels in a 10-GHz region at $E_{vib} = 1400$ cm^{-1}. This implies selectivity in the extent of IVR for these levels.[9] Such selectivity could reasonably be the result of symmetry restrictions on vibrational coupling. Thirdly, the quantity $|\langle a|\psi(t)\rangle|^2$ has been shown[7] to be a useful measure of vibrational chaos in the quantum regime. Regular, periodic variations in this quantity indicate nonchaotic behavior. In this sense, then, the herein reported a-type decays, which are regular and periodic, represent the observation of nonchaotic IVR. Having demonstrated a technique for probing molecular states that are the quantum analogs of quasiperiodic regular motion we shall, in a future publication, show how the observation of rapid decay describes the analog of irregular motion and the rapid spreading out of energy deposited in a local region.[10]

This work was supported by the National Science Foundation through Grant No. CHE-8211356. One of us (P.M.F.) is an IBM Predoctoral Fellow and one of us (A.H.Z.) is a Camille and Henry Dreyfus Foundation Teacher Scholar.

---

[1]See, e.g., N. Bloembergen and E. Yablonovitch, Phys. Today 31 (5), 23 (1978); A. H. Zewail, Phys. Today 33 (11), 27 (1980).

[2]For a review see D. W. Noid, M. L. Koszykowski, and R. A. Marcus, Annu. Rev. Phys. Chem. 32, 267 (1981).

[3]For a review see C. S. Parmenter, Faraday Discuss. Chem. Soc. 75, 7 (1983).

[4]A. Zewail, Faraday Discuss. Chem. Soc. 75, 315 (1983).

[5]S. Haroche, in *High Resolution Laser Spectroscopy*, edited by K. Shimoda (Springer-Verlag, Berlin, 1976), pp. 254–313.

[6]P. M. Felker and A. H. Zewail, Chem. Phys. Lett. 102, 113 (1983); the lack of influence of laser and detection polarizations on beats is discussed in this reference.

[7]M. D. Feit and J. A. Fleck, Jr., J. Chem. Phys. 80, 2578 (1984), and references therein.

[8]W. R. Lambert, P. M. Felker, and A. H. Zewail, to be published.

[9]Here, we have not considered the role of rotations in vibrational coupling. Experimental results to be published elsewhere show that the effect of rotations on modulated decays is primarily to enhance the rate of decay of quantum beat envelopes.

[10]For theoretical discussion see, e.g., G. Hose and H. S. Taylor, J. Chem. Phys. 84, 375 (1984).

APPENDIX III*

* Published paper: Peter M. Felker and Ahmed H. Zewail, Chem. Phys. Lett. **108**, 303 (1984).

Volume 108, number 4 CHEMICAL PHYSICS LETTERS 13 July 1984

DIRECT PICOSECOND TIME RESOLUTION OF DISSIPATIVE INTRAMOLECULAR VIBRATIONAL-ENERGY REDISTRIBUTION (IVR) IN ISOLATED MOLECULES

Peter M. FELKER * and Ahmed H. ZEWAIL **
Arthur Amos Noyes Laboratory of Chemical Physics †, California Institute of Technology, Pasadena, California 91125, USA

Received 22 May 1984

Direct picosecond time resolution of dissipative IVR is reported for the first time. For jet-cooled anthracene with E_{vib} = 1792 cm^{-1}, the *unrelaxed* fluorescence displays a fast decay of ≈75 ps, while the *relaxed* fluorescence displays a corresponding rise. The onset for dissipative IVR is related to the effective density of states and coupling matrix elements, and reflects the importance of time-resolved measurements.

1. Introduction

Using picosecond techniques in supersonic jet beams [1] we reported last year on the observation of restricted intramolecular vibrational-energy redistribution (IVR) in the large molecule anthracene [2]. The experimental results on jet-cooled anthracene at intermediate excess vibrational energies [2,3] (E_{vib} ≈ 1400 cm^{-1}) in S_1 have revealed the existence of IVR amongst a small number (≈3) of vibrational levels and have indicated magnitudes of vibrational coupling matrix elements (10^{-2}–0.3 cm^{-1}) that significantly influence this process. This information on multilevel vibrational coupling was obtained from the observation of spectrally dependent *phase-shifted* quantum beats (frequencies ranging from 0.2 to 11 GHz) in fluorescence decays. One important aspect of the IVR problem that has not been addressed, until now, is the experimental characterization in *real time* of IVR between a larger number of vibrational levels at higher energies. This characterization is necessary to establish the role that molecular parameters (total vibrational energy, molecular structure, vibrational density of states, etc.) play in affecting both the time scale and the extent of dissipative (irreversible) IVR.

Time-integrated fluorescence measurements [4], while having led the way in the study of IVR in this energy regime, are limited in that they provide no direct view of the process. Instead, from a given spectrum a redistribution rate is inferred from the time-integrated intensity ratio of vibrationally unrelaxed fluorescence (U) to vibrationally relaxed fluorescence (R), and the extent of IVR is inferred from the degree of congestion in the spectrum (see fig. 1). Such inferences can be ambiguous since it is not always apparent which bands in a spectrum are U and which are R, nor is it certain that spectral congestion and complexity are manifestations solely of *dynamical* IVR processes.

In this letter we report on the picosecond time resolution of U and R fluorescence in the emission spectrum of jet-cooled anthracene excited to E_{vib} = 1792 cm^{-1} in the S_1 manifold. The decays taken in the U region exhibit an initial fast component (≈75 ps) followed by a modulated long time decay. In contrast, the R-region fluorescence transients exhibit a finite rise time, the time scale of which matches the ≈75 ps component of the U-region decays, and subsequent long decay. We interpret these new results as direct evidence for the onset of dissipative IVR in anthracene

* IBM Predoctoral Fellow.
** Camille and Henry Dreyfus Foundation Teacher–Scholar.
† Contribution No. 7028.

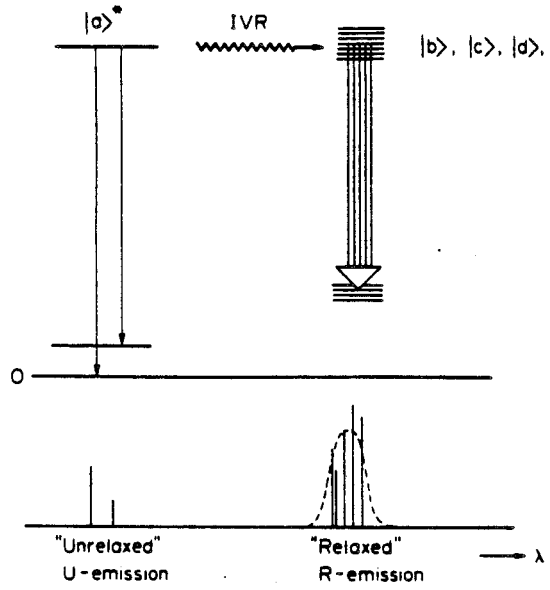

Fig. 1. An energy level diagram representing the dissipative flow of vibrational energy from the laser-prepared |a⟩ vibrational level to the manifold of coupled levels |b⟩, |c⟩, |d⟩,... . As indicated in the figure this process can be probed by fluorescence measurements made in the vibrationally unrelaxed (U) and relaxed (R) spectral regions.

and for its dynamical time scale at this E_{vib}. For comparison we present results for lower E_{vib}s where we observe no fast decay or buildup in the dispersed fluorescence.

2. Theory

Elsewhere [2,3] we have discussed the theory for restricted IVR and its predictions regarding experiments done in real time. Here, we shall be concerned with the dynamical behavior of the N harmonic (zero-order) S_1 vibrational levels |a⟩, |b⟩, |c⟩, ..., which are mutually coupled by anharmonic and/or vibration–rotation terms in the molecular Hamiltonian. In general, only one of the zero-order levels, say |a⟩, will have an appreciable Franck–Condon factor for absorption from the vibrationless level of S_0, |0⟩ (i.e. we take only |a⟩ as being optically active, see fig. 1). Consequently, δ-function excitation of a molecule from |0⟩ will give rise to the excited state

$$\psi(t) \sim \sum_{I=1}^{N} \alpha_{I_a} |I\rangle \exp(-iE_I t/\hbar) \exp(-\Gamma t/2) , \qquad (1)$$

where the $|I\rangle = \Sigma_{\gamma=a,b,\ldots} \alpha_{I\gamma} |\gamma\rangle$ are the molecular eigenstates resulting from the coupling of the zero-order levels |γ⟩, the $\alpha_{I\alpha}$s form a real, orthonormal, $N \times N$ matrix, the E_Is are the energies of the $|I\rangle$, and Γ is the decay rate of the eigenstates (taken for simplicity to be equal for all I). The contribution of a given zero-order level |γ⟩ to $\psi(t)$ is

$$P_\gamma(t) = |\langle\gamma|\psi(t)\rangle|^2$$

$$\sim \sum_{I,J=1}^{N} (\alpha_{I_a}\alpha_{I\gamma}\alpha_{J_a}\alpha_{J\gamma}) \exp[-(i\omega_{IJ} + \Gamma)t] ,$$

where $\omega_{IJ} = (E_J - E_I)/\hbar$. At $t = 0$, $\psi(0) \approx \Sigma\alpha_{I_a}\alpha_{I\gamma}|\gamma\rangle = |a\rangle$ by the orthonormality of the αs. As t increases, however, the phase terms in eq. (1) evolve and other zero-order states contribute to $\psi(t)$. This evolution is the quantum mechanical description of vibrational energy flow from the motion represented by |a⟩ to those motions represented by |b⟩, |c⟩, etc. The details of this IVR process (the number of levels involved, the time scale) depend on the particular details of the coupling between zero-order levels.

The evolution of $\psi(t)$ can be fruitfully probed by the temporal and spectral resolution of the fluorescence arising from $\psi(t)$. The usefulness of this experimental approach derives from the fact that emission to a given S_0 final state $|f_\gamma\rangle$, will generally gain its strength from just one zero-order excited state level |γ⟩ (again for reasons of Franck–Condon overlap). The intensity of such a fluorescence band (which we call γ-type) is

$$I_\gamma(t) \sim \sum_{I,J} (\alpha_{I_a}\alpha_{I\gamma}\alpha_{J_a}\alpha_{J\gamma}) \exp[-(i\omega_{IJ} + \Gamma)t]$$

and is, therefore, directly proportional to $P_\gamma(t)$. Thus, knowledge of the temporal behaviour of all the bands in the fluorescence spectrum gives one a direct indication of the evolution of the vibrational content of the excited state. On the other hand, if the decay of spectrally integrated fluorescence is measured this information is masked or lost.

In the limit of small N, *restricted* IVR occurs. Such a process is characterized by oscillatory energy flow

between the coupled vibrational levels. This is manifested in fluorescence decays as cosine modulation terms, the phases of which (0° or 180°) are dependent on fluorescence detection wavelength [2,3].

The evolution of $\psi(t)$ for larger N has been treated in the literature within the context of both the intermediate and statistical cases of radiationless transitions [5–8]. In such treatments, it is convenient to consider two quantities

$$P_a(t) = \left(\sum_I \alpha_{Ia}^4 + 2 \sum_{I>J} \alpha_{Ia}^2 \alpha_{Ja}^2 \cos(\omega_{IJ} t) \right) \exp(-\Gamma t) \tag{2a}$$

and

$$\sum_{\gamma=b,c,..} P_\gamma(t) = \sum_{\gamma=b,c,..} \left(\sum_I \alpha_{Ia}^2 \alpha_{I\gamma}^2 + 2 \sum_{I>J} (\alpha_{Ia}\alpha_{I\gamma}\alpha_{Ja}\alpha_{J\gamma}) \cos(\omega_{IJ} t) \right) \exp(-\Gamma t) \,. \tag{2b}$$

Eq. (2a) is the contribution of the initially prepared vibrational state $|a\rangle$ to $\psi(t)$ and eq. (2b) is the overall contribution to $\psi(t)$ of those states coupled to $|a\rangle$. Now for large N, the number (i.e. $\frac{1}{2}N(N-1)$) of cosine terms with different frequencies in eqs. (2) is sufficient to lead to a dephasing process whereby the sums over interference terms in eqs. (2a) and (2b) are large only for $t \leqslant \Delta^{-1}$, where Δ^{-1} is a measure of width of the distribution of ω_{IJ} values. (Δ is normally approximated by the quantity $2\pi \overline{V}^2 \rho$ [5,7], where $\overline{V}$ is a measure of the variance for vibrational coupling [7] and ρ is the density of interacting vibrational states.) Lahmani et al. [5] have shown that the quantum mechanical decays that are represented by eqs. (2) can be approximately reproduced by treating the kinetic scheme illustrated in fig. 1 if one makes the correspondence $k_i + k_r \leftrightarrow \Delta$ and $k_i/k_r \leftrightarrow N$, where k_i is the forward IVR "rate constant" from $|a\rangle$ to other modes and k_r is the reverse rate constant. The $P(t)$ values are treated as populations. Solving the population equations for this kinetic system yields

$$P_a(t) = (k_i + k_r)^{-1} \times \{k_i \exp[-(k_i + k_r + \Gamma)t] + k_r \exp(-\Gamma t)\} \leftrightarrow N^{-1}\{(N-1)\exp[-(\Gamma+\Delta)t] + \exp(-\Gamma t)\} \,, \tag{3a}$$

$$\sum_{\gamma \neq a} P_\gamma(t) = [k_i/(k_i + k_r)] \times \{\exp(-\Gamma t) - \exp[-(k_i + k_r + \Gamma)t]\} \leftrightarrow [(N-1)/N]\{\exp(-\Gamma t) - \exp[-(\Gamma+\Delta)t]\} \,. \tag{3b}$$

Thus, with the aid of this kinetic analogy, one can interpret the initial dephasing in eqs. (2) and (3) as giving rise to a dissipative IVR process by which vibrational population flows irreversibly out of $|a\rangle$ into the other vibrational states on a time scale Δ^{-1}, after which time a steady state is reached and the relative vibrational populations do not appreciably change. Of course, a kinetic model cannot describe completely a quantum dynamical process, except in the statistical limit. In particular, one might expect two deviations from eqs. (3a) and (3b). Firstly, the initial decay of $P_a(t)$ (or buildup of $\Sigma_\gamma P_\gamma(t)$) need not, in general, be exponential. Secondly, the long time decays of these quantities need not be monotonically decreasing functions but may, instead, exhibit quantum beats. Bearing this in mind, however, the simplicity of the kinetic results renders the kinetic model an important interpretive tool.

Now, as we have noted above, the values $P_\gamma(t)$ can be directly monitored by the temporal and spectral resolution of fluorescence. For large N, spectral congestion usually precludes the possibility of measuring decays for each type of band. Nevertheless, the optically active property of the $|a\rangle$ level, which allows its selective excitation as the initially prepared state, also effects a spectral separation of a-type fluorescence bands from the other types of bands [4]. In general, only a-type bands, which are called vibrationally unrelaxed bands (U), appear as discrete bands in the uncluttered region of the fluorescence spectrum just to the red of the excitation energy (fig. 1). For these bands, one expects decays of the form of eq. (3a). The other bands, which are called vibrationally relaxed (R), in general, appear further to the red in the fluorescence spectrum, in a congested region starting roughly at the wavelength of the $S_1 \rightarrow S_0$ 0–0 transition [4]. Without resolving individual bands, one expects the fluorescence decays in this region to approximate the expression given in eq. (3b). By measuring decays in these two regions one can derive parameters charac-

terizing the flow of energy from $|a\rangle$ to other $|\gamma\rangle$.

As a final point, it is worth noting that eqs. (3a) and (3b) provide a basis by which the rate of IVR (i.e. Δ) can be deduced by time-integrated fluorescence measurements of U intensity (I_U) versus R intensity (I_R). This derives from the fact that

$$I_U/I_R \approx \int P_a(t)\,dt \Big/ \int \sum_{\gamma=b,c,\ldots} P_\gamma(t)\,dt$$

$$\approx \Gamma/(\Gamma + \Delta) \qquad (4)$$

in the limit of fast IVR (i.e. $\Delta \gg \Gamma$). Thus, in this limit I_U/I_R becomes the ratio of the fluorescence decay rate to the rate of IVR. By obtaining the former (Γ) from conventional fluorescence measurements one can therefore deduce Δ. As we shall discuss later, this procedure could lead to erroneous rates for IVR.

3. Experimental

Details of the experimental apparatus and techniques may be found elsewhere [9]. Briefly, a free-jet expansion of 35 psi He and anthracene vapor (180°C) through a 100 μm pinhole was intersected 3 mm downstream from the orifice by the frequency doubled output ($\Delta t \approx 15$ ps, $\Delta\bar{\nu} \approx 2$ cm^{-1}) of a synchronously pumped, cavity dumped (4 MHz) dye laser. Fluorescence was detected at right angles, wavelength analyzed by a monochromator, and detected by a fast multichannel plate phototube. Fluorescence decays were measured by time-correlated single photon counting. The temporal response of the detection system (typically 80 ps fwhm) is now capable of resolving decays of $\approx$10 ps time constant. This feature is important for the reported experiments and for other recent measurements [3] of "very fast" quantum beats. By letting the anthracene sample run out and then measuring a "decay", the laser scatter contribution was found to be negligible for typical detection conditions. To assess the influence of intermolecular collisions on measured decays the laser-to-nozzle distance (X) was increased up to 10 mm (X/D = 100). No changes in decays were observed upon this variation.

4. Results

Fig. 2 presents the dispersed fluorescence spectrum

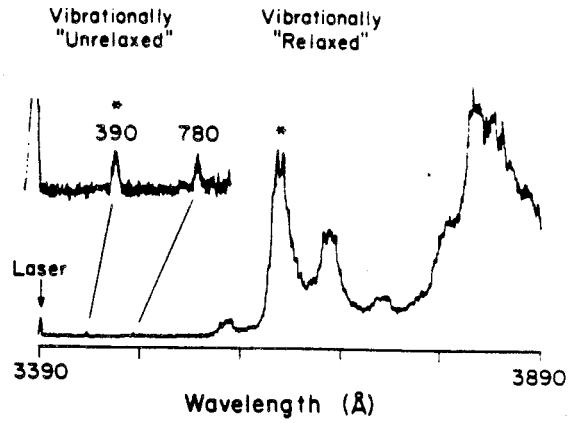

Fig. 2. The fluorescence spectra which result from the excitation of jet-cooled anthracene to E_{vib} = 1792 cm^{-1} in S_1. Spectral resolution was 1.6 A for the main spectrum and 3.2 A for the inset. The spectral position of the laser is marked by an arrow. Laser scatter contributes significantly only to the resonance fluorescence band. The asterisks mark the detection wavelengths for the decays of fig. 3.

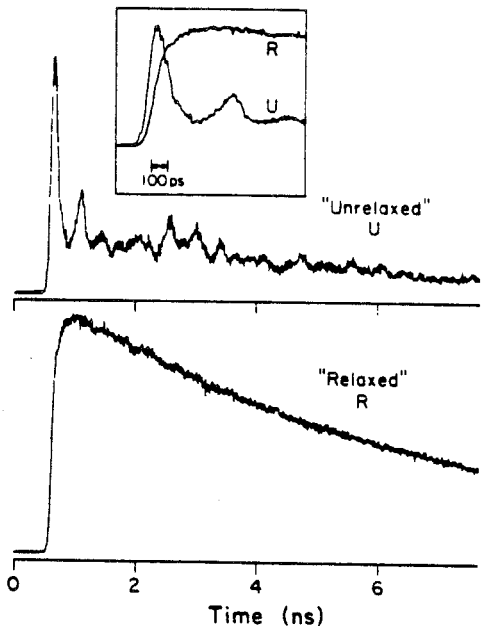

Fig. 3. Fluorescence decays of U and R emission from jet-cooled anthracene excited to E_{vib} = 1792 cm^{-1}. The inset shows the early time behavior of the decays. Detection wavelengths are indicated by asterisks in fig. 2. The detection spectral resolution was $\approx$20 A. The apparent ratio of fast to slow fluorescence in the U decay is less than the actual value, which relates to N in the text, due to the finite temporal response of detection and spectral resolution. Quantum beats were observed for R fluorescence decays when the spectral resolution was better (e.g. 3.2 A).

which results from excitation of jet-cooled anthracene to E_{vib} = 1792 cm^{-1} in S_1 (for spectroscopic data on jet-cooled anthracene, see refs. [9,10]). One may note two spectral regions: the one just to the red of the excitation energy ($\bar{\nu}_{ex}$) which contains two weak, well-resolved bands at shifts of 390 and 780 cm^{-1} from $\bar{\nu}_{ex}$ [9,10], and the congested region to the red of this, wherein almost all of the fluorescence intensity occurs. Knowing that the 390 cm^{-1} interval represents one quantum of the strongly optically active $a_g(12)$ S_0

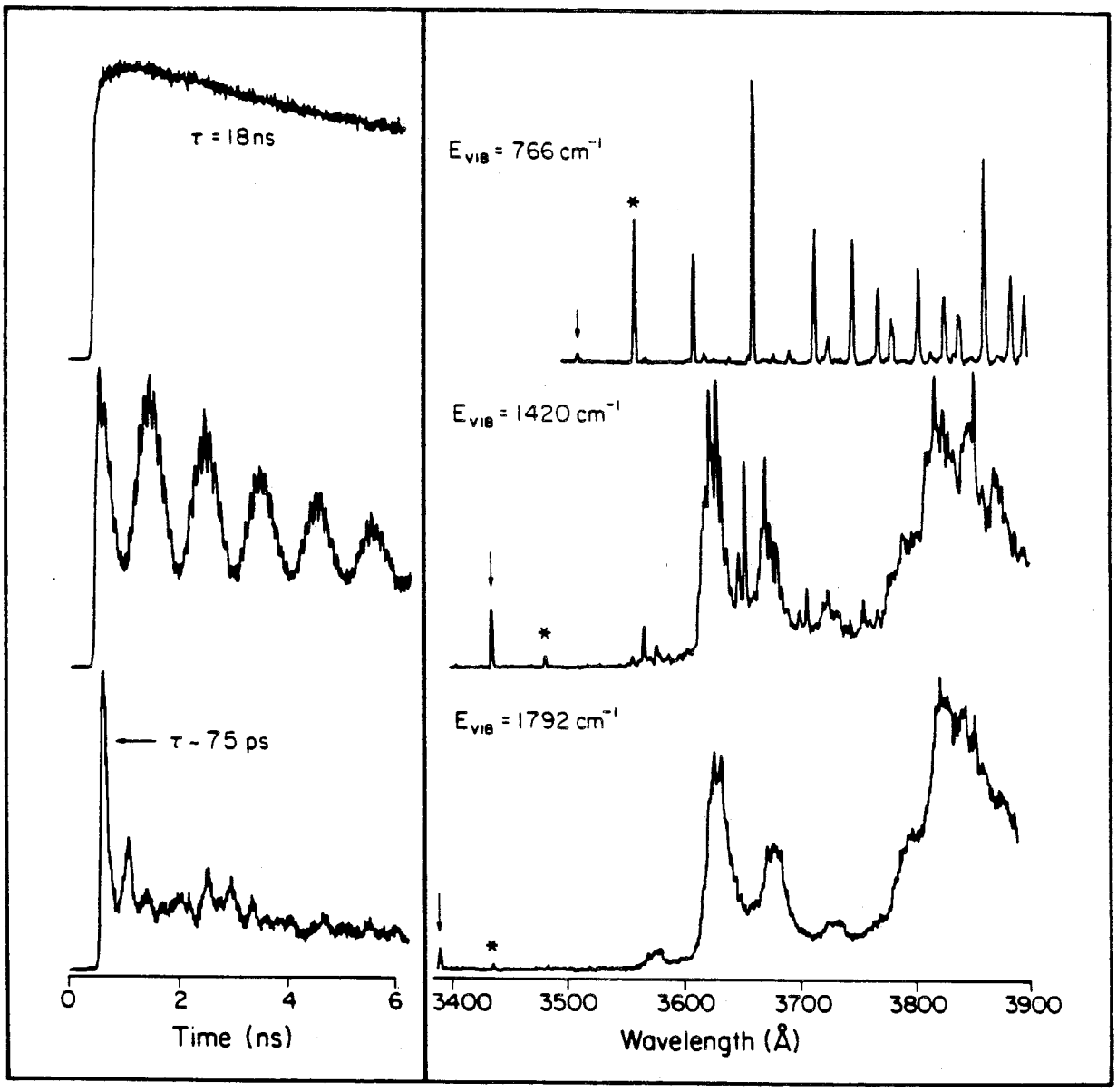

Fig. 4. U fluorescence decays and dispersed fluorescence spectra of jet-cooled anthracene for three values of E_{vib}. All decays were obtained by detection of the 390 cm^{-1} bands (marked by asterisks) in the various fluorescence spectra. The apparent rise of the decay for E_{vib} = 766 cm^{-1} is a result of the convolution of a long single exponential function with the system response function (width ≈80 ps). All fluorescence spectra were obtained with 1.6 Å resolution. Arrows mark the excitation wavelength for each spectrum.

mode [9,10], it is clear that the 390 and 780 cm^{-1} bands are U bands. On the other hand, the congested region has the characteristics typical of R fluorescence. In fig. 3 are the fluorescence decays obtained by detection of emission in the two regions (the detection wavelengths are marked by asterisks in fig. 2). The inset of the figure displays the early time behavior of the two decays. The relative temporal position of the two decays is real and has not been adjusted for display purposes. Neither the initial portion of the U decay nor the rise of the R decay are response function limited, as judged by decay simulations incorporating response function convolution effects.

Decays at other wavelengths have also been measured. The decay of the 780 cm^{-1} band was found to be the same as that of the 390 cm^{-1} band. Other decays measured in the congested region from 3620 to 3640 Å were found to vary with detection wavelength and to exhibit quantum beats. All such R decays, however, had finite risetimes comparable to that of the R decay in fig. 3.

As a point of reference, we display in fig. 4 typical temporal and spectral behaviors of anthracene fluorescence as a function of vibrational energy in S_1.

5. Discussion

5.1. IVR and intramolecular dephasing

The temporal behaviors of the U and R emissions reported herein are consistent with previous theoretical predictions derived from the quantum mechanical treatment of many level IVR. As such, they are interpreted as manifestations of dissipative IVR in anthracene at $E_{vib} = 1792\ cm^{-1}$. The fast (≈75 ps) decay of the U fluorescence and the rise of the R fluorescence correspond, respectively, to the intramolecular dephasing of interference terms in eqs. (2a) and (2b). Further comparison with theory is aided by use of the simple kinetic expressions, eqs. (3a) and (3b). Clearly, the U decay of fig. 3 has the approximate functional form of the sum of two exponentials (eq. (3a)). The initial ≈75 ps component is the irreversible IVR decay (dephasing) of the laser-prepared zero-order vibrational level. The R fluorescence decay, in turn, is approximated by the difference of two exponentials (eq. (3b)). The rise time of this decay represents the flow of energy into the vibrational levels coupled to the initially prepared state. The long time components of the U and R decays correspond to an intramolecular steady state wherein the distribution of vibrational energy remains approximately constant. In this regard, it is notable that the long time components are modulated for both U and R fluorescence (for good enough spectral resolution). This quantum effect, which cannot be handled by the kinetic model, indicates that the vibrational coupling at $E_{vib} = 1792\ cm^{-1}$ is best classified as being in the strong-coupled intermediate case [6–8]. Moreover, it shows that it is possible for IVR to exhibit partial recurrences and, yet, also be dissipative in nature!

5.2. Temporal versus spectral measurements of IVR

There are several points to be made concerning the ≈75 ps time scale for IVR ($\Delta \approx 13 \times 10^9\ s^{-1}$) deduced from the U decay of fig. 3. Firstly, it is instructive to compare this value to that which one obtains from eq. (4) by using $I_R/I_U \approx 600$ (from fig. 2) and the lifetime at this energy, $1/\Gamma = 6$ ns [9,10]. These numbers lead to $\tau_{IVR} \approx 10$ ps. This order of magnitude discrepancy between time-resolved and time-integrated results is due to a number of factors including the presence of U fluorescence in the R spectral region, approximations involved in the kinetic model leading to eq. (4), and/or experimental difficulties in measuring relative fluorescence intensities. In any case, it points up the difficulties involved in extracting Δ values from *time-integrated* measurements.

5.3. Homogeneous broadening and IVR

Since Δ is related to the bandwidth over which the |a⟩ level is spread through coupling with other vibrational levels, it could, in principle, be obtained by absorption or fluorescence excitation experiments. Associated with such measurements, however, are linewidth contributions from rotational inhomogeneous broadening, Doppler broadening, and overlapping vibronic transitions, all of which obscure the dynamically important broadening. Thus, a spectral linewidth measurement of Δ must be interpreted with some care. In cases where care is taken to consider or eliminate "trivial" spectral broadening the Δ value obtained can be related to an actual temporal measurement only if

the initial dephasing of U fluorescence or the rise time of R fluorescence can be measured. That is, temporal and spectral resulution of fluorescence is necessary; Δ is not related to the long time decay of U or R fluorescence. Since the apparent lifetime at this excess energy is 6 ns, the homogeneous broadening [11] (in a two-level approximation!) is $\Delta\nu_H = 1/\pi T_2 = 1/2\pi\tau$ = 26 MHz, assuming a Lorentzian line shape. In our case, however, the fast component alone will translate to a 2 GHz width. Therefore it is apparent that in the case where there is multilevel IVR *the apparent width and the apparent lifetime might not correspond;* only if the early time behavior is resolved would one know about such correspondence. This important point is also crucial to the dynamics of benzene in the channel-3 region [12].

5.4. Effective density of states for IVR

The measured Δ can be related to average molecular parameters via $\Delta \approx 2\pi\bar{V}^2\rho$. Now, $\rho_{vib}(1792\ cm^{-1}) \approx 120/cm^{-1}$. However, one would expect symmetry restrictions [13] on vibrational coupling to give a density of interacting states $\rho = \rho_{vib}/8$, assuming that anharmonic coupling is the dominant coupling mechanism. (The factor of 8 comes from the number of irreducible representations (D_{2h}) using the formula given in ref. [13].) Using $\rho = 15/cm^{-1}$ and $\Delta = 0.4\ cm^{-1}$ (13×10^9 Hz) one obtains $\bar{V} \approx 0.07\ cm^{-1}$. This value is quite consistent with the values for the matrix elements manifested in quantum beat modulated decays at intermediate energies in anthracene [2,3]. However, caution should be taken when discussing $\bar{V}$ since we already know from our quantum beat data that V can vary from 10^{-2} to at least 0.3 cm^{-1}. Also, if the spectral distribution of eigenstates is irregular such as it might be for moderate N (e.g. $N \approx 10$) it is difficult to relate Δ to a well-defined spectral width. A fuller treatment of this problem will be dealt with elsewhere.

5.5. Excess energy behavior

It is significant that the decay behavior exhibited by anthracene at $E_{vib} = 1792\ cm^{-1}$ does not occur at lower energies in the molecule (fig. 4). In fact, two regimes at lower energies may be identified and classified by the decay behavior of U bands. At the lowest energies (e.g. $E_{vib} = 766\ cm^{-1}$) all bands are U bands and the decays are single exponential. This energy regime corresponds to one in which IVR is negligible. U decays at intermediate energies [2,3] (e.g. $E_{vib} = 1420\ cm^{-1}$), on the other hand, are modulated by small numbers of Fourier components (1, 9.7, 10.7 GHz), but *do not display irreversible initial decays.* This energy regime corresponds to one in which IVR is restricted in nature. The overall trend of U decay behavior with energy is paralleled by spectral changes in fluorescence [9,10] (fig. 4) which reflect the increasing influence of IVR. Of course, this change with energy from *negligible* to *restricted* to *dissipative* IVR is what one would expect given the behavior of the vibrational density of states † with energy ($\approx 1/cm^{-1}$ at 766 cm^{-1}; $\approx 25/cm^{-1}$ at 1400 cm^{-1}; $\approx 120/cm^{-1}$ at 1792 cm^{-1}), assuming $\bar{V}$ does not change drastically with energy in this energy range of interest.

Acknowledgement

This material is based upon work supported by the National Science Foundation under Grant No. CHE-8211356.

† Our treatment here has not taken account of the influence of rotational level structure on observed fluorescence decays. In a subsequent publication we will present experimental and theoretical evidence which show that changes in vibrational coupling with rotational level are manifested in fluorescence decays as enhanced decay rates of quantum beat *envelopes.*

References

[1] A. Zewail, Faraday Discussions Chem. Soc. 75 (1983) 315; P.M. Felker and A.H. Zewail, in: Proceedings of the 1983 NATO Advanced Research Workshop, Acquafredda di Maratea, Italy, 5–11 June, 1983, to be published.
[2] P.M. Felker and A.H. Zewail, Chem. Phys. Letters 102 (1983) 113.
[3] P.M. Felker and A.H. Zewail, Phys. Rev. Letters, submitted for publication.
[4] C.S. Parmenter, Faraday Discussions Chem. Soc. 75 (1983) 7;
R.E. Smalley, J. Phys. Chem. 86 (1982) 3504.
[5] F. Lahmani, A. Tramer and C. Tric, J. Chem. Phys. 60 (1974) 4431.

[6] S. Mukamel and J. Jortner, in: Excited states, Vol. 3, ed. E.C. Lim (Academic Press, New York, 1977); S.A. Rice, in: Excited states, Vol. 2, ed. E.C. Lim (Academic Press, New York, 1975).
[7] C. Tric, Chem. Phys. 14 (1976) 189.
[8] A. Tramer and R. Voltz, in: Excited states, Vol.4. ed. E.C. Lim (Academic Press, New York, 1979); K.F. Freed and A. Nitzan, J. Chem. Phys. 73 (1980) 4765; S. Mukamel and R.E. Smalley, J. Chem. Phys. 73 (1980) 4156.
[9] W.R. Lambert, P.M. Felker and A.H. Zewail, J. Chem. Phys. (September, 1984), to be published.
[10] W.R. Lambert, P.M. Felker, J.A. Syage and A.H. Zewail, J. Chem. Phys. (September, 1984), to be published.
[11] M.J. Bruns, W.-K. Liu and A.H. Zewail, in: Spectroscopy and excitation dynamics of condensed molecular systems, Vol. 4, eds. V.M. Agranovich and R.M. Hochstrasser (North-Holland, Amsterdam, 1983) ch. 7, p. 301.
[12] E. Riedle, H.J. Neusser and E.W. Schlag, J. Phys. Chem. 86 (1982) 4847; E. Riedle and H.J. Neusser, J. Chem. Phys., to be published.
[13] S.M. Lederman, J.H. Runnels and R. Marcus, J. Phys. Chem. 87 (1983) 4364.

APPENDIX IV

FOURIER TRANSFORM COMPUTER PROGRAM

The printout below is the FORTRAN computer program used in analyzing data for this paper. It relies on the fact that the the Fourier transform of the convolution integral of two functions is equal to the product of the Fourier transforms of the two functions, to give information concerning the modulation depths and phases of beat components in decays for which the finite detection temporal resolution cannot be ignored. Further information and references are given in Chapter 4, section II-B. The program was written to run interactively on a PDP 11/23 computer.

```
      PROGRAM FMAIN
C     DESIGNED TO OBTAIN THE FOURIER TRANSFORM OF A DECAY OR RESIDUAL
C     SUCH THAT IT IS FREE OF CONVOLUTION EFFECTS
C     ONE SUBROUTINE: "FFT" A FAST FOURIER TRANSFORM ROUTINE USING UP
C     TO 4Ø96 POINTS (IN POWERS OF TWO)
C     FILES INPUT ARE THE RESPONSE FUNCTION FILE AND EITHER A DECAY
C     OR A RESIDUAL FILE
C     THE PROGRAM DOES THE FOLLOWING:
C     1. THE RESPONSE FUNCTION IS FOURIER TRANSFORMED
C     2. THE DECAY (OR RESIDUAL) IS FOURIER TRANSFORMED
C     3. THE DECAY TRANSFORM (COMPLEX NUMBERS) IS DIVIDED
C     BY THE RESPONSE TRANSFORM (COMPLEX NUMBERS)
C     4. EITHER THE REAL SPECTRUM (ABSORPTION) ARISING
C     FROM THIS PROCEDURE OR THE ABSOLUTE VALUE SPECTRUM
C     (POWER) ARISING FROM THIS IS OUTPUT
C     INTO THE DATA FILE NU. DEPENDING ON USER CHOICE
C
      DIMENSION XR(4Ø96),XI(4Ø96),FILE1(3),FILE2(3)
      N=4Ø96
      NU=12
      TYPE *,'INPUT THE RESPONSE, AND DATA FILE NAMES'
      ACCEPT 5,FILE1
      ACCEPT 5,FILE2
5     FORMAT (3A4)
      TYPE *,'IS THE DATA FILE A DECAY OR RESIDUAL FILE ?'
      ACCEPT 7,ANS
7     FORMAT(A1)
      TYPE *,'ENTER THE NO. OF POINTS IN THE DECAY/RESIDUAL
     1 FILE.'
      ACCEPT *,NPTS
      TYPE *,'ENTER THE HIGHEST FREQUENCY (IN CHANNELS)
     1 TO BE CONSIDERED.'
      ACCEPT *,NFREQ
      TYPE *,'DO YOU WANT A POWER OR AN AMPLITUDE SPECTRUM ?'
      ACCEPT 7,ANS2
C     INPUT THE RESPONSE
      OPEN(UNIT=4,NAME=FILE1,TYPE='OLD',ACCESS='DIRECT',
     1 RECORDSIZE=1Ø2Ø)
      READ(4'1) NNN,CT,ACC,(XR(I),I=1,NPTS)
C     NNN AND ACC ARE UNUSED, CT IS THE EXPERIMENTAL
C     VALUE OF PSEC PER
C     CHANNEL, AND XR(I) ARE THE DATA POINTS
      CLOSE(UNIT=4,DISP='SAVE')
C     ZERO FILL
      DO 6 I=NPTS+1,N
6     XR(I)=Ø.
C     FOURIER TRANSFORM THE RESPONSE
      CALL FFT(XR,XI,N,NU)
      TYPE *,'THE RESPONSE TRANSFORM IS DONE'
C     TEMPORARILY STORE THE RESPONSE TRANSFORM
      OPEN(UNIT=4,NAME='SAVE.DAT',TYPE='NEW',ACCESS='DIRECT'
     1 RECORDSIZE=2)
      DO 1Ø I=1,N
      WRITE(4'I) XR(I),XI(I)
      XR(I)=Ø.
1Ø    XI(I)=Ø.
      CLOSE(UNIT=4,DISP='SAVE')
C     INPUT THE DECAY OR RESIDUAL FILE
      IF(ANS1.EQ.'R') GO TO 15
      OPEN(UNIT=4,NAME=FILE2,TYPE='OLD',ACCESS='DIRECT',
     1 RECORDSIZE=1Ø2Ø)
      READ(4'1) NNN,CT,ACC,(XR(I),I=1,NPTS)
      CLOSE(UNIT=4,DISP='SAVE')
      GO TO 16
15    OPEN(UNIT=4,NAME=FILE2,TYPE='OLD',ACCESS='DIRECT',
```

```
C       FOURIER TRANSFORM THE DECAY OR RESIDUAL FILE
        CALL FFT(XR,XI,N,NU)
        TYPE *,'THE DECAY TRANSFORM IS DONE'
C       DIVIDE THE DECAY (OR RESIDUAL) TRANSFORM BY THE RESPONSE
        OPEN(UNIT=4,NAME='SAVE.DAT',TYPE='OLD',ACCESS='DIRECT',
     1  RECORDSIZE=2)
        DO 2Ø I=1,N
        READ(4'I) XR1,XI1
        F1=(XR1**2 +XI1**2)
        XR2=XR(I)
        XI2=XI(I)
        XR(I)=(XR1*XR2+XI1*XI2)/F1
2Ø      XI(I)=(XR1*XI2-XI1*XR2)/F1
        CLOSE(UNIT=4,DISP='DELETE')
C       WRITE THE NORMALIZED FOURIER SPECTRUM TO FILE NU.
        IF(ANS.EQ.'A') GO TO 25
        DO 22 I=1,NFREQ
22      XR(I)=SQRT(XR(I)**2+XR(N-I+1)**2 +XI(I)**2+XI(N-I+1)**2)
        GO TO 28
25      CONTINUE
        DO 27 I=1,NFREQ
27      XR(I)=XR(I)+XR(N-I+1)
28      CONTINUE
        DO 29 I=NFREQ+1,N
29      XR(I)=Ø.
C       FIND FMAX IN GHZ
        FMAX=FLOAT(NFREQ)*1ØØØ./(4Ø96.*CT)
        OPEN (UNIT=4,NAME='NU.',TYPE='NEW',ACCESS='DIRECT',
     1  RECORDSIZE=1Ø2Ø)
        WRITE(4'1) 1ØØØ,Ø.,FMAX,(XR(I),I=1,1ØØØ)
        CLOSE(UNIT=4,DISP='SAVE')
        RETURN
        END
```

```
      SUBROUTINE FFT(XREAL,XIMAG,N,NU)
C     FAST FOURIER TRANSFORM ROUTINE DESIGNED TO
C     TRANSFORM UP TO 4096 COMPLEX NUMBER INPUTS
C     WHICH ARE DESTROYED
C     AND TAKEN THE C PLACE OF BY THE TRANSFORM. THE
C     FREQUENCY RESOLUTION IS (1/T) C WHERE T IS THE
C     TOTAL TIME-RANGE OF THE INPUT FILE
      DIMENSION XREAL(1),XIMAG(1)
      EYE=(0.,1.)
      N2=N/2
      NU1=NU-1
      K=0
      DO 100 L=1,NU
102   DO 101 I=1,N2
      NP=IBITR(K/2**NU1,NU)
      P=FLOAT(NP)
      ARG=6.283185*P/FLOAT(N)
      C=COS(ARG)
      S=SIN(ARG)
      K1=K+1
      K1N2=K1+N2
      TREAL=XREAL(K1N2)*C+XIMAG(K1N2)*S
      TIMAG=-XREAL(K1N2)*S+XIMAG(K1N2)*C
      XREAL(K1N2)=XREAL(K1)-TREAL
      XIMAG(K1N2)=XIMAG(K1)-TIMAG
      XREAL(K1)=XREAL(K1)+TREAL
      XIMAG(K1)=XIMAG(K1)+TIMAG
101   K=K+1
      K=K+N2
      IF(K.LT.N) GO TO 102
      K=0
      NU1=NU1-1
100   N2=N2/2
      DO 103 K=1,N
      I=IBITR(K-1,NU)+1
      IF(I.LE.K) GO TO 103
      TREAL=XREAL(K)
      TIMAG=XIMAG(I)
      XREAL(K)=XREAL(I)
      XIMAG(K)=XIMAG(I)
      XREAL(I)=TREAL
      XIMAG(I)=TIMAG
103   CONTINUE
      N22=N/2
      GO TO 153
      DO 152 I=N22+1,N
      XREAL(I)=XIMAG(I-N22)
152   CONTINUE
153   CONTINUE
      RETURN
      END
      FUNCTION IBITR(J,NU)
      J1=J
      IBITR=0
      DO 200 I=1,NU
      J2=J1/2
      IBITR=IBITR*2+(J1-2*J2)
200   J1=J2
      RETURN
      END
```